Methods in
Molecular Biology 1327

Springer Protocols

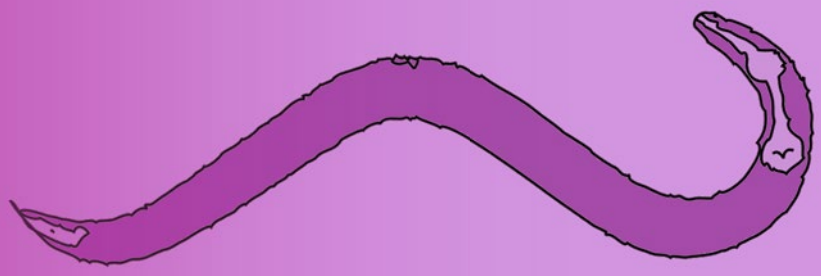

David Biron
Gal Haspel *Editors*

C.elegans

Methods and Applications

Second Edition

Humana Press

METHODS IN MOLECULAR BIOLOGY

Series Editor
John M. Walker
School of Life and Medical Sciences
University of Hertfordshire
Hatfield, Hertfordshire, AL10 9AB, UK

For further volumes:
http://www.springer.com/series/7651

C. elegans

Methods and Applications

Second Edition

Edited by

David Biron

Department of Physics, The James Franck Institution, The Institute for Biophysical Dynamics, The University of Chicago, Chicago, IL, USA

Gal Haspel

Federated Department of Biological Sciences, New Jersey Institute of Technology and Rutgers University, Newark, NJ, USA

Humana Press

Editors
David Biron
Department of Physics
The James Franck Institution
The Institute for Biophysical Dynamics
The University of Chicago
Chicago, IL, USA

Gal Haspel
Federated Department of Biological Sciences
New Jersey Institute of Technology
and Rutgers University
Newark, NJ, USA

ISSN 1064-3745 ISSN 1940-6029 (electronic)
Methods in Molecular Biology
ISBN 978-1-4939-2841-5 ISBN 978-1-4939-2842-2 (eBook)
DOI 10.1007/978-1-4939-2842-2

Library of Congress Control Number: 2015945342

Springer New York Heidelberg Dordrecht London

Printed on acid-free paper

Humana Press is a brand of Springer
Springer Science+Business Media LLC New York is part of Springer Science+Business Media (www.springer.com)

Preface

Tractable models such as the nematode *Caenorhabditis elegans* provide profound insight into a wide range of biological phenomena. It is the objective of any scientific effort to understand a natural phenomenon. Considerable effort and ingenuity are dedicated towards developing novel methods and approaches that will enable breakthroughs and progress.

C. elegans has a short life cycle—it matures during three days at room temperature—and is easy to cultivate. Under standard laboratory conditions, hermaphroditic nematodes self-fertilize but mating with males can be induced for experimental purposes. Therefore, genetic manipulations and the maintenance of mutant strains are comparatively simple. *C. elegans* was the first animal to have its genome fully sequenced and to this day, the genome is being annotated with increasing detail and accuracy. Genetic, genomic, anatomical, physiological, and other data are curated in publically accessible databases including Wormbase, Wormatlas, Wormweb, Wormwiring, and Wormbook.

The simple anatomy of *C. elegans* is a key advantage in and of itself. Determining the cell lineage, which is mostly invariant between individuals, enabled fundamental discoveries in developmental biology and the determination of cell fate. Likewise, the nervous system of *C. elegans* is compact—a hermaphrodite has but 302 neurons. This enabled White and colleagues to construct an anatomical map of neuronal connectivity, colloquially referred to as the "Mind of a Worm." The connectome of *C. elegans*—unique in its near completeness—is being refined since, and updated information is periodically made available to researchers in the field. It provides a powerful starting point for understanding how neuronal and molecular pathways regulate behavior. At the same time, the importance of nonsynaptic pathways is increasingly appreciated.

Novel experimental methods for genetic, cellular, and whole animal manipulations are being developed at a staggering rate. In recent years, reading an entire genome has become cost effective, writing or deleting genetic information in vivo has come to resemble editing text, the properties of optical reporters have improved dramatically, and the diversity of physiological parameters that can be monitored using unobtrusive measures has greatly expanded. Concurrent advances in computation, imaging, microfluidics, and prototyping enable bench-top experiments that were not previously possible. The number of addressable scientific questions scales rapidly with the number of available tools.

The aim of this volume is to provide a step-by-step guide for implementing a selection of these novel techniques in the lab. Each protocol in this volume is presented as a stand-alone chapter, specifically geared towards addressing practical needs without presuming prior knowledge of the technique at hand. We hope this volume can assist in addressing the subset of these questions that most intrigue you.

Chicago, IL, USA — ***David Biron***
Newark, NJ, USA — ***Gal Haspel***

Acknowledgment

This work was supported by the NSF IOS grant no. 1256989 (DB).

Contents

Contributors

Dirk R. Albrecht • *Department of Biomedical Engineering, Worcester Polytechnic Institute, Worcester, MA, USA; Department of Biology and Biotechnology, Worcester, MA, USA*

David Biron • *Department of Physics, The James Franck Institution, The Institute for Biophysical Dynamics, The University of Chicago, Chicago, IL, USA*

Christian Braendle • *Institut de Biologie Valrose, CNRS UMR7277, Nice, Cedex, France; INSERM U1091, Nice, Cedex, France; Université Nice Sophia Antipolis, UFR Sciences, Nice, Cedex, France*

André E.X. Brown • *Faculty of Medicine, MRC Clinical Sciences Centre, Imperial College, London, UK*

John A. Calarco • *FAS Center for Systems Biology, Harvard University, Cambridge, MA, USA*

Matthew A. Churgin • *Department of Bioengineering, University of Pennsylvania, Philadelphia, PA, USA*

Yifat Eliezer • *Genetics Department, Silberman Life Sciences Institute, The Hebrew University of Jerusalem, Jerusalem, Israel*

Christopher Fang-Yen • *Department of Bioengineering, University of Pennsylvania, Philadelphia, PA, USA; Department of Neuroscience,University of Pennsylvania, Philadelphia, PA, USA*

Ari E. Friedland • *Editas Medicine, Cambridge, MA, USA*

Christian Frøkjær-Jensen • *Howard Hughes Medical Institute, University of Utah, Salt Lake City, UT, USA; Department of Biology, University of Utah, Salt Lake City, UT, USA; Danish National Research Foundation Centre for Cardiac Arrhythmia, University of Copenhagen, Copenhagen, Denmark*

Caspar Glock • *Buchmann Institute for Molecular Life Sciences, Goethe University, Frankfurt, Germany; Institute of Biochemistry, Goethe University, Frankfurt, Germany*

Alexander Gottschalk • *Buchmann Institute for Molecular Life Sciences, Goethe University, Frankfurt, Germany; Institute of Biochemistry, Goethe University, Frankfurt, Germany*

Eric S. Haag • *Department of Biology, University of Maryland, College Park, MD, USA*

David H. Hall • *Albert Einstein College of Medicine, Center for C. elegans Anatomy, Bronx, NY, USA*

Sarah E. Hall • *Department of Biology, Syracuse University, Syracuse, NY, USA*

Michael Hendricks • *Department of Biology, McGill University, Montreal, QC, Canada*

Menachem Katz • *Laboratory of Developmental Genetics, The Rockefeller University, New York, NY, USA*

Ross C. Lagoy • *Department of Biomedical Engineering, Worcester Polytechnic Institute, Worcester, MA, USA*

Erel Levine • *Department of Physics and FAS Center for Systems Biology, Harvard University, Cambridge, MA, USA*

Dylan Lynch • *Department of Physics, The James Franck Inst., The Institute for Biophysical Dynamics, The University of Chicago, Chicago, IL, USA*
Laura Manning • *Department of Biological Sciences, University of Illinois at Chicago, Chicago, IL, USA*
Jatin Nagpal • *Buchmann Institute for Molecular Life Sciences, Goethe University, Frankfurt, Germany; Institute of Biochemistry, Goethe University, Frankfurt, Germany*
Iulia Neagu • *Department of Physics and FAS Center for Systems Biology, Harvard University, Cambridge, MA, USA*
Maria C. Ow • *Department of Biology, Syracuse University, Syracuse, NY, USA*
Nausicaa Poullet • *Institut de Biologie Valrose, CNRS UMR7277, Nice, Cedex, France; INSERM U1091, Nice, Cedex, France; Université Nice Sophia Antipolis, UFR Sciences, Nice, Cedex, France*
William J. Rice • *New York Structural Biology Center, New York, NY, USA*
Janet Richmond • *Department of Biological Sciences, University of Illinois at Chicago, Chicago, IL, USA*
Harold E. Smith • *National Institute of Diabetes and Digestive and Kidney Diseases, National Institutes of Health, Bethesda, MD, USA*
Cristel G. Thomas • *Department of Ecology and Evolutionary Biology, University of Toronto, Toronto, ON, Canada*
Nicholas F. Trojanowski • *Department of Bioengineering, University of Pennsylvania, Philadelphia, PA, USA; Department of Neuroscience, University of Pennsylvania, Philadelphia, PA, USA*
Eviatar I. Yemini • *Department of Biochemistry and Molecular Biophysics, Columbia University, New York, NY, USA*
Alon Zaslaver • *Genetics Department, Silberman Life Sciences Institute, The Hebrew University of Jerusalem, Jerusalem, Israel*

Chapter 1

Library Construction for Mutation Identification by Whole-Genome Sequencing

Harold E. Smith

Abstract

Next-generation sequencing provides a rapid and powerful method for mutation identification. Herein is described a workflow for sample preparation to allow the simultaneous mapping and identification of candidate mutations by whole-genome sequencing in *Caenorhabditis elegans*. The protocol is designed for small numbers of worms to accommodate classes of mutations, such as lethal and sterile alleles, that are difficult to identify by traditional means.

Key words Sequence variant detection, Polymorphism mapping, NGS library construction

1 Introduction

For more than a century, researchers have used classical genetics (random mutagenesis and phenotypic screening) in model species to identify the genes involved in biological pathways. The availability of both self and outcross modes of reproduction makes *Caenorhabditis elegans* ideally suited for such genetic screens. Historically, the ability to generate interesting mutations in worms has greatly exceeded the ability to identify causative sequence variants. Dozens or even hundreds of alleles might be recovered in a single mutant screen (e.g., [1, 2]). The analysis of such a large number of strains involves a daunting (but tractable) number of crosses—to discriminate recessive, dominant, and multigenic traits, to remove extraneous mutations through backcrossing, and to define complementation groups. However, identifying even a single gene of interest by the traditional techniques of positional mapping and transgene rescue is considerably more labor-intensive and time-consuming. As a practical consequence, the molecular identity of many alleles remains unknown.

In recent years, the application of next-generation sequencing technology to mutation identification in *C. elegans* has largely

David Biron and Gal Haspel (eds.), *C. elegans: Methods and Applications*, Methods in Molecular Biology, vol. 1327,
DOI 10.1007/978-1-4939-2842-2_1,

eliminated this bottleneck [3–5]. Whole-genome sequencing provides a catalog of all sequence variants within the strain of interest. By crossing the strain into a highly polymorphic genetic background, both positional information and novel mutations can be obtained [6, 7]. Software pipelines specifically designed for *C. elegans* greatly facilitate the identification of candidate genes [8, 9], which can be validated by secondary criteria such as RNAi [10].

The workflow for sample preparation for whole-genome sequencing consists of the following steps: (1) crossing the mutation-bearing strain to a polymorphic strain and picking homozygous F2 progeny; (2) isolating and shearing the genomic DNA (gDNA); and (3) constructing a gDNA library from the sheared sample. The indicated protocols produce sequence-ready libraries, and are designed to accommodate phenotypes (e.g., nonconditional lethality or sterility) that are typically difficult to analyze. The only limitation is that the allele of interest be recessive so that homozygous and heterozygous segregants can be distinguished.

Each step in this workflow is subject to considerable variation. The picking of F2 progeny (step 1) will be determined by the mutant phenotype in question. The gDNA isolation (step 2) is intended for small numbers of worms, but can be used for bulk samples as well. The library construction protocol (step 3) is specific to the Illumina sequencing platform (which, as of January 2015, was the most cost-effective), but alternative platforms are possible. In all cases, the reader is referred to Subheading 4 for relevant parameters to consider when using alternative methods.

2 Materials

2.1 Worm Growth and Mating

1. Dissecting microscope.
2. Worm pick (*see* **Note 1**).
3. NGM plates: In 2 L flask, mix 3 g NaCl, 17 g agar, 2.5 g peptone, and 975 mL H_2O. Autoclave to sterilize. Cool to 55 °C. Add 1 mL cholesterol (5 mg/mL in ethanol; do not autoclave), 1 mL 1 M $CaCl_2$, 1 mL 1 M $MgSO_4$, and 25 mL 1 M KPO_4, pH 6.0 (108.3 g KH_2PO_4, 35.6 g $K_2HPO_4 \cdot H_2O$, 1 L H_2O) (*see* **Note 2**). Dispense 14 mL into 6 cm petri plates. Cool plates to room temperature. Seed plates with ~50 μL OP50 culture (grown overnight in LB medium @ 37 °C). Incubate seeded plates overnight @ room temperature (*see* **Note 3**).
4. *E. coli* strain OP50 (*see* **Note 4**).
5. *C. elegans* strain CB4856 (*see* **Note 4**).

2.2 gDNA Isolation

1. M9 buffer: Mix 3 g KH_2PO_4, 6 g Na_2HPO_4, 5 g NaCl, and 1 mL 1 M $MgSO_4$ in 1 L H_2O; autoclave to sterilize.
2. TE buffer: Mix 10 mL 1 M Tris–HCl, pH 8.0 and 2 mL 0.5 M EDTA, pH 8.0 in 988 mL H_2O; autoclave to sterilize.
3. Worm lysis buffer: Mix 100 µL 1 M Tris–HCl (pH 8.0), 20 µL 5 M NaCl, 100 µL 0.5 M EDTA, 125 µL 10 % (v/v) SDS, and 655 µL H_2O.
4. Proteinase K, 10 mg/mL concentration.
5. RNase A, 10 mg/mL concentration.
6. Bioruptor sonicating water bath (Diagenode) or similar.
7. MinElute PCR purification kit (Qiagen) or similar.

2.3 Library Construction

1. NEBNext Ultra DNA library prep kit for Illumina (New England Biolabs).
2. EB: 10 mM Tris–HCl, pH 8.0 or 8.5.
3. AMPure XP beads (Agencourt).
4. Magnetic tube rack.
5. 80 % (v/v) ethanol; prepare fresh immediately before use.
6. Adapter oligonucleotides (*see* **Note 5**): Prepare @ 100 µM concentration in TE + 50 mM NaCl. Mix 25 µL each universal and index adapter oligonucleotide. Incubate in a thermal cycler 2 min @ 95 °C, decrease 1 °C each minute until reaching 25 °C (70 min), then hold @ 4 °C. Dilute to the indicated concentration immediately before use.
7. PCR primers (*see* **Note 6**): Prepare @ 25 µM concentration in TE.

3 Methods

3.1 Mating and F2 Selection (See Note 7)

1. Using a dissecting microscope and worm pick, transfer two to three young adult hermaphrodites containing the mutation of interest to a NGM plate seeded with OP50. Pick 10–12 adult males of strain CB4856 to the same plate. Allow to mate overnight @ room temperature (*see* **Note 8**).
2. Transfer each mated hermaphrodite to an individual fresh-seeded NGM plate. Incubate @ room temperature until the F1 progeny begin to reach the L4/young adult stages (~4 days) (*see* **Note 9**).
3. Pick 10–12 F1 L4/young adult hermaphrodites to a fresh-seeded NGM plate. Incubate @ room temperature until F2 progeny can be scored for the mutant phenotype (*see* **Note 10**).

3.2 gDNA Isolation

1. Pick homozygous F2 progeny into a 1.5 mL centrifuge tube containing 500 µL M9 (*see* **Note 11**).
2. Vortex briefly (3–5 s), then spin 60 s @ 1300 RCF.
3. Remove most of the M9 by pipette, taking care to avoid the pellet.
4. Resuspend in 500 µL M9 and repeat the wash at least four times (*see* **Note 12**).
5. Perform a final wash with 500 µL TE; spin 1 min at top speed; remove TE, leaving ~100 µL (*see* **Note 13**).
6. Add 400 µL worm lysis buffer to the worm sample; mix briefly.
7. Sonicate with the BioRuptor using the following settings: high power; 30 s on/30 s off; 2 × 15 min sonication time (*see* **Note 14**).
8. Add 50 µL proteinase K; mix well; incubate 1 h @ 65 °C, vortexing briefly at 10–15 min intervals to maintain suspension (*see* **Note 15**).
9. Add 20 µL RNase A; incubate 30 min @ 37 °C.
10. Purify sheared gDNA using a MinElute column (Qiagen) per the manufacturer's protocol; the final elution volume is 10 µL (*see* **Notes 16** and **17**).

3.3 Library Construction

3.3.1 End Repair and A-Tailing

1. Mix in 0.5 mL tube:

   10 µL sheared gDNA (2–10 ng)

   6.5 µL 10× end repair reaction buffer

   3 µL end prep enzyme mix

   45.5 µL H_2O
2. Incubate in a thermal cycler:

   30 min @ 20 °C

   30 min @ 65 °C

   Hold @ 4 °C

3.3.2 Adapter Ligation

1. Dilute the adapter to 1.5 µM in EB immediately before use (*see* **Note 18**).
2. Add the following and mix:

   15 µL blunt/TA ligase master mix

   2.5 µL adapter

   1 µL ligation enhancer
3. Incubate in a thermal cycler:

   15 min @ 20 °C

   Hold @ 4 °C

*3.3.3 AMPure XP Bead Clean-Up (**See Note 19**)*

1. Remove the reaction tube from the thermal cycler; add 83.5 µL beads; mix well by vortexing (*see* **Note 20**).
2. Incubate the reaction tube 5 min in a tube rack.
3. Place the reaction tube in the magnetic stand; incubate 5 min; remove and discard the supernatant (*see* **Note 21**).
4. Leave the reaction tube in the magnetic stand; add 200 µL freshly prepared 80 % (v/v) ethanol; incubate 30 s; carefully remove and discard the supernatant.
5. Repeat **step 4** twice, for a total of three washes.
6. Air-dry the beads in the open tube for 5 min on the magnetic stand.
7. Add 28 µL EB to elute the DNA; pipette or vortex to resuspend the bead pellet; incubate for 2 min in a tube rack; return to the magnetic stand for 5 min; transfer 23 µL of supernatant (containing the DNA) to a new 0.5 mL tube.

*3.3.4 PCR Amplification (See **Note 22**)*

1. Add the following and mix:

   1 µL primer TruSeq-1 @ 25 µM

   1 µL primer TruSeq-2 @ 25 µM

   25 µL NEBNext Q5 Hot Start HiFi PCR Master Mix
2. Incubate in a thermal cycler:

   One cycle of:

   30 s @ 98 °C

   12 cycles of:

   10 s @ 98 °C

   75 s @ 65 °C

   One cycle of:

   5 min @ 65 °C

   Hold @ 4 °C

*3.3.5 Final AMPure XP Bead Clean-Up (See **Note 23**)*

Follow the protocol above with the following differences:

Step 1. Add 50 µL beads.

Step 5. Repeat **step 4** once, for a total of two washes.

Step 7. Add 25 µL EB; transfer 20 µL.

The library is now ready for quantification, using a method suitable for DNA concentrations in the low ng/µL range (e.g., dye fluorometry or qPCR). UV absorbance is relatively insensitive and therefore not recommended. Library quality can be assessed using the Agilent Bioanalyzer with a high-sensitivity DNA chip to detect

the size distribution. If adapter dimer contamination (a discrete band of 121 bp) is observed, it can be removed by size fractionation via gel isolation or AMPure bead size selection. Libraries with different adapter indices can be pooled, or multiplexed. The recommended minimum sequencing depth for mutation identification is 20-fold genome coverage, or 2×10^9 bp. The amount of data one obtains is determined by the sequencing capacity of the instrument and the degree of multiplexing; consult your sequencing service provider for guidance. The data can be analyzed using any variety of variant-calling software. For ease of use, we recommend CloudMap [9] on the public Galaxy server (available at https://usegalaxy.org) [11–13].

4 Notes

1. Available commercially from www.wormstuff.com. Also, instructions for making worm picks are available online (e.g., http://openwetware.org/wiki/BISC_219/F10:_Gene_Linkage#Making_a_Worm_Pick or http://www.wormbook.org/wbg/articles/volume-19-number-1/a-better-worm-pick-handle).
2. NGM medium lacks antibiotics, so sterile technique is essential to prevent contamination. The cholesterol solution is flammable and does not require sterilization. The remaining solutions can be sterilized by autoclave or filtration. Airborne contaminants can be avoided by working in a laminar flow hood.
3. Plates can be stored seeded or unseeded in airtight containers @ 4 °C for several weeks.
4. Strains are available from the Caenorhabditis Genetics Center (http://www.cgc.cbs.umn.edu).
5. All oligonucleotide sequences are derived from the TruSeq sample prep kit (©2007–2012 Illumina, Inc. All rights reserved), and generated by annealing the universal adapter to the index adapter. Each index adapter contains a unique 6mer; replace 'NNNNNN' with the indicated sequence in Table 1.

Table 1
Index sequences

1 ATCACG	5 ACAGTG	9 GATCAG
2 CGATGT	6 GCCAAT	10 TAGCTT
3 TTAGGC	7 CAGATC	11 GGCTAC
4 TGACCA	8 ACTTGA	12 CTTGTA

Libraries with different indices can be pooled (multiplexed) for sequencing.

Universal adapter (sequence 5′–3′; * = phosphorothioate bond):

AATGATACGGCGACCACCGAGATCTACACTCTTTCCC TACACGACGCTCTTCCGATC*T

Index adapter (5′–3′; p = 5′ phosphate; * = phosphorothioate bond):

p ~ GATCGGAAGAGCACACGTCTGAACTCCAGTCAC<u>N NNNNN</u>ATCTCGTATGCCGTCTTCTGCTT*G

6. Primer sequences (5′–3′):

   TruSeq-1: AATGATACGGCGACCACCGAG
   TruSeq-2: CAAGCAGAAGACGGCATACGAG

7. For strains that do not require mapping, begin with gDNA isolation (Subheading 3.2).
8. The mutation-bearing strain may be homozygous (preferable) or heterozygous (for phenotypes that preclude mating, such as nonconditional sterility or lethality). Conditional alleles that require maintenance @ 15 °C should be allowed to mate for 24 h. Mutations that impair mating efficiency may require more hermaphrodites to insure success.
9. Successful mating produces equal numbers of male and hermaphrodite outcross progeny, which are first distinguishable at the L4 stage. Use only those plates with successful mating, especially when the starting strain is heterozygous.
10. For heterozygous starting strains, only half of the F1 progeny will contain the mutation; therefore, the number of picked F1s should be doubled. Temperature-sensitive alleles should be incubated at the nonconditional temperature to allow discrimination of homozygous F2 mutants.
11. The number of animals to pick is determined by the stage of development: 200 mid-stage embryos or 50 adult hermaphrodites is the recommended minimum. For larger samples, wash with ≥10× volumes of TE per volume of packed worms.
12. Washing is critical to remove as much of the OP50 bacteria as possible and minimize the amount of contaminating DNA in the sequencing library. Viable animals contain OP50 in the intestine. To remove, incubate the animals in M9 for 30 min with gentle shaking followed by multiple washes.
13. Samples can be frozen at −80 °C at this point if desired. To continue, thaw in ice bath and proceed with **step 6**.
14. Sonication disrupts the sample and shears the genomic DNA. If using a different instrument, parameters should be

optimized to produce sheared gDNA in the 100–300 bp size range. Care should be taken to minimize sample heating and foaming.

15. The suspension should be clear by the end of incubation, indicating complete digestion.
16. Column purification kits from other vendors may be substituted. Be sure that the protocol is compatible with samples containing ~1 % SDS.
17. The amount of sheared gDNA should be 2–10 ng, which can be quantified by dye fluorometry (e.g., Qubit) or qPCR. Remember to increase the elution volume accordingly, leaving a final volume of 10 μL after quantification.
18. Excess adapters can ligate and produce dimers, which are effective competitors for PCR amplification and sequencing. At the lower limit of input (2 ng), the adapters should be diluted fivefold to 0.3 μM to minimize dimer formation.
19. Resuspend beads by vortexing immediately before pipetting; perform all incubations at room temperature.
20. Depending upon your magnetic stand, it may be necessary to transfer the sample to a tube of different size (e.g., 1.5 mL).
21. The solution will clear as beads adhere to the side of the tube adjacent to the magnet. When removing the supernatant, pipette slowly and carefully to avoid the bead pellet and bound gDNA.
22. At the lower limit of input gDNA (2 ng), the number of amplification cycles should be increased from 12 to 15.
23. Alternatively, a MinElute column can be used for the final clean-up.

Acknowledgments

I would like to thank Sevinc Ercan for sharing the small-scale gDNA isolation protocol. This work was supported by the Intramural Research Program of the National Institutes of Health, National Institute of Diabetes and Digestive and Kidney Diseases, and is subject to the NIH Public Access Policy.

References

1. Brenner S (1974) The genetics of *Caenorhabditis elegans*. Genetics 77:71–94
2. Hirsh D, Vanderslice R (1976) Temperature-sensitive developmental mutants of *Caenorhabditis elegans*. Dev Biol 49:220–235
3. Sarin S, Prabhu S, O'Meara MM et al (2008) *Caenorhabditis elegans* mutant allele identification by whole-genome sequencing. Nat Methods 5:865–867
4. Sarin S, Bertrand V, Bigelow H et al (2010) Analysis of multiple ethyl methanesulfonate-mutagenized *Caenorhabditis elegans* strains by whole-genome sequencing. Genetics 185: 417–430

5. Zuryn S, Le Gras S, Jamet K et al (2010) A strategy for direct mapping and identification of mutations by whole-genome sequencing. Genetics 186:427–430
6. Wicks SR, Yeh RT, Gish WR et al (2001) Rapid gene mapping in *Caenorhabditis elegans* using a high density polymorphism map. Nat Genet 28:160–164
7. Doitsidou M, Poole RJ, Sarin S et al (2010) *C. elegans* mutant identification with a one-step whole-genome-sequencing and SNP mapping strategy. PLoS One 5:e15435
8. Bigelow H, Doitsidou M, Sarin S et al (2009) MAQGene: software to facilitate *C. elegans* mutant genome sequence analysis. Nat Methods 6:549
9. Minevich G, Park DS, Blankenberg D et al (2012) CloudMap: a cloud-based pipeline for analysis of mutant genome sequences. Genetics 192:1249–1269
10. Fire A, Xu S, Montgomery MK et al (1998) Potent and specific genetic interference by double-stranded RNA in *Caenorhabditis elegans*. Nature 391:806–811
11. Giardine B, Riemer C, Hardison RC et al (2005) Galaxy: a platform for interactive large-scale genome analysis. Genome Res 15:1451–1455
12. Blankenberg D, von Kuster G, Coraor N et al (2010) Galaxy: a web-based genome analysis tool for experimentalists. Curr Prot Mol Biol Unit 19.10.1–21
13. Goecks J, Netrutenko A, Taylor J et al (2010) Galaxy: a comprehensive approach for supporting accessible, reproducible, and transparent computational research in the life sciences. Genome Biol 11:R86

Chapter 2

Fundamentals of Comparative Genome Analysis in *Caenorhabditis* Nematodes

Eric S. Haag and Cristel G. Thomas

Abstract

The genome of the nematode *Caenorhabditis elegans* was the first of any animal to be sequenced completely, and it remains the "gold standard" for completeness and annotations. Even before the *C. elegans* genome was completed, however, biologists began examining the generality of its features in the genomes of other *Caenorhabditis* species. With many such genomes now sequenced and available via WormBase, *C. elegans* researchers are often confronted with how to interpret comparative genomic data. In this article, we present practical approaches to addressing several common issues, including possible sources of error in homology annotations, the often complex relationships between sequence similarity, orthology, paralogy, and gene family evolution, the impact of sexual mode on genome assemblies and content, and the determination and use of synteny as a tool.

Key words Comparative genomics, Phylogeny, Homology, Paralog, Ortholog

1 Introduction

The sequencing of the *C. elegans* genome in 1998 [1] was a landmark in modern biology. For experimental biologists, it became possible to perform reverse-genetic experiments genome-wide [2–5], create reporter transgene constructs [6], and quantify expression of all genes simultaneously (e.g. [7–10]). For workers in other systems, it inspired the development of genomic methods. Most relevant here, however, it also served as a beachhead from which to launch comparative studies with close relatives of *C. elegans* [11]. Indeed, large-scale characterization of the genomes of non-*elegans* species of *Caenorhabditis* began well before 1998. In 1981, Butler et al. found abundant differences in electrophoretic mobility of homologous enzymes from *C. elegans* and *C. briggsae* [12], implying a surprising amount of molecular divergence in these anatomically very similar animals. An early study of vitellogenin homologs [13] confirmed that homologous sequences between these species were indeed highly divergent, yet also noted

David Biron and Gal Haspel (eds.), *C. elegans: Methods and Applications*, Methods in Molecular Biology, vol. 1327,
DOI 10.1007/978-1-4939-2842-2_2,

that remaining conservation is likely to represent important functional constraints. In the mid-1990s the Genome Sequencing Center at Washington University in St. Louis generated 12 Mbp of *C. briggsae* sequence from large-insert clones. This relatively small amount of sequence was immediately used by many authors, and a few years later an entire assembly was produced by Waterston and his colleagues [14]. As whole-genome shotgun methods were improved and their costs reduced, many new *Caenorhabditis* species were added to the collection, most quickly populating WormBase with varying degrees of curation (http://www.wormbase.org). More recently, multispecies whole-genome comparisons have shed light on subjects as diverse as discovery of noncoding RNAs [15], the introduction of insertion–deletion mutations [16], and the evolution of sexually dimorphic gene expression [17].

In 2015, a user of WormBase examining a *C. elegans* gene page will see a number of fields related to homology. These include both named (e.g. "*Cre-unc-119*") and unnamed (e.g. CBG12344) homologs from other *Caenorhabditis* nematodes, as well as from much more distant relatives, such as *Pristionchus*, parasitic nematodes from different families, mouse, *Drosophila*, human, and various fish. This information puts relationships of "your favorite gene" a mouse-click away, and has greatly increased the speed with which homologs can be found. Yet at the same time, most determinations of homology are based on automated annotation pipelines, and are subject to errors of various sorts. Here, we summarize the major sources of imprecision in homology assignments, present a simple dichotomous key to guide a researcher to a well-supported model of gene evolution, and discuss some computational approaches to working with large datasets.

2 *Caveat Emptor*: Sources of Ambiguity in Homology Assignment

The genome assembly for *C. elegans* is of exceptional quality, but this is not generally true for most other *Caenorhabditis* species. There are two reasons for this discrepancy, as discussed below in Subheadings 2.1 and 2.2.

2.1 Assembly Approach

C. elegans was meticulously assembled using a minimal tiling path of large-insert clones [1], an approach generally not taken in subsequent projects. There was also a wealth of genetic data supporting the linkage of particular sequences on the same chromosome. These resources led to an assembly with very few gaps. In contrast, other species were sequenced using the whole-genome shotgun approach, which produces fragmented assemblies that are far from chromosome-level. In addition, the only non-*elegans Caenorhabditis* species with significant genetic markers tied to the physical map is

C. briggsae [18–20]. The fragmentation of genomes immediately reduces the ability to use local and global synteny information to inform homology determination.

2.2 The Interaction of Mating System, Heterozygosity, and Gene Number

C. elegans, *C. briggsae*, and *C. tropicalis* (formerly *C.* sp. 11; [21]) produce self-fertile hermaphrodites. As a result, individuals are often completely homozygous in nature, and no inbreeding depression is seen in these species [22–24]. Being naturally devoid of allelic variation, even nearly identical sequences can confidently be recognized as duplications, even if they are on different sequence contigs. This is not true, however, of obligately outcrossing *Caenorhabditis*, such as *C. remanei* [25]. These organisms have high levels of allelic divergence, up to 14 % at silent positions in *C. brenneri* [26]. Moreover, among the allelic variants are abundant recessive deleterious mutations, which lead to severe inbreeding depression [22].

The presence of abundant recessive deleterious mutations, which is normally tolerated in the large populations of outcrossing *Caenorhabditis*, creates a special challenge for genome sequencing. Inbreeding is the simplest way to reduce heterozygosity in a genome, but is less effective than expected in outcrossing species due to balanced polymorphisms [27]. In some cases large fractions of the genome can remain heterozygous. In combination with automated gene annotation, many redundant allelic variants are added that appear to the end-user as highly similar paralogs. In addition, diverged haplotypes can contribute to fragmentation of other parts of the genome by partitioning sequence reads into two competing assemblies. *Post hoc* distinction of alleles from recently diverged paralogs is nontrivial, as the most abundant class of *bona fide* gene duplicates is the most recent [28], so that no simple sequence identity threshold suffices to parse duplicates from alleles. After the initial demonstration of the severity of heterozygosity in outcrossing *Caenorhabditis* genome assemblies [27], improved pipelines were developed [26, 29] to systematically recognize (and even exploit) such regions. However, as of this writing the depiction of unrecognized alternative alleles as paralogs remains an issue.

Mating system also impacts the size and gene content of genome assemblies in a surprisingly predictable fashion. The number of gene predictions for obligately outcrossing species is consistently larger than for selfing species, and fewer distinct mRNAs are detected in their transcriptomes [17]. This is likely due to the interaction between relaxed selection on mating-related traits [30, 31] and sex-biased transmission of chromosomes that favors loss of larger size variants by drift in partially selfing species [32].

2.3 Phylogeny vs. Raw Similarity

In an idealized world of molecular evolution in which gene loss and duplication do not occur, and rates of molecular evolution are even across a gene family, orthologs will show a greater similarity

than any other possible inter-species pairings. In these cases, simple heuristics for inferring orthologs, such as reciprocal best BLAST hits [14, 33], will generally identify the ortholog, even if there are related paralogs as well. However, it is common for rates of molecular evolution to be uneven, and in some gene families gain and loss are commonplace. In extreme cases, little orthology remains despite the presence of consistently large gene families (e.g. [34]). This is often only clear after inferring a phylogenetic tree. In WormBase, most *Caenorhabditis* homologs of *C. elegans* genes have been run through automated pipelines (reviewed in ref. 35), such as TreeFam [36], Imparanoid [33], and OrthoMCL [37]. Their outputs, in combination with more focused analyses, are currently presented in the "curated nematode orthologs" section of the WormBase gene page. These tools represent major advances over raw similarity, but should nevertheless be regarded as preliminary. Particularly difficult to recognize are cases of parallel and/or complementary loss of members of established subfamilies (Fig. 1). For example, the most similar *C. briggsae* genes to *C. elegans fbf-1* and *fbf-2* are *Cbr-puf-1*, *Cbr-puf-1.2*, *and Cbr-puf-2*, and they were initially inferred to be orthologous [38]. However, the inclusion of homologs from *C. japonica*, *C. remanei*, and *C. brenneri* revealed that they were actually members of two distinct and ancient PUF subfamilies that had experienced reciprocal losses in the *C. elegans* and *C. briggsae* lineages [39]. For such cases, careful alignment and appropriate taxon sampling is essential to clarify the situation (*see* Subheading 4 below).

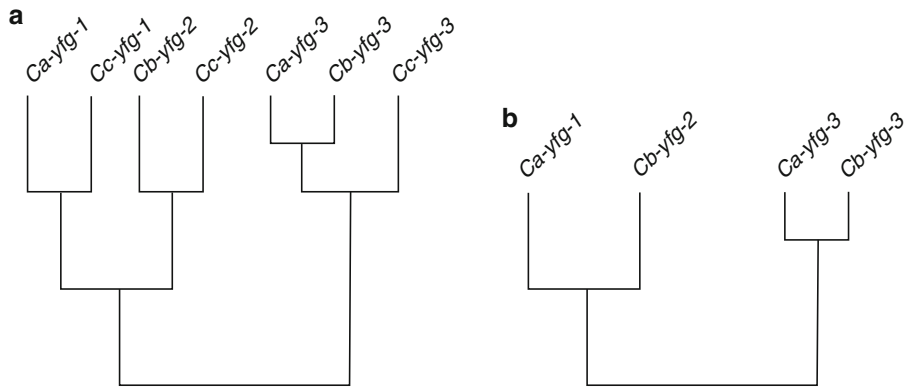

Fig. 1 Misleading effects of insufficient taxon sampling. We consider three hypothetical *Caenorhabditis* species, *Ca, Cb, and Cc*. (**a**) The last common ancestor of these three species had three paralogs of *y*our *f*avorite *g*ene, *yfg-1, yfg-3,* and *yfg-3*. However, species *Cb* has lost its *yfg-1* paralog, and *Ca* its *yfg-2*. (**b**) When species *Cc* is omitted from consideration, however, the complementary losses are not apparent, and *Ca-yfg-1* and *Cb-yfg-2* could be erroneously inferred to be orthologs

3 A Decision Tree for Assessing Gene Homology in Nematode Genome Assemblies

Definitive studies of homology relationships are time-consuming, and still form entire research publications. However, an experimental biologist not trained in molecular phylogenetics often needs a "quick and dirty" way to sift through various homologs that is still defensible. In this spirit, we present a sort of key, similar in layout to that used in species identification, to help guide scrutiny of homologs. The assumption is that the researcher will be starting with a single *C. elegans* query gene, which may or may not be part of a family, and that the goal is to identify the orthologous gene (if one exists) for a specific second species among the potentially numerous homologs listed in WormBase gene pages. It also provides a way to quickly verify that an annotated ortholog really is orthologous.

1) *Zero homologs.* The complete absence of related sequences in gene predictions for another *Caenorhabditis* assembly is rare, but can happen for a number of reasons:
   (a) A homologous sequence may be present in the assembly, but is not annotated. This possibility can be tested by searching the genomic DNA with the protein sequence of the *C. elegans* using TBLASTN [40], which compares the protein query to conceptual translations, in all six possible reading frames, of the genome.
   (b) There may be a homolog, but it falls in a gap in sequence coverage. In this case, examination of syntenic genes may reveal the gap.
   (c) The absence may be a biological reality. As noted above, thousands of genes were likely lost in the *C. elegans* genome after the transition to self-fertility. Genes specific to *C. elegans* are rarer, but exist and can even encode essential factors [41].
2) *Exactly one homolog.* This single homolog is likely to be the ortholog, barring unrecognized homologs in sequence or annotation gaps. Conserved flanking genes (local synteny; [42]) often (but not always) confirm the diagnosis.
3) *Exactly two homologs.*
   (a) The two homologs are nearly identical to each other (e.g. over 90 % at the nucleotide level). These may be recent duplicates or retained alleles.
      (i) If allelic:

(1) The two homologs will be on different sequence contigs, one of which is usually short (<15 kb).

(2) Flanking genes that are single-copy in *C. elegans* will tend to also be present in two copies in this species.

(3) The two homologs are autosomal (male hemizygosity of the X prevents recessive deleterious alleles from accumulating).

(4) Noncoding sequences (introns, 3′ UTR, flanking DNA) will align easily, though with some insertions and deletions (e.g. [43]).

(ii) If recently duplicated paralogs:

(1) The two homologs are likely to be in tandem or near each other on the same large sequence contig.

(2) The two homologs may be X-linked.

(3) Noncoding sequences may be highly diverged.

(4) The two homologs are more likely to be in the high-recombination peripheral domains than in the central "cluster" domain [20, 44].

(b) The two homologs are quite divergent, e.g. over 10 % at the amino acid level. They are likely to be duplicates (paralogs).

(i) The *C. elegans* query also has two or more diverged copies. The duplication may have occurred before the last common ancestor of it and the other species. A simple distance-based phylogeny (*see* 4 Phylogeny Tips below) could confirm or reject this.

(ii) The *C. elegans* query has no within-species paralog. This would suggest that either *C. elegans* lost a copy, or that the other species experienced a duplication after it diverged from their common ancestor. Adding homologs from a more distantly related species and creating a sequence-based phylogeny usually clarifies which is the case.

(4) *Three or more homologs.* Allelism is an insufficient explanation; gene copy number has definitely evolved.

(1) The *C. elegans* query has two or more related sequences in *C. elegans* (*see* 2bi above). Many cases of large multigene families exist in nematode genomes (e.g. [45]), and most require a phylogenetic approach to understand.

(2) The *C. elegans* query has no within-species paralog (i.e. a 1:3+ situation). Either expansion or contraction has occurred in one of the species (*see* 2bii above).

4 Phylogeny Tips

As noted above, when a many-to-many relationship exists between related sequences in different species, a phylogeny (or "gene tree") is the only way to achieve clarity. A full treatment of how to infer molecular phylogenies is beyond the scope of this paper, and we refer the reader to other sources (e.g. [46, 47]). However, we can offer here some simple rules of thumb for nematode sequences that will greatly increase the utility of trees obtained:

- *Use protein sequences (not coding DNA) to infer the tree.* Between most *Caenorhabditis* species there has been complete mutational saturation of silent sites [48], whose inclusion would thus only introduce noise into the analysis.
- *Only confidently alignable sequences should be used for the analysis.* Identity need not be consistently high if there are conserved motifs to serve as landmarks (e.g. [49]).
- *Inclusion of more taxa often produces a better result.* For example, though the most similar *C. briggsae* genes to *C. elegans fbf-1* and *fbf-2* are *Cbr-puf-1*, *Cbr-puf-1.2*, *and Cbr-puf-2*, and were initially inferred to be orthologous [38] the inclusion of homologs from *C. japonica*, *C. remanei*, and *C. brenneri* revealed that they were actually members of two distinct and ancient PUF subfamilies that had experienced reciprocal losses in the *C. elegans* and *C. briggsae* lineages [39].

5 Scaling Up

Most of the tests described above can be performed for a handful of genes with little trouble using only the WormBase web site, and there are many suitable software tools that can be used to infer phylogenies from sequence alignments. However, in some cases finding homologs, if not necessarily orthologs, of large sets of query genes (e.g. >100) is desirable. In these cases, we offer the following compendium of specific methods.

5.1 Genome-Scale Sequence Datasets

Working with large sets of genes, or genome wide is possible thanks to resources available on the ftp website of WormBase (ftp://ftp.wormbase.org/pub/wormbase/; also linked at the bottom of the WormBase main page). For each release of WormBase, text files containing the data upon which the website is built are available for

download. This is particularly useful for species other than *C. elegans*, for which data are not necessarily retrievable through the use of WormMart or WormMine or do not exist yet (e.g. BLASTP hits or orthology assignments), or when analyzing a large set of genes. In addition, for reasons stated above, it might sometimes be preferable or necessary to determine orthology relationships for a family of related sequences independently.

The number of sequence files for each species varies depending on the status of the genomic assembly and annotations, availability of expression data, and curation of any given species at each WormBase release. All genome draft assemblies, except for those of *C. elegans* and *C. briggsae*, are fragmented in numerous scaffolds. The filenames are generally self-explanatory, and for the purpose of identifying homologs only a few are useful: genome draft sequences are stored in FASTA-format files (plain text with a specific header line for each sequence) ending with "genomic.fa," and if they exist, coding sequences in those ending with "cds_transcripts.fa." Annotations of the genomic scaffolds, including the positions of exons and introns of gene predictions, end with "annotations.gff3" or "annotations.gff2."

5.2 Running Batch BLAST Searches from the Command Line

Identifying allelic scaffolds (*see* above) can be a first step in sorting potential gene paralogs from allelic variants. Once these have been recognized, orthologs are often provisionally identified as best reciprocal BLAST hits. When dealing with a large set of genes, this process can be automated with command-line BLAST [50], which can be downloaded from ftp://ftp.ncbi.nlm.nih.gov/blast/executables/blast+/LATEST/. Once installed onto a desktop or laptop computer, command-line searches are initiated through the Terminal (Unix or Mac) or Command Prompt (Windows) applications. This is most easily done by placing the relevant BLAST databases and query files in the same, or in closely linked, directories.

Though less familiar to many experimental biologists than web-based BLAST servers, there are major advantages to using command-line BLAST. One is flexibility. Any number of CDS sequences can be input as queries in a batch, up to the entire set of predictions for a given species. This set of sequences can be compared to either another set of gene predictions, filtered or not to remove allelic variants, or to genomic sequences. The latter case should generate more than one high-confidence hit per CDS sequence, but in simple cases only one per exon. Another advantage to command-line BLAST is the ability to quickly vary the values of the parameters for BLAST as well as for subsequent filtering. The threshold above which a hit is considered significant might vary depending on the accuracy and completeness of the assembly or set of CDS sequences, as well as on the degree of divergence between species and level of heterozygosity found within each species. The latter especially matters when using sequences from outcrossing species generated

in-house (rather than those stored on WormBase), since the degree and location of heterozygous regions is unknown, and more than one individual contributes their DNA to sequencing.

As noted above, a sensible BLAST *E*-value threshold between best reciprocal hits is not enough to indicate orthology. When working with large gene sets, additional parameters to be considered include the proportion of each gene's length involved in the alignment, the degree of identity over the length of the alignment, and for close relatives, conservation of micro-synteny. Additionally, in the case of genomic sequences hits, the alignments corresponding to potential exons must be colinear to the query sequence. Once the output files have been generated, BLAST alignments can be sorted through efficiently with appropriate Perl or Python scripts.

5.3 Identifying All Members of a Gene Family

Another common task is to identify the entire set of genes in a family, as defined by possession of one or more protein domains, a specific motif, or a highly conserved region. In these cases, a number of options are available. For short motifs that can be represented by a simple regular text expression, Perl or Python scripts can be used to search sequences directly. In more complex cases, a tool like HMMER [51, 52] can generate a profile from the shared features, and be used to comb through CDS or genomic sequence databases to identify occurrences. The same considerations as for BLAST searches apply here as well to sensibly determine homology. Phylogenetic analysis of the genes' relationships to one another is required to assign accurately orthology.

References

1. The C. elegans Sequencing Consortium (1998) Genome sequence of the nematode *C. elegans*: a platform for investigating biology. Science 282:2012–2018
2. Colaiacovo MP, Stanfield GM, Reddy KC, Reinke V, Kim SK, Villeneuve AM (2002) A targeted RNAi screen for genes involved in chromosome morphogenesis and nuclear organization in the *Caenorhabditis elegans* germline. Genetics 162(1):113–128
3. Gonczy P, Echeverri C, Oegema K, Coulson A, Jones SJ, Copley RR, Duperon J, Oegema J, Brehm M, Cassin E, Hannak E, Kirkham M, Pichler S, Flohrs K, Goessen A, Leidel S, Alleaume AM, Martin C, Ozlu N, Bork P, Hyman AA (2000) Functional genomic analysis of cell division in *C. elegans* using RNAi of genes on chromosome III. Nature 408(6810): 331–336
4. Simmer F, Moorman C, van der Linden AM, Kuijk E, van den Berghe PV, Kamath RS, Fraser AG, Ahringer J, Plasterk RH (2003) Genome-wide RNAi of *C. elegans* using the hypersensitive *rrf-3* strain reveals novel gene functions. PLoS Biol 1(1), E12
5. Edgley M, D'Souza A, Moulder G, McKay S, Shen B, Gilchrist E, Moerman D, Barstead R (2002) Improved detection of small deletions in complex pools of DNA. Nucleic Acids Res 30(12), e52
6. Boulin T, Etchberger J, Hobert O (2006) Reporter gene fusions. In: WormBook, The *C. elegans* Research_Community, Editor 2006
7. Gerstein MB, Lu ZJ, Van Nostrand EL, Cheng C, Arshinoff BI, Liu T, Yip KY, Robilotto R, Rechtsteiner A, Ikegami K, Alves P, Chateigner A, Perry M, Morris M, Auerbach RK, Feng X, Leng J, Vielle A, Niu W, Rhrissorrakrai K, Agarwal A, Alexander RP, Barber G, Brdlik CM, Brennan J, Brouillet JJ, Carr A, Cheung MS, Clawson H, Contrino S, Dannenberg LO, Dernburg AF, Desai A, Dick L, Dose AC, Du

J, Egelhofer T, Ercan S, Euskirchen G, Ewing B, Feingold EA, Gassmann R, Good PJ, Green P, Gullier F, Gutwein M, Guyer MS, Habegger L, Han T, Henikoff JG, Henz SR, Hinrichs A, Holster H, Hyman T, Iniguez AL, Janette J, Jensen M, Kato M, Kent WJ, Kephart E, Khivansara V, Khurana E, Kim JK, Kolasinska-Zwierz P, Lai EC, Latorre I, Leahey A, Lewis S, Lloyd P, Lochovsky L, Lowdon RF, Lubling Y, Lyne R, MacCoss M, Mackowiak SD, Mangone M, McKay S, Mecenas D, Merrihew G, Miller DM III, Muroyama A, Murray JI, Ooi SL, Pham H, Phippen T, Preston EA, Rajewsky N, Ratsch G, Rosenbaum H, Rozowsky J, Rutherford K, Ruzanov P, Sarov M, Sasidharan R, Sboner A, Scheid P, Segal E, Shin H, Shou C, Slack FJ, Slightam C, Smith R, Spencer WC, Stinson EO, Taing S, Takasaki T, Vafeados D, Voronina K, Wang G, Washington NL, Whittle CM, Wu B, Yan KK, Zeller G, Zha Z, Zhong M, Zhou X, Ahringer J, Strome S, Gunsalus KC, Micklem G, Liu XS, Reinke V, Kim SK, Hillier LW, Henikoff S, Piano F, Snyder M, Stein L, Lieb JD, Waterston RH (2010) Integrative analysis of the *Caenorhabditis elegans* genome by the modENCODE project. Science 330(6012): 1775–1787

8. Reinke V, Gil IS, Ward S, Kazmer K (2004) Genome-wide germline-enriched and sex-biased expression profiles in *Caenorhabditis elegans*. Development 131(2):311–323
9. Kim SK, Lund J, Kiraly M, Duke K, Jiang M, Stuart JM, Eizinger A, Wylie BN, Davidson GS (2001) A gene expression map for *Caenorhabditis elegans*. Science 293(5537): 2087–2092
10. Reinke V, Smith HE, Nance J, Wang J, Van Doren C, Begley R, Jones SJ, Davis EB, Scherer S, Ward S, Kim SK (2000) A global profile of germline gene expression in *C. elegans*. Mol Cell 6(3):605–616
11. Haag E, Pilgrim D (2005) Harnessing Caenorhabditis genomics for evolutionary developmental biology. Curr Genomics 6:579–588
12. Butler MH, Wall SM, Luehrsen KR, Fox GE, Hecht RM (1981) Molecular relationships between closely related strains and species of nematodes. J Mol Evol 18(1):18–23
13. Zucker-Aprison E, Blumenthal T (1989) Potential regulatory elements of nematode vitellogenin genes revealed by interspecies sequence comparison. J Mol Evol 28(6): 487–496
14. Stein L et al (2003) The genome sequence of *Caenorhabditis briggsae:* a platform for comparative genomics. PLoS Biol 1:166–192
15. Lu ZJ, Yip KY, Wang G, Shou C, Hillier LW, Khurana E, Agarwal A, Auerbach R, Rozowsky J, Cheng C, Kato M, Miller DM, Slack F, Snyder M, Waterston RH, Reinke V, Gerstein MB (2011) Prediction and characterization of noncoding RNAs in *C. elegans* by integrating conservation, secondary structure, and high-throughput sequencing and array data. Genome Res 21(2):276–285
16. Jovelin R, Cutter AD (2013) Fine-scale signatures of molecular evolution reconcile models of indel-associated mutation. Genome Biol Evol 5(5):978–986
17. Thomas CG, Li R, Smith HE, Woodruff GC, Oliver B, Haag ES (2012) Simplification and desexualization of gene expression in self-fertile nematodes. Curr Biol 22:2167–2172
18. Hillier LW, Miller RD, Baird SE, Chinwalla A, Fulton LA, Koboldt DC, Waterston RH (2007) Comparison of *C. elegans* and *C. briggsae* genome sequences reveals extensive conservation of chromosome organization and synteny. PLoS Biol 5(7), e167
19. Koboldt DC, Staisch J, Thillainathan B, Haines K, Baird SE, Chamberlin HM, Haag ES, Miller RD, Gupta BP (2010) A toolkit for rapid gene mapping in the nematode *Caenorhabditis briggsae*. BMC Genomics 11:236
20. Ross J, Koboldt D, Staisch J, Chamberlin H, Gupta BP, Millller R, Baird S, Haag E (2011) *Caenorhabditis briggsae* recombinant inbred line genotypes reveal inter-strain incompatibility and the evolution of recombination. PLoS Genet 7(7), e1002174
21. Félix M-A, Braendle C, Cutter AD (2014) A streamlined system for species diagnosis in Caenorhabditis (Nematoda: Rhabditidae) with name designations for 15 distinct biological species. PLoS One 9(4), e94723
22. Dolgin ES, Charlesworth B, Baird SE, Cutter AD (2007) Inbreeding and outbreeding depression in Caenorhabditis nematodes. Evolution 61(6):1339–1352
23. Barriére A, Félix MA (2005) High local genetic diversity and low outcrossing rate in *Caenorhabditis elegans* natural populations. Curr Biol 15(13):1176–1184
24. Cutter AD, Felix MA, Barriere A, Charlesworth D (2006) Patterns of nucleotide polymorphism distinguish temperate and tropical wild isolates of *Caenorhabditis briggsae*. Genetics 173(4): 2021–2031
25. Cutter AD, Baird SE, Charlesworth D (2006) High nucleotide polymorphism and rapid decay of linkage disequilibrium in wild populations of *Caenorhabditis remanei*. Genetics 174(2):901–913

26. Dey A, Chan CK, Thomas CG, Cutter AD (2013) Molecular hyperdiversity defines populations of the nematode *Caenorhabditis brenneri*. Proc Natl Acad Sci U S A 110(27): 11056–11060
27. Barriere A, Wang S, Pekarek E, Thomas C, Haag E, Ruvinsky I (2009) Detecting heterozygosity in shotgun genome assemblies: lessons from obligately outcrossing nematodes. Genome Res 19:470–480
28. Lynch M, Conery JS (2000) The evolutionary fate and consequences of duplicate genes. Science 290(5494):1151–1155
29. Huang S, Chen Z, Huang G, Yu T, Yang P, Li J, Fu Y, Yuan S, Chen S, Xu A (2012) HaploMerger: reconstructing allelic relationships for polymorphic diploid genome assemblies. Genome Res 22(8):1581–1588
30. Cutter AD (2008) Reproductive evolution: symptom of a selfing syndrome. Curr Biol 18(22):R1056–R1058
31. Thomas CG, Woodruff GC, Haag ES (2012) Causes and consequences of the evolution of reproductive mode in Caenorhabditis nematodes. Trends Genet 28(5):213–220
32. Wang J, Chen PJ, Wang GJ, Keller L (2010) Chromosome size differences may affect meiosis and genome size. Science 329(5989):293
33. Ostlund G, Schmitt T, Forslund K, Kostler T, Messina DN, Roopra S, Frings O, Sonnhammer EL (2010) InParanoid 7: new algorithms and tools for eukaryotic orthology analysis. Nucleic Acids Res 38(Database issue):D196–D203
34. Nayak S, Goree J, Schedl T (2005) *fog-2* and the evolution of self-fertile hermaphroditism in Caenorhabditis. PLoS Biol 3, e6
35. Altenhoff A, Dessimoz C (2012) Chpt. 9: Inferring orthology and paralogy. In: Anisimova M (ed) Evolutionary genomics, statistical and computational methods, vol 1. Humana Press, New York, pp 259–279
36. Li H, Coghlan A, Ruan J, Coin LJ, Heriche JK, Osmotherly L, Li R, Liu T, Zhang Z, Bolund L, Wong GK, Zheng W, Dehal P, Wang J, Durbin R (2006) TreeFam: a curated database of phylogenetic trees of animal gene families. Nucleic Acids Res 34(Database issue): D572–D580
37. Li L, Stoeckert CJ Jr, Roos DS (2003) OrthoMCL: identification of ortholog groups for eukaryotic genomes. Genome Res 13(9): 2178–2189
38. Lamont LB, Crittenden SL, Bernstein D, Wickens M, Kimble J (2004) FBF-1 and FBF-2 regulate the size of the mitotic region in the *C. elegans* germline. Dev Cell 7(5):697–707
39. Liu Q, Stumpf C, Wickens M, Haag ES (2012) Context-dependent function of a conserved translational regulatory module. Development 139:1509–1521
40. Zhang J, Zhang Z, Miller W, Lipman DJ (1997) Gapped BLAST and PSI-BLAST: a new generation of protein database search programs. Nucleic Acids Res 25:3389–3402
41. Zhang T, Sun Y, Tian E, Deng H, Zhang Y, Luo X, Cai Q, Wang H, Chai J, Zhang H (2006) RNA-binding proteins SOP-2 and SOR-1 form a novel PcG-like complex in *C. elegans*. Development 133(6):1023–1033
42. Kuwabara PE, Shah S (1994) Cloning by synteny: identifying *C. briggsae* homologues of *C. elegans* genes. Nucleic Acids Res 22: 4414–4418
43. Haag ES, Ackerman AD (2005) Intraspecific variation in *fem-3* and *tra-2*, two rapidly coevolving nematode sex-determining genes. Gene 349:35–42
44. Rockman MV, Kruglyak L (2009) Recombinational landscape and population genomics of *Caenorhabditis elegans*. PLoS Genet 5(3), e1000419
45. Thomas JH, Kelley JL, Robertson HM, Ly K, Swanson WJ (2005) Adaptive evolution in the SRZ chemoreceptor families of *Caenorhabditis elegans* and *Caenorhabditis briggsae*. Proc Natl Acad Sci U S A 102(12):4476–4481
46. Swofford D, Olsen G, Waddell P, Hillis D (1996) Chpt. 11: Phylogenetic inference. In: Hillis D, Moritz C, Mable B (eds) Molecular systematics. Sinauer Associates, Sunderland, MA
47. Whelan S (2008) Inferring trees. In: Keith J (ed) Bioinformatics, vol 1, Data, sequence analysis, and evolution. Humana Press, Totowa, NJ, pp 287–309
48. Cutter AD, Dey A, Murray RL (2009) Evolution of the *Caenorhabditis elegans* genome. Mol Biol Evol 26(6):1199–1234
49. Haag ES, Wang S, Kimble J (2002) Rapid coevolution of the nematode sex-determining genes *fem-3* and *tra-2*. Curr Biol 12(23): 2035–2041
50. Altschul SF, Gish W, Miller W, Myers EW, Lipman DJ (1990) Basic local alignment search tool. J Mol Biol 215(3):403–410
51. Eddy S (2001) HMMER: profile hidden Markov models for biological sequence analysis., Available from: http://hmmer.wustl.edu
52. Finn RD, Clements J, Eddy SR (2011) HMMER web server: interactive sequence similarity searching. Nucleic Acids Res 39(Web Server issue):W29–W37

Chapter 3

Genetic Methods for Cellular Manipulations in *C. elegans*

Menachem Katz

Abstract

Neuron manipulation in vivo by ablation, activation, or inactivation, and regulation of gene expression, is essential for dissecting nervous system function. Here we describe genetic means for neuron manipulation in the nematode *C. elegans*, and provide protocols for generating transgenic animals containing these genetic tools.

Key words *C. elegans*, Microinjection, Transgenic worms, Cell-ablation, Optogenetic, Neuronal-silencing, Neuronal-activation

1 Introduction

How neuronal circuits form and function are central questions in neuroscience. *C. elegans* is an excellent model for addressing these questions. An adult hermaphrodite has a compact nervous system of 302 neurons, each of which develops in an invariant manner. The animal is transparent, enabling observation and manipulation of neurons in vivo, and exhibits diverse behaviors. These properties, together with a completely reconstructed neuronal connectome, allow neuronal functions within circuits to be dissected at high resolution.

Cell ablation is frequently used to analyze the roles of specific neurons within a network. In *C. elegans*, directed neuron elimination by laser microsurgery was initially used to dissect the neuronal circuits of sensory responses and feeding [1–4]. This method allows the elimination of almost any neuron in the first larval stage (L1), or of neuronal progenitor cells in the developing embryo. However, it is labor intensive and generates a limited number of ablated animals [5], making it unsuitable for studies of behavior, which involve scoring a large number of animals. Advances in genetic engineering now allow individual neurons to be killed by cell-specific expression of genes that induce apoptosis [6–10], degeneration [11, 12], or necrosis [13–15]. Such genetic ablations

David Biron and Gal Haspel (eds.), *C. elegans: Methods and Applications*, Methods in Molecular Biology, vol. 1327,
DOI 10.1007/978-1-4939-2842-2_3,

are less laborious than laser ablation, and result in reproducible cell killing in transgenic animals that can be propagated indefinitely. Genetic ablations targeted to specific neurons can also be controlled in time, either by light-induced enzymatic activity [13–15] or by heat-induced gene expression [6] (for a description of these tools *see* Table 1). Gene knockouts in specific neurons [16–18] can serve not only to define endogenous gene function, but also to study neuronal activities (*see* Table 1).

Although effective, cell and gene ablation often cannot be used to study subtle and/or complex aspects of neuronal activity. A number of methods for finer manipulation of intact neurons in living and behaving animals have been developed. These are summarized in Table 1, and include chronic or acute inhibition of neuronal activity by membrane hyperpolarization [19–28] or by blocking neurotransmitter release [29, 30]. Genetic methods for acute or chronic activation of neurons also exist [29, 31–38]. Temporal manipulation of neuronal activity over a wide range of time scales, from slow developmental processes to rapid behavioral responses, can be accomplished using tools with varying activation kinetics. Moreover, several neurons can be differentially manipulated in the same animal by combining chemical and optogenetic regulation, or by using a combination of light-induced enzymes with non-overlapping activation wavelengths. Optogenetic tools, however, have some limitations. Blue-violet light is toxic to *C. elegans*; thus proteins that are activated at longer wavelengths are preferred. Limiting the intensity and duration of illumination or using pulsed light can also help to overcome toxicity. Importantly, *C. elegans* avoid blue-violet light, complicating behavioral analysis. While this can be overcome using animals in which the light receptor (LITE-1) is mutated [32], such *lite-1* mutants have locomotory defects, limiting their use in various behavioral assays.

Genetic manipulations often require cell-specific promoters, which may not be available for a given neuron at a given developmental time. A number of methods have been developed to overcome this constraint. For example, cell killing by caspase reconstitution allows each of the two caspase fragments to be expressed using promoters with broad cell specificity. Cell death, however, would only ensue in cells expressing both promoters [6]. A similar strategy employs the combinatorial action of recombinases such as FLP or Cre [29, 39, 40]. Here, one promoter is used to drive the expression of a transgene preceded by a transcription termination site flanked by FRT or loxP recombination sites. Expression of the appropriate recombinase using a second partially overlapping promoter recombines out the termination site allowing specific gene expression. Using optogenetic tools, cell specificity can be achieved by restricting illumination to the cell and time of interest. Methods for automatic cell-specific illumination in freely moving animals have been developed [27, 41, 42], but are of low throughput.

Table 1
Genetic tools for neuronal manipulation

Gene	Cellular process	Comments	References
1.1. Cell elimination			
Chronic			
ced-3/4	Apoptosis	*ced-3* and *ced-4* are apoptotic genes that can induce cell death upon ectopic expression if they are integrated to the genome and homozygous Cons: The efficiency of cell killing is moderate, where some cells are more resistant than others. Efficiency can increase by using *ced-9* mutant animals	[8]
recCaspase (*ced-3;* caspase-3)	Apoptosis	*ced-3*/caspase-3 are cloned in two separate fragments that mimic the proteolytically cleaved subunits. Each fragment is fused to an antiparallel leucine-zipper dimerization motif Co-expression of the subunits generates constitutively active caspase that leads to cell death Integration to the genome and homozygous expression can increase efficiency Since each fragment is expressed under a separate promoter, it can be used to achieve cell-specific ablation when a cell-specific promoter is unavailable. Moreover, this system can be used for inducible cell killing, if a heat-shock promoter regulates expression of one of the subunits	[6]
egl-1	Apoptosis	*egl-1* is a BH3-containing activator of the apoptotic pathway. Ectopic expression of EGL-1 can induce cell death	[9, 10]
Diphtheria toxin	Apoptosis	A catalytic fragment of the diphtheria toxin (DT-A), which induces cell death by blocking protein synthesis	[7, 48]
mec-4	Degeneration	A dominant mutant of *mec-4*, a mechanotransduction channel, which can lead to cell swelling and degeneration when ectopically expressed	[11]
deg-3	Degeneration	A dominant hyperactive mutant of *deg-3*, a subunit of the acetylcholine receptor, which can lead to channel opening, cell swelling, and degeneration Cons: Effective in only a limited subset of neurons that endogenously express *des-2*, which is required to form a functional acetylcholine receptor	[12]

(continued)

Table 1
(continued)

Gene	Cellular process	Comments	References
Inducible			
KillerRed	Necrosis	A type II photosensitizer that produces superoxide anion radicals following induction by green light, which results in neuronal death Plasma membrane targeting of KillerRed increases its efficiency Cons: Some neurons are resistant to KillerRed. Efficiency can be increased by using animals with mutated *sod-1*, which normally protects from cytoplasmic reactive oxygen species (ROS)	[13, 15]
MiniSog	Necrosis	Mini singlet oxygen generator (miniSog) is a small monomeric fluorescent flavoprotein that upon blue light illumination induces ROS production and cell death. Effective cell death is achieved by mitochondrial-targeting of miniSog	[14]
1.2. Neuronal inhibition			
Chronic			
unc-103 (gf)	Hyperpolarization	Gain-of-function mutation of ERG-like potassium channel (UNC-103) that induces membrane hyperpolarization	[26]
twk-18(gf)	Hyperpolarization	A constitutively active mutation in a two-P domain K^+ channel (TWK-18) that induces membrane hyperpolarization	[22, 23]
Tetanus toxin (TeTx)	Blocks synaptic transmission	Expression of the light chain of TeTx blocks synaptic vesicle release through synaptobrevin cleavage	[29, 30]
Inducible			
Histamine/ Cl^- channel	Hyperpolarization	*C. elegans* does not use histamine as a neurotransmitter, and is insensitive to this molecule at low concentrations. Ectopic expression of the inhibitory *Drosophila* histamine-gated chloride channel (HisCl1) together with histamine treatment results in graded neuronal silencing	[25]
NpHR/Halo	Hyperpolarization	Halorhodopsin is a light-gated Cl^- pump that is activated with yellow light	[20, 28]
Arch	Hyperpolarization	Archaerhodopsin-3 (Arch) is a green-yellow light-activated, outward-directed proton pump with higher inward currents compared to NpHR	[19, 21, 24]

(continued)

Table 1
(continued)

Gene	Cellular process	Comments	References
Mac	Hyperpolarization	A blue-green light-activated outward-directed proton pump with higher inward currents compared to NpHR	[19, 21, 27]
1.3. Neuronal activation			
Chronic			
pkc-1/ttx-4	Increases dense core vesicle (DCV) release	A gain-of-function mutation that induces neuronal activity by induction of DCV transmission and neuropeptide release	[29, 36, 37]
Inducible			
lite-1	Depolarization	LITE-1 is a novel gustatory receptor (Gr) family-related ultraviolet light receptor Upon UV illumination it induces activation of guanylate cyclase and (cGMP)-sensitive cyclic nucleotide-gated (CNG) channels, which results in neuronal depolarization. LITE-1 activation does not require the addition of all-*trans* retinol (ATR) Cons: LITE-1 activity requires the expression of DAF-11, TAX-2, and TAX-4; thus it can only work in a subset of neurons. It requires strong violet light illumination for activation	[32, 33]
ChR2	Depolarization	Channelrhodopsin-2 (ChR2) is a blue-light-activated cation channel. ChR2 response is fast, inducing depolarization within the millisecond time scale. Slower variants for long-term manipulation (step function opsins, SFOs) are also available ChR2 requires the addition of the cofactor all-*trans* retinal (ATR), which is provided to the worms by feeding with bacteria soaked in ATR	[31, 34, 35]
PAC	Induces synaptic vesicle release	Blue-light-activated adenylyl cyclase increases intracellular concentrations of the second messenger cAMP, leading to the induction of synaptic vesicle release Cons: Since cAMP serves as second messenger in various cellular processes cAMP induction might have pleiotropic effects	[38]

(continued)

Table 1
(continued)

Gene	Cellular process	Comments	References
1.4. Cell-specific gene inactivation			
rde-1	Cell-specific rescue of the RNAi response	*rde-1* mutant animals are resistant to RNAi. Cell-specific expression of RDE-1 can rescue the RNAi response cell autonomously. This allows the use of feeding-RNAi method, which is easy to use and applicable for high-throughput screens Cons: Feeding-RNAi is inefficient in neurons. Using sensitized mutant such as *rrf-3*, *lin-15b*, *eri-1*, or *nre-1* can increase efficiency	[18]
Sense and antisense sequences of gene of interest		Expression, under cell-specific promoters, of sense and antisense RNA corresponding to a gene of interest. This method works well in neurons without the need of using RNAi-sensitized mutants Cons: Not efficient for high-throughput screens	[17]
CRISPR/Cas-9 genome editing		The Clustered Regularly Interspaced Short Palindromic Repeats (CRISPR) and CRISPR-associated nuclease (Cas-9) can be used to knock in loxP sites within a gene of interest. Cre expression under a cell-specific promoter will then induce a directed deletion mutation, resulting in cell-specific gene inactivation	[16]

There are many ways to manipulate neurons in a living organism. The approaches described above are based on transgenic techniques. Below is a detailed protocol for generation of transgenic animals by DNA microinjection.

2 Materials

2.1 Equipment

1. Axiovert 200, inverted microscope with a gliding stage and 10× and 40× Plan-Neofluar lenses (Zeiss, Oberkochen, Germany). (Or other equivalent inverted microscopes.)
2. Needle holder, connected to a coarse manipulator and a Three-axis Oil Hydraulic Micromanipulator (Narishige Int. USA, East Meadow, NY). (Or other microinjection manipulator systems.)
3. FemtoJet, electronic microinjector with a built-in compressor (Eppendorf, Hamburg, Germany). (Alternatively, pressurized injection systems could also be used.)

4. Needle puller: Laser-based micropipette puller, P-2000 (Sutter Instrument, Novato, CA, USA). (Filament heating-based micropipette puller could also be used.)
5. Standard dissecting stereomicroscope.

2.2 Buffers

1. M9 buffer (1 l): 3 g KH_2PO_4, 6 g Na_2HPO_4, 5 g NaCl, and 1 ml 1 M $MgSO_4$. Add H_2O to 1 l, and autoclave.
2. NGM agar (1 l): 3 g NaCl, 17 g agar, 2.5 g peptone. Add 975 ml of H_2O, and autoclave. Allow to cool to ~50 °C, and then add 1 ml $CaCl_2$ (1 M), 1 ml $MgSO_4$ (1 M), 25 ml potassium phosphate (1 M, pH 6), and 1 ml cholesterol (5 mg/ml in EtOH).
3. TE buffer: For 100 ml, mix 200 µl EDTA (0.5 M, pH 8), 1 ml Tris–HCl (1M, pH 8), and 98.8 ml H_2O.

2.3 Other

1. Agarose.
2. Cover slips, 24 × 50 × 1.5 mm.
3. Halocarbon 700 oil (Sigma Chemical Company, St. Louis, MO, USA).
4. A worm pick: A platinum wire connected to a Pasture pipette. The end of the pick should be slightly wide and flat.
5. NGM plates seeded with OP50 *Escherichia coli* bacteria. Dispense 10 ml of NGM agar into 6 cm petri dishes, allow to solidify overnight. Inoculate OP50 *Escherichia coli* bacteria in 500 ml LB, and incubate at 37 °C overnight. Seed NGM agar plates with OP50 bacteria. Allow the bacteria to dry and form a lawn by incubating the plates at room temperature for 2 days.
6. Worms: L4 hermaphrodites (around 50) picked a day before injection onto a fresh OP50-seeded plate, so that on the day of injection there will be many well-fed young adult animals, with a single row of eggs (*see* **Note 1**).
7. Capillaries: Borosilicate glass capillaries with filament (4 in., 1/0.58 OD/ID (mm), World Precision Inst., Sarasota, FL, USA) (*see* **Note 2**).

3 Methods

To generate transgenic lines for neuronal manipulations, animals are transformed with DNA encoding the appropriate genetic tool (Table 1). The most common method of transformation is DNA microinjection. In brief, DNA is injected into a distal gonadal arm, which contains a central core cytoplasm shared by many germ cell nuclei. Injected DNA can be taken up into the nuclei of mature oocytes as high-copy extrachromosomal arrays, which segregate

randomly and transmit to subsequent generations with variable frequency, creating transgenic lines. The following protocol is based on [43] (*see* **Notes 3** and **4**).

The following steps should be done before starting the injection procedure:

3.1 Preparing Injection Pads (*See* Note 5)

1. Dissolve 2 % agarose in water by heating it in a microwave until boiling, and mix well.
2. Using a Pasteur pipette, place a drop of hot agarose on a cover slip.
3. Immediately place another cover slip on top to flatten it. The size of the agarose pad should be approximately 2 cm in diameter.
4. Once the agarose has solidified, slide off the top cover slip.
5. Place the cover slips with the agarose pads in an open box, and cover loosely with an aluminum foil (which serves to prevent dust from sticking to the agar).
6. Allow to dry for several days.
7. Injection pads can be stored indefinitely; thus it is advised to prepare many at once.

3.2 Preparing Microinjection Needles (According to Needle Puller P-2000 (Sutter Instruments) User Manual)

1. Turn the machine power switch on. Allow the machine to warm up with the lid closed for about 15 min.
2. Load the desired program. Parameters for needle pulling are varied, and should be defined individually (*see* **Note 6**). We are using the following parameters: HEAT, 275; FIL, 2; VEL, 45; DEL, 250; and PUL, 150.
3. Loosen clamping knob on the puller bar.
4. Place the capillary in the V-groove of the puller bar, slide it about 2 cm beyond the clamp, and tighten the knob. Be careful to hold the capillaries only at the edges.
5. Depress the spring stop on each puller bar to release them from their catch position.
6. Pull both bars towards each other using the finger bars. Hold bars in position using the thumb and index finger from one hand.
7. Using your free hand, loosen both clamping knobs and carefully slide the capillary through the holes in the side of the shroud and into V-groove of the opposite puller bar.
8. Tighten down clamping knobs.
9. Close the lid and press “PULL.” Needle pulling will take a few seconds.
10. Loosen the clamping knobs and remove the pulled needles from the puller bars.

11. Place the pulled needles in an empty box with a strip of modeling clay in the bottom. Push the needle slightly into the clay such that the tip of the needle is hanging free in space (*see* **Note 7**). On the day of injection:

3.3 Preparing DNA for Injection

1. Prepare 20 µl DNA mixture in TE buffer containing the desired plasmid DNA (according to Table 1), and a co-injection marker (*see* **Notes 8** and **9**). Total DNA concentration is 100–150 ng/µl (*see* **Note 10**). If the total concentration is less than 100 ng/µl, add an empty pBlueScript vector to the mixture.
2. Spin at maximal speed for 30 min using a bench-top microcentrifuge at 4 °C.
3. To prevent dust and other small particles from clogging the needle, use only the upper portion of the solution to load needles.
4. The DNA mixture could be kept at 4 °C for several days, or in −20 °C for a few months, but will need to be respun for a few minutes before use.

3.4 Loading the Needle with DNA

1. Make a ring of adhesive tape, where the adhesive side is facing out, and stick it to the side of a table or a shelf. This will be used to hold the needle.
2. Pipette around 0.5 µl of DNA to the back (unpulled) side of the needle, adhere the needle vertically on the adhesive tape, and allow it to stand for about 5 min. By capillary action the DNA mixture will flow to the tip of the needle (*see* **Note 2**).
3. Verify that the mixture flowed down to the tip of the needle by holding the needle up to the light. Look at the needle under a dissecting microscope to make sure that there are no large air bubbles at the tip. If there are, discard the needle and load a new one.

3.5 Mounting the Needle on the Microscope and Breaking the Needle

1. Before you start, make sure that the three knobs of the micromanipulator are set in the middle (5) and the needle holder is at about a 30° angle to the microscope stage.
2. Unscrew the end cup of the needle holder that is mounted to the microscope.
3. Insert the needle to the end cup from the back (unpulled) end, until a few millimeters of the back end of the needle protrudes from the end cup.
4. Screw the end cup tightly back onto the needle holder.
5. With the coarse manipulator make sure that the needle is placed high enough to prevent it from colliding with the stage.

6. Turn on the FemtoJet microinjector and wait for the pressure to build up (injection pressure should be 1700 hPa and compensation pressure 50 hPa).
7. To center the needle in the field of view, close the transmitted light diaphragm and turn the light intensity to maximum. Using the knobs of the coarse manipulator bring the needle to a position such that only the very tip of the needle is strongly illuminated. Make sure that the needle is not too low on the *z*-axis. Reopen the transmitted light diaphragm and dim the light.
8. Place a capillary on a cover slip and apply a drop of microinjection oil on it in the center. This will stabilize the capillary.
9. Put this capillary on the microscope, perpendicular to the needle. Using a 10× objective focus on the middle of the capillary in the *z*-axis. You should see clear dark lines on both sides of the capillary.
10. Carefully lower the needle into the oil, and use the micromanipulator to bring it close to the capillary. Make sure to keep the tip of the needle always in focus to prevent accidental breakage.
11. While pressing the injection foot paddle, use the micromanipulator to move the needle until it slightly touches the capillary, and immediately retract it back. A constant flow of liquid at a moderate speed should be released from the tip of the needle into the oil. This step is tricky and might require some practice before getting the right size opening.
12. Raise the needle using the micromanipulator. The needle is aligned, open, and ready for injection.

3.6 Mounting the Worm on the Injection Pad

1. Place a small drop of oil on the cover slip next to the agarose pad.
2. Flame to clean the edge of a pick. Dip it into the oil and then use a dissecting microscope to pick a worm that is outside of the bacterial lawn. Drop the worm into the oil droplet on the injection pad. Allow the worm to swim in the oil for a few seconds (*see* **Note 11**).
3. Scoop the worm from the oil and place it on the agarose pad. Allow the worm to adhere to the agarose by gently spreading out the oil on either side of the worm. To avoid dehydration, you may need to add more oil once the worm is immobilized, and the following steps should be performed quickly (*see* **Note 12**).

3.7 Injection

1. Place the injection pad on the stage and use the 10× objective to orient the worm in a way that the dorsal side (where the distal part of the gonad is located) is facing the needle. By moving the stage, position the worm at about 15°–45° to the needle.

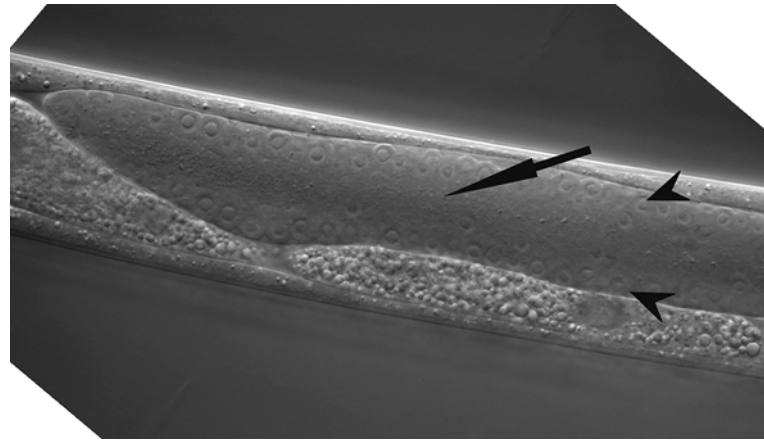

Fig 1 Microinjection into the distal gonad arm. For microinjection, the needle is inserted into the core syncytium of the gonad (an *arrow*). The cytoplasmic core is at the correct focal plane for injection, when two rows of germ cell nuclei are visible (*pointed arrowheads*)

2. Lower the needle carefully until it is in the field of view.
3. Move to the 40× objective and focus on the core of one of the two distal gonad syncytia. When the syncytial gonad arm is in the right focal plane it should be visualized as two rows of nuclei (on either sides of the gonad wall) with a clear cytoplasm in the middle (*see* Fig. 1). If a continuous sheet of nuclei is observed, you are probably at the surface of the gonad, and need to lower the plane of focus.
4. Carefully lower the tip of the needle into focus using the micromanipulator. Using the X–Y-axis knobs place the needle near the center of this syncytium, gently touching the worm cuticle.
5. Very gently move the worm by moving the stage. First push it up so that the needle will create a little curving in the worm cuticle, and then move it to the right, so that the needle penetrates the body wall and enters the gonad. Once the needle is inside the gonad, pull the worm away slightly to make sure that the tip of the needle is floating at the center of the cytoplasmic core.
6. To inject the DNA, press the food pedal for few seconds. You should see the gonad expanding and a flow of liquid in both the distal and proximal directions. You want to fill the gonad with as much solution as possible, but without letting the DNA solution spill out of the needle hole.
7. While still applying the pressure (to prevent the needle from clogging) pull the worm away from the needle by moving the stage to the left.
8. Raise the needle, and move the injection pad to the dissecting microscope (*see* **Note 13**).

3.8 Recovery of the Worm

1. Under the dissecting microscope, pipette 0.5 μl of M9 buffer on the worm. A healthy worm will be released from the agar pad and will start swimming in the buffer.
2. Use a bacteria-coated pick to transfer the worm to a seeded NGM plate.
3. Allow the worm to recover for around 30 min.

3.9 Selection for Transgenic Worms

1. Pick two to three injected worms onto a seeded NGM plate and incubate at 20–25 °C.
2. Three days after injection, score the first generation (F1) for the transgenic phenotype under a standard or fluorescence-dissecting microscope, depending on the co-injection marker used. Pick transgenic F1s individually onto separate plates (*see* **Note 14**).
3. Three to four days later, score the F2 generation for stable transgenic lines. A line is defined if several transgenic animals are identified on the same plate, indicating a germ line transmission of the array.
4. Maintain several of these lines, by selecting for the transgenic worms (*see* **Note 15**). Alternatively, the extrachromosomal array can be integrated into the genome [44] (*see* **Note 16**). This step is essential for proper expression of some of the genes that were reviewed here.

4 Notes

1. The DNA mixture is injected into the cytoplasmic syncytium at the distal gonad arm, which can be easily identified in young adult hermaphrodites. Older animals tend to accumulate a large amount of eggs in the proximal side of their gonads, reducing the volume of the syncytium in the distal part, which complicates the identification and needle insertion into the syncytium.
2. These capillaries have a fine filament adhered to their inner wall, which allows efficient backfilling of the DNA mixture to the tip of the needle by capillary force.
3. An informative video describing the process of microinjection can be found here: http://www.jove.com/video/833/generation-of-stable-transgenic-c-elegans-using-microinjection.
4. An alternative method to injection is gene bombardment, which is based on coating micro-gold particles with DNA and using high pressure to bombard the worms. Despite the low rate of transformation, which requires starting with a large number of animals, transgenes are usually integrated into the genome at low copy number, generating stable transgenic lines [45].

5. The agarose on the injection pads is used to immobilize the worms during the injection procedure. Worms stick to pad due to absorption of water from the worm into the agarose; therefore, it is essential that the pad is completely dry.
6. Good needles are essential for successful injection. The parameters for needle pulling will vary between different needle puller models, different types of capillaries, and personal preferences. In general, the tip of the needle should be sharp (whereupon breaking the opening is narrow, ~1 μm), and rigid. This allows for easy insertion of the needle into the gonad, and a moderate liquid flow. If the tip of a capillary tapers too gradually it will result in an ending that is very sharp but too flexible. Conversely, if the tip tapers too quickly the needle will be rigid but too wide. Thus a good needle is a fine balance between the two.
7. Pulled needles can be stored for only a few weeks due to the liquid properties of the glass.
8. To identify transgenic progeny of an injected animal a visible or selectable marker should be included in the injection mix. Dominant or recessive markers can be used. The advantage of dominant markers is that they allow transformation of any *C. elegans* strain. A popular dominant marker is the pRF4 plasmid, which encodes a mutated *rol-6(su1006)* gene that results in a "roller" phenotype. This phenotype is easy to score under a standard dissecting microscope. However, since it severely affects the pattern of worm locomotion, it is not suitable for behavior analysis. Markers that drive strong expression of a fluorescence protein in a subset of cells are ideal for behavioral analysis, as they usually do not affect neuronal or muscular activity. This includes expression of fluorescence proteins under *myo-2*, *elt-2*, or *unc-122* promoters (which will drive expression in pharyngeal muscle, gut, and coelomocytes, respectively). The drawback of fluorescence markers is that selection of transgenic animals under a dissecting microscope equipped with fluorescent optics is required. For recessive markers, a rescue construct is added to the DNA mix to rescue a mutant phenotype (such as *unc-119*, *lin-15*, and *pha*-1). This require working with mutant strains that might have an affect on animal development or behavior and thus might complicate neurobiology studies.
9. An alternative approach to working with plasmids is to generate a fusion between the desired regulatory promoter and a gene of interest using PCR and injecting the PCR product directly to the worms [46].
10. If the working concentration for a plasmid is unknown, 30–50 ng/μl is a standard starting concentration. Some plasmid can be toxic, or have pleiotropic functions at high concentration.

In these cases concretions should be titrated down to as low as 1–5 ng/μl. On the other hand, some promoters drive very low expression levels, and hence injection of plasmids at higher concentration is required.

11. Allowing worms to swim in the oil will minimize the transfer of bacteria and liquids to the agar pad, thus facilitating the immobilization of the worm and preventing clogging of the needle with bacteria.
12. Experience users can mount and inject more than one worm at a time (up to ten worms if very skilled). If injecting more than one worm, it is important to use the pick to align the worms in the same orientation to minimize the need to change the orientation of the pad relative to the needle between injections.
13. Once you are confident with injection you can inject both gonad arms of the same worm to increase the rate of success. If you are injecting more than one worm at a time, move to the next worm on the pad, until all the worms have been injected.
14. Each transgenic F1 is considered an independent transformant, even if several come from the same injected P0.
15. DNA injection results in the formation of a large extrachromosomal array that is formed by homologous and nonhomologous recombination of plasmids (or linear DNA) injected. Those arrays that are transmitted to subsequent generations differ in the efficiency of transmission (5–95 %) and in the levels of gene expression. Therefore it is advised to keep more than one transgenic line.
16. Bombardment [45] and the MosSCI [47] techniques can be used to generate low- or single-copy transgene integration to the genome, respectively. Thus if integrated lines with low to moderate transgene expression levels are desired, it is advised to consider these methods before starting the above protocol for generating transgenic worms.

Acknowledgment

I would like to thank Shai Shaham, Aakanksha Singhvi, In Hae Lee, and Sean Wallace for comments and discussions on this manuscript.

References

1. Avery L, Horvitz HR (1989) Pharyngeal pumping continues after laser killing of the pharyngeal nervous system of C. elegans. Neuron 3:473–485
2. Bargmann CI, Hartwieg E, Horvitz HR (1993) Odorant-selective genes and neurons mediate olfaction in C. elegans. Cell 74: 515–527

3. Bargmann CI, Horvitz HR (1991) Chemosensory neurons with overlapping functions direct chemotaxis to multiple chemicals in C. elegans. Neuron 7:729–742
4. Chalfie M, Sulston JE, White JG et al (1985) The neural circuit for touch sensitivity in Caenorhabditis elegans. J Neurosci 5:956–964
5. Fang-Yen C, Gabel CV, Samuel AD et al (2012) Laser microsurgery in Caenorhabditis elegans. Methods Cell Biol 107:177–206
6. Chelur DS, Chalfie M (2007) Targeted cell killing by reconstituted caspases. Proc Natl Acad Sci U S A 104:2283–2288
7. Fares H, Greenwald I (2001) Genetic analysis of endocytosis in Caenorhabditis elegans: coelomocyte uptake defective mutants. Genetics 159:133–145
8. Shaham S, Horvitz HR (1996) Developing Caenorhabditis elegans neurons may contain both cell-death protective and killer activities. Genes Dev 10:578–591
9. Conradt B, Horvitz HR (1998) The C. elegans protein EGL-1 is required for programmed cell death and interacts with the Bcl-2-like protein CED-9. Cell 93:519–529
10. Procko C, Lu Y, Shaham S (2011) Glia delimit shape changes of sensory neuron receptive endings in C. elegans. Development 138: 1371–1381
11. Harbinder S, Tavernarakis N, Herndon LA et al (1997) Genetically targeted cell disruption in Caenorhabditis elegans. Proc Natl Acad Sci U S A 94:13128–13133
12. Treinin M, Chalfie M (1995) A mutated acetylcholine receptor subunit causes neuronal degeneration in C. elegans. Neuron 14:871–877
13. Kobayashi J, Shidara H, Morisawa Y et al (2013) A method for selective ablation of neurons in C. elegans using the phototoxic fluorescent protein, KillerRed. Neurosci Lett 548: 261–264
14. Qi YB, Garren EJ, Shu X et al (2012) Photoinducible cell ablation in Caenorhabditis elegans using the genetically encoded singlet oxygen generating protein miniSOG. Proc Natl Acad Sci U S A 109:7499–7504
15. Williams DC, Bejjani RE, Ramirez PM et al (2013) Rapid and permanent neuronal inactivation in vivo via subcellular generation of reactive oxygen with the use of KillerRed. Cell Rep 5:553–563
16. Dickinson DJ, Ward JD, Reiner DJ et al (2013) Engineering the Caenorhabditis elegans genome using Cas9-triggered homologous recombination. Nat Methods 10:1028–1034
17. Esposito G, Di Schiavi E, Bergamasco C et al (2007) Efficient and cell specific knock-down of gene function in targeted C. elegans neurons. Gene 395:170–176
18. Qadota H, Inoue M, Hikita T et al (2007) Establishment of a tissue-specific RNAi system in C. elegans. Gene 400:166–173
19. Chow BY, Han X, Dobry AS et al (2010) High-performance genetically targetable optical neural silencing by light-driven proton pumps. Nature 463:98–102
20. Han X, Boyden ES (2007) Multiple-color optical activation, silencing, and desynchronization of neural activity, with single-spike temporal resolution. PLoS One 2:e299
21. Husson SJ, Liewald JF, Schultheis C et al (2012) Microbial light-activatable proton pumps as neuronal inhibitors to functionally dissect neuronal networks in C. elegans. PLoS One 7:e40937
22. Kawano T, Po MD, Gao S et al (2011) An imbalancing act: gap junctions reduce the backward motor circuit activity to bias C. elegans for forward locomotion. Neuron 72:572–586
23. Kunkel MT, Johnstone DB, Thomas JH et al (2000) Mutants of a temperature-sensitive two-P domain potassium channel. J Neurosci 20:7517–7524
24. Okazaki A, Sudo Y, Takagi S (2012) Optical silencing of C. elegans cells with arch proton pump. PLoS One 7:e35370
25. Pokala N, Liu Q, Gordus A et al (2014) Inducible and titratable silencing of Caenorhabditis elegans neurons in vivo with histamine-gated chloride channels. Proc Natl Acad Sci U S A 111:2770–2775
26. Reiner DJ, Weinshenker D, Tian H et al (2006) Behavioral genetics of Caenorhabditis elegans unc-103-encoded erg-like K(+) channel. J Neurogenet 20:41–66
27. Stirman JN, Crane MM, Husson SJ et al (2011) Real-time multimodal optical control of neurons and muscles in freely behaving Caenorhabditis elegans. Nat Methods 8:153–158
28. Zhang F, Wang LP, Brauner M et al (2007) Multimodal fast optical interrogation of neural circuitry. Nature 446:633–639
29. Macosko EZ, Pokala N, Feinberg EH et al (2009) A hub-and-spoke circuit drives pheromone attraction and social behaviour in C. elegans. Nature 458:1171–1175
30. Schiavo G, Benfenati F, Poulain B et al (1992) Tetanus and botulinum-B neurotoxins block neurotransmitter release by proteolytic cleavage of synaptobrevin. Nature 359:832–835
31. Boyden ES, Zhang F, Bamberg E et al (2005) Millisecond-timescale, genetically targeted optical control of neural activity. Nat Neurosci 8:1263–1268

32. Edwards SL, Charlie NK, Milfort MC et al (2008) A novel molecular solution for ultraviolet light detection in Caenorhabditis elegans. PLoS Biol 6:e198
33. Liu J, Ward A, Gao J et al (2010) C. elegans phototransduction requires a G protein-dependent cGMP pathway and a taste receptor homolog. Nat Neurosci 13:715–722
34. Nagel G, Brauner M, Liewald JF et al (2005) Light activation of channelrhodopsin-2 in excitable cells of Caenorhabditis elegans triggers rapid behavioral responses. Curr Biol 15:2279–2284
35. Nagel G, Szellas T, Huhn W et al (2003) Channelrhodopsin-2, a directly light-gated cation-selective membrane channel. Proc Natl Acad Sci U S A 100:13940–13945
36. Okochi Y, Kimura KD, Ohta A et al (2005) Diverse regulation of sensory signaling by C. elegans nPKC-epsilon/eta TTX-4. EMBO J 24:2127–2137
37. Sieburth D, Madison JM, Kaplan JM (2007) PKC-1 regulates secretion of neuropeptides. Nat Neurosci 10:49–57
38. Weissenberger S, Schultheis C, Liewald JF et al (2011) PACalpha—an optogenetic tool for in vivo manipulation of cellular cAMP levels, neurotransmitter release, and behavior in Caenorhabditis elegans. J Neurochem 116: 616–625
39. Davis MW, Morton JJ, Carroll D et al (2008) Gene activation using FLP recombinase in C. elegans. PLoS Genet 4:e1000028
40. Schmitt C, Schultheis C, Pokala N et al (2012) Specific expression of channelrhodopsin-2 in single neurons of Caenorhabditis elegans. PLoS One 7:e43164
41. Guo ZV, Hart AC, Ramanathan S (2009) Optical interrogation of neural circuits in Caenorhabditis elegans. Nat Methods 6: 891–896
42. Leifer AM, Fang-Yen C, Gershow M et al (2011) Optogenetic manipulation of neural activity in freely moving Caenorhabditis elegans. Nat Methods 8:147–152
43. Mello C, Fire A (1995) DNA transformation. Methods Cell Biol 48:451–482
44. Way JC, Wang L, Run JQ et al (1991) The mec-3 gene contains cis-acting elements mediating positive and negative regulation in cells produced by asymmetric cell division in Caenorhabditis elegans. Genes Dev 5:2199–2211
45. Praitis V, Casey E, Collar D et al (2001) Creation of low-copy integrated transgenic lines in Caenorhabditis elegans. Genetics 157: 1217–1226
46. Hobert O (2002) PCR fusion-based approach to create reporter gene constructs for expression analysis in transgenic C. elegans. Biotechniques 32:728–730
47. Frokjaer-Jensen C, Davis MW, Hopkins CE et al (2008) Single-copy insertion of transgenes in Caenorhabditis elegans. Nat Genet 40: 1375–1383
48. Collier RJ (1975) Diphtheria toxin: mode of action and structure. Bacteriol Rev 39:54–85

Chapter 4

A Fusion PCR Method for Expressing Genetic Tools in *C. elegans*

Yifat Eliezer and Alon Zaslaver

Abstract

C. elegans offer a unique opportunity for understanding computation in neural networks. This is largely due to their relatively compact neural network for which a wiring diagram is available. Recent advances in genetic tools for interrogating neural activity (e.g., optogenetics) make *C. elegans* particularly compelling as they can be expressed in many different combinations in target individual neurons. Thus, the prospect to decipher principles underlying functionality in neural networks largely depends on the ease by which transgenic animals can be generated. Traditionally, to generate transgenic animals one would inject a plasmid containing the gene of interest under the regulation of the cell- or lineage-specific promoter. This often requires laborious cloning steps of both the gene and the promoter. The Hobert lab has developed a simpler protocol in which linear PCR fragments can be injected to generate transgenic animals. Relying on this PCR fusion-based method, here we provide a detailed protocol that we have optimized for expressing various genetically encoded calcium indicators and optogenetic tools in individual or sets of neurons. We use these simple procedures to generate multiple constructs within a very short time frame (typically 1–2 days).

Key words *C. elegans*, Transgenics, Fusion PCR, Genetic ablations, Fluorescent reporters

1 Introduction

Caenorhabditis elegans provide an excellent model system widely used in biological research [1]. Neuroscience is one appealing field for which *C. elegans* confer a key advantage: their neural network is relatively simple and compact (302 neurons in total) and a full neuronal wiring diagram is available [2]. In addition, *C. elegans* are compatible with a wide variety of molecular and genetic manipulations. In particular, it is possible to generate transgenic worms that carry DNA of choice [3]. The DNA, whether injected as a supercoiled plasmid or in a linearized form, is organized into extrachromosomal high-molecular-weight arrays, and is usually transmissible and stable for many generations [4]. Since first introducing the DNA injection method to *C. elegans*, many studies were performed

David Biron and Gal Haspel (eds.), *C. elegans: Methods and Applications*, Methods in Molecular Biology, vol. 1327,
DOI 10.1007/978-1-4939-2842-2_4,

by tagging individual, or a set of cells, with many different reporter genes [5–7].

In recent years, we witness major advances in the molecular tools developed for interrogating neural activity. These include various genetically encoded calcium indicators (GECIs) [8–10] and optogenetic tools [11, 12]. Thus, the prospect of expressing these optogenetic and GECI tools in target neurons makes *C. elegans* a powerful system for studying dynamics and computation in neural networks with single-neuron resolution.

Much of the success of interrogating neural circuit dynamics depends on the ease by which we can generate transgenic worms. Cloning the gene of interest downstream to a desired promoter can be a tedious process and often requires many steps of DNA purification and cloning. To minimize time and labor, the Hobert laboratory (University of Columbia) has developed a convenient and fast method where linear PCR products are injected to produce transgenic lines [13–15]. In this method, the gene of interest is fused to the promoter region using a single-fusion PCR reaction. Moreover, injection of vector-free DNA fragments was shown to improve transgene expression [16]. We find this method to be particularly useful as we aim to express various proteins (e.g., calcium indicators or optogenetic tools) fused to many different neuron-specific promoters.

In our lab we use this established technique for large-scale and rapid production of promoter-gene fusions. These fusion PCR products are then injected to animals to successfully generate transgenic lines. Here we provide a detailed protocol that is based on the method developed originally by the Hobert lab for fusing two overlapping PCR products [13–15]. We add guidelines and notes that helped us improve this technique and customize it for expressing GECIs in target neurons. This method involves one step of cloning the reporter gene into the Fire-lab vector pPD95.77 [17] (chosen for its robust expression of genes and its restriction sites; *see* **Note 1**), followed by three simple PCR reactions. All three PCR reactions can be performed in 1 day such that the fusion-PCR product can be ready for microinjection within a very short time frame.

2 Materials

2.1 Promoter Cloning

1. Worm lysis buffer: 50 mM KCl, 10 mM Tris–HCl (pH 8.3), 2.5 mM $MgCl_2$, 0.45 % NP-40 (IGEPAL), 0.45 % Tween-20, 0.01 % gelatin, 2 mg/mL proteinase K.
2. Wild-type worms: N2 is the wild-type strain. It could be obtained from CGC.
3. Primers: According to the desired promoter, reverse primer should contain a 5′ overhang (cca agt tgt tag cgt atc cat cgt tgt gag tg). This overhang is complementary to the 5′ end of the

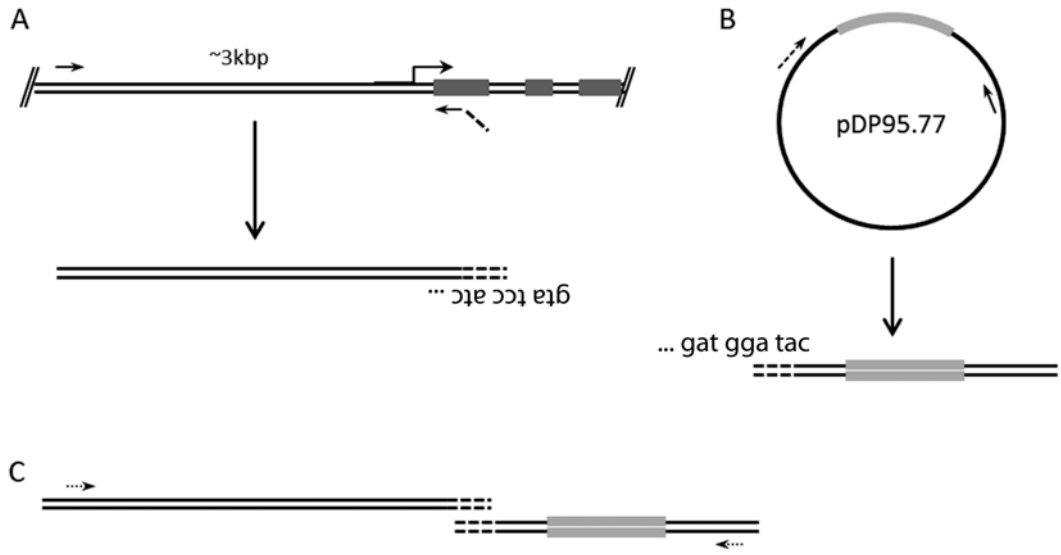

Fig. 1 Schematic representation of the three PCR reactions needed for fusion PCR. (**a**) PCR amplification of the required promoter from genomic DNA. *Bent arrow* represents the transcription start site. Primers are the *short arrows. Dashed lines*, including the primer extension, represent the region of sequence homology between PCR product no. 1 and PCR product no. 2. (**b**) PCR amplification of the gene from the pPD95.77 vector. In *grey* is the gene of interest. Primers are the *short arrows. Dashed lines* represent the region of sequence homology between PCR product no. 1 and PCR product no. 2. (**c**) Fusion PCR reaction between PCR products no. 1 and 2. *Dashed arrows* denote the nested primers used in the reaction

gene of interest PCR product amplified from the pPD95.77 vector (Fig. 1a).

4. PCR reagents: High-fidelity DNA polymerase, polymerase buffer, dNTPs.
5. 1 % agarose gel.
6. DNA cleaning column.

2.2 Cloning Reporter Gene

1. pPD95.77 plasmid: Can be acquired from Addgene or other worm laboratories. This plasmid contains an artificial intron for enhanced expression of the gene and an *unc-54* 3′ UTR for the stabilization of the RNA transcript. For insertion of the gene the pPD95.77 harbors an AgeI and EcoRI restriction sites.
2. Reporter plasmid: Could also be obtained from Addgene or colleagues. If a plasmid is not available but the sequence of the transgene is known, it could be cloned from transgenic animals as described here for promoter cloning.
3. Primers for amplification of the gene: Should be ordered with restriction sites.
4. PCR reagents: High-fidelity DNA polymerase, polymerase buffer, dNTPs.

5. AgeI and EcoRI restriction enzymes, ligase, gel purification kit.
6. 1 % agarose gel.
7. DNA cleaning column.

Primers for amplification of the gene from the pPD95.77: pPD95.77 fwd (cac tca caa cga tgg ata c), pPD95.77 rev (cgc tta cag aca agc tgt). The fwd primer is the reverse complement of the aforementioned overhang. Therefore, the resulting PCR product will complement the overhang from the promoter amplification (Fig. 1b) and enable the following fusion PCR reaction.

2.3 Fusion PCR

1. PCR reagents: High-fidelity DNA polymerase, polymerase buffer, dNTPs.
2. Primers: The forward primer is a nested primer about 100 bp downstream from the beginning of the promoter PCR product. Therefore, it should be designed together with the primers for cloning the promoter (see left dashed arrow in Fig. 1c). The reverse primer is pPD95.77 rev nested (atc acc gaa acg cgc gag acg) (see right dashed arrow in Fig. 1c), upstream of the reverse primer of the reporter. If a different vector than pPD95.77 is used as a carrier for the reporter gene then both of the reporter primers and the fusion reverse primer need to be designed accordingly.
3. 1 % agarose gel.

3 Methods

Generation of a promoter-gene fusion requires two PCR products; the first is the promoter, which is amplified from genomic DNA of wild-type (N2) worms, and the second is the gene of interest, which in our case is cloned into the Fire lab vector pPD95.77 and amplified from there. This is followed by a third reaction in which we use nested primers in order to amplify the fused, partially overlapping, PCR products.

The fusion reaction is depicted in Fig. 1. The first PCR fragment is the required promoter amplified from genomic DNA (Fig. 2a). The second fragment is the gene of interest and flanking regions from the pPD95.77 plasmid (Fig. 2b). The reverse primer of the promoter includes an overhang, which corresponds to the 5′ sequence of the second PCR fragment (*see* Subheading 2).

In the first step of the third reaction (Fig. 3a), following denaturation of the two fragments, the 3′-end of the promoter is annealed to the 5′ of the gene, and this overlapping region functions as a primer, allowing the DNA polymerase to elongate these sequences and create a primary promoter-gene fusion.

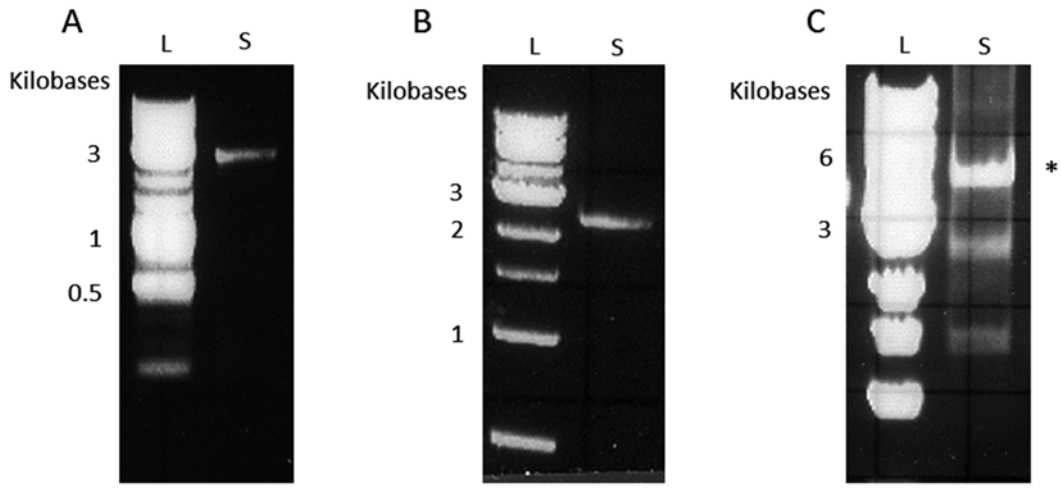

Fig. 2 Representative images of the three PCR products on gels. (**a**) *sra-6* gene promoter amplified from N2 worm genomic DNA. (**b**) GCaMP6m calcium indicator amplified from pPD95.77 (including the vectors' flanking regions). (**c**) Fusion PCR between the *sra-6* promoter and GCaMP6m. *Asterisk* marks the whole fusion product. "L" is the ladder and "S" is the sample lane

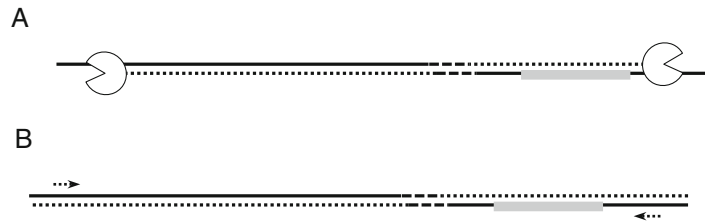

Fig. 3 Schematic representation of the fusion PCR reaction. (**a**) The first step of the reaction where the region of sequence homology acts as primers for elongation by DNA polymerase ("packman" shapes). (**b**) The second step of the reaction depicts the amplification of the entire fusion fragment following the addition of the nested primers (*dashed arrows*)

In the second step of this reaction (Fig. 3b), two nested primers are added to the reaction tube. These primers amplify the promoter-gene fusions that were generated in the first part of the reaction (Fig. 2c).

3.1 Amplifying the Promoter from Genomic DNA

1. Preparation of genomic DNA from N2 worms: Ten young adult worms (*see* **Note 2**) are dissolved in 50 μL of worm lysis buffer. The tube is transferred to −80 °C for 30 min, then to 65 °C for 60 min, and 95 °C for 10 min (for the inactivation of the proteinase K). Genomic DNA can then be stored at −20 °C for a few months.

2. Primer design for promoter amplification: *C. elegans* promoters are typically positioned in the 3 kbp stretch of DNA upstream of the gene. Choose sequences of 20–24 bp that flank this region (*see* **Notes 3**–**5**).

   The reverse primer should have a 5′ overhang (*see* Subheading 2) that corresponds to the sequence of the pPD95.77—the 5′ of the PCR product amplified from the plasmid (*see* **Note 6**).

3. Use the designed primers for promoter amplification. The PCR volume is 25 μL. Run 2.5 μL on 1 % agarose gel and verify that the band is of the right size (*see* **Note 7**). Following the verification, the PCR product should be cleaned on a column, and DNA concentration can then be measured (*see* **Note 8**).

3.2 Cloning and Amplifying the Gene of Interest

1. To clone the gene of interest into the pPD95.77 plasmid we amplify the gene from any given source by using primers which have restriction site extensions. We use the AgeI restriction site for the forward (fwd) primer, and EcoRI restriction site for the reverse (rev) primer. There is no need to insert bases between the primer sequence and the restriction site sequence (*see* **Note 9**).
2. Insertion of the gene into the pPD95.77 is by standard techniques of restriction, gel purification and ligation (*see* **Note 10**). One needs to verify the proper insertion of the gene by sequencing. Additionally, as mentioned before, this plasmid contains an unc-54 3′ UTR. One should also verify that this fragment is still intact in the plasmid. To boost expression, the fusion PCR product will contain the unc-54 3′ UTR and the synthetic intron that precedes it on the vector.
3. Fusion PCR reactions can be performed using the pPD95.77 vector containing the gene of interest. The primers used are the primers designated “pPD95.77 fwd” and “pPD95.77 rev” in the previous section. The annealing temperature used is 60 °C and denaturation and elongation temperatures are as recommended by the polymerase manufacturer. The duration of denaturation, annealing, and elongation are typically recommended by the polymerase manufacturer as well. The final volume of the PCR is 25 μL.
4. To verify that the PCR reaction succeeded, run 2.5 μL form the reaction on 1 % agarose gel. The product should be the size of the gene plus ~0.5 kbp from the flanking vector sequences. This amplicon contains the artificial intron followed by the gene and the unc-54 3′ UTR. Following the verification, the PCR product should be cleaned on a column and the concentration of the DNA concentration should be determined using standard spectrophotometry methods (*see* **Note 11**).

3.3 Fusion PCR of the Promoter and Gene

1. *Primary elongation to produce the full fusion*: Transfer a similar amount of the gene and promoter PCR products (between 10 and 50 ng) to a PCR tube. Add dNTPs, buffer, and enzyme, and adjust the volume to 50 μL with DDW. Primers are *not* added to this reaction (*see* **Note 12**). Perform a short PCR of ten cycles with the annealing temperature of 50–58 °C.
2. *Nested amplification of the fusion product*: Add 1 μL of each of the two nested primers to the PCR tube; the fwd primer is the promoter-specific nested primer, and the rev primer is the primer designated pPD95.77 rev nested in Subheading 2 (*see* Fig. 1). Perform an additional PCR, this time with 30 cycles and an annealing temperature ranging from 55 to 68 °C, depending on the Tm of the promoters' nested primer.
3. Run 5 μL from the PCR on gel. Verify that the band is of the right size (*see* **Notes 13** and **14**). No need for additional cleanup; the fusion PCR is ready for microinjection. Use an estimation of the concentration according to the band intensity compared to the DNA ladder bands, and inject between 20 and 40 ng/μL of the PCR product (*see* **Notes 15** and **16**; [18, 19]).

4 Notes

1. One can use any other vectors for cloning the gene of interest provided that the primers for the first PCR reaction (gene amplification) and the rev nested primer for the third reaction (fusion PCR) are redesigned accordingly.
2. When preparing genomic DNA, picked worms should be young and gravid; this yields more DNA.
3. It is recommended to check the literature before deciding on the size of the promoter. Many gene promoters have already been characterized.
4. The primers for amplifying the promoter should have approximately 50 % GC content, and the annealing temperature should be similar for both primers (between 50 and 65 °C).
5. Run BLAST analysis on the promoter primers you choose in order to validate that you have a *unique* sequence and avoid nonspecific products.
6. When calculating the Tm of the promoter reverse primer, do not take the 5′ overhang into consideration.
7. If more than one band appears on the gel when verifying the promoter PCR product, try to use a more stringent *annealing* temperature.
8. The cleanup of the two first PCR products is not mandatory. It may even be preferable to leave them not cleaned [13]. When doing so, use an estimation of the DNA concentration

based on their band intensity compared to the DNA ladder band intensity.

9. It is highly recommended to add between four and six bases before the restriction site when designing the primers for cloning genes into the pPD95.77 plasmid; this improves the restriction reaction.
10. An alternative and faster method that can be used for cloning the gene of interest into the pPD95.77 vector is the restriction-free cloning, which also relies on PCR. A detailed description of this method can be found in [20].
11. When PCR amplifying the reporter gene from the pPD95.77 vector results in low yield, try to adjust the annealing temperature to the enzyme you are working with. Alternatively, try to extend the elongation time.
12. Note that you do *not* add primers to the first step of the fusion PCR.
13. Sometimes additional nonspecific bands appear in the gel verifying the fusion PCR. If the desired band is the most intense one, there should be no problem injecting it as is (*see* Fig. 2c). However, if the desired band is very weak compared to other nonspecific ones, try to change the annealing temperature used in the second reaction of the fusion PCR.
14. Sometimes the fusion PCR band is surrounded by a DNA smear; this also should not interfere with the successful injection of the fusion PCR.
15. The fusion PCR product can be injected concurrently with other fusion PCR products or with other plasmids (linearized or not).
16. When fusion PCR yield is low, injections are still possible. We have successfully generated transgenic worms even when injecting as low as 2 ng/μL. This is not ideal, but nevertheless works.

This work was supported by the I-CORE grant.

References

1. Brenner S (1974) The genetics of Caenorhabditis elegans. Genetics 77(1):71–94
2. White JG et al (1986) The structure of the nervous system of the nematode Caenorhabditis elegans. Philos Trans R Soc Lond B Biol Sci 314(1165):1–340
3. Mello C, Fire A (1995) DNA transformation. Methods Cell Biol 48:451–482
4. Stinchcomb DT et al (1985) Extrachromosomal DNA transformation of Caenorhabditis elegans. Mol Cell Biol 5(12):3484–3496
5. Lynch AS, Briggs D, Hope IA (1995) Developmental expression pattern screen for genes predicted in the C. elegans genome sequencing project. Nat Genet 11(3): 309–313
6. Chalfie M et al (1994) Green fluorescent protein as a marker for gene expression. Science 263(5148):802–805
7. Troemel ER et al (1995) Divergent seven transmembrane receptors are candidate chemosensory receptors in C. elegans. Cell 83(2): 207–218
8. Chen TW et al (2013) Ultrasensitive fluorescent proteins for imaging neuronal activity. Nature 499(7458):295–300

9. Nakai J, Ohkura M, Imoto K (2001) A high signal-to-noise Ca(2+) probe composed of a single green fluorescent protein. Nat Biotechnol 19(2):137–141
10. Tian L et al (2009) Imaging neural activity in worms, flies and mice with improved GCaMP calcium indicators. Nat Methods 6(12):875–881
11. Lorenz-Fonfria VA, Heberle J (2014) Channelrhodopsin unchained: structure and mechanism of a light-gated cation channel. Biochim Biophys Acta 1837(5):626–642
12. Sparta DR et al (2013) Optogenetic strategies to investigate neural circuitry engaged by stress. Behav Brain Res 255:19–25
13. Hobert O (2002) PCR fusion-based approach to create reporter gene constructs for expression analysis in transgenic C. elegans. Biotechniques 32(4):728–730
14. Delidow BC et al (1993) Polymerase chain reaction: basic protocols. Methods Mol Biol 15:1–29
15. Boulin T, Etchberger JF, Hobert O (2006) Reporter gene fusions. WormBook. pp 1–23
16. Etchberger JF, Hobert O (2008) Vector-free DNA constructs improve transgene expression in C. elegans. Nat Methods 5(1):3
17. Fire A, Harrison SW, Dixon D (1990) A modular set of lacZ fusion vectors for studying gene expression in Caenorhabditis elegans. Gene 93(2):189–198
18. Evans TC (ed) (2006) Transformation and microinjection. WormBook
19. Katz (2014) this volume
20. van den Ent F, Lowe J (2006) RF cloning: a restriction-free method for inserting target genes into plasmids. J Biochem Biophys Methods 67(1):67–74

Chapter 5

Transposon-Assisted Genetic Engineering with Mos1-Mediated Single-Copy Insertion (MosSCI)

Christian Frøkjær-Jensen

Abstract

Transgenesis in model organisms is necessary to determine the function, expression, and subcellular localization of gene products. In *Caenorhabditis elegans*, injected DNA can be propagated as multicopy extrachromosomal arrays but transgenes in arrays are mosaic, over-expressed in some tissues and silenced in the germline. Here, a method to insert a transgene into a specific genomic location called Mos1-mediated single-copy insertion (MosSCI) is described. Single-copy insertion allows transgene expression at levels that approximate endogenous gene expression as well as expression in the germline.

Key words Mos1 transposon, Transgenesis, Mos1 single-copy insertion (MosSCI), Universal insertion sites, Germline expression, Endogenous levels of gene expression

1 Introduction

Transgenic *C. elegans* are most often generated by injection of DNA into the gonad of adult hermaphrodites [1]. Injected plasmids form repetitive extrachromosomal arrays that contain between 100 and 200 copies. In each cell division extrachromosomal arrays can be lost and the DNA is therefore transmitted at variable frequency to progeny. Arrays have the advantage that they are easy to generate and transgene expression is often high, which is beneficial for fluorescence microscopy for example. Arrays have the disadvantages that expression is variable between different strains and transgenes are frequently over-expressed relative to the endogenous expression level. Furthermore expression from extrachromosomal arrays in the germline [2] is efficiently silenced through small RNA pathways [3–6]. Several alternatives to extrachromosomal array transgenesis have been developed to overcome these limitations: biolistic transformation [7], low-copy transgene insertion by ultraviolet and trimethylpsoralen mutagenesis [8], and more recently Cas9-mediated genome engineering [9, 10].

David Biron and Gal Haspel (eds.), *C. elegans: Methods and Applications*, Methods in Molecular Biology, vol. 1327,
DOI 10.1007/978-1-4939-2842-2_5,

Here, I describe the method Mos1-mediated single-copy insertion (MosSCI) that allows insertion of single copies of transgenes into well-defined genomic locations throughout the genome. The method was developed based on the observation that the Mos1 DNA transposon from *Drosophila mauritiana* is active in the *C. elegans* germline [11] and that transgenic DNA can be inserted into the genome following Mos1 excision [12]. With MosSCI, transgene insertions are generated by transient expression of the Mos1 transposase by injection and insertions are identified based on positive and negative selection markers (Fig. 1) [13, 14]. Transgenes can be inserted into different genomic locations by cloning the transgene into distinct targeting vectors [14] or into a single, universal targeting vector [15]. Inserted transgenes can be expressed at levels that approximate endogenous expression levels and in tissues that are typically refractory to expression from arrays, such as the hermaphrodite and male germline [14].

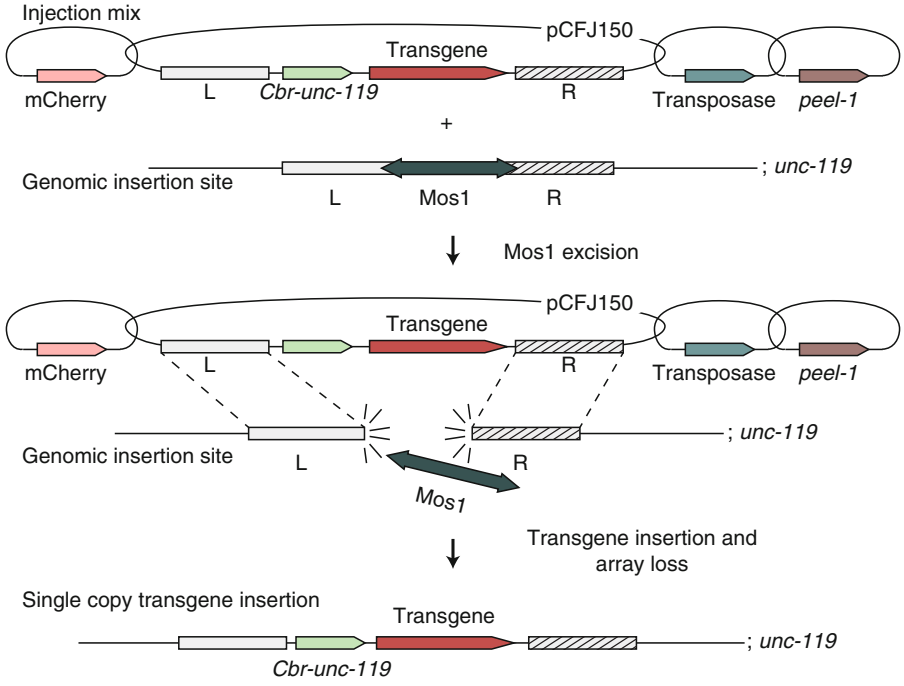

Fig. 1 Schematic of Mos1-mediated single-copy insertion (MosSCI). Targeted transgene insertion relies on generating a double-strand break (DSB) at a specific chromosomal location and a repair template that contains homology to the DSB. Mos1 mobilization by transposase injection creates the DSB. The targeting vector (here pCFJ150) contains homology to the DSB. DNA repair copies the transgene and the selection marker (*Cbr-unc-119*) into the genome. The fluorescent (mCherry) and inducible (*peel-1*) selection markers are used to select against the array

2 Materials

To generate MosSCI insertions it is necessary to have access and familiarity with standard *C. elegans* equipment and reagents, including NGM plates, a microinjection setup, a pipette puller to make injection needles, a fluorescence dissection microscope, and incubators at 20, 25, and 37 °C. All injection strains should be maintained at 20 °C on NGM plates seeded with HB101 bacteria (*see* **Note 1**). Additional information about strains, plasmids, and protocols can be found at the website www.wormbuilder.org.

2.1 MosSCI Insertion Strains

1. Injection strains: Request a strain corresponding to the desired transgene insertion site (Table 1). All strains are available from the *Caenorhabditis elegans* Genetics Center (CGC, www.cbs.umn.edu/research/resources/cgc). Choose the insertion site based on whether germline expression is required and what experiments you plan to do (*see* **Note 2**). For example, do not choose a site that is genetically linked to any mutant backgrounds you plan to cross the transgene into.

2.2 MosSCI Targeting Vectors

1. Generate a targeting vector corresponding to the chosen insertion site (Table 2). All vectors are available from Addgene (www.addgene.org/Erik_Jorgensen/). Vectors for three-fragment Gateway multisite cloning™ (Life Technologies) or for standard restriction fragment cloning are available. Use standard molecular biology protocols to insert the transgene of choice into the targeting vector.
2. Make transfection-grade DNA preparations of the targeting vector(s) (*see* **Note 3**).

Table 1
MosSCI insertion strains

Locus	Genetic position	Chromosomal position	Strain	Germline expression
unc-119 selection				
ttTi4348	I:–5.32	I: 2.85 MB	EG6701	Yes
ttTi4391	I:7.93	I: 11.27 MB	EG6702	No
ttTi5605	II:0.77	II: 8.42 MB	EG6699	Yes
cxTi10816	IV:1.41	IV: 5.01 MB	EG6703	Yes
cxTi10882	IV:–0.05	IV: 4.24 MB	EG6700	Yes (variable)
ttTi14024	X:22.84	X: 15.57 MB	EG6705	Late stages only
unc-18 selection				
ttTi4348	I:–5.32	I: 2.85 MB	EG6032	Yes

Table 2
MosSCI targeting vectors

Locus	Selection marker	Three-fragment Gateway™ vector	Multiple cloning site vector
ttTi4348	*Cbr-unc-119*	pCFJ210	pCFJ352
	unc-18	pCFJ448	pCFJ676
ttTi4391	*Cbr-unc-119*	pCFJ604	pCFJ353
ttTi5605	*Cbr-unc-119*	pCFJ150	pCFJ350
cxTi10816	*Cbr-unc-119*	pCFJ212	pCFJ356
cxTi10882	*Cbr-unc-119*	pCFJ201	pCFJ351
ttTi14024	*Cbr-unc-119*	pCFJ606	pCFJ355

Table 3
Universal insertion sites

Locus	Genetic position	Chromosomal position	Strain	Genomic environment	Germline expression
NeoR and unc-18 landing site					
oxTi185	I:1.17	I: 6.50 MB	EG8078	Intergenic	Yes
oxTi179	II:1.73	II: 9.83 MB	EG8079	In ZK938.3	Yes
oxTi444	III:–0.85	III: 7.01 MB	EG8080	In *lgc-38*	Yes
oxTI177	IV:7.43	IV: 13.05 MB	EG8081	In *scl-10*	Yes
oxTi365	V:1.52	V: 8.64 MB	EG8082	In *asp-13*	Yes
Pmyo-2:GFP:H2B and unc-18 landing site					
oxTi354	V:5.59	V: 13.78 MB	EG8083	In F53C11.3	Yes

2.3 Universal MosSCI Insertion Strains

1. Universal injection strains: A set of strains contain a universal landing site (Table 3), which are all compatible with a single targeting vector (Table 4). The strains contain a Mos1 transposon flanked by two selection markers (NeoR and *unc-18*(+) or *Pmyo-2*:GFP:H2B) (Fig. 2). The selection markers are convenient for moving a transgene insertion into other genetic backgrounds by following neomycin resistance or pharyngeal GFP fluorescence.

2.4 Universal MosSCI Targeting Vectors

1. Generate a universal targeting vector (Table 5) by your preferred cloning method. Transgenes in the universal vectors can be inserted into any of the six universal insertion sites and the insertion location only depends on which strain is injected.
2. Make transfection-grade DNA preparations of targeting vector(s).

Table 4
Universal targeting vector

Locus	Selection marker	Three-fragment Gateway™ vector	Multiple cloning site vector
Universal insertion sites	*Cbr-unc-119*	pCFJ150	pCFJ350

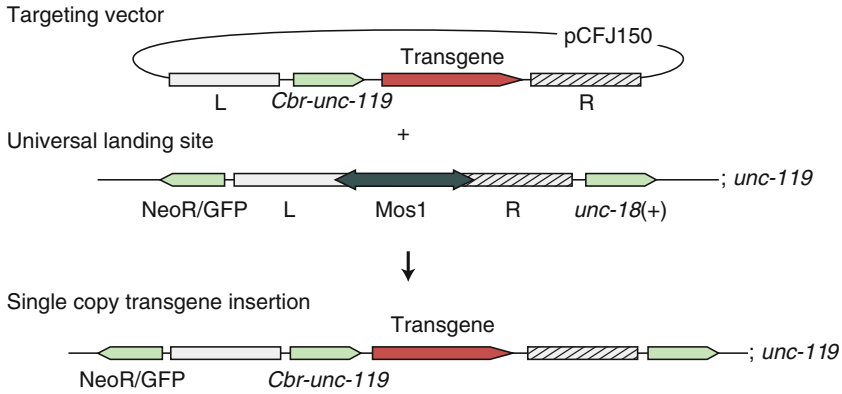

Fig. 2 Schematic of universal MosSCI sites. The universal MosSCI system relies on a set of landing sites that were introduced into locations across the genome. Because the sequence flanking the Mos1 transposon is identical for all insertion sites the same targeting vector (pCFJ150) can be used for insertion. The universal landing sites furthermore contain a selection marker adjacent to the insertion sites (NeoR or P*myo-2*:GFP) that facilitates following a MosSCI insertion in genetic crosses

Table 5
Co-injection markers

Plasmid	Description	Transgene
pCFJ601	Induces Mos1 transposition by injection	P*eft-3*:Mos1 transposase
pMA122	Negative selection, heat-shock inducible	P*hsp-16.41*:*peel-1*:*tbb-2* UTR
Red fluorescent markers		
pGH8	Visual array marker: Red, nervous system, cytosolic	P*rab-3*:mCherry:*unc-54* UTR
pCFJ90	Visual array marker: Red, pharynx, cytosolic	P*myo-2*:mCherry:*unc-54* UTR
pCFJ104	Visual array marker: Red, body wall muscle, cytosolic	P*myo-3*:mCherry:*unc-54* UTR
Green fluorescent markers		
pCFJ420	Visual array marker: Green, ubiquitous, nuclear	P*eft-3*:GFP:H2B:*tbb-2* UTR
pCFJ421	Visual array marker: Green, pharynx, nuclear	P*myo-2*:GFP:H2B:*tbb-2* UTR

2.5 Co-injection Markers

1. Make transfection-grade DNA preparations of all co-injection markers.
2. 2× red co-injection mix: 100 ng/μl pCFJ601, 20 ng/μl pMA122, 20 ng/μl pGH8, 5 ng/μl pCFJ90, 10 ng/μl pCFJ104 (*see* **Note 4**). Make 2× stock solution and store at −20 °C.
3. 2× green co-injection mix: 100 ng/μl pCFJ601, 20 ng/μl pMA122, 20 ng/μl pCFJ420, 5 ng/μl pCFJ421. Make 2× stock solution and store at −20 °C.

3 Methods

3.1 MosSCI Injections

1. Centrifuge the 2× co-injection mix and the targeting vector at highest speed on a tabletop microcentrifuge for 2 min.
2. Make 20 μl injection solution by mixing 10 μl of the 2× co-injection mix (*see* **Note 5**) with the targeting vector to a final concentration of 10–50 ng/μl. Bring the final concentration of DNA up to 100 ng/μl with a DNA ladder without dye or another inert stuffer DNA. Add molecular grade purified water to a final volume of 20 μl.
3. Immediately before injection, centrifuge the injection mix at highest speed on a tabletop microcentrifuge for 2 min.
4. Pick relatively healthy and unstarved young adult hermaphrodites for injection from strains maintained at 20 °C (*see* **Note 6**). Pick animals from the strain corresponding to the targeting vector (Tables 2 and 4).
5. Generate transgenic animals by following standard protocols for injection ([1] and Chapter 3) (*see* **Note 7**).
6. Place one to three injected animals on individual NGM plates seeded with OP50. Place NGM plates with injected animals in 25 °C incubator (*see* **Note 8**).

3.2 Isolation of Transgenic Animal with Single-Copy Insertion

1. After approximately 1 week and the injected animals have starved out the plate, heat-shock plates with injected animals for 1 h at 37 °C. Place animals at room temperature after the heat-shock. Animals with extrachromosomal arrays die from the heat-shock whereas animals with a transgene insertion survive (*see* **Note 9**).
2. The day after heat-shock, screen plates for transgene insertions with a fluorescence dissection microscope. Animals with transgene insertions are rescued for the mutant phenotype (*unc-119* or *unc-18*) but do not contain any of the fluorescent co-injection markers (*see* **Note 10**).
3. Pick three to four animals from each plate with a transgene insertion to a single NGM plate seeded with OP50 (*see* **Note 11**).

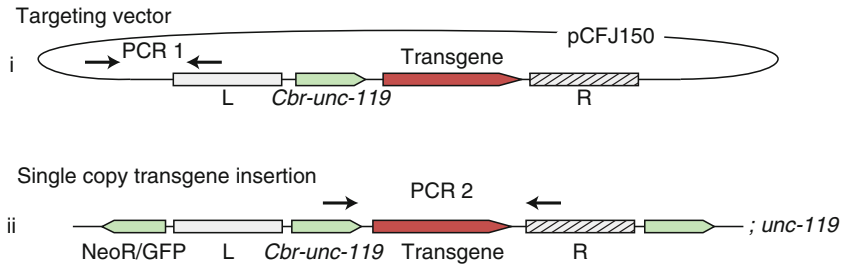

Fig. 3 Validation of MosSCI insertions. Approximately 15 % of MosSCI insertions contain one of the two errors, either dual insertion of the transgene or indels within the transgene. To validate full-length, single-copy insertions two strategies are used: (*i*) a PCR designed to detect the junction between the bacterial backbone of the targeting vector and the homology region. This DNA should not be present in the final strain and a positive PCR band therefore indicates a dual insertion. (*ii*) PCR amplification of the inserted transgene: Indels are typically large enough (approx. 1 kb [14]) to be detected by gel electrophoresis. For large transgenes, splitting the PCR into several smaller amplifications will facilitate the detection of aberrant insertions

4. 2–3 days later, verify that the selected animals do not express fluorescent co-injection markers and pick a single, clonal animal *with eggs* to a new plate from each plate. Only pick one insertion from each plate to ensure that all insertions are independent and treat each insertion as an independent allele (*see* **Note 12**).
5. In the following generation, pick four to eight clonal animals to individual plates to establish a strain that is homozygous for the insertion (*see* **Note 13**).

3.3 Validation of Single-Copy Transgene Insertion

1. If the inserted transgene contains a fluorescent marker (GFP for example), check each independent strain for fluorescence (*see* **Note 14**).
2. If insertion of only a single copy of the transgene is important then validate the strain by PCR amplification on genomic DNA derived from the strain with oligos designed to amplify the junction between the plasmid backbone and the homology regions that flank the transgene in the targeting vector (Fig. 3). Use the targeting vector as a positive control and N2 genomic DNA as a negative control for the PCR reaction. Single-copy insertions do not contain the plasmid backbone and should therefore not result in a visible amplification band.
3. Validate intact, full-length transgene insertions by PCR amplification across the entire transgene, either as a single amplicon or as separate amplicons using oligos that do not anneal in non-transgenic animals (*see* **Note 15**). Use N2 genomic DNA as the negative control for PCR reactions.
4. Give each validated MosSCI strain an allele name using the "Si" nomenclature corresponding to the lab allele designation (*see* **Note 16**).

4 Notes

1. *unc-119* and *unc-18* animals propagated on HB101 bacteria are healthier than mutant animals propagated on standard OP50 bacteria. HB101 bacteria is available from the *Caenorhabditis elegans* Genetics Center (CGC). Injections into relatively healthy animals are much more efficient than into starved animals. I therefore take great care to maintain relatively healthy animals by picking three individual adult animals to three separate spots on a recently seeded HB101 plate on a daily basis. The progeny from these picked animals are ready for injection after approx. 3–5 days.
2. Expression in the germline was tested with the ubiquitous *dpy-30* promoter driving GFP:histone expression. P*dpy-30* is highly sensitive to genomic position effects (CFJ, unpublished observations) and other germline-specific promoters may behave differently.
3. Preparation of injection plasmids (co-injection plasmids as well as targeting vectors) with a plasmid purification method that yields transfection-grade plasmids significantly improves the number of F1 progeny generated from each injection [15]. I routinely use the kit PureLink HQ miniPlasmid DNA Purification kit (Life Technologies).
4. In my experience, using all three fluorescent co-injection markers significantly reduces the number of false positive insertions.
5. I recommend using co-injection markers that are not homologous to the transgene; for example, for a GFP-tagged transgene I recommend using the mCherry markers. The repair process which copies the transgene into the genomic location is likely to be inhibited by the presence of several different homologous templates in the injection mix.
6. To facilitate freezing and handling, the strains contain an extrachromosomal array with *unc-119* rescue. Before MosSCI injections this array needs to be lost and injections should be performed into *unc-119* mutant animals.
7. The number of injected animals necessary to generate a single MosSCI insertion will depend on the transgene (for example, larger transgenes >10 kb are more difficult to insert) and on how experienced the researcher is at injecting. In my experience, insertions are generated in 10–50 % of injected animals but for researchers with less experience the insertion frequency is often closer to 1–5 %. Adjust the number of injections according to the size of the transgene and your injection experience.
8. The MosSCI insertion frequency appears to be independent of temperature [15] but there are two advantages to placing

animals at 25 °C. First, the animals develop faster and can be screened for insertions faster. Second, a higher percentage of MosSCI insertions are expressed in the germline when the injected animals are placed at 25 °C (Frøkjær-Jensen, unpublished observations). Even genotypically identical insertions do not necessarily express the transgene in the same way in the germline because of stochastic silencing by small RNAs [16].

9. Most animals with extrachromosomal arrays typically die within approx. 4 h of the heat-shock and plates can be scored the same day if necessary. Generally it is easier to score the animals the following day when even highly mosaic animals have died from the heat-shock.
10. Mostly, the negative selection with *peel-1* is very efficient with only a low frequency of false positives (approx. 10 %). However some laboratories report a much higher frequency of false positives. The plates can be screened for MosSCI insertions even in the absence of the negative selection marker but I suggest trying a higher concentration of the pMA122 plasmid if false positives occur at >10 % of rescued animals after the heat-shock.
11. Following injection and heat-shock the animals show a high frequency of sterility. Picking a single L1 animal with a transgene insertion is therefore often not enough to establish a line. Instead, I pick several L1 animals from the same plate and only select a clonal animal when they have become adults and the absence or presence of eggs is obvious.
12. When the Mos1 element is excised it sometimes inserts into another genomic location. So even if each strain contains the same insertion it is possible that the genetic background is different.
13. There is strong selection towards homozygosity of the transgene insertion, so the longer a mixed population is propagated the higher the proportion of homozygous animals will be.
14. Single-copy insertions are often dimmer than extrachromosomal arrays and the strains should therefore be checked for fluorescence on a microscope with high magnification.
15. Approximately 15 % of MosSCI insertions are either dual insertions or imperfect insertions that contain indels. In the absence of phenotypic rescue or consistent GFP fluorescence between several independent alleles, it is therefore important to validate each MosSCI insertion.
16. Alleles are designated by the lab-specific designation followed by “Si.” For example, the allele designation for Erik Jorgensen’s lab is “ox” and all MosSCI alleles are therefore named oxSi together with an allele number.

Acknowledgements

Strains with Mos1 elements were generated by the nemaGENETAG consortium. This work was supported by a postdoctoral fellowships from the Lundbeck and Carlsberg Foundations. The research was performed in the laboratory of Erik M. Jorgensen at University of Utah and supported by NIH grant 1R01GM095817 (E.M.J.) and Howard Hughes Medical Institute (E.M.J.).

References

1. Mello CC, Kramer JM, Stinchcomb D, Ambros V (1991) Efficient gene transfer in *C. elegans*: extrachromosomal maintenance and integration of transforming sequences. EMBO J 10: 3959–3970
2. Kelly WG, Xu S, Montgomery MK, Fire A (1997) Distinct requirements for somatic and germline expression of a generally expressed *Caenorhabditis elegans* gene. Genetics 146: 227–238
3. Fischer SEJ, Pan Q, Breen PC, Qi Y, Shi Z, Zhang C et al (2013) Multiple small RNA pathways regulate the silencing of repeated and foreign genes in *C. elegans*. Genes Dev 27: 2678–2695
4. Grishok A, Sinskey JL, Sharp PA (2005) Transcriptional silencing of a transgene by RNAi in the soma of *C. elegans*. Genes Dev 19:683–696
5. Tabara H, Sarkissian M, Kelly WG, Fleenor J, Grishok A, Timmons L et al (1999) The rde-1 gene, RNA interference, and transposon silencing in *C. elegans*. Cell 99:123–132
6. Vastenhouw NL, Fischer SEJ, Robert VJP, Thijssen KL, Fraser AG, Kamath RS et al (2003) A genome-wide screen identifies 27 genes involved in transposon silencing in *C. elegans*. Curr Biol 13:1311–1316
7. Praitis V, Casey E, Collar D, Austin J (2001) Creation of low-copy integrated transgenic lines in *Caenorhabditis elegans*. Genetics 157:1217–1226
8. Kage-Nakadai E, Kobuna H, Funatsu O, Otori M, Gengyo-Ando K, Yoshina S et al (2012) Single/low-copy integration of transgenes in *Caenorhabditis elegans* using an ultraviolet trimethylpsoralen method. BMC Biotechnol 12:1
9. Chen C, Fenk LA, de Bono M (2013) Efficient genome editing in *Caenorhabditis elegans* by CRISPR-targeted homologous recombination. Nucleic Acids Res 41, e193
10. Dickinson DJ, Ward JD, Reiner DJ, Goldstein B (2013) Engineering the *Caenorhabditis elegans* genome using Cas9-triggered homologous recombination. Nat Methods 10: 1028–1034
11. Bessereau JL, Wright A, Williams DC, Schuske K, Davis MW, Jorgensen EM (2001) Mobilization of a Drosophila transposon in the *Caenorhabditis elegans* germ line. Nature 413: 70–74
12. Robert V, Bessereau J-L (2007) Targeted engineering of the *Caenorhabditis elegans* genome following Mos1-triggered chromosomal breaks. EMBO J 26:170–183
13. Frøkjær-Jensen C, Davis MW, Ailion M, Jorgensen EM (2012) Improved Mos1-mediated transgenesis in *C. elegans*. Nat Methods 9:117–118
14. Frøkjaer-Jensen C, Davis MW, Hopkins CE, Newman BJ, Thummel JM, Olesen S-P et al (2008) Single-copy insertion of transgenes in *Caenorhabditis elegans*. Nat Genet 40: 1375–1383
15. Frøkjær-Jensen C, Davis MW, Sarov M, Taylor J, Flibotte S, LaBella M et al (2014) Random and targeted transgene insertion in *Caenorhabditis elegans* using a modified Mos1 transposon. Nat Methods 11:529–534
16. Shirayama M, Seth M, Lee H-C, Gu W, Ishidate T, Conte D Jr et al (2012) piRNAs initiate an epigenetic memory of nonself RNA in the *C. elegans* germline. Cell 150: 65–77

Chapter 6

Creating Genome Modifications in *C. elegans* Using the CRISPR/Cas9 System

John A. Calarco and Ari E. Friedland

Abstract

The clustered, regularly interspaced, short, palindromic repeat (CRISPR)-associated (CAS) nuclease Cas9 has been used in many organisms to generate specific mutations and transgene insertions. Here we describe a method using the *S. pyogenes* Cas9 in *C. elegans* that provides a convenient and effective approach for making heritable changes to the worm genome.

Key words *C. elegans*, CRISPR, Cas9, Genome editing, Genome engineering

1 Introduction

Clustered, regularly interspaced, short, palindromic repeats (CRISPR) and the CRISPR-associated endonuclease Cas9 have recently been used to generate custom mutations, indels, and transgene insertions in a wide variety of organisms, including *Caenorhabditis elegans* [1–3]. Through this exciting technology, cells in the *C. elegans* germ line can be targeted with *Streptococcus pyogenes* Cas9 and its associated guide RNAs to produce transgenic strains as desired. Thus far, the method requires microinjection of Cas9 and single-guide RNA (sgRNA) components into the gonads of adult hermaphrodites to generate both somatic and heritable, germline mutations. Several research groups have successfully generated mutants by injection of different combinations of Cas9 and sgRNA encoded by DNA on plasmids, through injection of RNA, and even direct injection of Cas9 protein [4–13]. Here, we describe our method of choice, which relies solely on the use of DNA plasmids that encode Cas9 nuclease driven by a strong promoter with expression in the germline and U6 snRNA promoter-driven sgRNAs [7, 10]. However, different approaches may have

David Biron and Gal Haspel (eds.), *C. elegans: Methods and Applications*, Methods in Molecular Biology, vol. 1327,
DOI 10.1007/978-1-4939-2842-2_6,

different advantages depending on the type of genome modification required, and it is recommended to additionally consult the other references cited in this protocol.

2 Materials

2.1 Worm Strains and Maintenance

1. The worm strain N2 from Bristol [14] is used for all experiments. This can be acquired from the *Caenorhabditis* Genetics Center (CGC).
2. Incubator set to 25 °C and incubator or water bath set to 34 °C.
3. OP50: This bacterial strain can also be acquired from the CGC.
4. 6 cm seeded nematode growth medium (NGM) agar plates: For 1 L of NGM agar media, mix 3 g NaCl, 17 g agar, 2.5 g peptone, and water to a final volume of 972 mL, and autoclave. After autoclaving and cooling to 50 °C, using sterile technique add 1 mL of 1 M $CaCl_2$, 1 mL of 1 M $MgSO_4$, 25 mL of 1 M potassium phosphate buffer pH 6, and 1 mL of cholesterol (5 mg/mL stock in ethanol). Dispense media into plates and allow to solidify at room temperature overnight. Seed plates with a diluted overnight culture of *Escherichia coli* strain OP50. Allow seeded bacteria to dry and grow to a lawn for 24 h at room temperature. Plates can be stored at 4 °C for several weeks in sealed containers.

Worms are maintained essentially as described in [14].

2.2 Plasmids for Generating Indels

1. Peft-3::Cas9-SV40_NLS::tbb-2 3′UTR: A plasmid expressing Cas9 under a strong promoter with activity in the germ line. Available through Addgene (http://www.addgene.org/46168/).
2. PU6::klp-12_sgRNA: A plasmid expressing a high-efficiency sgRNA targeting the *klp-12* gene. This plasmid can serve both as a positive control plasmid for establishing good cleavage conditions, and a vector for cloning new sgRNA targeting sequences. Available through Addgene (http://www.addgene.org/46170/).
3. pCFJ104 (Pmyo-3::mCherry::unc-54 3′UTR): A plasmid used as a co-injection marker to label transgenic F1 progeny. Animals carrying this marker express mCherry in body wall muscles (*see* **Note 1**). Available through Addgene (http://www.addgene.org/19328/).

2.3 Additional Plasmids/DNA for Homologous Recombination and Transgene Insertion

1. pCFJ90 (Pmyo-2::mCherry::unc-54 3′UTR): A plasmid used as a co-injection marker to label transgenic F1 progeny. Animals carrying this marker express mCherry in the pharynx (*see* **Note 1**). Available through Addgene (http://www.addgene.org/19327/).
2. pMA122 (Phsp-16.41::peel-1::tbb-2 3′UTR): A negative selection marker used to select against animals carrying extrachromosomal arrays and assist with identifying animals that have endogenous locus insertions (*see* **Note 2**). Available through Addgene (http://www.addgene.org/34873/).
3. pDD04 (contains Prps-27::neoR::unc-54 3′UTR): A plasmid that can be used as a source of a transgene expressing a neomycin resistance cassette in *C. elegans*. Useful for positive selection of animals carrying insertions in the genome (*see* **Note 3**). Available through Addgene (http://www.addgene.org/26393/).
4. pDD104 (Peft-3::Cre::tbb-2 3′UTR): A plasmid that expresses Cre recombinase under the control of the strong *eft-3* promoter. Can be used to excise unwanted selection cassettes after selection has been performed. Available through Addgene (http://www.addgene.org/47551/).
5. Any standard cloning vector with a multiple cloning site, to be used for making custom repair templates.
6. N2 genomic DNA: Used to amplify homology arm regions and other transgene components.

2.4 Molecular Cloning

1. High-fidelity DNA polymerase and dNTPs.
2. Gibson Assembly cloning kit (NEB).
3. sgRNA oligonucleotides:

   P1 (U6prom EcoRI F): CGGGAATTCCTCCAAGAACT CGTACAAAAATGCTCT

   Primer P1 is an upstream primer to amplify a PCR product including the U6 promoter and new sgRNA targeting sequence.

   P2: ($N_{20\text{-}RC}$)CTGCAGGTGCAAACATTTAGATTTGCAAT TCAATTATATAG (where $N_{20\text{-}RC}$ is the reverse complementary sequence of the N_{20} target sequence used in primer P3).

   Primer P2 will be used with Primer P1 to amplify the upstream U6 promoter and new sgRNA targeting sequence.

   P3: (N_{20})GTTTTAGAGCTAGAAATAGCAAGTTA (where N_{20} represents the sgRNA target sequence).

   Primer P3 is a forward primer used to incorporate the new sgRNA targeting sequence and amplify the sgRNA scaffold.

   P4 (U6prom HindIII R): CGGAAGCTTCACAGCCGAC TATGTTTGGCGT.

Primer P4 will be used with Primer P3 to amplify the new sgRNA targeting sequence and sgRNA scaffold region.

4. EcoRI and HindIII restriction enzymes.
5. T4 DNA ligase and 10× ligase buffer (Thermo Scientific, EL0014).
6. DH5-alpha library efficiency competent cells.
7. Gel extraction kit and PCR purification kit.
8. Plasmid miniprep kit (Thermo Scientific, K0503) and midiprep kit (Qiagen, 12143) (*see* **Note 4**).

2.5 Microinjection Setup

1. Microinjector apparatus, which generally includes an inverted microscope with suitable filters for differential interference contrast (DIC) microscopy and equipped with low (10×) and high (40×) lenses. Additional items include a micromanipulator for manipulating the injection needle during injection, a pressure-regulated pump, and a capillary needle puller. For details *see* ref. 15.
2. Dry agarose pads: Prepare 2 % agarose solution in sterile ddH_2O, and melt agarose in microwave. Using a Pasteur pipette with a broken tip as a dropper, place one drop of molten agarose solution on a 22 × 40 mm glass cover slip, and place another cover slip on top of the drop. Allow to solidify for several minutes at room temperature and remove top cover slip. Allow pads to air-dry overnight. We generally prepare many of these pads at once and store them in a cover slip container.
3. Halocarbon oil: For immersion of animals on agarose pads prior to injection.
4. M9 medium: 22 mM KH_2PO_4, 22 mM Na_2HPO_4, 85 mM NaCl, 1 mM $MgSO_4$. For recovery of animals after injection.
5. Glass capillaries: For pulling injection needles for microinjection.

2.6 Drug Selection and Screening

1. G418 disodium salt (Sigma, A1720-5G): Dilute in water to 25 mg/mL concentration. Filter sterilize.
2. Single-worm lysis buffer: 50 mM KCl, 10 mM Tris-HCl pH 8.0, 2.5 mM $MgCl_2$, 0.45 % NP-40, 0.45 % Tween-20, 100 μg/mL proteinase K.

3 Methods

3.1 sgRNA Design and Selection Considerations

1. In our original study [7], we identified genomic target sequences for sgRNAs that were of the form $G/A(N)_{19}NGG$. We required the first nucleotide to be a purine because previous studies suggested that RNA polymerase III promoters (like

our U6 promoter driving sgRNA expression) more efficiently transcribe when the +1 base is a purine. We have now demonstrated that additional nonhomologous sequence can be added to the 5′ end of transcribed sgRNAs while maintaining their cleavage efficiency (A.E.F. and J.A.C., unpublished results). This observation allows for enhanced flexibility of target site selection, where the restriction on genomic target sequence is now simply N_{20}NGG (*see* Fig. 1a for details).

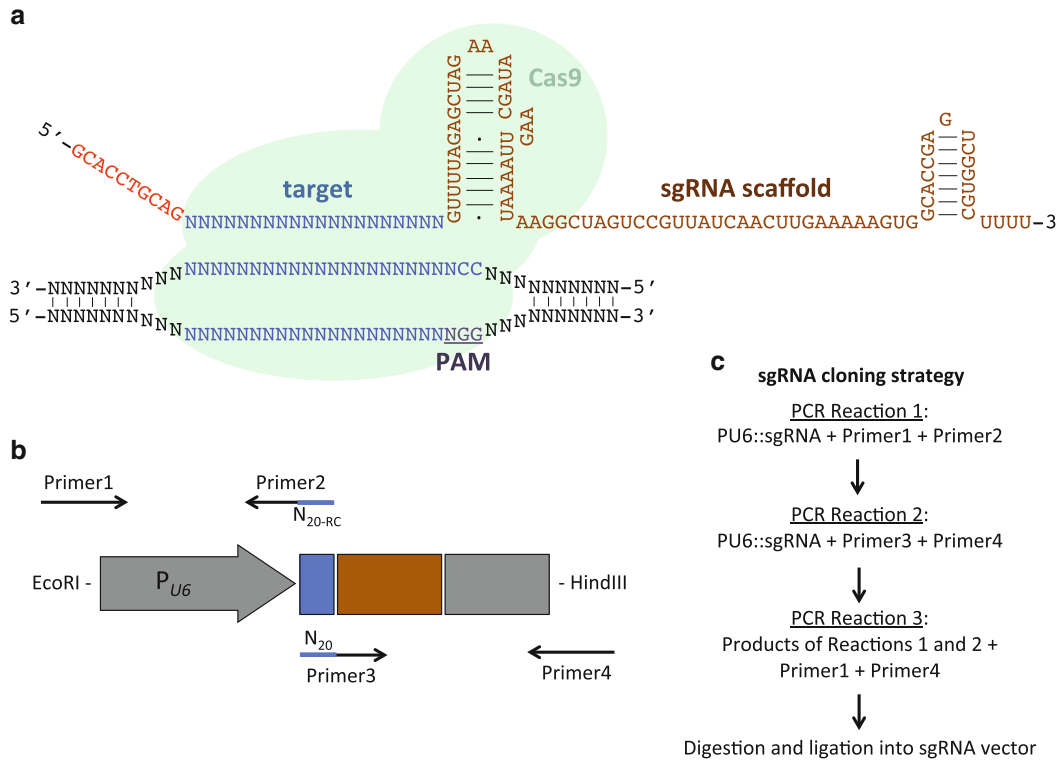

Fig. 1 Schematic of sgRNA architecture and cloning. (**a**) Diagram of sgRNA after expression from U6 promoter. *Red highlighted sequence* is additional heterologous sequence included at the 5′ end of the sgRNA. The G at the 5′ end serves as a purine at position +1 for efficient transcription from the U6 promoter. The *blue* (N_{20}) *sequence* represents the target sequence, chosen by scanning an appropriate region of genomic DNA (diagramed below the Cas9/sgRNA complex) of the form (N_{20})NGG, where the NGG is the protospacer adjacent motif (PAM—highlighted in *purple*). The *orange* highlighted text is the sgRNA scaffold, required for interactions with Cas9. Cas9 is depicted in *light blue*. (**b**) Organization of primers for cloning new sgRNAs. *Grey block arrow* and *grey block* represent upstream promoter and downstream genomic sequence, respectively, surrounding a U6 snRNA gene. *Blue block* represents the target sequence of interest for the sgRNA, and the *dark orange block* represents the sgRNA scaffold sequence. Primers 1 and 4 introduce EcoRI and HindIII sites, and primers 2 and 3 incorporate the new target sequence by PCR stitching (*blue lines* on *black arrows*, $N_{20\text{-RC}}$ and N_{20}, respectively). (**c**) Scheme for cloning new sgRNAs by PCR stitching. PCR reactions 1 and 2 are carried out in parallel, and then the products of these reactions are used as templates in a second-round PCR step (reaction 3). The final product is then digested and cloned into the sgRNA vector

2. If knockout of a protein-coding gene is desired, sgRNAs should target sequences near the 5′ end of known open reading frames. This will make any sequence disruptions likely to create frameshifts early in the coding sequence and premature termination codons.
3. Where possible, it is also desirable to look for target sequences that have a restriction enzyme recognition sequence containing the cut site a few bases upstream of the protospacer-adjacent motif PAM. This will facilitate prescreening F1 progeny by restriction fragment length polymorphism (RFLP) assays. However, this last consideration is not a requirement because there are alternative methods that can be used to verify the presence of an indel (see below).
4. Several sgRNAs should be tested for a given locus. We have observed significantly different efficiency (up to an order of magnitude) in our ability to generate heritable mutations when comparing independent sgRNAs targeting the same genetic locus. A recent study has indicated that sgRNAs with two terminal G nucleotides (i.e N18GG) in the 20mer targeting sequence can lead to dramatic increases in cleavage efficiency [16].

3.2 Cloning New sgRNA Plasmids

1. Amplify upstream (reaction 1) and downstream (reaction 2) sgRNA amplicons using PU6::klp-12_sgRNA as a template (*see* Fig. 1b, c for schematic and outline). Primers P2 and P3 will incorporate the new sgRNA targeting sequence ($N_{20\text{-}RC}$ and N_{20}, respectively) in Subheading 2.4:

Reaction 1

34 μL ddH_2O

10 μL 5× HF buffer

1 μL 10 mM dNTP mix

1.25 μL 10 μM P1

1.25 μL 10 μM P2

2 μL 50 ng/μL PU6::klp-12_sgRNA vector

0.5 μL Phusion polymerase

Total volume: 50 μL

Reaction 2

34 μL ddH_2O

10 μL 5× HF buffer

1 μL 10 mM dNTP mix

1.25 μL 10 μM P3

1.25 μL 10 μM P4

2 μL 50 ng/μL PU6::klp-12_sgRNA vector

0.5 μL Phusion polymerase

Total volume: 50 μL

2. Run reactions in a thermal cycler with the following program: 98 °C for 45 s (98 °C for 30 s, 55 °C for 30 s, 72 °C for 15 s) × 35 cycles, 72 °C for 5 min, and 4 °C hold.
3. Gel purify PCR amplicons from reaction 1 and reaction 2 by agarose gel electrophoresis (1 % agarose gel) and using a gel extraction kit (*see* **Note 5**).
4. Amplify a stitched sgRNA amplicon by using amplicons from reaction 1 and reaction 2 as templates (reaction 3).

Reaction 3

34 μL ddH_2O

10 μL 5× HF buffer

1 μL 10 mM dNTP mix

1.25 μL 10 μM P1

1.25 μL 10 μM P4

1 μL amplicon from reaction 1 (5–10 ng)

1 μL amplicon from reaction 2 (5–10 ng)

0.5 μL Phusion polymerase

Total volume: 50 μL

5. Run reaction in a thermal cycler with the following program: 98 °C for 45 s (98 °C for 30 s, 55 °C for 30 s, 72 °C for 30 s) × 35 cycles, 72 °C for 5 min, and 4 °C hold.
6. Clean up PCR amplicon from reaction 3 using a PCR purification kit.
7. Digest PU6::klp-12_sgRNA and clean PCR amplicon from **step 6** with EcoRI and HindIII restriction enzymes. Gel purify digested vector backbone and PCR amplicon using agarose gel electrophoresis (1 % agarose gel).
8. Ligate the digested amplicon with the digested PU6::klp-12_sgRNA vector (reaction 4). A control ligation with vector only will help assess enrichment of transformed bacteria carrying amplicon insertions in the vector (reaction 5).

Reaction 4

$(16 - x - y)$ μL ddH_2O

xμL digested vector (50 ng)

yμL digested stitched amplicon (40 ng)

2 μL 10× T4 DNA ligase buffer

2 μL T4 DNA ligase

Total volume: 20 μL

Reaction 5 (control ligation)

$(16 - x)$ µL ddH_2O

xµL digested vector (50 ng)

2 µL 10× T4 DNA ligase buffer

2 µL T4 DNA ligase

Total volume: 20 µL

9. Incubate ligation reactions at room temperature for 1 h. Transform 5 µL of each ligation reaction into 45 µL DH5alpha competent cells according to the manufacturer's recommendations, and then spread bacteria onto LB + ampicillin plates. Incubate at 37 °C overnight.
10. Pick and grow up bacterial colonies from plate containing bacteria transformed with reaction 4, purify plasmids, and screen for insertion of sgRNA cassette by standard restriction digest analysis.
11. Further verify correct sgRNA insert by sequencing the vector by Sanger sequencing using primers P1 and P4.

3.3 Inject Cas9 and sgRNA Plasmids

1. The day before injection, pick L4-stage animals on NGM agar plates seeded with OP50 bacteria. Allow the animals to develop overnight at room temperature. Animals will reach adulthood the next day for injection.
2. On the day of injection, prepare the injection mix using the following concentrations of plasmids (*see* **Notes 4**, **6**, and **7**):

   50–200 ng/µL Peft-3::Cas9-SV40_NLS::tbb-2 3′UTR

   50–200 ng/µL PU6::sgRNA vector of interest

   5 ng/µL pCFJ104 (or other co-injection marker)
3. Inject and recover animals as described in [15]. For an efficient sgRNA, injecting 15–20 animals should be sufficient to obtain progeny with germline indels.
4. Place two or three injected animals per plate on NGM agar plates seeded with OP50. Incubate animals at 25 °C.

3.4 Screening Animals for Heritable Indels

1. Three to four days after injection, pick F1 progeny (generally L4-young adult animals) expressing mCherry in body wall muscle cells. Pick 40–50 animals, placing one to three animals per plate. Incubate transgenic F1 progeny at 25 °C for 2 days to allow these animals to generate F2 progeny.
2. After 2 days, place single F1 mothers in 6 µL lysis buffer and incubate animals in thermal cycler under the following conditions: 60 °C for 1 h, 95 °C for 15 min, and 4 °C hold.
3. Using an aliquot of the lysed animal solution as a template, amplify the genomic region by PCR using primers surrounding

the sgRNA-targeted sequence. For all downstream validation methods, a 200–300 bp amplicon would be an appropriate length.

4. Several options exist for verifying heritable indel mutations:
   (a) If an sgRNA was designed to target a region that also overlaps a site cleaved by a restriction enzyme, PCR amplicons from lysed F1 animals can be screened by digestion with the appropriate restriction enzyme followed by agarose gel electrophoresis [7]. Animals carrying indel mutations that have disrupted the restriction endonuclease cleavage site will show incomplete digestion patterns on a gel.
   (b) Amplicons from lysed F1 animals can also be screened using the CEL-1 and/or T7 endonuclease assays [9, 17].
   (c) It has recently been demonstrated that F1 PCR products can also be screened for the presence of indels simply by resolving potential heteroduplexes (which migrate anomalously) by electrophoresis on a 6 % polyacrylamide gel [18].
   (d) Amplicons from lysed F1 animals can also be directly sequenced by Sanger sequencing. Heterozygous mutations can be resolved by analysis of sequencing traces [7].
5. Once F1 animals harboring indels are identified, F2 progeny from the original plates can be retrieved, and homozygotes can be obtained and monitored for inheritance of the mutation in subsequent generations (*see* **Note 8**).

3.5 Considerations for Generating Custom Insertions

1. *Type of insertion or mutation desired*: A number of different strategies have proven to be effective for insertion of small tags like His, Myc, or FLAG epitopes, as well as single-point mutations into animals. The use of single-stranded oligonucleotides coupled with either TALEN- or CRISPR/Cas9-mediated cleavage has been effective at inserting small indels or inserting FRT sites into defined loci to enable larger deletion alleles to be generated [9, 12, 19, 20]. For insertion of larger tags or more complex genome editing events, introducing a repair template with longer homology arms (generally via a plasmid) has been a preferred method of choice [4, 6, 10]. However, a recent study has demonstrated that length of homology arms can be shortened to as little as 30–60 base pairs when the template is injected as a linear molecule [20].
2. *Selection or screen*: In several cases reported, the CRISPR/Cas9 system can be efficient enough at generating custom insertions of large cassettes (promoter::GFP transgenes) such that simply screening for these insertions is possible, in particular if the resultant transgenic animal phenotype is easy to score (i.e., a visible phenotype or fluorescent pattern) [10, 21] (Fig. 2a).

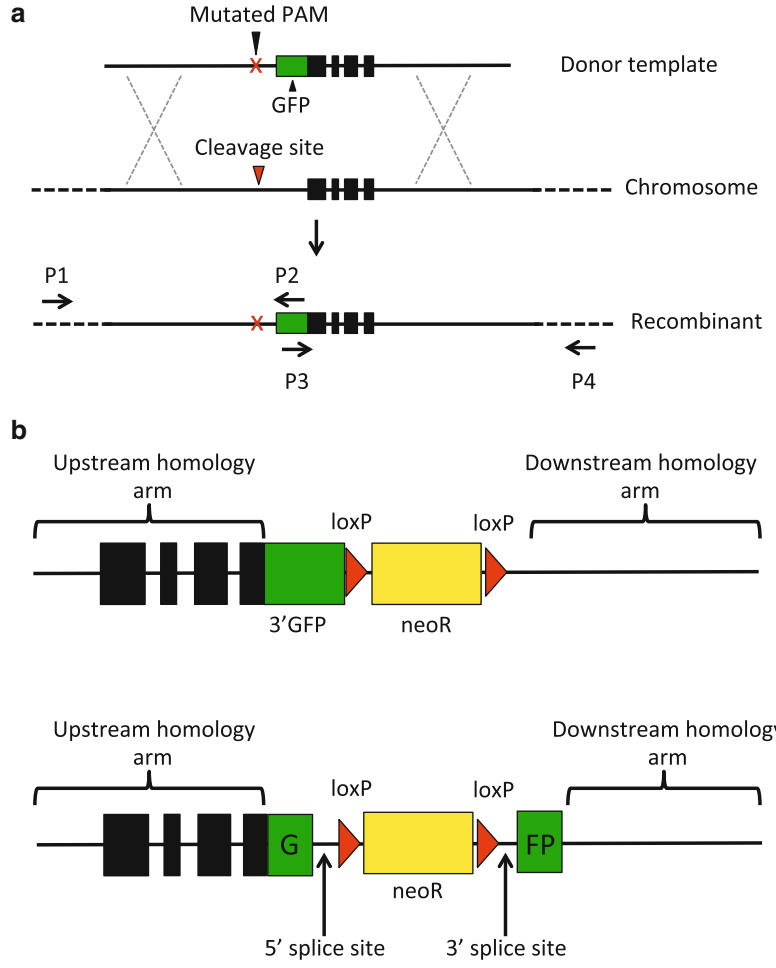

Fig. 2 Design suggestions for homologous recombination-mediated gene targeting. (**a**) Screening method. In this method, the transgene of interest (in this example a GFP transgene, *green block*) is cloned into a donor repair template together with homologous regions in the vicinity of a genomic site targeted by an sgRNA/Cas9 complex. If the region being targeted by Cas9 will be in the donor repair template, it is recommended to introduce a silent mutation in the PAM sequence (*red X*) to avoid the donor being cleaved by Cas9. Insertions can then be directly screened in F1 animals transgenic for a marker of interest by a PCR strategy using primers specific to the transgene and primers that lie outside the homology regions used in the donor template (*dashed lines*). Alternatively, insertions can be screened visually if homologous recombination events introduce a visible phenotype. (**b**) Selection method. Two transgene options are depicted. The *top panel* introduces a GFP tag immediately after the 3′ end of the coding sequence of a gene of interest. A neomycin resistance cassette (*yellow block*) flanked by loxP sites (*red triangles*) is positioned immediately downstream of the GFP tag. After selection and insertion of the transgene, the resistance cassette can be removed by injecting Cre recombinase, leaving a single loxP site at the beginning of the 3′UTR. The *bottom panel* depicts a second strategy where the loxP-neomycin resistance cassette-loxP is located within a heterologous constitutively spliced intron, inserted in a split GFP coding sequence. After selection and insertion of the transgene, Cre recombinase can once again be used to excise the cassette, leaving the single loxP site contained in the heterologous intron, which would be spliced out in mature mRNAs

A screening approach has the advantage of not requiring selectable markers to be included in the transgene and experimental design, especially if these selectable markers are undesirable and require special genetic backgrounds. A disadvantage of a screening approach is that if the efficiency of obtaining a transgenic is low, it can be quite laborious to recover a rare transformed animal from the population of non-transgenic animals. Several recent studies have suggested that germ cells that have undergone genome editing at one locus have a higher likelihood to also be edited at a locus of interest [19, 21]. In light of these results, the use of a co-injection strategy using combinations of sgRNAs and/or repair templates giving visible phenotypes can assist in reducing the number of animals required to be screened for insertions of interest [16, 19, 21, 22]. However, in other cases a selection approach may also be appropriate (Fig. 2b), and several selection schemes have been created to make this strategy effective [4, 6]. Below, we present a selection strategy that works using a positive selection cassette conferring neomycin resistance (neoR) [23] that can later be excised by Cre/loxP recombination [6], and a negative selection plasmid expressing the toxin PEEL-1 [24, 25].

3. *Preselecting a suitable sgRNA for homologous recombination experiments*: In most cases, we recommend testing the cleavage efficiency of several sgRNAs surrounding an intended site of transgene-mediated homologous recombination as described in Subheading 3.4. Once an sgRNA is found to have suitable cleavage efficiency, it can be used for transgene-mediated homologous recombination.

3.6 Creating a Donor Repair Template for Homologous Recombination

1. Amplify upstream and downstream homology arms (~1–1.5 kb genomic fragments) (*see* **Notes 9** and **10**) by PCR using N2 genomic DNA as a template. PCR primers should include 25 nucleotides that share terminal homology to neighboring cloning fragments for the downstream Gibson assembly [26, 27] cloning step (*see* Fig. 2b for design suggestions).
2. Amplify NeoR cassette with primers Px and Py using pDD04 as a template. Again, PCR primers should include 25 nucleotides that share homology with neighboring cloning fragments for the Gibson assembly cloning step (*see* Fig. 2b for design suggestions).
3. Amplify the transgene of interest. Again, include 25 nucleotides of terminal homology in primer sequences for Gibson assembly step.
4. Gel purify amplified PCR products along with an appropriate linearized cloning vector (*see* **Note 11**).
5. Stitch together PCR fragments and vector using the Gibson assembly approach [26], as recommended by the manufacturer.

6. Transform bacteria with incubated Gibson assembly reactions. Proceed to grow and screen bacterial colonies as described above by standard molecular cloning techniques.

3.7 Injecting Animals for Homologous Gene Targeting

1. The day before injection, pick L4-stage animals on NGM agar plates seeded with OP50 bacteria. Allow the animals to develop overnight at room temperature. Animals will reach adulthood the next day for injection.
2. On the day of injection, prepare the injection mix using the following concentrations of plasmids:

   50 ng/μL Peft-3::Cas9-SV40_NLS::tbb-2 3′UTR

   50 ng/μL PU6::sgRNA vector of interest

   50 ng/μL donor repair template plasmid (*see* **Note 12**)

   5 ng/μL pCFJ104

   2.5 ng/μL pCFJ90

   10 ng/μL pMA122
3. Inject and recover animals as described in [15]. We recommend injecting at least 60 animals, but possibly more depending on the quality of injections.
4. Place two to three injected animals per plate on 6 cm NGM agar plates seeded with OP50. Incubate animals at 25 °C.

3.8 Selection of Animals with Custom Transgene-Mediated Genome Modifications

1. When a significant number of transgenic F1 progeny (Pmyo-2 and Pmyo-3::mCherry positive) are visible, usually 24–48 h after injected animals have been incubating at 25 °C, add 500 μL of a 25 mg/mL solution of G418 directly to each plate. Swirl G418 solution to ensure that the entire plate is coated with liquid, and return plates to the 25 °C incubator without their lids to allow the antibiotic solution to absorb into the plates. When the plates are fully dry, cover them once again with their lids.
2. (a) Allow plates to fully starve out (usually 7–10 days). After positive selection, only animals with insertions and animals carrying extrachromosomal arrays should be alive. In order to select against animals carrying extrachromosomal arrays (which should contain the Phsp-16.41::peel-1 toxin transgene), the animals are heat shocked in one of the two ways: incubation in an air incubator for 2 h at 34 °C, or incubation in a water bath for 2 h at 34 °C (*see* **Note 13**). Allow worms to recover for at least 4 h at 25 °C. Proceed to optional **step 2b** or directly to **step 3**.

   (b) (Optional) For each plate that still has healthy-looking animals, pick 10–20 animals that are moving well and have lost all fluorescent injection markers and place on a fresh NGM agar plate with OP50 and containing G418 as

prepared in **step 1**. Alternatively, the heat-shocked plates could be chunked onto fresh antibiotic plates. Allow animals to grow for one additional generation. This step is generally not necessary, but confirms that animals are indeed G418 resistant and have not simply escaped selection.

3. Pick ten healthy-looking animals that have lost all fluorescent injection markers and single to ten NGM agar plates. Incubate animals at 25 °C for 2 days to allow these animals to generate progeny.
4. After 2 days, place single mothers in 6 μL lysis buffer and incubate animals in thermal cycler under the following conditions: 60 °C for 1 h, 95 °C for 15 min, and 4 °C hold.
5. Using an aliquot of the lysed animal solution, test for insertions by PCR at both recombination boundaries using primers that anneal outside the termini of the homology arms used in the donor repair template, as well as primers specific to custom genetic modification (Fig. 2a). In cases where PCR products of the correct size are detected at both boundaries, return to plates where mothers originated from and screen progeny to recover animals homozygous for the desired genome modification.
6. Perform follow-up assays to confirm proper insertion of desired modification. For example, in the case of insertion of a fluorescent protein tag or some other epitope, the modification could be assessed by fluorescence microscopy, immunofluorescence, or a western blot (*see* **Note 14**).
7. (Optional) If the neoR selection cassette is unwanted in the final transgenic animal, it can be removed by injecting Cre recombinase into animals homozygous for insertions essentially as described in the scheme by Dickinson and colleagues [6] (*see* **Note 15**).

4 Notes

1. Any co-injection marker plasmid that confers an easy-to-score phenotype could be substituted for pCFJ104 and pCFJ90.
2. An additional highly effective negative selection scheme to eliminate animals with extrachromosomal arrays has been developed [28] using the strain DA1316 (*avr-14(ad1302) I*; *avr-15(ad1051) glc-1(pk54) V*). These animals are resistant to the drug ivermectin, and animals carrying extrachromosomal arrays with plasmid pCCM416 (Pmyo-2::avr-15) will not survive on plates containing ivermectin.

3. Additional drug resistance cassettes, conferring puromycin resistance [29], hygromycin resistance [4], and blasticidin resistance [21], are also available and could be used for a similar purpose.
4. For best injection results, prepare plasmid DNA with Qiagen midi kits. However, we have also had success with standard miniprep kits (we use the Thermo Scientific GeneJET purification kit). We have heard anecdotes that purity of DNA plasmids that are used in *C. elegans* gonad injections is critical, and less pure solutions that are obtained from minipreps can potentially result in toxicity, mixed results, or even a failure to acquire transgenic progeny.
5. Although gel purification is not generally necessary for PCR stitching, the original PCR template used in reactions 1 and 2 contains an sgRNA cassette that targets the *klp-12* locus. Gel purification helps ensure that the original template is not utilized in amplification cycles in reaction 3.
6. We frequently use our klp-12 targeting plasmid to test injection conditions. The cleavage efficiency of this guide RNA is quite high under optimal conditions (~80 % of F1 progeny contain an indel), and there is a restriction enzyme site just upstream of the PAM which enables easy screening with an RFLP assay.
7. We have found that when injecting higher concentrations (200 ng/μL) of Cas9 and sgRNA vectors we have noticed higher efficiency of generating heritable indels. If it is found that injecting at these concentrations results in too much toxicity, we recommend reducing the concentrations as needed.
8. A limited number of studies have suggested that off-target cleavage and indels do not occur in *C. elegans* [5–7]. However, we recommend that transgenic animals be outcrossed several times to ensure that any additional background mutations should be eliminated.
9. We base 1 kb as a minimum length for each homology arm as a reasonable length, because this is the minimum homology arm length we have used thus far to obtain transgenic animals [10]. We are uncertain whether longer or shorter homology arms would increase or decrease efficiency, respectively. This is a parameter that could be manipulated.
10. During construction of a donor vector for homology-dependent repair, put a silent mutation in the PAM sequence if possible so that the guide RNA that is used to generate the double-strand break in the DNA at the genomic locus is not effective at targeting the donor sequence. This silent mutation optimally maintains the amino acid sequence of the gene that is being targeted, but inhibits PAM recognition of the donor.

11. We generally prepare any standard cloning vector by linearizing it with one or two convenient restriction enzymes. We then design our transgene/selection cassette PCR primers to include 25 nucleotides of terminal homology with the 5′ and 3′ ends of the linearized vector, in preparation for Gibson assembly.
12. As noted above in **Note 4**, the suggested injection mix concentrations for the Cas9, sgRNA, and donor repair template serve as a good starting point. All three of these concentrations can be adjusted if excessive toxicity is observed.
13. Both incubation in an air incubator or water bath have been demonstrated to work [24], but we generally take the extra effort to use the water bath method.
14. As mentioned in **Note 7**, we recommend that transgenic animals be outcrossed several times to ensure that any additional background mutations should be eliminated.
15. In the study of Dickinson and colleagues [6], an *unc-119* selectable marker is used and transgenesis is performed in an *unc-119(ed3)* genetic background, making it easier to identify animals that lost the selection marker (by identifying animals that have reverted to displaying an uncoordinated phenotype). However, recombination is fairly efficient, and can also be screened by looking for loss of the cassette by PCR genotyping using primers flanking the loxP sites.

Acknowledgements

We would like to thank the many investigators who have contributed to the recent developments in genome editing and transgenesis techniques in *C. elegans*. These studies have been referenced throughout our manuscript and should be consulted for additional advice and tips for genome editing. In particular, we thank the Jorgensen, Dupuy, and Goldstein laboratories for the development of highly useful selectable markers and strategies that are effective for both Mos- and CRISPR/Cas9-based editing approaches. Many of the approaches and reagents described by these groups have been helpful in establishing the current methodology described here. We have also greatly appreciated excellent collaborations with Yonatan Tzur, Monica Colaiacovo, Kevin Esvelt, and George Church which led to the original protocol that the current approach is based upon. We also thank Heesun Kim, Masaki Shirayama, and Craig Mello for continued stimulating discussions regarding improvements in this exciting technology. Our work has been supported by US National Institutes of Health Early Independence Award (1DP5OD009153) and additional support from Harvard University to J.A.C. and a Ralph Ellison/American Federation for Aging Research postdoctoral fellowship to A.E.F.

References

1. Mali P et al (2013) Cas9 as a versatile tool for engineering biology. Nat Methods 10:957–963
2. Frokjaer-Jensen C (2013) Exciting prospects for precise engineering of Caenorhabditis elegans genomes with CRISPR/Cas9. Genetics 195:635–642
3. Waaijers S, Boxem M (2014) Engineering the Caenorhabditis elegans genome with CRISPR/Cas9. Methods 68(3):381–388
4. Chen C et al (2013) Efficient genome editing in Caenorhabditis elegans by CRISPR-targeted homologous recombination. Nucleic Acids Res 41, e193
5. Chiu H et al (2013) Transgene-free genome editing in Caenorhabditis elegans using CRISPR-Cas. Genetics 195:1167–1171
6. Dickinson DJ et al (2013) Engineering the Caenorhabditis elegans genome using Cas9-triggered homologous recombination. Nat Methods 10:1028–1034
7. Friedland AE et al (2013) Heritable genome editing in C. elegans via a CRISPR-Cas9 system. Nat Methods 10:741–743
8. Katic I, Grosshans H (2013) Targeted heritable mutation and gene conversion by Cas9-CRISPR in Caenorhabditis elegans. Genetics 195:1173–1176
9. Lo TW et al (2013) Precise and heritable genome editing in evolutionarily diverse nematodes using TALENs and CRISPR/Cas9 to engineer insertions and deletions. Genetics 195:331–348
10. Tzur YB et al (2013) Heritable custom genomic modifications in Caenorhabditis elegans via a CRISPR-Cas9 system. Genetics 195:1181–1185
11. Waaijers S et al (2013) CRISPR/Cas9-targeted mutagenesis in Caenorhabditis elegans. Genetics 195:1187–1191
12. Zhao P et al (2014) Oligonucleotide-based targeted gene editing in C. elegans via the CRISPR/Cas9 system. Cell Res 24:247–250
13. Cho SW et al (2013) Heritable gene knockout in Caenorhabditis elegans by direct injection of Cas9-sgRNA ribonucleoproteins. Genetics 195:1177–1180
14. Brenner S (1974) The genetics of Caenorhabditis elegans. Genetics 77:71–94
15. Kadandale P et al (2009) Germline transformation of Caenorhabditis elegans by injection. Methods Mol Biol 518:123–133
16. Farboud B, Meyer BJ (2015) Dramatic enhancement of genome editing by CRISPR/Cas9 through improved guide RNA design. Genetics 199:959–971
17. Hwang WY et al (2013) Efficient genome editing in zebrafish using a CRISPR-Cas system. Nat Biotechnol 31:227–229
18. Sugi T et al (2014) Versatile strategy for isolating transcription activator-like effector nuclease-mediated knockout mutants in Caenorhabditis elegans. Dev Growth Differ 56:78–85
19. Arribere JA et al (2014) Efficient marker-free recovery of custom genetic modifications with CRISPR/Cas9 in Caenorhabditis elegans. Genetics 198(3):837–846
20. Paix A et al (2014) Scalable and versatile genome editing using linear DNAs with microhomology to cas9 sites in Caenorhabditis elegans. Genetics 198(4):1347–1356
21. Kim H et al (2014) A co-CRISPR strategy for efficient genome editing in Caenorhabditis elegans. Genetics 197:1069–1080
22. Ward JD (2015) Rapid and precise engineering of the Caenorhabditis elegans genome with lethal mutation co-conversion and inactivation of NHEJ repair. Genetics 199:363–3377
23. Giordano-Santini R et al (2010) An antibiotic selection marker for nematode transgenesis. Nat Methods 7:721–723
24. Frokjaer-Jensen C et al (2014) Random and targeted transgene insertion in Caenorhabditis elegans using a modified Mos1 transposon. Nat Methods 11:529–534
25. Frokjaer-Jensen C et al (2012) Improved Mos1-mediated transgenesis in C. elegans. Nat Methods 9:117–118
26. Gibson DG (2011) Enzymatic assembly of overlapping DNA fragments. Methods Enzymol 498:349–361
27. Gibson DG et al (2009) Enzymatic assembly of DNA molecules up to several hundred kilobases. Nat Methods 6:343–345
28. Shirayama M et al (2012) piRNAs initiate an epigenetic memory of nonself RNA in the C. elegans germline. Cell 150:65–77
29. Semple JI et al (2012) Generating transgenic nematodes by bombardment and antibiotic selection. Nat Methods 9:118–119

Chapter 7

Observing and Quantifying Fluorescent Reporters

Michael Hendricks

Abstract

Genetically encoded fluorescent reporters take advantage of *C. elegans*' transparency to allow noninvasive, in vivo observation and recording of physiological processes in intact animals. Here, I discuss the basic microscope components required to observe, image, and measure fluorescent proteins in live animals for students and researchers who work with *C. elegans* but have limited experience with fluorescence imaging and analysis.

Key words: Microscopy, Fluorescent proteins, Digital image analysis

1 Introduction

1.1 Fluorescent Molecules and Microscopy

Fluorescence occurs when an electron returns to its ground state after excitation to a higher energy state, emitting a photon. Fluorescent proteins commonly used in biology contain a fluorophore—the chemical moiety that absorbs and emits light—that is excited by a shorter wavelength of light and emits at a longer wavelength. Fluorophores have a range of wavelengths over which they are excited by or emit light, referred to as their excitation (or absorption) spectrum and emission spectrum, respectively. By using appropriate filters, this difference in the excitation and emission spectra allows the fluorescently labeled molecules or structure of interest to be observed with minimal background from the excitation light source.

Figure 1 shows a simplified schematic of a fluorescence microscope. In this example, a white light source is passed through a filter that transmits light only in a specific range of wavelengths. "Band-pass" filters such as this are usually specified by the middle wavelength and range over which they transmit light. For example, "BP470/40" is a band-pass filter that transmits light ranging from 450 to 490 nm. In contrast, a dichroic filter reflects light below a certain wavelength but allows light to pass above this wavelength.

David Biron and Gal Haspel (eds.), *C. elegans: Methods and Applications*, Methods in Molecular Biology, vol. 1327,
DOI 10.1007/978-1-4939-2842-2_7,

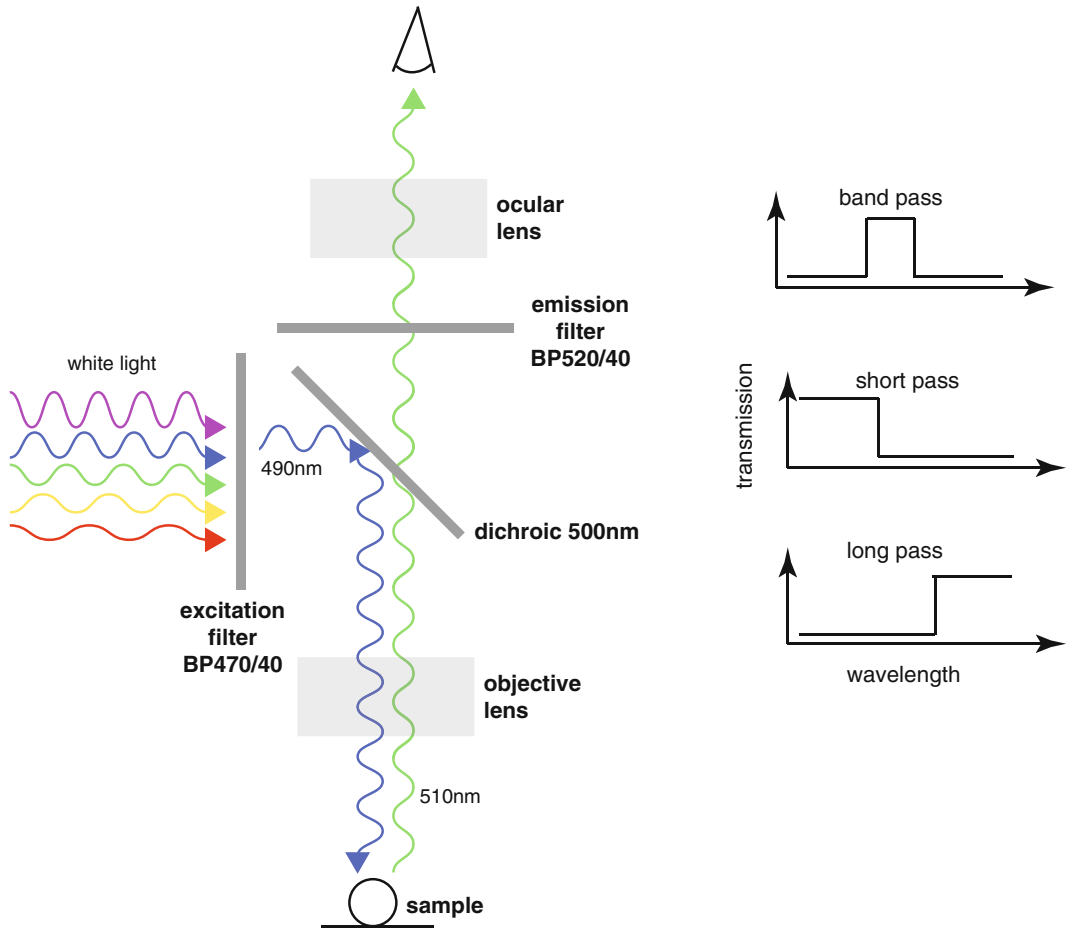

Fig. 1 Schematic of a light path in a simple fluorescence microscope. At *right* are graphical representations of common filter types encountered in fluorescence microscopy. See main text for details

In this example, the dichroic filter reflects anything below 500 nm through the objective lens and onto the sample, including the blue (490 nm) light coming through excitation filter. Green fluorescence (510 nm) from the sample, in contrast, passes through the dichroic because of its longer wavelength.

Most fluorescence microscopes share this basic organization. Combinations of dichroic, excitation, and emission filters are usually sold assembled in "filter cubes" appropriate for particular fluorophores and fitting specific brands of microscope.

1.2 Fluorescent Proteins in Biology

While the use of green fluorescent protein (GFP) and its many variants is now ubiquitous in biology, *C. elegans* has the distinction of being the first multicellular organism in which GFP was demonstrated to be a useful in vivo marker for labeling cells [1]. Several common ways in which fluorescent markers are used are described below.

1. *As a marker for a specific cell type or tissue.* Endogenous DNA regulatory sequences cloned upstream of GFP (or other fluorescent protein) coding sequences are used to drive the expression in a subset of cells. This is most commonly used for comparative studies of the number, morphology, presence, or development of the same cells or tissues in different animals. A large number of regulatory sequence-cell type relationships have been determined for *C. elegans.*
2. *To estimate endogenous gene expression patterns and dynamics.* Upstream genomic sequences from a gene of interest are used to drive the expression of a visible marker. This allows inference of normal expression pattern or regulation of expression under different conditions. A major caveat is that the results of such an experiment are not determinative of an endogenous expression pattern, which requires supplemental evidence from in situ mRNA hybridization or immunohistochemistry. One can never be sure that all positive and negative regulatory elements have been included, so the observed GFP transgene expression pattern may misrepresent the true expression pattern.
3. *To monitor the subcellular localization of a protein of interest.* In most cases, GFP can be expressed as a fusion protein with a gene product of interest without preventing proper protein localization or function (the ability of the fusion transgene to rescue a mutant phenotype is often a good test of this assumption). This allows the observation of the subcellular localization and dynamics of the tagged protein, though one most bear in mind the possibility of artifacts caused by excessive or ectopic expression.
4. *As a physiological reporter.* The most recently developed type of genetically encoded fluorescent probes are those that indicate changes in ion concentrations, pH, voltage, or other physiochemical processes. While the molecular mechanisms vary, these fall into two general classes:
   (a) *Reporters based on change in intensity of a single fluorophore.* A reporter protein consists of a fluorescent fusion protein that binds a molecule of interest. Binding induces a conformational change that alters the amount fluorescence emission, usually by altering solvent access to the fluorophore, thus changing its protonation state and fluorescence. Fluorescence intensity thus provides an indirect measurement of changes in concentration. This type of reporter is simpler to image and analyze, but is more susceptible to motion artifacts.
   (b) *Reporters that rely on interactions between two fluorophores.* For the latter, the most common type is based on Förster resonance energy transfer (FRET). FRET occurs when two complementary fluorophores are in close proximity

and dipole-dipole coupling occurs between a "donor" in its excited state and an "acceptor." The most commonly used FRET pair in biological imaging consists of a CFP (cyan) donor and YFP (yellow) acceptor. When the reporter is in a tertiary conformation that allows the FRET interaction to occur, excitation of CFP will cause indirect emission from YFP. The ratio of CFP:YFP fluorescence is thus a measure of the relative amount of ligand-bound reporter. Because it is ratiometric, FRET measurements are less sensitive to motion artifacts.

2 Materials

Because of the huge spectrum of possible reporters, protocols for handling and mounting animals, and microscope and camera styles and models, what follows will attempt to describe general principles and for observing and recording fluorescent signals in live *C. elegans*. Engineered transgenes are available as plasmid DNA. Many commonly used transgenes are available through Addgene (www.addgene.org). Published constructs not available in public repositories should be provided by authors on request.

2.1 Fluorescent Reporters Used in C. elegans

Static fluorescent reporters include dyes and fluorescent proteins, such as variants of GFP (EGFP, CFP) and DsRED (mCherry) that are used as general cellular markers. Fluorescent proteins can be targeted through the addition of trafficking signals, for example to the nucleus or plasma membrane. Fluorescent proteins are also often fused proteins of interest.

1. DAF-16:GFP is normally localized to the cytosol, but upon environmental stress is nuclear localized [2], providing a real-time readout of the animal's physiological state.
2. Fusion of GFP to synaptic proteins has been a powerful tool for screening for mutations in synaptic growth and morphology [3, 4].
3. Chemical dyes: Some fluorescent dyes (FITC and lipophilic dyes such as DiI and DiO) are preferably taken up by amphid and phasmid neurons, and abnormal or absent "dye-filling" has been used to screen for development defects in sensory structures [5].

Dynamic, genetically encoded sensors change their optical properties based on binding or modification by a physiological substrate of interest.

Calcium

1. One of the earliest in vivo uses of the FRET-based calcium indicator Cameleon was in *C. elegans* muscles and neurons [6, 7].

2. The non-ratiometric Ca^{2+} indicator GCaMP (and its variants) has become the standard calcium-imaging reagent in *C. elegans* [8, 9]. The latest versions of GCaMP (GCaMP5, GCaMP6) exhibit improved signal-to-noise and faster. Looger lab website for details. Available through Addgene. The website of Loren Looger's lab is a good way to keep up to date with GCaMP technology.
3. RCaMP is structurally similar to GCaMP, but is based on mRuby instead of GFP. It is excited in by green light and emits red [10].
4. G-GECOs are a family of genetically encoded calcium indicators that vary in their excitation/emission wavelengths [11]. They have not been extensively used in *C. elegans*, and some early attempts suggest that they may not perform as well as GCaMPs in nematode neurons. However, the possibility of a wide range of multispectral calcium-imaging tools is intriguing.

Voltage

The use of genetically encoded voltage reporters in *C. elegans* is in its infancy, but has enormous promise. Early-generation reporters suffered from low signal-to-noise and suboptimal kinetics.

1. Arclight and its variants range in fluorescence amplitude from ~8 to 35 %, with an associated trade-off in speed [12].
2. Two new variants of the Archaerhodopsin-3 proton pump, Archer1 and Archer2, have been recently validated in *C. elegans* sensory neurons [13]. Stimulus conditions that give maximal calcium responses in the AWC sensory neuron showed 40 % increases in Archer1 fluorescence. Archers can be used as voltage sensory when excited by red (655 nm) light; under green light they play the more familiar Archaerhodopsin role of hyperpolarizing pumps.
3. A FRET-based voltage sensor class called VSFP-Butterflies has been recently developed [14] and has reportedly been successfully optimized for *C. elegans.*

A variety of other physiological reporters have been used in *C. elegans* or show significant promise for future use:

1. Clomeleons are FRET-based *chloride* reporters [15, 16], which potentially provide a crucial means of interrogating inhibitory synaptic connections and may be of particular interest to *C. elegans* researchers due to the prevalence of transmitter-gated chloride channels. All current chloride sensors suffer from a high degree of pH dependence.
2. *Redox* state can be measured through expression of genetically encoded redox sensors [17, 18].

3. The difference between vesicular and extracellular *pH* has been exploited to observe synaptic vesicle fusion using the pH-sensitive GFP variant pHluorin fused to synaptobrevin (SNB-1) to create synaptopHluorin [19, 20].
4. A single-wavelength *glutamate* (iGluSnFR) sensory was recently published by the Looger lab, allowing direct visualization of glutamate release [21].

2.2 Transgenic Worms

The design of plasmid DNA constructs for creating transgenic *C. elegans* is beyond the scope of this chapter. For a guide to creating transgenic worms by microinjection, *see* Chapter 3. Many transgenic strains are available from the *C. elegans* Genetics Stock Center at the University of Minnesota, and published strains can usually be obtained by contacting the authors directly.

2.3 Microscope Equipped with Fluorescence Components

A fluorescence microscope with a digital camera is essential. Again, there are too many variations available to address the use of specific equipment, and what follows are general guidelines. Many markers can be observed under relatively low-magnification fluorescence stereomicroscopes. Detailed morphology or quantitative measurement often requires increased magnification and the use of high-numerical-aperture objective lenses found on compound microscopes. Your microscope must be equipped with a light source and filter sets that are appropriate to the properties of the fluorophore you wish to observe.

3 Methods

3.1 Mounting and Immobilization

Live animals must be mounted in a way that permits observation and either allows or restricts movement according to experimental design. Observing and recording from immobilized animals is much simpler, and several methods can be used:

1. *Anesthetics.* Worms can be immobilized with anesthetics such as levamisole or low levels of sodium azide on agar pads and observed through cover slips. This is often not desirable as these compounds may interfere with the physiological processes in question. They are usually appropriate for observing cellular expression patterns or morphology.
2. *Cyanoacrylate glue.* Gluing worms to agar pads is the preferred method for electrophysiological recordings and is commonly used for imaging experiments as well [22].
3. *Microfluidic devices.* A huge number of designs have proliferated for small fluid channel chips for restraining, sorting, observing, and stimulating live worms. These have the advantage of avoiding the use of drugs or harsh chemicals, but require some specialized materials and preparation, reviewed in Chapter 12.

4. *Nanoparticle immobilization.* A simple method of immobilizing worms on agar using submicron polystyrene beads was recently reported [23]. Friction between the beads and the agar and cover slip prevents movement and allows for long-term imaging without the use of drugs and simple recovery of animals after imaging.

3.2 Acquiring Images

Documenting your fluorescent reporter requires a camera. Once again, a huge range exists, from inexpensive point-and-shoot equivalents that are useful for routine documentation to highly specialized cameras with enormous sensitivity and speed. Some general principles for digital imaging are useful to bear in mind. These parameters are commonly found as adjustable settings in digital imaging software.

1. A grayscale digital picture consists of an array of pixels, each with a single numerical value assigned (discussed in more detail in **Note 1**). Most imaging software allow you to view a histogram of the distribution of pixel values in your image. It is usually important to make sure that this entire distribution lies within the dynamic range of the camera for the current setting. Both minimum and maximum (also called a saturated pixel) values should be avoided for any pixel in a structure of interest, as this will distort measurements made later. In addition, some cameras can be damaged by long-term saturation.
2. Pixel values are a function of illumination intensity, exposure time, and both intrinsic and adjustable properties of the camera sensor. The light intensities used for fluorescence microscopy can be noxious or harmful to *C. elegans* over time. Lower intensity illumination and longer exposure times are less harmful, but increase noise and motion artifacts and decrease sensitivity. Shorter exposure times with higher illumination address these problems, but can be damaging or aversive to the organism and cause photobleaching of the fluorophore. Optimizing these competing parameters is essential for each sample and experimental condition.
3. For time-lapse acquisition, a frame rate must be set as well. Determining an optimal frame rate depends on the exposure time (the sampling interval must be greater than the exposure time) and on the temporal features of the signal you wish to measure. This is discussed in more detail in **Note 2**.

3.3 Image Analysis and Measurement

Digital image analysis requires specialized software. Often, acquisition software includes some analysis tools. Excellent free resources also exist. For imaging in biology, by far the best choice for straightforward analysis is ImageJ, in particular the Fiji ImageJ distribution (http://fiji.sc/Fiji) [24, 25]. A huge number of free ImageJ plug-ins exist that perform functions that once required software costing thousands of dollars.

1. *Image segmentation*. Segmentation refers to the process of defining or selecting objects or regions of interest (ROI) within an image.
   (a) Perhaps the simplest form of segmentation is based on pixel value. The "Threshold" function in Fiji allows users to select pixels that are within a selected range of values.
   (b) Alternatively, ROIs can be manually defined using drawing tools. Multiple ROIs can be defined in the ROI Manager.
2. *Motion correction*. In time-lapse images, some amount of movement is inevitable. There are two primary approaches to dealing with objects of interest moving between frames:
   (a) Frames can be automatically aligned using stack registration algorithms included in Fiji or available as ImageJ plug-ins. This is preferred when the image contains minor motion artifacts, and allows selection of a single ROI that is appropriate across all frames.
   (b) Algorithms that segment and track moving objects across multiple frames are available, though these are more complex. This approach is required when multiple objects of interest move relative to one another throughout the time series.
3. *Measurement*. Fiji can measure a number of attributes of the pixels contained within an ROI as part of a defined object. For intensity, normally the mean pixel value of the object is measured.
4. *Normalization and analysis*. Raw pixel values are not informative with respect to the absolute amounts of a fluorescent reporter. In time lapse, it is common practice to select a baseline value corresponding and to measure intensity changes relative to this baseline. Differences in raw pixel values can arise from many sources, including expression level, illumination intensity, mounting method, and camera acquisition settings. For this reason comparing intensities across animals is difficult; however for a given set of carefully controlled imaging conditions, fluorescence intensity of a static reporter can, for example, be used as a proxy for expression level.

4 Notes

1. Digital images:
   (a) A simple way to think of a digital camera is as a sensor array that assigns values based on the number of photons collected over a given time period (the exposure time). "Bit depth" refers to the range of possible values for each pixel.

An *n*-bit image has $2n$ values for each pixel. Common image formats include 8-bit (0–255), 12-bit (0–4095), and 14-bit (0–16383). Larger bit depths greatly increase file size, but provide a greater dynamic range.

(b) Generally, compressed file formats should not be used for quantitative imaging. The most commonly found uncompressed file formats are TIFFs (*t*agged *i*mage *f*ile *f*ormat, which can be single or multi-layer) and AVI (*a*udio *v*ideo *i*nterleave, for uncompressed movies).

2. Considerations for time-lapse imaging:

(a) *Optimal frame rates.* Undersampling occurs when the frame rate is too low to accurately measure events at a frequency of interest, introducing aliasing artifacts. The Nyquist-Shannon Theorem gives a simple metric for determining frame rate: the sampling rate must be at least 2× the frequency of the lowest bandwidth events you wish to measure. For example, if you wish to measure a signal at 5 Hz, you must image at a minimum of ten frames per second.

(b) *Motion artifacts.* Long exposure times and inadequate immobilization contribute to motion artifacts. The most common artifact consists of "smearing" of a fluorescent object over the course of an exposure. The major effects are to increase the apparent size of the object and decrease its mean fluorescence intensity. A second common motion artifact is caused by shifts in focal plane caused by muscle contractions. Depending on the source of the problem, suspected motion artifacts can be controlled for in several ways:

- Decreased exposure times.
- Improved immobilization.
- Comparison or ratio measurement with a static fluorescent reporter.

Acknowledgments

Images in Fig. 2 were provided by Claudia Wever (a), Sebastian Schmeisser (b), and Pratik Kadekar (c). I thank David Biron for constructive feedback.

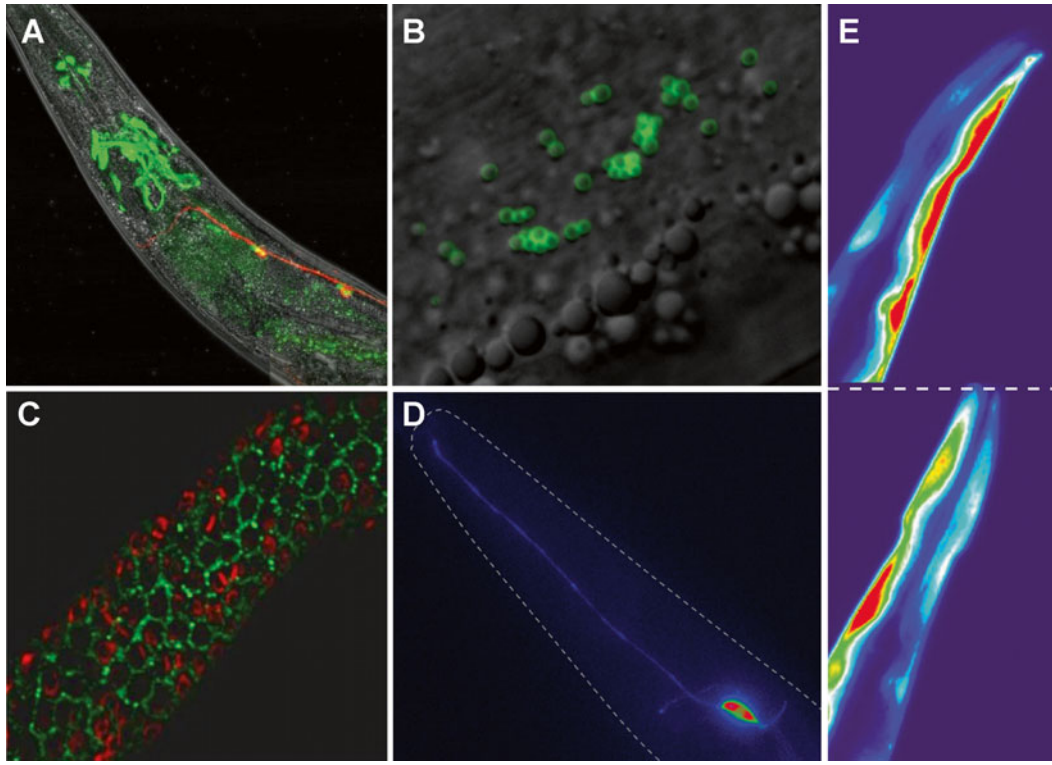

Fig. 2 Example of in vivo fluorescent reporters. (**a**) The promoter of *acc-1* driving the expression of GFP in neurons of the head. (**b**) A GFP fusion to DGAT-2 labels lipid droplets in muscles. (**c**) Actin filaments (GFP, *green*) and nuclei (DAPI, *red*) in the adult germ line. (**d**) The genetically encoded calcium indicator GCaMP3 (pseudocolored) expressed in the AWC sensory neuron. (**e**) GCaMP3 (pseudocolored) expressed in muscles under the *myo-3* promoter during a ventral (*top*) and dorsal (*bottom*) anterior body bend

References

1. Chalfie M, Tu Y, Euskirchen G et al (1994) Green fluorescent protein as a marker for gene expression. Science 263:802–805
2. Henderson ST, Johnson TE (2001) *daf-16* integrates developmental and environmental inputs to mediate aging in the nematode *Caenorhabditis elegans*. Curr Biol 11:1975–1980
3. Colón-Ramos DA, Margeta MA, Shen K (2007) Glia promote local synaptogenesis through UNC-6 (netrin) signaling in *C. elegans*. Science 318:103–106
4. Zhen M, Huang X, Bamber B et al (2000) Regulation of presynaptic terminal organization by *C. elegans* RPM-1, a putative guanine nucleotide exchanger with a RING-H2 finger domain. Neuron 26:331–343
5. Herman RK (1984) Analysis of genetic mosaics of the nematode *Caneorhabditis elegans*. Genetics 108:165–180
6. Kerr R, Lev-Ram V, Baird G et al (2000) Optical imaging of calcium transients in neurons and pharyngeal muscle of *C. elegans*. Neuron 26:583–594
7. Miyawaki A, Griesbeck O, Heim R et al (1999) Dynamic and quantitative Ca^{2+} measurements using improved cameleons. Proc Natl Acad Sci U S A 96:2135–2140
8. Tian L, Hires SA, Mao T et al (2009) Imaging neural activity in worms, flies and mice with improved GCaMP calcium indicators. Nat Methods 6:875–881
9. Schrödel T, Prevedel R, Aumayr K et al (2013) Brain-wide 3D imaging of neuronal activity in

Caenorhabditis elegans with sculpted light. Nat Methods 121:785–794

10. Akerboom J, Carreras Calderón N, Tian L et al (2013) Genetically encoded calcium indicators for multi-color neural activity imaging and combination with optogenetics. Front Mol Neurosci 6:2
11. Zhao Y, Araki S, Wu J et al (2011) An expanded palette of genetically encoded Ca^{2+} indicators. Science 333:1888–1891
12. Han Z, Jin L, Platisa J et al (2013) Fluorescent protein voltage probes derived from ArcLight that respond to membrane voltage changes with fast kinetics. PLoS One 8, e81295
13. Flytzanis NC, Bedbrook CN, Chiu H et al (2014) Archaerhodopsin variants with enhanced voltage-sensitive fluorescence in mammalian and *Caenorhabditis elegans* neurons. Nat Commun 5:4894
14. Mishina Y, Mutoh H, Song C et al (2014) Exploration of genetically encoded voltage indicators based on a chimeric voltage sensing domain. Front Mol Neurosci 7:78
15. Berglund K, Schleich W, Wang H et al (2008) Imaging synaptic inhibition throughout the brain via genetically targeted Clomeleon. Brain Cell Biol 36:101–118
16. Arosio D, Ratto GM (2014) Twenty years of fluorescence imaging of intracellular chloride. Front Cell Neurosci 8:258
17. Ostergaard H, Henriksen A, Hansen FG et al (2001) Shedding light on disulfide bond formation: engineering a redox switch in green fluorescent protein. EMBO J 20:5853–5862
18. Romero-Aristizabal C, Marks DS, Fontana W et al (2014) Regulated spatial organization and sensitivity of cytosolic protein oxidation in *Caenorhabditis elegans*. Nat Commun 5:5020
19. Dittman JS, Kaplan JM (2006) Factors regulating the abundance and localization of synaptobrevin in the plasma membrane. Proc Natl Acad Sci U S A 103:11399–11404
20. Ohno H, Kato S, Naito Y et al (2014) Role of synaptic phosphatidylinositol 3-kinase in a behavioral learning response in *C. elegans*. Science 345:313–317
21. Marvin JS, Borghuis BG, Tian L et al (2013) An optimized fluorescent probe for visualizing glutamate neurotransmission. Nat Methods 10:162–170
22. Schafer WR (2006) Neurophysiological methods in *C. elegans*: an introduction. WormBook 1–4
23. Kim E, Sun L, Gabel CV et al (2013) Long-term imaging of *Caenorhabditis elegans* using nanoparticle-mediated immobilization. PLoS One 8, e53419
24. Schneider CA, Rasband WS, Eliceiri KW (2012) NIH Image to ImageJ: 25 years of image analysis. Nat Methods 9:671–675
25. Schindelin J, Arganda-Carreras I, Frise E et al (2012) Fiji: an open-source platform for biological-image analysis. Nat Methods 9:676–682

Chapter 8

Microbial Rhodopsin Optogenetic Tools: Application for Analyses of Synaptic Transmission and of Neuronal Network Activity in Behavior

Caspar Glock, Jatin Nagpal, and Alexander Gottschalk

Abstract

Optogenetics was introduced as a new technology in the neurosciences about a decade ago (Zemelman et al., Neuron 33:15–22, 2002; Boyden et al., Nat Neurosci 8:1263–1268, 2005; Nagel et al., Curr Biol 15:2279–2284, 2005; Zemelman et al., Proc Natl Acad Sci USA 100:1352–1357, 2003). It combines optics, genetics, and bioengineering to render neurons sensitive to light, in order to achieve a precise, exogenous, and noninvasive control of membrane potential, intracellular signaling, network activity, or behavior (Rein and Deussing, Mol Genet Genomics 287:95–109, 2012; Yizhar et al., Neuron 71:9–34, 2011). As *C. elegans* is transparent, genetically amenable, has a small nervous system mapped with synapse resolution, and exhibits a rich behavioral repertoire, it is especially open to optogenetic methods (White et al., Philos Trans R Soc Lond B Biol Sci 314:1–340, 1986; De Bono et al., Optogenetic actuation, inhibition, modulation and readout for neuronal networks generating behavior in the nematode Caenorhabditis elegans, In: Hegemann P, Sigrist SJ (eds) Optogenetics, De Gruyter, Berlin, 2013; Husson et al., Biol Cell 105:235–250, 2013; Xu and Kim, Nat Rev Genet 12:793–801, 2011). Optogenetics, by now an "exploding" field, comprises a repertoire of different tools ranging from transgenically expressed photo-sensor proteins (Boyden et al., Nat Neurosci 8:1263–1268, 2005; Nagel et al., Curr Biol 15:2279–2284, 2005) or cascades (Zemelman et al., Neuron 33:15–22, 2002) to chemical biology approaches, using photochromic ligands of endogenous channels (Szobota et al., Neuron 54:535–545, 2007). Here, we will focus only on optogenetics utilizing microbial rhodopsins, as these are most easily and most widely applied in *C. elegans*. For other optogenetic tools, for example the photoactivated adenylyl cyclases (PACs, that drive neuronal activity by increasing synaptic vesicle priming, thus exaggerating rather than overriding the intrinsic activity of a neuron, as occurs with rhodopsins), we refer to other literature (Weissenberger et al., J Neurochem 116:616–625, 2011; Steuer Costa et al., Photoactivated adenylyl cyclases as optogenetic modulators of neuronal activity, In: Cambridge S (ed) Photswitching proteins, Springer, New York, 2014). In this chapter, we will give an overview of rhodopsin-based optogenetic tools, their properties and function, as well as their combination with genetically encoded indicators of neuronal activity. As there is not "the" single optogenetic experiment we could describe here, we will focus more on general concepts and "dos and don'ts" when designing an optogenetic experiment. We will also give some guidelines on which hardware to use, and then describe a typical example of an optogenetic experiment to analyze the

Caspar Glock and Jatin Nagpal contributed equally.

David Biron and Gal Haspel (eds.), *C. elegans: Methods and Applications*, Methods in Molecular Biology, vol. 1327,
DOI 10.1007/978-1-4939-2842-2_8,

function of the neuromuscular junction, and another application, which is Ca^{2+} imaging in body wall muscle, with upstream neuronal excitation using optogenetic stimulation. To obtain a more general overview of optogenetics and optogenetic tools, we refer the reader to an extensive collection of review articles, and in particular to volume 1148 of this book series, "Photoswitching Proteins."

Key words: *C. elegans*, Optogenetics, Neuron, Muscle, Synapse, Behavior, Channelrhodopsin-2, Halorhodopsin, Archaerhodopsin, Mac, Calcium imaging, RCaMP

1 Introduction

Optogenetics allows analyzing genetic determinants of synaptic transmission at the neuromuscular junction, as well as the causative role of single neurons in the generation of behavior [1], or their effects on signaling within neuronal circuits [2–8]. This involves activators and inhibitors, which can be used as single tools or in combination in different nodes of a neuronal network [5, 9]. Rhodopsin optogenetic tools are most commonly used. Opsins consist of seven transmembrane helices and require the vitamin A-related organic molecule retinal as a cofactor. When retinal is bound, the functional opsins are called rhodopsins. Retinal isomerizes upon the absorption of a photon, thus triggering a conformational change of the protein, which then enters a distinct photocycle [10–12]. Whereas type I rhodopsins combine the two tasks of light sensation and (passive or active) ion flux across the plasma membrane, type II rhodopsins are G-protein-coupled proteins that activate intracellular signal transduction pathways. Channelrhodopsin-2 (ChR2), a blue light-gated cation channel [13, 14], was the first microbial rhodopsin to be used for depolarizing neurons [15] and further to modulate behavior in a living organism [16]. In later studies, the yellow light-activated chloride pump Halorhodopsin (NpHR) was used to hyperpolarize neurons [17]. Besides NpHR, archaerhodopsin (Arch) and the fungal rhodopsin Mac [18, 19] have emerged as further inhibitory optogenetic tools. Nowadays, the optogenetic toolbox comprises a wide variety of rhodopsins and variants thereof that are used to directly activate, directly inhibit, or to indirectly modulate neurons [20].

The experimental outcomes of optogenetic manipulations are evident by behavioral, electrical, or optical readouts [21]. Combination of electrical recording and optical stimulation constitutes a powerful way to analyze the functionality of distinct neuronal connections [22, 23], but is less easily applied in *C. elegans*. Here, this methodology is feasible to investigate different mutants with pre- or postsynaptic defects to understand and/or determine their impact on synaptic transmission [24–27]. Optical readouts of neuronal or network function are mostly obtained by calcium imaging. Genetically encoded calcium indicators (GECIs) permit a cell type-specific observation of neuronal activity [28, 29].

However, the spectral overlap between the action spectrum of the optogenetic tool and the excitation spectrum of the GECI complicates this approach [30]. Most applications in *C. elegans* thus lie in the combination of optogenetic actuation and simultaneous analysis of animal behavior [16, 24, 31–39].

2 Materials

2.1 Optogenetic Activation: Depolarizing Membrane Potential

Channelrhodopsin-2 and other microbial rhodopsin-based optogenetic activators enable a spatiotemporally precise control of genetically targeted neurons. This optogenetic activation allows us to study their causative role in generating diverse behaviors.

2.2 Channelrhodopsin-2

Channelrhodopsin-2 (ChR2) is a directly light-gated cation channel endogenous to the green alga *Chlamydomonas reinhardtii*, where it is enriched in the so-called eye spot region, mediating phototaxis and photophobic responses [14, 40]. ChR2 requires all-*trans*-retinal (ATR) as a cofactor [41]. This light-absorbing chromophore is embedded within the hydrophobic core of the seven transmembrane (TM) helices, where retinal binds covalently to a conserved lysine residue of TM domain seven by forming a Schiff base [42]. A protonation of the Schiff base shifts the absorption of light into the blue range of the spectrum (around 470 nm). Upon absorption of a photon, retinal isomerizes from the all-*trans* to the 13-*cis* configuration in less than 50 ns and triggers a conformational change of the protein that causes the opening of the channel [13, 14]. This induces an inward rectifying current for different monovalent (e.g., Na^+, K^+, H^+) and some divalent cations, including (minute amounts of) Ca^{2+}, and in the native context of a cell, particularly a neuron, thus depolarizes its plasma membrane [14–16].

The extent of current mediated by ChR2, as compared to other ion channels, is rather small (ca. 40 fS in contrast to ca. 40–60 pS in the case of a nAChR) [43]. In nonspiking neurons of *C. elegans*, all of the current required to activate a neuron has to be provided by ChR2, while in (mammalian) neurons firing action potentials, one "just" needs to reach threshold [44]. This implies that ChR2 expression levels need to be high, such that "strong" promoters should be used. However, there are more light-sensitive and more conductive/better expressing variants of ChR2 available nowadays, which one can use as alternatives (see below).

The light-induced conductive state of ChR2 is part of a photocycle (Fig. 1) that underlies the mechanism of the channel [12]. In the dark, ChR2 is in the ground state D470. After absorption of a blue photon (maximal activation is reached with light of ca. 460 nm; however, as the rhodopsin spectrum is rather broad, light between ca. 350 and ca. 530 nm can activate ChR2), the intermediate state

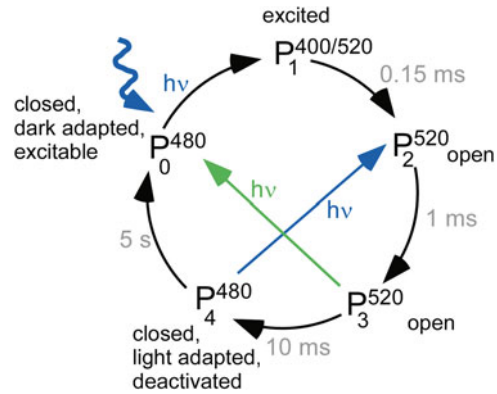

Fig. 1 Photocycle of Channelrhodopsin, adapted from [11]. Blue light induces the conducting state, but can also short-circuit the light-adapted dark state to the open state. Green light can lead to channel closure

P500 is formed within nanoseconds by the light-induced isomerization of retinal. The following deprotonation of the Schiff base to the extracellular side converts the protein to the P350 state within ca. 25 μs. Reprotonation of the Schiff base from the cytoplasmic side leads to the conducting state P520 [11, 43, 45], which is in a pH-dependent equilibrium with the deprotonated form P390. Upon closing, the channel changes to the intermediate states $P480_a$ and $P480_b$ before it eventually recovers to the ground state after ca. 45 s. In a flash-photolysis (i.e., a "single-photon") experiment, the latter is the rate-limiting step of the photocycle, in which hydrogen bonds of amino acids change and backbone rearrangements occur. However, during continuous blue light, $P480_b$ absorbs a photon to be directly converted into the early P500 intermediate, thereby circumventing the ground state D470. Thus, after a brief peak current, involving all available channels, steady state currents occur, as a distinct proportion of channels in the dynamic equilibrium can be converted again to open state after channel closure, i.e., the stationary-state level results from the desensitization of a fraction of channels. The larger the proportion of channels in the light-sensitive state, the more can be opened by light. The shorter the time required for channel closure and reactivation, the more channels can regain a light-sensitive state. From these effects, a higher steady state current will result. This has been achieved by certain mutations, e.g., in the "high-efficiency" E123T variant [46]. Upon repeated stimulation, ChR2 exhibits a desensitized state, which leads to reduced initial peak currents in successive trials. Desensitized channels recover in the dark only slowly, with a typical time constant around 5 s, influenced by the extracellular pH and the membrane potential [14, 24]. Once the channel is open, it closes by spontaneous progression through the photocycle. However,

channel closure may also be achieved by green light illumination of the of P520 state [45]. In sum, size and the kinetic properties of the ChR2 photocurrent are a result of the described photocycle, the ion selectivity, and the time constants of activation, deactivation, and inactivation [10].

In comparison to rhodopsins of higher eukaryotes, retinal does not dissociate from its opsin molecule after activation, but thermally reisomerizes to the initial all-*trans* state [47]. Because nematodes do not generate ATR, exogenous ATR has to be added to the bacteria lawn in order to render the channel functional [16]. However, transgenic animals grown without ATR can serve as convenient negative controls for ChR2 experiments in *C. elegans*.

2.2.1 ChR2 Variants with Distinct Functional Properties for Specific Applications

ChR2 is a powerful tool, but there is also room for improvement. Thus, ChR2 variants that enable specific optogenetic applications were engineered by site-directed mutagenesis, yielding channels with altered ion selectivity and conductance, spectral properties, or photocycle kinetics. The mutated residues are often near the retinal-binding pocket or in close proximity of the putative pore of the channel. ChR2 with histidine 134 mutated to arginine, ChR2(H134R), shows a twofold extended open state life time, a twofold higher Na^+ sensitivity and a twofold lower degree of inactivation [16, 48]. Conversely, the mutation of glutamate 123 to threonine, ChR2(E123T), shortens closing kinetics significantly and is thus capable to elicit firing frequencies in neurons with more than 200 Hz [46]. Another variant, the ChR1/2 chimera ChIEF [48], carrying the mutation I170V, has been used to elicit very fast depolarization of neurons for electron microscopy analyses of the stimulated neuromuscular junction [49]. Mutation of threonine 159 to cysteine, ChR2(T159C), displays up to tenfold enhanced photocurrents, due to higher conductance and/or better plasma membrane trafficking, as well as faster kinetics [50, 51]. The mutation leucine 132 to cysteine, ChR2(L132C), exhibits an enhanced calcium conductance by sixfold [52]. ChR2 was also altered to allow long-term manipulation at low light intensities. The mutation of the residue cysteine 128 to serine (C128S) significantly delays the closing of the channel in the dark to several minutes; thus a large proportion of the channels accumulates in the open state. Similar effects were found for the D156A mutant and C128S; D156A double mutant [53, 54]. This effectively reduces the light intensity required to achieve activation, and both effects allow stimulating cells in the long term (even for hours) without the need for continuous intense blue light exposure that would be harmful. Alike wild-type ChR2, this variant can be turned off by yellow or green light [31, 55]. In general, we find that combining the H134R mutation with the above mentioned mutations improves the function in *C. elegans*, for unknown reasons. Last, variants of ChR have been generated that have altered activation spectral peaks. The chimeric protein C1V1, composed of *Chlamydomonas reinhardtii* ChR1 and *Volvox carteri*

ChR1, with two additional mutations, is activated with green light instead of blue light [53, 56]. However, due to the naturally broad absorption band of rhodopsins, it can still respond to blue light, and is furthermore quite light sensitive. Thus, in order to allow for independent blue and green activation of two distinct neuron populations, with ChR2 and C1V1-ETET, respectively, the highly efficient ChR2(H134R; T159C) double mutant should be used (to allow efficient activation with blue light while not co-activating C1V1), and the relative expression levels of the two proteins need to be carefully titrated [51].

2.3 Optogenetic Inhibition: Hyperpolarizing Membrane Potential

The ability to silence the activity of genetically defined neurons in a temporally precise fashion allows investigating the causative role of the defined neuron cell type in driving the behavior. When used in combination with channelrhodopsins, optogenetic inhibitors enable multimodal optical interrogation of neural circuits [17, 19].

2.3.1 Halorhodopsin

Optical inhibition of neural activity was first achieved using the yellow light-gated chloride pump Halorhodopsin (NpHR), from the archaeon *Natronomonas pharaonis* [17]. When expressed in *Xenopus* oocytes, it produced vectorial, hyperpolarizing inward currents associated with chloride influx into the cell, with a peak photocurrent observed at 590 nm excitation. Illumination with yellow light potently inhibited action potential firing in cultured hippocampal neurons expressing NpHR. Activation of NpHR in *C. elegans* body wall muscle cells resulted in the extension of the worm's body due to hyperpolarization and relaxation of muscle cells. In contrast to ChR2, which is a channel that is opened by absorption of a photon to allow passage of many ions, NpHR as a pump allows for only one ion to be transported per photocycle. Thus, as is true for ChR2, though for different reasons, also NpHR requires robust plasma membrane expression. Unfortunately, the protein traffics inefficiently to the plasma membrane in eukaryotes. Hence, molecular engineering of NpHR, comprising incorporation of ER export and trafficking motifs from mammalian membrane proteins, was performed [57, 58]. However, incorporating these plasma membrane targeting signals in NpHR did not enhance NpHR's ability to photo-inhibit excitable cells in worms as these signals are not conserved in *C. elegans* [19]. Thus, for a strong and robust inhibition, massive overexpression of NpHR is required in worms, such that enough protein makes it into the plasma membrane. This is not always possible, unless a strong promoter is used to drive its expression, which limits the neuronal networks that can be investigated in this ideal model system for optogenetics.

2.3.2 Archaerhodopsin and Mac

As alternative to NpHR for neuronal photoinhibition, light-driven outward-directed proton pumps were discovered or characterized for utilization in optogenetics in an extensive screen of microbial opsins carried out by Chow and colleagues [18]. Archaerhodopsin-3,

known as Arch, from *Halorubrum sodomense*, and Mac, from the fungus *Leptosphaeria maculans*, are activated by yellow-green and blue-green wavelengths of light, respectively, and express well on the neural plasma membrane. The magnitude of photocurrents mediated by outward proton flux through Arch and Mac are higher than those with NpHR's chloride influx, making them more potent photoinhibitors. Both Mac and Arch have been effectively utilized to inhibit excitable cells in *C. elegans* [19, 33]. Using behavioral assays and current recordings on dissected muscle cells expressing NpHR, Mac, or Arch, Husson and colleagues showed that Arch is the most potent hyperpolarizer when illuminated with yellow-green light. Also, the action spectrum of Mac is blue-shifted as compared to NpHR and Arch (primary peaks of their action spectra are 550 nm for Mac, 566 nm for Arch, and 590 nm for NpHR). Using the nociceptive ASH network, they also demonstrated that Mac and Arch can be used to interfere with downstream signaling in networks in which upstream neurons are stimulated by ChR2, using multimodal illumination strategies. A concern with the usage of the proton pumps is the gradual elevation of proton concentration in the extracellular space, which might have deleterious or nonspecific effects on the activity of neurons. However, the pseudocoelom is also well buffered, so this may not be too problematic.

3 Methods

3.1 Specific Application of Optogenetics to Investigate Synaptic Function

C. elegans is particularly suited to study mechanisms of chemical synaptic transmission. The basic synaptic machinery involved in neurotransmission is conserved from *C. elegans* to mammals. The distinct advantage of working in worms is that most mutants affecting pre- or postsynaptic function are viable, and can be analyzed in adult animals, unlike in mammals. However, the physiological tools used to study synaptic function in worms—pharmacological and behavioral assays, as well as electrophysiological recording of neuronal activity [59–63]—are either slow and tedious or technically challenging. Here, optogenetics offers advantages as it allows noninvasive stimulation in intact moving animals, is repeatable, is specific for stimulation of a neuron type, and causes the release of the neurotransmitter at the synaptic sites only. In 2008, Liewald et al. introduced optogenetic investigation of neurotransmission (OptIoN), which uses photo-induced electrical activity to affect behavior, or to drive transmission at dissected neuromuscular junctions (NMJ), in a quantitative and time-resolved manner. Selective and repetitive photostimulation of cholinergic or GABAergic neurons can be used to examine mutants for defects in various aspects of synaptic function [24, 26, 27]. Following on, Liu et al. also studied graded synaptic transmission at the NMJ using ChR2-mediated photostimulation [25]. Optogenetic stimulation followed by electron

microscopic analysis of the synaptic ultrastructure has also yielded new insights into the maintenance of synaptic vesicle pools and synaptic activity [49, 64]. The basics of conducting an optogenetics experiment in worms is described below.

3.1.1 Expression of Optogenetic Proteins

Optogenetic activators and inhibitors are expressed using appropriate promoters. There are promoters known which can drive expression specifically in many if not all tissues and cell types in *C. elegans*. However, there are a very few promoters that drive expression specifically in only single (pairs of) neuron(s), which is particularly important for applications in this small nervous system, as every single neuron is expected to have a distinct role or even several roles. Thus, for optogenetic manipulation of a single cell or cell type, either combinatorial genetic approaches using intersectional promoter strategies with Cre or FLP recombinases should be used [65–68]. Alternatively, or in combination, patterned illumination with digital micromirror devices (DMDs), LCD projectors, etc. have been employed [30, 33, 34, 69]. The *myo-3* promoter, driving expression in body wall muscle cells, is commonly used to express and assess the efficacy of new optogenetic proteins [16, 17, 19, 51]. This is convenient, as photoactivation or inhibition of muscle cells leads to a straightforward behavioral readout (body contraction or elongation, respectively). Also, muscle cells are relatively more accessible than neurons to electrophysiological characterization of the optogenetic proteins [24, 70]. For dos and don'ts regarding the usage of the different optogenetic tools, *see* **Notes 1** and **2**.

3.1.2 Worm Rearing

Transgenic worms expressing the desired optogenetic protein are cultivated on standard NGM plates and fed with *E. coli* OP50. The microbial rhodopsins require all-*trans*-retinal (ATR) as a cofactor, which has to be exogenously supplied in the OP50 that is fed to the worms [16, 24]. Animals for optogenetic analyses are cultivated on NGM plates with OP50 supplemented with 2.5–5 μM ATR (calculated with respect to the volume of NGM in the culture dish) for one generation at 20 °C in the dark. Typically, 1 μl 100 mM ATR stock solution in EtOH is mixed with 1000 μl of OP50 culture, and 200–300 μl of this mixture is spread onto the top of the NGM plates. Thus, ATR is not mixed into the NGM medium itself. As a control, animals of the same genotype are grown on NGM plates without ATR. About 18 h before the experiments, L4 larvae, grown on ATR plates, are placed on fresh ATR plates.

3.1.3 Illumination

1. An epi-fluorescence microscope with a mercury lamp as light source and standard band-pass filters for the desired excitation wavelength can be used to induce a behavioral response in transgenic animals. Optogenetic proteins expressed in *C. elegans* are commonly activated with light intensities in the 0.5–5 mW/mm^2 range.

2. The precise light intensity needs to be measured, e.g., with a light meter, where the sensor is placed under the microscope instead of the culture dish, at the focal plane that would be used for worm imaging during the experiment. The diameter of the spot of light can be measured when focused on a piece of paper through a "Neubauer" chamber (used for cell counting, with a μm grating). Of course, it can also be calculated from the specifications of the microscope and objective used.
3. Duration of the light stimulus is set with a computer-controlled shutter. For a typical behavioral response, e.g., from mechanosensory neurons, a 500 ms light stimulus is sufficient. For full muscle contraction to be achieved, a 2 s or longer light stimulus should be used.
4. LEDs with the desired wavelength are also commonly used as excitation light sources. Patterned single cell illumination [34, 69], and see above, is another means to provide illumination, even of single neurons in freely moving animals.

3.1.4 Video Analysis

1. The locomotion behavior of the worms on a solid NGM substrate can be quantified and several locomotion parameters like the worm body length, velocity, body bending angles, frequency of turns, etc. can be obtained (for a review of different tracking and behavior analysis systems available for *C. elegans*, *see* ref. 71).
2. For quantitative analysis of worm body length, consecutive frames (e.g., 30 frames per second) from the captured videos are extracted as individual images. Individual images are converted into binary images (black and white), background subtracted, and skeletonized into a single pixel thick backbone. This image processing can be automatized with custom written ImageJ or Matlab scripts [24, 51, 69, 72]. The body length of the worm is recorded as the length of the backbone obtained after skeletonization.
3. Worm length is normalized by the mean length before the light stimulation and followed over hundreds of consecutive video frames. Length chronograms of multiple worms are then averaged and the length profiles of test vs. control strain can be plotted [24]. For single time points, body length can also be measured "by hand," by drawing a segmented line along the backbone of the animal, e.g., using ImageJ, and determining the length in pixels.
4. For precise annotation of the different aspects of locomotion, different worm-tracking packages based on machine vision tools have been developed by the worm research community [71]. These tracker systems can be combined with optogenetic experiments that require spatially and temporally precise illumination of the worm with various colors of light [33, 34, 69].

3.2 Combining Optogenetic Actuation with Ca^{2+} Imaging

Ca^{2+} imaging provides a noninvasive way to monitor the activity of muscles and neurons in *C. elegans* in close to real time. This can be achieved in fully intact worms, due to the optical transparency of the animal. Different genetically encoded calcium indicators (GECIs) have been designed to visualize and quantify intracellular calcium levels [28, 29, 73–76]. For chemically synthesized Ca^{2+} sensitive dyes, we refer the reader to other reviews; application of such dyes in *C. elegans* is challenging due to the difficulty to get them across the cuticle. Instead, GECIs are preferred to capitalize on the genetic tractability of *C. elegans.* Since GECIs are built entirely from proteins, they may be expressed in targeted cells under a tissue-specific promoter. There are two major classes of GECIs: The FRET-based indicators such as cameleons [28] and Tn-XXL [76], as well as the single-fluorophore indicators, such as the GCaMPs and GECOs [29, 73–75, 77].

Cameleons have been extensively used in *C. elegans* to monitor neural activity [78–81]. These GECIs use Förster resonance energy transfer (FRET) to indicate changes in Ca^{2+} concentration [28, 82]. FRET is a distance- and orientation-dependent, radiation-free transfer of energy from donor to acceptor chromophore (e.g., CFP and YFP), which results in the loss and gain of fluorescence of donor and acceptor molecule, respectively. In Cameleons CFP and YFP are connected via calmodulin and the calmodulin-binding peptide M13. When calmodulin binds Ca^{2+} ions, it undergoes a conformational change, binds M13, and thus affects CFP/YFP FRET efficiency. The ratio between YFP and CFP fluorescence serves as a measure for the Ca^{2+} concentration [28, 78], and the ratiometric nature allows to control for focus artifacts of the fluorescent signals, particularly in experiments with freely behaving animals.

The non-FRET Ca^{2+} indicators consist of a single circularly permuted (cp) GFP-variant that is fused to calmodulin at its C-terminus and to M13 at its N-terminus. Binding of Ca^{2+} causes the M13 and calmodulin domains to interact and to alter the environment of the chromophore (exclude water), which changes the brightness of the indicator [73, 83]. Examples for single-fluorophore GECIs are the GCaMPs, originally introduced by Nakai et al. in 2001 [29], and the GECOs [77]. Since then, GCaMPs have been improved continuously by using structure-based mutagenesis, with GCaMP6 as the most recent version [74, 75]. These Ca^{2+} indicators are prone to movement and focus artifacts. Thus, they are usually co-expressed with a reference fluorophore with a nonoverlapping fluorescence, which must not alter with calcium concentration [84], to allow distinction of Ca^{2+}-induced vs. focus-dependent fluorescence intensity changes.

The combination of optogenetic modulators with calcium indicators constitutes a powerful approach to study neuronal functionality. However, the overlap of spectral channels is often problematic.

ChR2 and CFP, GFP or YFP excitation spectra largely overlap; thus it is virtually impossible to image Cameleons or GCaMPs without concomitantly activating the ChR2-containing cell. One, however "dirty" approach is to compare stimulating one cell with ChR2 and imaging a linked cell with Cameleon or GCaMP, and to perform this experiment twice, once with, and a second time without ATR. In the case of the ATR experiment, one will not achieve a stable "baseline" Ca^{2+} trace, however. Another approach is to spatially restrict the actuation and the imaging light, provided that the cells to be imaged and the cell to be activated are spatially distinct from one another. This has recently been achieved by patterned illumination using a DMD-based illumination system in combination with a tracking system [30, 34]. A much less demanding approach is provided by using a spectrally shifted (relative to ChR2) Ca^{2+} indicator, namely RCaMP [85]. RCaMP is based on the red fluorescent protein mRuby. In 2012, Husson and colleagues used RCaMP as an optical readout for the excitation of the forward command neuron PVC by upstream photoactivation of the sensory PVD neuron [32]. Thus, the combination of ChR2 and RCaMP is feasible for the analysis of neuron to neuron and neuron to muscle communications. A similar, actually more potent red fluorescent Ca^{2+} indicator is R-GECO, which is based on the mApple protein [77]. However, R-GECO is not suited for optogenetic applications, as it shows photoconversion/photoactivation in response to blue illumination for concomitant ChR2 stimulation, which leads to a large increase in the red fluorescent signal, irrespective of the Ca^{2+} concentration [85]. A typical experiment combining optogenetic activation with in vivo Ca^{2+} imaging of the induced activity in body wall muscle cells is described below.

1. Animals expressing RCaMP in body wall muscle cells and ChR2 in the neuron of interest (e.g., in locomotion command neurons) may be investigated to assess muscular calcium changes during photostimulation of the command neurons (mediated via evoked or inhibited activity of the motor neurons). One day prior to the experiment, L4 larvae are transferred to NGM plates seeded with bacteria, and supplemented with 2.5–5 μM ATR (from a 100 mM EtOH stock solution), calculated with respect to the amount of NGM in the culture dish; control animals are transferred to plates without ATR.
2. On the day of the experiment, up to three animals are picked onto a 10 % agar pad (w/v, in M9 buffer) and are fully immobilized by using 0.1 μm polystyrene beads [86].
3. RCaMP fluorescence is monitored with a 10× air objective lens on an inverted fluorescence microscope. Two high power light-emitting diodes (LEDs) with the respective wavelengths of 470 nm for ChR2 excitation and 590 nm for RCaMP excitation are used as light sources. A beam splitter couples

both LEDs to enable a simultaneous illumination of the specimen, thus allowing the excitation of RCaMP and the photostimulation of ChR2 in parallel. A double band-pass excitation filter permits wavelengths of 479 and 585 nm from the illuminator to pass onto a 605 nm beam splitter that reflects the light towards the sample. Eventually, the emitted light is filtered by a 647/57 band-pass barrier filter that allows only wavelengths about 647 nm to pass towards the eye or the detector. In order to run different photostimulation protocols, a Lambda SC Smart Shutter controller (Sutter Instrument Company) can be used to switch the power supply of the 470 nm LED through TTL pulses. Videos are obtained with a CCD camera or a sCMOS camera at a frame rate of 20 fps. Micro-Manager freeware (https://www.micro-manager.org/) can be used to adjust video settings. The exposure time is set to 30 ms and frames are binned to 4×4 pixels. The light power is adjusted to 1 mW/mm^2 at 470 nm.

4. For analysis, the image sequences can be analyzed using ImageJ (http://imagej.nih.gov/ij/). Animals are segmented into regions of interest (ROI) by only circumscribing the RCaMP expressing areas. The mean fluorescence intensity values are calculated for every ROI at every frame. A region outside the animal is chosen as background and subtracted from the mean fluorescence values. The traces for each ROI are normalized (Eq. 1):

$$F_{\text{all}} = \frac{\left(F - F_0\right)}{F_0} \tag{1}$$

F_0 is the mean fluorescence of the first 100 video frames. The increase of the signal due to autofluorescence caused by the photostimulation is circumvented by normalizing the fluorescence values of the illumination period, with F_0 as the first frame of the illumination.

4 Notes

1. Dos and Don'ts when using ChR2

   As ChR2 is a low-efficiency Na^+ channel, high expression levels need to be achieved. Thus, multicopy extrachromosomal arrays are required that should be integrated into the genome. In some cases, we observed robust effects only after integration, e.g., for activation of PVD neurons, only 5 % of the transgenic animals showed PVD-evoked escape behavior, while after integration, 100 % of the animals responded [32]. Single-copy

genomic integration, e.g., by MosSCI [87], is thus not suitable to generate optogenetic strains (at least not with ChR2(H134R)).

Of course, as *C. elegans* neurons produce graded potentials, higher blue light intensity also increases the ChR2-mediated effects [25, 26]. However, as *C. elegans* has an intrinsic light response to avoid UV and blue light, mediated by the *lite-1* receptor [88], any optogenetic experiment using ChR2 runs the risk of activating the photoavoidance response in addition to the ChR2-evoked behavioral response. This is particularly true when prolonged (>300–500 ms) photostimulation of the neuron of interest is required to evoke an observable behavioral response. There are two possibilities to distinguish the specific from the nonspecific photoresponse: (1) Run the experiment with two groups of animals—one cultivated with, the other without ATR—and compare the behavioral response. This is problematic, however, if the behavior is actually modulated by the photoavoidance. (2) Perform the experiment in a *lite-1(ce314)* mutant background, which largely lacks the photophobic responses. This is to be done with caution, however, as *lite-1* mutants are not wild type, and for example exhibit slowed locomotion, particularly in swimming assays. Generally, as little blue light as necessary to evoke the full response should be used (both with respect to duration and intensity), and more light-sensitive variants of ChR2 can be used (C128S or H134R; T159C, see above) that mediate effects at light intensities that evoke almost no photophobic responses.

All-*trans* retinal itself has some nonspecific effects on *C. elegans*, (e.g., animals show slightly deeper body bending with ATR), and too much ATR actually becomes toxic. Thus the concentration of ATR should be kept as low as possible, while still evoking maximal activity. This can be titrated for the specific application. Keep in mind that ATR is prone to oxidation and photo damage, so keep the plates in the dark and do not use them if they are older than 4–5 days.

2. Dos and Don'ts when using inhibitory rhodopsins

As a word of caution, Arch and Mac, possibly due to their enhanced membrane insertion in *C. elegans*, actually can cause toxicity when overexpressed, unlike NpHR. Our observations are that expressing lots of NpHR in body wall muscle (80 ng/µl injected DNA) had no negative effects on viability or muscle physiology, despite the presence of large intracellular protein aggregates. In contrast, similar amounts of Arch and Mac caused animals to be sick and muscle cells to show aberrant membrane protrusions ("blebbing"). This could be avoided by expressing much less (<10 ng/µl injected DNA), while still maintaining more potent inhibition than with NpHR [19].

Also, while yellow light required for NpHR activation does not evoke photophobic responses, and thus can be applied in wild-type animals, the blue-green light wavelengths needed for Arch activation do evoke photophobicity. Thus, such experiments should be done in *lite-1* mutants, particularly if prolonged inhibition is required. Also for photoinhibition experiments, always include controls like the same transgenic animals cultivated without ATR and perform experiments in wild type, with and without ATR, but with the same light exposure.

References

1. White JG, Southgate E, Thomson JN, Brenner S (1986) The structure of the nervous system of the nematode Caenorhabditis elegans. Philos Trans R Soc Lond B Biol Sci 314: 1–340
2. Zemelman BV, Lee GA, Ng M, Miesenbock G (2002) Selective photostimulation of genetically chARGed neurons. Neuron 33:15–22
3. Zemelman BV, Nesnas N, Lee GA, Miesenbock G (2003) Photochemical gating of heterologous ion channels: remote control over genetically designated populations of neurons. Proc Natl Acad Sci USA 100:1352–1357
4. Rein ML, Deussing JM (2012) The optogenetic (r)evolution. Mol Genet Genomics 287: 95–109
5. De Bono M, Schafer WR, Gottschalk A (2013) Optogenetic actuation, inhibition, modulation and readout for neuronal networks generating behavior in the nematode Caenorhabditis elegans. In: Hegemann P, Sigrist SJ (eds) Optogenetics. De Gruyter, Berlin
6. Szobota S, Gorostiza P, Del Bene F, Wyart C, Fortin DL, Kolstad KD, Tulyathan O, Volgraf M, Numano R, Aaron HL, Scott EK, Kramer RH, Flannery J, Baier H, Trauner D, Isacoff EY (2007) Remote control of neuronal activity with a light-gated glutamate receptor. Neuron 54:535–545
7. Weissenberger S, Schultheis C, Liewald JF, Erbguth K, Nagel G, Gottschalk A (2011) PACalpha—an optogenetic tool for in vivo manipulation of cellular cAMP levels, neurotransmitter release, and behavior in Caenorhabditis elegans. J Neurochem 116:616–625
8. Steuer Costa W, Liewald J, Gottschalk A (2014) Photoactivated adenylyl cyclases as optogenetic modulators of neuronal activity. In: Cambridge S (ed) Photswitching proteins, vol 1148, Methods in molecular biology. Springer, New York, pp 161–175
9. Xu X, Kim SK (2011) The early bird catches the worm: new technologies for the Caenorhabditis elegans toolkit. Nat Rev Genet 12:793–801
10. Fenno L, Yizhar O, Deisseroth K (2011) The development and application of optogenetics. Annu Rev Neurosci 34:389–412
11. Bamann C, Kirsch T, Nagel G, Bamberg E (2008) Spectral characteristics of the photocycle of channelrhodopsin-2 and its implication for channel function. J Mol Biol 375:686–694
12. Stehfest K, Hegemann P (2010) Evolution of the channelrhodopsin photocycle model. Chemphyschem 11:1120–1126
13. Nagel G, Ollig D, Fuhrmann M, Kateriya S, Musti AM, Bamberg E, Hegemann P (2002) Channelrhodopsin-1: a light-gated proton channel in green algae. Science 296: 2395–2398
14. Nagel G, Szellas T, Huhn W, Kateriya S, Adeishvili N, Berthold P, Ollig D, Hegemann P, Bamberg E (2003) Channelrhodopsin-2, a directly light-gated cation-selective membrane channel. Proc Natl Acad Sci USA 100: 13940–13945
15. Boyden ES, Zhang F, Bamberg E, Nagel G, Deisseroth K (2005) Millisecond-timescale, genetically targeted optical control of neural activity. Nat Neurosci 8:1263–1268
16. Nagel G, Brauner M, Liewald JF, Adeishvili N, Bamberg E, Gottschalk A (2005) Light activation of channelrhodopsin-2 in excitable cells of Caenorhabditis elegans triggers rapid behavioral responses. Curr Biol 15:2279–2284
17. Zhang F, Wang LP, Brauner M, Liewald JF, Kay K, Watzke N, Wood PG, Bamberg E, Nagel G, Gottschalk A, Deisseroth K (2007) Multimodal fast optical interrogation of neural circuitry. Nature 446:633–639
18. Chow BY, Han X, Dobry AS, Qian X, Chuong AS, Li M, Henninger MA, Belfort GM, Lin Y, Monahan PE, Boyden ES (2010) High-performance genetically targetable optical neural silencing by light-driven proton pumps. Nature 463:98–102

19. Husson SH, Liewald JF, Schultheis C, Stirman JN, Lu H, Gottschalk A (2012) Microbial light-activatable proton pumps as neuronal inhibitors to functionally dissect neuronal networks in C. elegans. PLoS One 7, e40937
20. Mattis J, Tye KM, Ferenczi EA, Ramakrishnan C, O'Shea DJ, Prakash R, Gunaydin LA, Hyun M, Fenno LE, Gradinaru V, Yizhar O, Deisseroth K (2011) Principles for applying optogenetic tools derived from direct comparative analysis of microbial opsins. Nat Methods 9:159–172
21. Yizhar O, Fenno LE, Davidson TJ, Mogri M, Deisseroth K (2011) Optogenetics in neural systems. Neuron 71:9–34
22. Gradinaru V, Thompson KR, Zhang F, Mogri M, Kay K, Schneider MB, Deisseroth K (2007) Targeting and readout strategies for fast optical neural control in vitro and in vivo. J Neurosci 27:14231–14238
23. Petreanu L, Huber D, Sobczyk A, Svoboda K (2007) Channelrhodopsin-2-assisted circuit mapping of long-range callosal projections. Nat Neurosci 10:663–668
24. Liewald JF, Brauner M, Stephens GJ, Bouhours M, Schultheis C, Zhen M, Gottschalk A (2008) Optogenetic analysis of synaptic function. Nat Methods 5:895–902
25. Liu Q, Hollopeter G, Jorgensen EM (2009) Graded synaptic transmission at the Caenorhabditis elegans neuromuscular junction. Proc Natl Acad Sci USA 106: 10823–10828
26. Schultheis C, Brauner M, Liewald JF, Gottschalk A (2011) Optogenetic analysis of GABAB receptor signaling in Caenorhabditis elegans motor neurons. J Neurophysiol 106:817–827
27. Stirman JN, Brauner M, Gottschalk A, Lu H (2010) High-throughput study of synaptic transmission at the neuromuscular junction enabled by optogenetics and microfluidics. J Neurosci Methods 191:90–93
28. Miyawaki A, Llopis J, Heim R, McCaffery JM, Adams JA, Ikura M, Tsien RY (1997) Fluorescent indicators for Ca^{2+} based on green fluorescent proteins and calmodulin. Nature 388:882–887
29. Nakai J, Ohkura M, Imoto K (2001) A high signal-to-noise Ca(2+) probe composed of a single green fluorescent protein. Nat Biotechnol 19:137–141
30. Guo ZV, Hart AC, Ramanathan S (2009) Optical interrogation of neural circuits in Caenorhabditis elegans. Nat Methods 6:891–896
31. Schultheis C, Liewald JF, Bamberg E, Nagel G, Gottschalk A (2011) Optogenetic long-term manipulation of behavior and animal development. PLoS One 6, e18766
32. Husson SJ, Costa WS, Wabnig S, Stirman JN, Watson JD, Spencer WC, Akerboom J, Looger LL, Treinin M, Miller DM III, Lu H, Gottschalk A (2012) Optogenetic analysis of a nociceptor neuron and network reveals ion channels acting downstream of primary sensors. Curr Biol 22:743–752
33. Stirman JN, Crane MM, Husson SJ, Wabnig S, Schultheis C, Gottschalk A, Lu H (2011) Real-time multimodal optical control of neurons and muscles in freely behaving Caenorhabditis elegans. Nat Methods 8:153–158
34. Leifer AM, Fang-Yen C, Gershow M, Alkema MJ, Samuel AD (2011) Optogenetic manipulation of neural activity in freely moving Caenorhabditis elegans. Nat Methods 8:147–152
35. Piggott BJ, Liu J, Feng Z, Wescott SA, Xu XZS (2011) The neural circuits and synaptic mechanisms underlying motor initiation in C. elegans. Cell 147:922–933
36. Kocabas A, Shen CH, Guo ZV, Ramanathan S (2012) Controlling interneuron activity in Caenorhabditis elegans to evoke chemotactic behaviour. Nature 490:273–277
37. Pirri JK, McPherson AD, Donnelly JL, Francis MM, Alkema MJ (2009) A tyramine-gated chloride channel coordinates distinct motor programs of a Caenorhabditis elegans escape response. Neuron 62:526–538
38. Busch KE, Laurent P, Soltesz Z, Murphy RJ, Faivre O, Hedwig B, Thomas M, Smith HL, de Bono M (2012) Tonic signaling from O(2) sensors sets neural circuit activity and behavioral state. Nat Neurosci 15:581–591
39. Zimmer M, Gray JM, Pokala N, Chang AJ, Karow DS, Marletta MA, Hudson ML, Morton DB, Chronis N, Bargmann CI (2009) Neurons detect increases and decreases in oxygen levels using distinct guanylate cyclases. Neuron 61:865–879
40. Kateriya S, Nagel G, Bamberg E, Hegemann P (2004) "Vision" in single-celled algae. News Physiol Sci 19:133–137
41. Lawson MA, Zacks DN, Derguini F, Nakanishi K, Spudich JL (1991) Retinal analog restoration of photophobic responses in a blind Chlamydomonas reinhardtii mutant. Evidence for an archaebacterial like chromophore in a eukaryotic rhodopsin. Biophys J 60: 1490–1498
42. Kato HE, Zhang F, Yizhar O, Ramakrishnan C, Nishizawa T, Hirata K, Ito J, Aita Y, Tsukazaki T, Hayashi S, Hegemann P, Maturana AD, Ishitani R, Deisseroth K, Nureki O (2012) Crystal structure of the channelrhodopsin light-gated cation channel. Nature 482:369–374

43. Feldbauer K, Zimmermann D, Pintschovius V, Spitz J, Bamann C, Bamberg E (2009) Channelrhodopsin-2 is a leaky proton pump. Proc Natl Acad Sci U S A 106:12317–12322
44. Husson SJ, Gottschalk A, Leifer AM (2013) Optogenetic manipulation of neural activity in C. elegans: from synapse to circuits and behaviour. Biol Cell 105:235–250
45. Ritter E, Stehfest K, Berndt A, Hegemann P, Bartl FJ (2008) Monitoring light-induced structural changes of Channelrhodopsin-2 by UV-visible and Fourier transform infrared spectroscopy. J Biol Chem 283:35033–35041
46. Gunaydin LA, Yizhar O, Berndt A, Sohal VS, Deisseroth K, Hegemann P (2010) Ultrafast optogenetic control. Nat Neurosci 13:387–392
47. Haupts U, Tittor J, Bamberg E, Oesterhelt D (1997) General concept for ion translocation by halobacterial retinal proteins: the isomerization/switch/transfer (IST) model. Biochemistry 36:2–7
48. Lin JY, Lin MZ, Steinbach P, Tsien RY (2009) Characterization of engineered channelrhodopsin variants with improved properties and kinetics. Biophys J 96:1803–1814
49. Watanabe S, Liu Q, Davis MW, Hollopeter G, Thomas N, Jorgensen NB, Jorgensen EM (2013) Ultrafast endocytosis at Caenorhabditis elegans neuromuscular junctions. eLife 2, e00723
50. Berndt A, Schoenenberger P, Mattis J, Tye KM, Deisseroth K, Hegemann P, Oertner TG (2011) High-efficiency channelrhodopsins for fast neuronal stimulation at low light levels. Proc Natl Acad Sci USA 108:7595–7600
51. Erbguth K, Prigge M, Schneider F, Hegemann P, Gottschalk A (2012) Bimodal activation of different neuron classes with the spectrally red-shifted channelrhodopsin chimera C1V1 in Caenorhabditis elegans. PLoS One 7, e46827
52. Kleinlogel S, Feldbauer K, Dempski RE, Fotis H, Wood PG, Bamann C, Bamberg E (2011) Ultra light-sensitive and fast neuronal activation with the Ca(2)+-permeable channelrhodopsin CatCh. Nat Neurosci 14:513–518
53. Yizhar O, Fenno LE, Prigge M, Schneider F, Davidson TJ, O'Shea DJ, Sohal VS, Goshen I, Finkelstein J, Paz JT, Stehfest K, Fudim R, Ramakrishnan C, Huguenard JR, Hegemann P, Deisseroth K (2011) Neocortical excitation/inhibition balance in information processing and social dysfunction. Nature 477:171–178
54. Bamann C, Gueta R, Kleinlogel S, Nagel G, Bamberg E (2010) Structural guidance of the photocycle of channelrhodopsin-2 by an interhelical hydrogen bond. Biochemistry 49:267–278
55. Berndt A, Yizhar O, Gunaydin LA, Hegemann P, Deisseroth K (2009) Bi-stable neural state switches. Nat Neurosci 12:229–234
56. Prigge M, Schneider F, Tsunoda SP, Shilyansky C, Wietek J, Deisseroth K, Hegemann P (2012) Color-tuned channelrhodopsins for multiwavelength optogenetics. J Biol Chem 287:31804–31812
57. Gradinaru V, Thompson KR, Deisseroth K (2008) eNpHR: a Natronomonas halorhodopsin enhanced for optogenetic applications. Brain Cell Biol 36:129–139
58. Gradinaru V, Zhang F, Ramakrishnan C, Mattis J, Prakash R, Diester I, Goshen I, Thompson KR, Deisseroth K (2010) Molecular and cellular approaches for diversifying and extending optogenetics. Cell 141:154–165
59. Miller KG, Alfonso A, Nguyen M, Crowell JA, Johnson CD, Rand JB (1996) A genetic selection for Caenorhabditis elegans synaptic transmission mutants. Proc Natl Acad Sci USA 93: 12593–12598
60. Richmond J (2005) Synaptic function. WormBook 1–14
61. Richmond JE (2006) Electrophysiological recordings from the neuromuscular junction of C. elegans. WormBook 1–8
62. Francis MM, Maricq AV (2006) Electrophysiological analysis of neuronal and muscle function in C. elegans. Methods Mol Biol 351: 175–192
63. Sieburth D, Ch'ng Q, Dybbs M, Tavazoie M, Kennedy S, Wang D, Dupuy D, Rual JF, Hill DE, Vidal M, Ruvkun G, Kaplan JM (2005) Systematic analysis of genes required for synapse structure and function. Nature 436:510–517
64. Kittelmann M, Liewald JF, Hegermann J, Schultheis C, Brauner M, Steuer Costa W, Wabnig S, Eimer S, Gottschalk A (2013) In vivo synaptic recovery following optogenetic hyperstimulation. Proc Natl Acad Sci 110(32):E3007–E3016
65. Davis MW, Morton JJ, Carroll D, Jorgensen EM (2008) Gene activation using FLP recombinase in C. elegans. PLoS Genet 4, e1000028
66. Macosko EZ, Pokala N, Feinberg EH, Chalasani SH, Butcher RA, Clardy J, Bargmann CI (2009) A hub-and-spoke circuit drives pheromone attraction and social behaviour in C. elegans. Nature 458:1171–1175
67. Schmitt C, Schultheis C, Pokala N, Husson SJ, Liewald JF, Bargmann CI, Gottschalk A (2012) Specific expression of channelrhodopsin-2 in single neurons of Caenorhabditis elegans. PLoS One 7, e43164

68. Voutev R, Hubbard EJ (2008) A "FLP-Out" system for controlled gene expression in Caenorhabditis elegans. Genetics 180: 103–119
69. Stirman JN, Crane MM, Husson SJ, Gottschalk A, Lu H (2012) A multispectral optical illumination system with precise spatiotemporal control for the manipulation of optogenetic reagents. Nat Protoc 7:207–220
70. Richmond JE, Davis WS, Jorgensen EM (1999) UNC-13 is required for synaptic vesicle fusion in C. elegans. Nat Neurosci 2:959–964
71. Husson SJ et al. (2012) Keeping track of worm trackers. WormBook, ed. The C. elegans Research Community. WormBook. doi/10.1895/wormbook.1.156.1, http://www.wormbook.org.
72. Stephens GJ, Johnson-Kerner B, Bialek W, Ryu WS (2008) Dimensionality and dynamics in the behavior of C. elegans. PLoS Comput Biol 4, e1000028
73. Baird GS, Zacharias DA, Tsien RY (1999) Circular permutation and receptor insertion within green fluorescent proteins. Proc Natl Acad Sci USA 96:11241–11246
74. Akerboom J, Chen TW, Wardill TJ, Tian L, Marvin JS, Mutlu S, Calderon NC, Esposti F, Borghuis BG, Sun XR, Gordus A, Orger MB, Portugues R, Engert F, Macklin JJ, Filosa A, Aggarwal A, Kerr RA, Takagi R, Kracun S, Shigetomi E, Khakh BS, Baier H, Lagnado L, Wang SS, Bargmann CI, Kimmel BE, Jayaraman V, Svoboda K, Kim DS, Schreiter ER, Looger LL (2012) Optimization of a GCaMP calcium indicator for neural activity imaging. J Neurosci 32:13819–13840
75. Tian L, Hires SA, Mao T, Huber D, Chiappe ME, Chalasani SH, Petreanu L, Akerboom J, McKinney SA, Schreiter ER, Bargmann CI, Jayaraman V, Svoboda K, Looger LL (2009) Imaging neural activity in worms, flies and mice with improved GCaMP calcium indicators. Nat Methods 6:875–881
76. Mank M, Santos AF, Direnberger S, Mrsic-Flogel TD, Hofer SB, Stein V, Hendel T, Reiff DF, Levelt C, Borst A, Bonhoeffer T, Hubener M, Griesbeck O (2008) A genetically encoded calcium indicator for chronic in vivo two-photon imaging. Nat Methods 5:805–811
77. Zhao Y, Araki S, Wu J, Teramoto T, Chang YF, Nakano M, Abdelfattah AS, Fujiwara M, Ishihara T, Nagai T, Campbell RE (2011) An expanded palette of genetically encoded Ca(2)(+) indicators. Science 333:1888–1891
78. Kerr R, Lev-Ram V, Baird G, Vincent P, Tsien RY, Schafer WR (2000) Optical imaging of calcium transients in neurons and pharyngeal muscle of C. elegans. Neuron 26:583–594
79. Hilliard MA, Apicella AJ, Kerr R, Suzuki H, Bazzicalupo P, Schafer WR (2005) In vivo imaging of C. elegans ASH neurons: cellular response and adaptation to chemical repellents. EMBO J 24:63–72
80. Suzuki H, Kerr R, Bianchi L, Frokjaer-Jensen C, Slone D, Xue J, Gerstbrein B, Driscoll M, Schafer WR (2003) In vivo imaging of C. elegans mechanosensory neurons demonstrates a specific role for the MEC-4 channel in the process of gentle touch sensation. Neuron 39:1005–1017
81. Suzuki H, Thiele TR, Faumont S, Ezcurra M, Lockery SR, Schafer WR (2008) Functional asymmetry in Caenorhabditis elegans taste neurons and its computational role in chemotaxis. Nature 454:114–117
82. Nagai T, Yamada S, Tominaga T, Ichikawa M, Miyawaki A (2004) Expanded dynamic range of fluorescent indicators for Ca(2+) by circularly permuted yellow fluorescent proteins. Proc Natl Acad Sci USA 101:10554–10559
83. Nagai T, Sawano A, Park ES, Miyawaki A (2001) Circularly permuted green fluorescent proteins engineered to sense Ca^{2+}. Proc Natl Acad Sci USA 98:3197–3202
84. Kerr RA, Schafer WR (2006) Intracellular Ca^{2+} imaging in C. elegans. Methods Mol Biol 351:253–264
85. Akerboom J, Carreras Calderón N, Tian L, Wabnig S, Prigge M, Tolö J, Gordus A, Orger MB, Severi KE, Macklin JJ, Patel R, Pulver SR, Wardill TJ, Fischer E, Schüler C, Chen T-W, Sarkisyan KS, Marvin JS, Bargmann CI, Kim DS, Kügler S, Lagnado L, Hegemann P, Gottschalk A, Schreiter ER, Looger LL (2013) Genetically encoded calcium indicators for multi-color neural activity imaging and combination with optogenetics. Front Mol Neurosci 6:2
86. Kim E, Sun L, Gabel CV, Fang-Yen C (2013) Long-term imaging of Caenorhabditis elegans using nanoparticle-mediated immobilization. PLoS One 8, e53419
87. Frokjaer-Jensen C, Davis MW, Hopkins CE, Newman BJ, Thummel JM, Olesen SP, Grunnet M, Jorgensen EM (2008) Single-copy insertion of transgenes in Caenorhabditis elegans. Nat Genet 40:1375–1383
88. Edwards SL, Charlie NK, Milfort MC, Brown BS, Gravlin CN, Knecht JE, Miller KG (2008) A novel molecular solution for ultraviolet light detection in Caenorhabditis elegans. PLoS Biol 6, e198

Chapter 9

Simultaneous Optogenetic Stimulation of Individual Pharyngeal Neurons and Monitoring of Feeding Behavior in Intact *C. elegans*

Nicholas F. Trojanowski and Christopher Fang-Yen

Abstract

Optogenetic approaches have proven powerful for examining the role of neural circuits in generating behaviors, especially in systems where electrophysiological manipulation is not possible. Here we describe a method for optogenetically manipulating single pharyngeal neurons in intact *C. elegans* while monitoring pharyngeal behavior. This approach provides bidirectional and dynamic control of pharyngeal neural activity simultaneously with a behavioral readout and has allowed us to test hypotheses about the roles of individual pharyngeal neurons in regulating feeding behavior.

Key words: Optogenetics, Feeding behavior, Small circuits, Pharynx, In vivo optogenetics, *C. elegans*

1 Introduction

The nematode *C. elegans* is a powerful tool for studying the function of neural circuits, in large part due to its genetic tractability and known synaptic connectivity [1, 2]. Since it is not currently possible to electrophysiologically manipulate the activity of the *C. elegans* nervous system in intact animals [3], the primary method for studying the roles of specific neurons in behavior has been ablation of these neurons in young larvae using a laser beam followed by observation of behavior in adults [4, 5]. However, laser ablation is a permanent, unidirectional manipulation of a neural circuit that does not easily allow the assessment of functional redundancy or developmental compensation [6]. It is therefore suboptimal for understanding dynamic phenomena like neural activity.

David Biron and Gal Haspel (eds.), *C. elegans: Methods and Applications*, Methods in Molecular Biology, vol. 1327,
DOI 10.1007/978-1-4939-2842-2_9,

Optogenetic techniques, which involve using light-sensitive ion channels to manipulate neural activity and behavior, are ideal for precise temporal control of neural activity in behaving animals, as they afford bidirectional and dynamic manipulation [7]. To date, most optogenetic experiments in *C. elegans* have been performed by illuminating the entire worm after expressing light-sensitive proteins in a desired subset of neurons [8]. However, the cellular specificity of this approach—and therefore its utility for functionally dissecting neural circuits—has been limited by the difficulty of finding a promoter that drives gene expression only in the desired neurons. Genetic intersection approaches have been used [9–12], but even these are not guaranteed to provide the desired overlap. Furthermore, when using promoters with high cellular specificity, a different strain is required to study each subset of neurons, making it impossible to study the functions of multiple neurons in a single worm. To solve this problem, multiple groups have developed different methods for using patterned light to illuminate arbitrary parts of the worm corresponding to neurons of interest. The first of these studies was done using immobilized worms and optically monitoring calcium levels in neurons of interest [13]. More recent work has used locomotion as a behavioral readout of circuit function [14–16].

Here, we describe a method for using spatially restricted optogenetic illumination to investigate the behavioral effects of manipulating individual neurons in the pharynx (feeding organ). The pharyngeal neural circuit is one of the simplest in the worm, containing 20 neurons of 14 classes. However, experiments in which each of the 14 classes of pharyngeal neurons was ablated found only three classes for which ablation caused a clearly identifiable deficit in feeding behavior [17], perhaps due to circuit redundancy. Using an optogenetic approach, we uncovered genetic and neural degeneracy in the circuit for excitation of pharyngeal pumping [18].

We use a digital micromirror device (DMD) to focus light in defined patterns on worms that express light-sensitive excitatory (e.g., blue-light-sensitive ion channel Channelrhodopsin-2 (ChR2)) [19] or inhibitory microbial opsins (e.g., blue-light-powered proton pump (Mac) from *Leptosphaeria maculans*) [20–22]. To stimulate single neurons, we take advantage of the fact that pharynx is internal and use polystyrene beads to immobilize worms [23]. This affords submicron spatial resolution without pharmacological manipulation. We use particle image velocimetry to automatically track movement of pharyngeal muscles during optogenetic manipulations. This approach improves on both the lack of specificity present in typical optogenetic experiments and the lack of sensitivity and intraobserver variability inherent in manual observation [24].

2 Materials

1. Optical table (at least 1.5 m × 1.2 m surface).
2. 473 nm laser (e.g., Shanghai Laser and Optics Century model BL473T3-150).
3. Leica DMI3000B inverted microscope and associated filter cubes.
4. Leica Plan Apo 63× oil immersion objective lens with N.A. = 1.4.
5. Photometrics DV2 multichannel imaging system.
6. Cooled CCD camera with software capable of 30 frames per second (e.g., Andor iXon 885 and Andor SOLIS software).
7. 1024 by 768 pixel digital micromirror device (DMD) with Discovery 4100 Explorer software (Discovery 4100 DLP, Texas Instruments/Digital Light Innovations).
8. Power meter (e.g., Coherent FieldMate).
9. MATLAB software.
10. Aluminum mounting box for DMD control board (approx. 15 cm × 20 cm).
11. 6.24 mm focal length aspheric lens (e.g., Thorlabs C110TME-A).
12. 75 mm focal length planoconvex lens (e.g., Thorlabs LA1608-A).
13. 100 mm focal length, 2-in. diameter achromatic lens (e.g., Thorlabs AC508-100-A).
14. 2 200 mm focal length, 2-in. diameter achromatic lenses (e.g., Thorlabs AC508-200-A).
15. ~7 mirrors (e.g., Thorlabs PF20-03-P01 and PF10-03-P01).
16. Two irises (e.g., Thorlabs ID15).
17. Longpass dichroic filter (e.g., Thorlabs DMLP490R).
18. Hardware for mounting each optic.
    (a) Post holders (e.g., Thorlabs UPH3).
    (b) Posts (e.g., Thorlabs TR3).
    (c) Lens and mirror mounts (e.g., Thorlabs LMR1, LMR2, KM100, KM200).
    (d) Post clamps (e.g., Thorlabs RA45).
    (e) 1/4"–20 cap screws (e.g., Thorlabs HW-KIT2).
    (f) 8–32 cap screws (e.g., Thorlabs HW-KIT3).
19. Sodium fluorescein.

20. NGM buffer (NGM from [25] but without agar, cholesterol, or peptone).
21. Agarose.
22. Serotonin HCl.
23. Slides and coverslips.
24. 0.5 mm thick plastic shim stock (Ardus Yellow 0.020 Inches).
25. 250 mL beaker.
26. 50 mL centrifuge tube.
27. Disposable spatulas (e.g., VWR International 80081-188).
28. 2.5 % (v/v) suspension of 50 nm diameter polystyrene beads (Polysciences 08691-10).
29. Transgenic nematode strains expressing opsins in neurons of interest.

3 Methods

The methods will be described in five sections: (**a**) Building the rig, (**b**) Constructing the worm strains, (**c**) Immobilizing the worms, (**d**) Performing the experiments, and (**e**) Analyzing the data.

3.1 Building the Rig

In the optical setup, a laser beam is first expanded in diameter by about ten times by a telescope consisting of two lenses (Fig. 1). This laser beam is routed via mirrors to the DMD, which restricts the beam to a set of pixels selected by computer. Next, the image on the DMD is relayed to an intermediate image plane of the microscope with 2× magnification using lenses with focal lengths 100 and 200 mm. Finally the image is relayed again to the worm via a relay lens system composed of a 200 mm focal length lens and the objective lens. The steps for constructing this setup are described below, and a schematic is depicted in Fig. 1.

Before starting work, obtain the appropriate laser protection eyewear, light curtains, and other safety equipment. Consult your laser safety protection officer to determine what is needed.

1. Place the microscope and laser on an optical table and secure them so that they will not inadvertently move in relationship to the rest of the table (*see* **Note 1**).
2. Mount each mirror or lens in an appropriate mount, and attach each mount to a post and post holder. Fasten post holders to the table in an out of the way location so that they are secure while you are performing the other steps.
3. Mount the DMD by attaching the DMD to a KM200 mirror mount and attaching the control board to the mounting case using screws and board standoffs. Ensure that the DMD power cable can be plugged in to the control board after mounting.

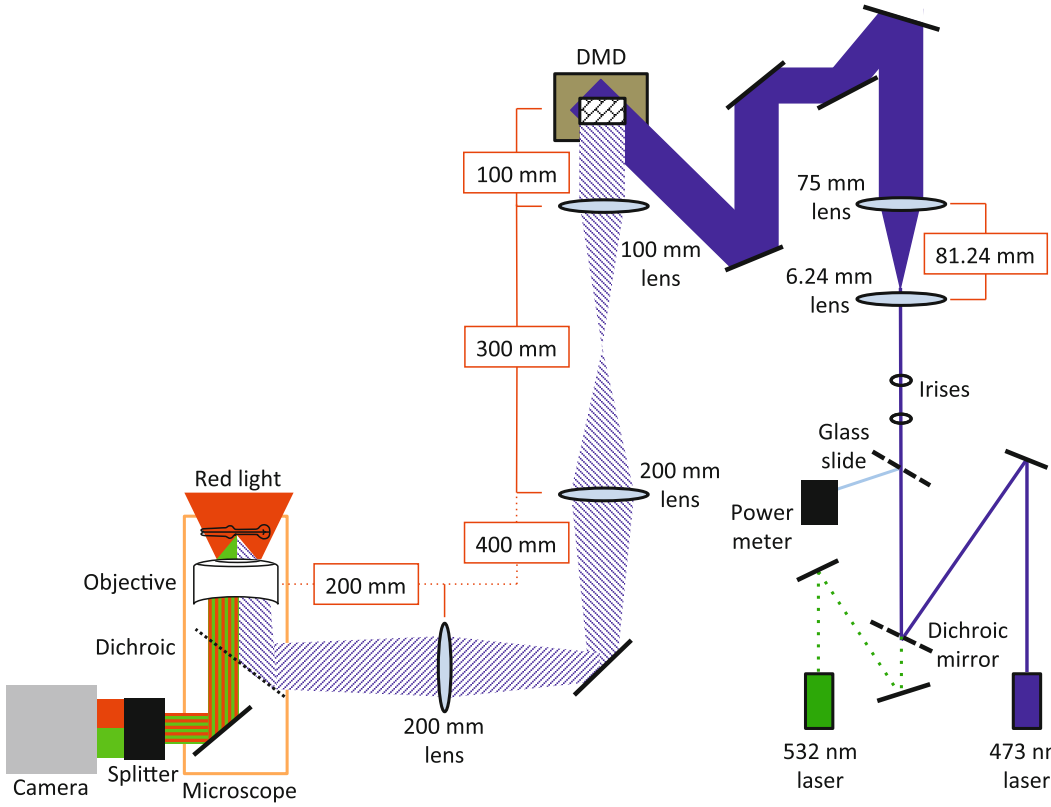

Fig. 1 Setup for single neuron stimulation of pharyngeal neurons. Light leaves the blue laser and is reflected off a mirror (*black line*) and dichroic beam splitter. A small percentage of the light is then reflected to a power meter to monitor laser output. The light then passes through two irises before being expanded through a telescope composed of two lenses. The beam is then, through a series of mirrors, reflected onto the DMD (*brown box*) such that it covers the entire grid of mirrors. This beam then passes through a series of lenses along the light path. It then enters the microscope through an auxiliary port, where it is reflected by a dichroic on a custom filter cube into the back of the objective. The stage of the microscope is illuminated with *red* light. This *red* light and the *green* light emitted by fluorescent proteins then pass through a DV2 beam splitter, which separates the red and green channels, which are then recorded by a camera

4. Place two irises in the path of the laser, and adjust them and the laser so that the laser beam is perfectly horizontal and passes directly through the center of the irises.
5. Place the 6.24 mm focal length lens and the 75 mm focal length lens so they are 81.24 mm apart (the sum of the focal lengths), beyond the irises. The lenses should be oriented according to their design specifications, with the sides designed for short conjugate distance facing each other.
6. Align these lenses so the beam passes through the center of the lenses and is collimated (i.e., neither converging nor diverging) after exiting the 75 mm focal length lens (*see* **Note 2**).
7. Install a filter cube and dichroic filter that reflects light from the desired port through the back of the objective. For GFP

optics, use a longpass dichroic filter that reflects wavelengths shorter than 500 nm and transmits wavelengths longer than 500 nm (*see* **Note 3**).

8. Place one of the 200 mm lenses 200 mm away from the back of the objective, along the light path, with the curved side facing the microscope (*see* **Note 4**).
9. Place the other 200 mm lens 400 mm beyond the first 200 mm lens, along the light path. The curved side should face away from the microscope (*see* **Note 5**).
10. Place the 100 mm lens 300 mm beyond the furthest 200 mm lens. The curved side should face the 200 mm lens.
11. Place the DMD 100 mm beyond the 100 mm lens. Screw down loosely, as the position will likely need to be adjusted later (*see* **Note 6**).
12. Plug in the DMD and use the Discovery 4100 Explorer software to set it so that all the mirrors are in the ON position.
13. Use mirrors as necessary to project the laser beam onto the DMD (*see* **Note 7**).
14. Adjust the angle of the DMD so that with the mirrors in the ON position, the laser beam is reflected along the optical path of the microscope, through the center of the 100 and 200 mm lenses (*see* **Note 8**).
15. Place a glass slide at an angle in the light path shortly after the beam leaves the laser by taping the slide to an optical post (*see* **Note 9**).
16. Set up the power meter so the light reflected off the glass slide hits the center of the sensor.
17. Place a red filter in the transillumination light path to enable behavioral observation during the optogenetics experiments without off-target stimulation effects.
18. To allow independent analysis of the green (GFP/targeting) and red (brightfield/behavior) signals, attach the DV2 and camera to the imaging port of the microscope.
19. Align the DV2 according to the instructions that come with the device (*see* **Note 10**).
20. Register the DMD coordinates to the field of view of the camera. Create a series of images that contain a square moving in a matrix across the DMD (*see* **Note 11**).
21. Prepare a slide with a thin layer of 1 M sodium fluorescein in water or glycerol between two shims under a coverslip and place it on the microscope stage.
22. Pass the series of images to the DMD (**step 20**) and record where (if at all) a fluorescent spot appears on the camera.

23. Compute the correspondence matrix of the coordinates passed to the DMD and coordinates where fluorescence was detected.
24. Use this matrix to define an image transformation between the DMD and the camera.

3.2 Creating Worm Strains

1. In general, the same strains that are used for whole worm optogenetics can be used for this method (*see* **Note 12**).
2. These worms should be grown in the dark following standard procedures. Where needed, add 2 μL of 100 mM all-*trans* retinal (ATR) in ethanol to the bacterial suspension immediately before seeding (*see* **Note 13**).
3. Laser ablations, if desired, can be performed as previously described [4, 5].

3.3 Preparing Agarose Pads

1. Prepare six slides by placing 0.5 mm thick shims, approximately 1 cm by 2 cm, on each end of each slide.
2. Prepare agarose pads by mixing 0.20 g agarose and 4 mg 5-HT into 2 mL of NGM (10 % agarose, 10 mM 5-HT) in a 50 mL centrifuge tube (*see* **Note 14**).
3. Swirl the mixture gently so that the agarose is evenly dispersed in the liquid rather than a large clump, but avoid getting too much of the mixture on the sides of the tube.
4. Rest the lid on top of the centrifuge tube, but do not screw it on.
5. Place the centrifuge tube in a 250 mL beaker.
6. Fill the beaker to ~50 mL with tap water, just above the level of liquid in the centrifuge tube.
7. Microwave the beaker and centrifuge tube for 50 s at high power, at which point the agarose mixture should be clear, and may have some bubbles.
8. Using a disposable plastic spatula, place a drop of agarose mixture about 1 cm in diameter onto the middle of a slide prepared with shims and immediately cover this slide with a second slide (*see* **Note 15**).
9. Make slides until all the agarose has been used (*see* **Note 16**).
10. Allow slides to set for at least 1 min before adding worms.

Note: **Steps 11–16** should be performed quickly for optimal immobilization.

11. Load 1.5 μL of a 2.5 % (v/v) suspension of 50 nm diameter polystyrene beads into a 20 μL pipettor [23] (*see* **Note 17**).
12. Remove top slide from one of the pads and place the slide with the pad onto a plate lid on the microscope stage.

13. Use bacteria to stick up to ten worms onto the bottom of a worm pick, but do not put them on the pad yet.
14. Expel the 1.5 μL of beads onto the pad.
15. Gently, and as quickly as possible, place the pick into the beads and allow the worms to transfer into the beads on the pad (*see* **Note 18**).
16. Quickly place a coverslip on top of the pad to immobilize the worms.
17. Wait 5–10 min before performing experiments to allow the worms to habituate.

3.4 Performing the Experiments

1. Set the frame rate of the camera and the laser power (*see* **Note 19**).
2. Place a slide on the microscope stage and find a worm at 10× on the microscope under brightfield illumination (*see* **Note 20**).
3. Switch to 63× and move the pharynx of the worm into the center of the field of view under brightfield illumination (*see* **Note 21**).
4. Manually take a *z*-stack of the pharyngeal neurons by illuminating the entire field using the DMD, and focusing through the relevant regions. This illumination period should be less than 1 s.
5. If desired, use MATLAB to convert the images into JPEG files. MATLAB scripts for this and all other steps are available upon request (*see* **Note 22**).
6. Identify the images in the *z*-stack that most clearly show the neurons of interest.
7. Use the roipoly function in MATLAB to select the regions of these images you would like to use to stimulate each neuron (*see* **Note 23** and Fig. 2b, c).
8. Use MATLAB to create an image mask that contains the value 1 for the region you outlined in the previous step and the value 0 elsewhere, and transform this file into DMD coordinates using the transformation computed in step A23 (*see* **Note 24**).
9. Create a Discovery 4100 script that tells the DMD which images to display and at which times they should be displayed (*see* **Note 25**).
10. Acquire a baseline recording of behavior without any illumination (*see* **Note 26**).
11. Run each script while recording from both the red and green channels (*see* **Note 27**).

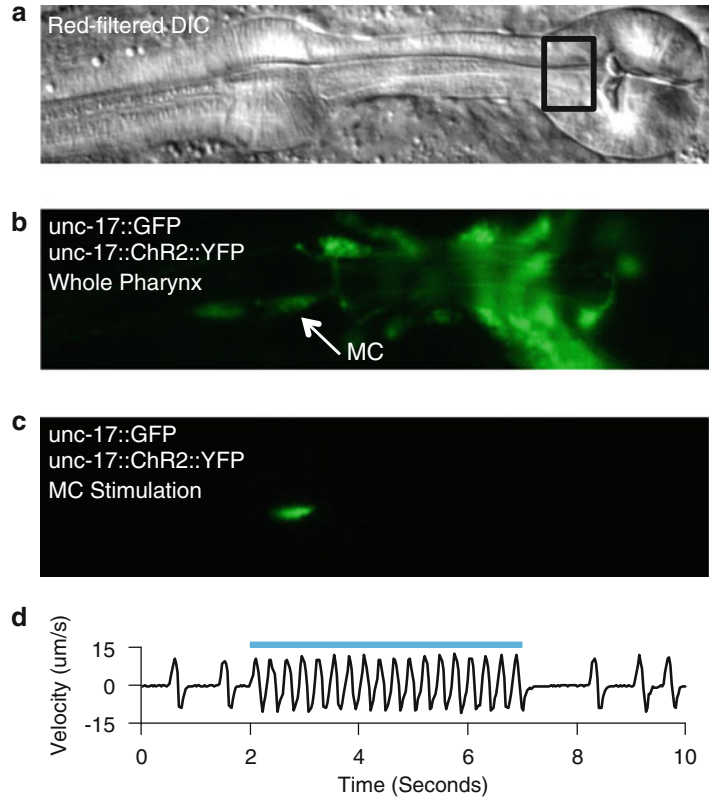

Fig. 2 Stimulation of single pharyngeal neurons. (**a**) DIC image of the pharynx. *Black* box denotes region used for velocity calculations. (**b**) Wide field GFP fluorescence image of the same field of view as in (**a**). The *arrow* points to an MC soma. (**c**) GFP fluorescence image of the same field of view as in (**a**) and (**b**), during selective illumination of an MC soma. (**d**) Velocity from PIV algorithm during ChR2-mediated stimulation of the MC neurons. Each peak in the velocity represents a pump. The *blue* bar represents timing of laser illumination. Modified from Trojanowski et al. [18] with permission from American Physiological Society

3.5 Analyzing the Data

The following steps should be repeated for each experiment:

1. If desired, convert the images into JPEG files (*see* **Note 22**).
2. Use the roipoly function in MATLAB to draw a ROI around the brightest part of the neuron that was stimulated during the experiment (*see* **Note 28**).
3. Use MATLAB to track the pixel intensity of this region over the course of experiment.
4. Use MATLAB to identify the times at which the intensity of this region sharply increased or decreased. These are the times at which the stimulus was turned on and off, respectively.

5. Use MATLAB to select the rectangular region of the terminal bulb just anterior to the grinder (*see* **Note 29** and Fig. 2a).
6. Using the freely available package PIVlab, a Time-Resolved Digital Particle Image Velocimetry Tool for MATLAB, track the velocity of this region over time (*see* **Note 30** and Fig. 2d).
7. Use this trace of velocity over time to identify the times at which a pump occurred by drawing a threshold and recording the times at which a positive-going threshold crossing occurs (*see* **Note 31**).
8. Determine the number of pumps that occur during each interval in which the stimulus is on or off (*see* **Note 32**).
9. Divide the number of pumps in a stimulus interval by the length of that stimulus interval to find the average pump rate (*see* **Note 33**).

4 Notes

1. Our setup uses a Leica DMI3000B inverted microscope with a Leica Plan Apo 63× oil immersion objective lens with N.A. = 1.4. Any microscope with a port that allows direct access to the back of the objective should suffice. An inverted microscope may be easier to set up due to the lower height of the fluorescence illumination path, but an upright microscope could be used as well.
2. The distance between the 6.24 mm lens and the 75 mm lens must be ~81.24 mm, but the distances from 75 mm lens to the irises, between the irises, and between the irises and the laser, can be arbitrary. Our rig is partially designed to work with a 532 nm laser as well as a 473 nm laser, so we use a system of mirrors and a dichroic beam splitter to allow us to use these two lasers through the same optical path. If you only wish to use one laser, you can aim it directly through the irises, though we find it useful to have the beam reflect off at least one mirror before entering the irises, because it is easier to precisely adjust the tilt angle of the mirror than that of the laser.
3. For the Leica DMI3000B, the fluorescent light port in the rear of the microscope contained optics of unknown parameters, so we used a side auxiliary port and custom filter cube (Nuhsbaum Inc.) that allowed direct access to the back of the objective.
4. You should adjust this position so that a sharp back-scattered image through the objective forms 200 mm away beyond the lens. It is difficult to measure the 200 mm distance from the back of the objective to this lens precisely, so you may need to adjust this lens empirically later. If this lens needs to be adjusted

after all the other lenses are set up, it may be easier to adjust the position of the microscope rather than move all the optics.

5. Due to spatial constraints, we put a mirror between the 200 mm lenses. This is fine so long as the total distance along the light path between the lenses is 400 mm.
6. The 100 mm distance here should be adjusted empirically so that a crisp back-scattered image from the microscope appears on the DMD and is centered on the grid of mirrors, covering it completely.
7. The laser beam should just barely cover the DMD. If this is not the case, then you likely need to adjust the two smaller lenses so that the beam is not changing in size after it exits the 75 mm lens.
8. To do this, the light must be incident onto the DMD from the lower right, if you are facing the DMD. We find that is easiest to use multiple mirrors to reflect the laser beam at the correct angle, as this provides multiple degrees of freedom for adjustment.
9. This will allow a large amount of the light to pass through but will reflect a small fraction without disrupting the direction of the laser beam. You can measure the light power reflected and the light power at the objective to determine the percentage of light that is reflected, and use this relationship to determine the light power at the objective at any time.
10. Alternatively, a beam splitter could be built in-house with similar optics to those in the DV2.
11. In order to target a specific region of the microscope stage, you must first identify the DMD coordinates that correspond to this region. This process will need to be repeated if any of the optics are inadvertently bumped, so make sure that all of the optics are tightly fastened to the table before beginning this step.
12. It is essential that the opsin of interest is tagged with an appropriate fluorescent protein (we used blue light to excite ChR2 and Mac, so we used opsins tagged with YFP or GFP). However, we found that for some transgenes the ChR2::YFP was not bright enough to resolve neuron processes (e.g., *zxIs6[unc-17p::ChR2(H134R)::YFP+lin-15(+)]*), likely because the ChR2 is membrane bound. After confirming expression in the relevant cell bodies, we crossed strains containing dim transgenes into a strain that expressed cytoplasmic GFP under the same promoter (we used *vsIs48[unc-17::GFP]*). We found this particularly useful for looking at off-target effects during ablation experiments, were we wanted to determine the effect of stimulating processes near a cell body after killing the cell body.

13. We stored ATR-seeded plates at 4 °C for up to 1 week before use.
14. We make the agarose mixture fresh for each experiment. 5-HT is necessary for inducing a basal pumping rate during immobilization. Other drugs can be added at this step as desired, though we found that adding too many ionic salts (more than 10 mM) caused the polystyrene beads to clump and made immobilization difficult.
15. We have found that the flexibility of the plastic spatulas makes it easier to get all the agarose out of the centrifuge tube, compared to stainless steel spatulas, and their low thermal mass may prevent premature cooling of the agarose.
16. We are usually able to make 6 slides from 2 mL of agarose solution.
17. We store 100 μL aliquots of polystyrene beads at 4 °C between uses.
18. When the pads contain 5-HT, the beads clump quickly after they are added to the pad, which reduces the quality of immobilization. Thus, we try to have the beads on the pad for as little time as possible before we add the cover slip.
19. We use an exposure time of 30 ms, which produces a frame rate of 32.7 Hz. We set the laser power so that the irradiance of the laser at the objective is approximately 37 mW/mm^2, well above the saturation irradiance of ChR2 [26]. These settings can be adjusted to increase the visibility of the fluorescent signal, if necessary.
20. Because of the way the DV2 splits the camera field of view, it is important that the head of the worm is close to aligned with the long direction of each channel's field of view (within ~30°). If the head is not aligned in this manner, rotate the slide or select a different worm on the slide. Do not rotate the camera, or you will have to re-register the DMD and camera images.
21. It is important that the grinder is visible in the camera's field of view, since its motion will later be used to quantify feeding rate. It is also important that the locations of the neurons of interest are visible in the camera. For pharyngeal neurons, this should not be an issue as long as the worm is aligned as described in **Note 20**.
22. The Andor iXon 885 and Andor SOLIS software produce images as multipage TIFF files. We find it easier to work with JPEG files than multipage TIFF files, but this is a lossy compression and may increase noise.
23. This should be a region slightly larger than the cell body—about 2–3 μm in diameter—to allow constant stimulation as the neural cell bodies move during the pump. It is important that the neuron of interest remains in this region during the

entire experiment, because the fluorescent signal from this neuron will be used to determine the times of stimulation *post hoc*. Counterintuitively, we found it difficult to immobilize some paralyzed mutants, in which case we found it necessary to use a substantially larger stimulus region to ensure the neuron of interest was stimulated during the entire experiment.

24. The DMD mirrors can be set in either the ON or OFF position, so we pass an image that contains 1 s (representing ON) in locations corresponding to the area of the stage we wish to illuminate and 0 s (representing OFF) elsewhere.
25. The DMD works by reading in images that represent the pattern it should display and displaying this pattern, then pausing for a defined period, then reading in the next file, and so on. For our experiments, we begin with an all-off image for 5 s, followed by 5 s of illumination of the neuron of interest, followed by an all-off image for 5 s, repeating up to ten times and ending with an all-off image.
26. We record the baseline for 30 s.
27. We wait 2–3 min between running each script, i.e., between each neuron we stimulate. We found that the behavior was most robust when experiments were performed within 90 min of immobilization.
28. Here we find it better to use a ROI smaller than that used for the experiment, because it is easier to detect changes in brightness when just looking at the brightest parts of the neuron.
29. We found that using a rectangle that extends from the anterior edge of the terminal bulb to the grinder, and is just slightly wider than the grinder, provides the best signal.
30. Tracking the velocity of this region over time will show a series of spikes, each representing a pump: a positive change in velocity represents the movement of the grinder towards the posterior and a negative change in velocity represents anterior movement.
31. We found that using a threshold of half of the maximum velocity provided high sensitivity and specificity, though a wide range of threshold values will give the same result on a good recording.
32. We did this for each stimulus interval by finding the number of pumps for which the value (pump time-stimulus time) was greater than 0 but less than the time between when the stimulus turned on and when it turned off.
33. The pumping rate during the stimulus-off windows is sometimes lower than the initial baseline, likely due to post-excitatory inhibition, so we typically do not use these values for looking at the effect of neuron stimulation. Rather, we use the pumping rate that we get from step D10 as the baseline.

Acknowledgements

We thank Olivia Padovan-Merhar for assistance writing MATLAB scripts and David Raizen for valuable comments and suggestions. Some strains were provided by Alexander Gottschalk and the *Caenorhabditis* Genetics Center (CGC), which is funded by National Institutes of Health (NIH) Office of Research Infrastructure Programs (P40-OD-010440). This work was supported by the National Institute of Neurological Disorders and Stroke of the NIH under Award R01-NS-084835 (C. Fang-Yen), the National Heart, Lung, and Blood Institute of the NIH Award T31-HL-07953 (N.F. Trojanowski; principal investigator: Allen I. Pack), the Ellison Medical Foundation (C. Fang-Yen), and an Alfred P. Sloan Foundation Research Fellowship (C. Fang-Yen).

References

1. Xu XZS, Kim SK (2011) The early bird catches the worm: new technologies for the Caenorhabditis elegans toolkit. Nat Rev Genet 12:793–801. doi:10.1038/nrg3050
2. Bargmann CI, Marder E (2013) From the connectome to brain function. Nat Methods 10:483–490. doi:10.1038/nmeth.2451
3. Goodman MB, Lindsay TH, Lockery SR, Richmond JE (2012) Electrophysiological methods for Caenorhabditis elegans neurobiology. Methods Cell Biol 107:409–436. doi:10.1016/B978-0-12-394620-1.00014-X
4. Bargmann CI, Avery L (1995) Laser killing of cells in Caenorhabditis elegans. Methods Cell Biol 48:225–250
5. Fang-Yen C, Gabel CV, Samuel ADT et al (2012) Laser microsurgery in Caenorhabditis elegans. Methods Cell Biol 107:177–206. doi:10.1016/B978-0-12-394620-1.00006-0
6. Steger KA, Shtonda BB, Thacker CM et al (2005) The C. elegans T-type calcium channel CCA-1 boosts neuromuscular transmission. J Exp Biol 208:2191–2203. doi:10.1242/jeb.01616
7. Deisseroth K (2010) Optogenetics. Nat Methods 8:26–29. doi:10.1038/nmeth.f.324
8. Husson SJ, Gottschalk A, Leifer AM (2013) Optogenetic manipulation of neural activity in C. elegans: from synapse to circuits and behaviour. Biol Cell doi: 10.1111/boc.201200069
9. Voutev R, Hubbard EJA (2008) A "FLP-Out" system for controlled gene expression in Caenorhabditis elegans. Genetics 180:103–119. doi:10.1534/genetics.108.090274
10. Davis MW, Morton JJ, Carroll D, Jorgensen EM (2008) Gene activation using FLP recombinase in C. elegans. PLoS Genet 4, e1000028. doi:10.1371/journal.pgen.1000028
11. Wei X, Potter CJ, Luo L, Shen K (2012) Controlling gene expression with the Q repressible binary expression system in Caenorhabditis elegans. Nat Methods 9:391–395. doi:10.1038/nmeth.1929
12. Schmitt C, Schultheis C, Husson SJ et al (2012) Specific expression of channelrhodopsin-2 in single neurons of Caenorhabditis elegans. PLoS One 7, e43164. doi:10.1371/journal.pone.0043164.t004
13. Guo ZV, Hart AC, Ramanathan S (2009) Optical interrogation of neural circuits in Caenorhabditis elegans. Nat Methods 6:891–896. doi:10.1038/nmeth.1397
14. Leifer AM, Fang-Yen C, Gershow M et al (2011) Optogenetic manipulation of neural activity in freely moving Caenorhabditis elegans. Nat Methods 8:147–152. doi:10.1038/nmeth.1554
15. Stirman JN, Crane MM, Husson SJ et al (2011) Real-time multimodal optical control of neurons and muscles in freely behaving Caenorhabditis elegans. Nat Methods 8:153–158. doi:10.1038/nmeth.1555
16. Kocabas A, Shen C-H, Guo ZV, Ramanathan S (2012) Controlling interneuron activity in Caenorhabditis elegans to evoke chemotactic behaviour. Nature 1–6. doi: 10.1038/nature11431
17. Avery L, You Y-J (2012) C. elegans feeding. Wormbook 1–23. doi: 10.1895/wormbook.1.150.1
18. Trojanowski NF, Padovan-Merhar O, Raizen DM, Fang-Yen C (2014) Neural and genetic

degeneracy underlies Caenorhabditis elegans feeding behavior. J Neurophysiol 112: 951–961. doi:10.1152/jn.00150.2014

19. Zhang F, Wang L-P, Brauner M et al (2007) Multimodal fast optical interrogation of neural circuitry. Nature 446:633–639. doi:10.1038/nature05744
20. Chow BY, Han X, Dobry AS et al (2010) High-performance genetically targetable optical neural silencing by light-driven proton pumps. Nature 463:98–102. doi:10.1038/nature08652
21. Waschuk SA, Bezerra AG, Shi L, Brown LS (2005) Leptosphaeria rhodopsin: bacteriorhodopsin-like proton pump from a eukaryote. Proc Natl Acad Sci U S A 102: 6879–6883. doi:10.1073/pnas.0409659102
22. Okazaki A, Takahashi M, Toyoda N, Takagi S (2014) Optical silencing of C. elegans cells with light-driven proton pumps. Methods 68:425–430. doi:10.1016/j.ymeth.2014.02.030
23. Kim E, Sun L, Gabel CV, Fang-Yen C (2013) Long-term imaging of Caenorhabditis elegans using nanoparticle-mediated immobilization. PLoS One 8, e53419. doi:10.1371/journal.pone.0053419.g005
24. Raizen DM, Song B-M, Trojanowski NF, You Y-J (2012) Methods for measuring pharyngeal behaviors. Wormbook 1–13. doi: 10.1895/wormbook.1.154.1
25. Stiernagle T (2006) Maintenance of C. elegans. Wormbook. doi: 10.1895/wormbook.1.101.1
26. Grossman N, Nikolic K, Toumazou C, Degenaar P (2011) Modeling study of the light stimulation of a neuron cell with channelrhodopsin-2 mutants. IEEE Trans Biomed Eng 58:1742–1751. doi:10.1109/TBME.2011.2114883

Chapter 10

High-Pressure Freeze and Freeze Substitution Electron Microscopy in *C. elegans*

Laura Manning and Janet Richmond

Abstract

While traditional chemical fixation methods for *C. elegans* electron microscopy (EM) have provided invaluable anatomical and structural information, the development of high-pressure freeze (HPF) and freeze substitution (FS) protocols offers advantages for high-resolution imaging. Specimens prepared using HPF methodology exhibit fewer distortion artifacts due to fixation and dehydration, have improved antigenicity, and result in a more physiologically accurate structural representation of the worm. In the HPF technique, freely moving worms are frozen at high-pressure (2100 bar) and low temperature (−180 °C) within milliseconds. These conditions prevent the formation of ice crystals that can damage cellular structures. Samples then undergo FS, during which worms are slowly brought to room temperature while substituting amorphous ice with organic solvents to preserve tissue in its near native state and provide contrast for imaging. FS can be performed in an automatic freeze substitution (AFS) machine or in makeshift, temperature controlled chambers. Fixed worms can be embedded in plastic resin and further processed for a variety of imaging techniques. Samples then viewed using scanning (SEM) or transmission electron microscopy (TEM) will show enhanced preservation of organelles, cell morphology, and antigenicity for immunocytochemistry.

Key words High-pressure freeze, Freeze substitution, Electron microscopy

1 Introduction

For optimal resolution, traditional chemical fixation methods used for EM require the cuticle of the worm to be breached to increase permeability across this thick structure. Worms must then incubate in highly concentrated fixative for hours before structures are fully immobilized. Both the hyperosmotic conditions associated with these methods and disruption of the worm's hydrostatic pressure result in shrinkage of extracellular space and distortion of membrane and organelle morphology [1]. In contrast, freezing the animal within milliseconds captures the intact worm in a near physiological state and allows fixatives to diffuse into the interior of the worm as it is brought to room temperature over several days. Furthermore, freezing at high pressure (2100 bar) and low temperature

David Biron and Gal Haspel (eds.), *C. elegans: Methods and Applications*, Methods in Molecular Biology, vol. 1327,
DOI 10.1007/978-1-4939-2842-2_10,

(−180 °C) in a high-pressure freezer converts tissue to a vitrified state. Vitreous ice in the sample occupies the same space as water rather than forming larger crystalline ice structures that can cause cellular components to change shape, size, and position during dehydration and chemical fixation.

After freezing, samples undergo stepwise thawing from −180 °C to room temperature over 1–7 days while incubated in chemical fixatives and are finally embedded in appropriate resins. A variety of solvents and incubation parameters have been used in FS. Common precipitating fixatives are methanol, anhydrous acetone, uranyl acetate, and tannic acid. These are combined with oxidizing agents such as osmium tetroxide or potassium permanganate that crosslink lipids and deposit heavy metals in the tissue to provide mechanical strength and visual contrast during imaging. Choice of solvents will depend on the focus of analysis. A stronger fixative, such as osmium tetroxide, will preserve tissue more effectively, improving resolution, but strongly reduces antigenicity.

This chapter will focus on two protocols: one designed for morphometric analysis and one for immunocytochemical analysis. For an excellent review of alternative methods and variations on the protocols detailed here, see [2].

Ultimately, high-pressure freezing is a versatile first step in preparing worms for high-resolution imaging. New developments such as cryosectioning, tomography and 3D reconstruction, focused ion beam (FIB) scanning electron microscopy (SEM), and correlative light and electron microscopy (CLEM) continue to emerge and capitalize on this exceptional method for rapid fixation [2].

2 Materials

2.1 High-Pressure Freezing

1. High-pressure freezing machine (Fig. 1) (*see* **Note 1**).
2. Liquid nitrogen (LN_2).
3. LN_2 dewars for storage and transfer.
4. Unloading workstation (Fig. 2) (*see* **Note 2**).
5. Insulated long tweezers.
6. Insulated forceps.
7. Toothpicks.
8. 2 mL Nalgene cryotubes (Fig. 3) (*see* **Note 3**).
9. Marker to label cryotubes.
10. Cryocanes.
11. Cryoprotective gloves.
12. Dissecting light microscope (*see* **Note 4**).
13. 2 × 100 mL Petri dishes lined with filter paper (*see* **Note 5**).

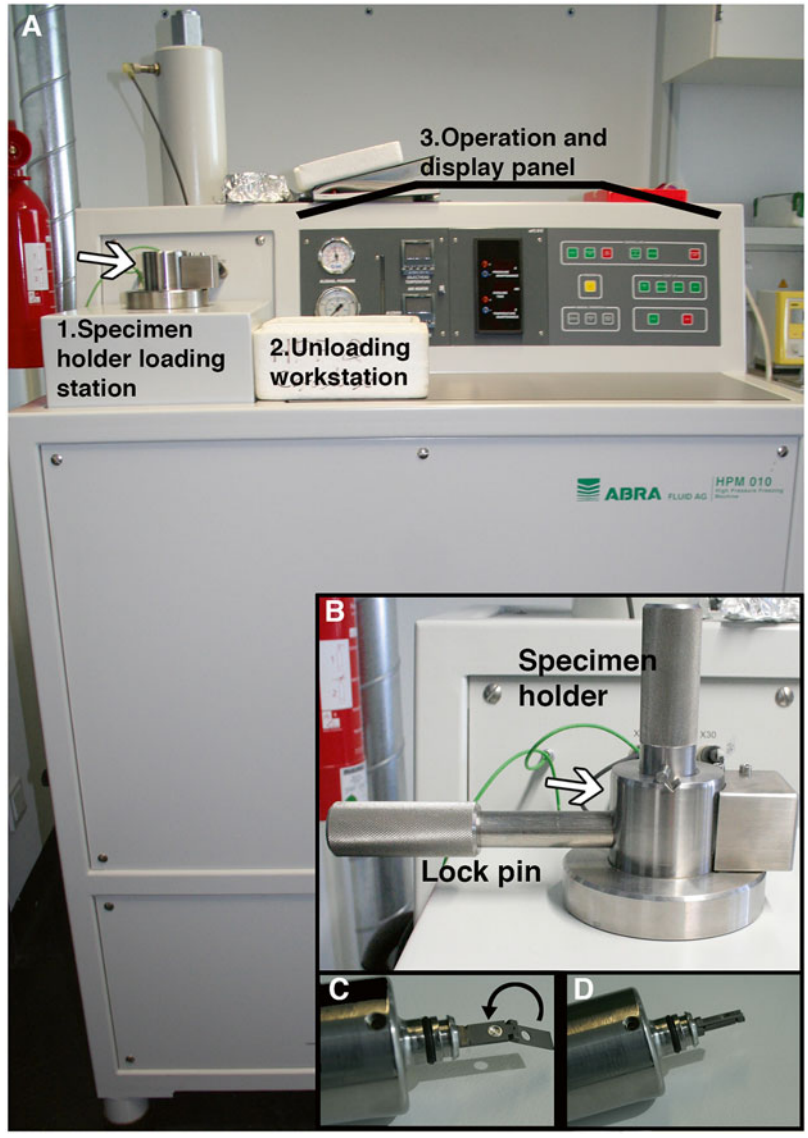

Fig. 1 (**a**) BAL-TEC HMP010 high-pressure freezer machine. (**b**) Specimen holder loading station with inserted specimen holder and lock pin. Hold the specimen holder with the right hand and the lock pin with the left hand to minimize the transfer time of the frozen sample in the specimen holder to the unloading workstation. (**c**) Open specimen holder containing specimen carrier. Close hinge and rotate to tighten as seen in (**d**) before loading into the loading station

14. Specimen carriers (Fig. 4) (*see* **Note 6**).
15. Cryoprotectant (*see* **Note 7**).
16. Micropipettor (1–10 μL) and tips.
17. ddH_2O.
18. Fine-tip forceps.

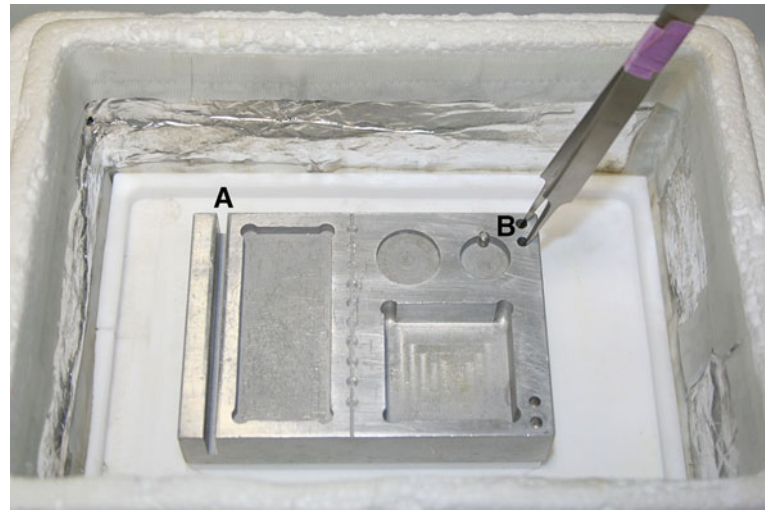

Fig. 2 Unloading workstation. (**a**) Groove to help unscrew the specimen holder. Wedge the specimen holder in this groove and rotate it to unscrew the container-carrying portion of the holder. Use the flat surfaces provided by the working platform to manipulate the specimen carriers, always maintaining the carrier and tools submerged under LN_2. (**b**) Precool forceps and other tools before they contact the specimen carrier

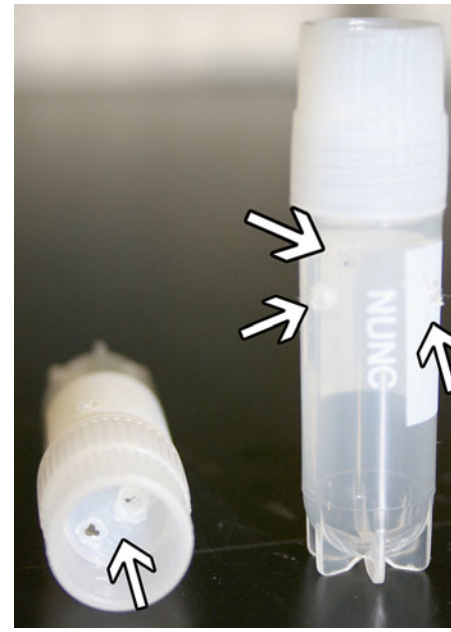

Fig. 3 Nalgene cryotubes for storage of frozen planchettes in LN_2. Create holes in the sides and caps of the tubes as indicated by the arrows in order to facilitate filling the tubes with LN_2 and to prevent them from bursting

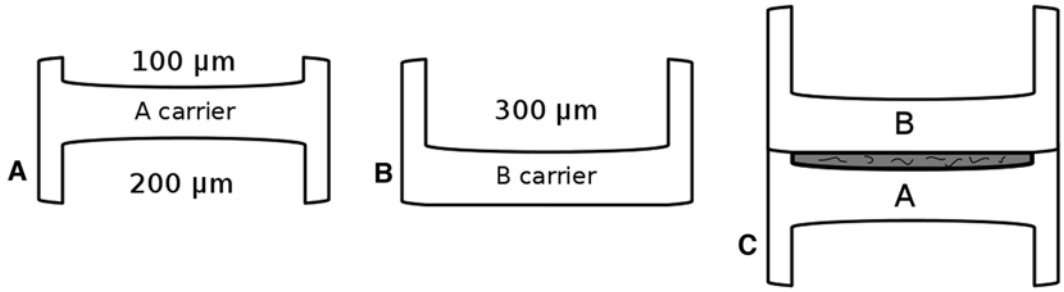

Fig. 4 Specimen carriers (or planchettes). Type (**a**) carriers have a 100 µm well on one side and a 200 µm well on the other side. Type (**b**) carriers have a 300 µm well on one side and are flat on the other side. (**c**) Load cryoprotectant and worms into the 100 µm well side of an (**a**) carrier, then place a (**b**) carrier flat side down on top of the (**a**) carrier to create a sandwich

19. Animals to be frozen, on agar plates.
20. Worm pick.
21. Hair dryer.
22. Paper towels, Kim wipes.

2.2 Freeze Substitution

1. Freeze substitution device (Fig. 5a) (*see* **Note 8**).
2. Anhydrous EMS-grade acetone (≤0.5 % H_2O).
3. Freeze substitution solution.
   (a) 50 mL conical tubes.
   (b) Spatula.
   (c) For morphological analysis.
      - 0.1 % Tannic acid (TA) in acetone.
      - 2 % OsO_4 in acetone.
   (d) For immunocytochemistry.
      - 1.5 % Uranyl acetate (UA) in acetone.
      - UV light source attachment for AFS2.
4. Solution transfer equipment.
   (a) Universal chambers and plastic lids (Fig. 5e).
   (b) Flow-through ring (Fig. 5d) (see Note 9).
   (c) Plastic capsule inserts with mesh bottoms (Fig. 5d).
5. Disposable plastic pipettes.
6. Two large forceps for handling cryotubes.
7. Fine-tip forceps for handling planchettes.
8. Insulated workstation (see Note 10).
9. LN_2 in small pitcher or dewar.

Fig. 5 Freeze substitution device and materials. (**a**) Leica AFS2. Note the LN_2 connection for filling the machine using a funnel attachment, the AFS chamber where samples will incubate, and the mouse-controlled programming screen. (**b**) Close-up of AFS chamber containing universal chambers. A minimum of one waste chamber and one reagent chamber should be present along with any sample-containing universal chambers. (**c**) Wash setup in AFS chamber. One pipet is used for washing with new solution and the other marked waste pipet is used for disposing of waste to prevent contamination. (**d**) Flow-through ring and mesh-bottom vial inserts. Cut a notch in one of these rings to aid in recording sample position. Insert a mesh-bottom vial tube into each sample-containing arm of the ring. (**e**) Universal chamber and plastic lid (**f**) Universal chamber containing flow-through ring with mesh-bottom vial inserts. Samples will incubate in this chamber, while reagents and waste are stored in empty universal chambers. Cover this chamber with the inverted plastic lid when not in use to prevent evaporation of solutions

2.3 Embedding

1. Embedding Kit (*see* **Note 11**).
2. Rotating shaker.
3. Incubator at 60 °C.
4. 2 mL Eppendorf tubes.
5. Parafilm.
6. Dissecting microscope with light source suitable for worm picking.
7. Fine-tip syringe needles (28G3/8) to handle fixed worms.
8. Toothpicks.
9. Disposable wide tip plastic pipettes.
10. Disposable 100 mm Petri dishes.
11. Thin embedding.
    (a) Glass slides (2/strain).
    (b) Teflon spray.
12. Latex gloves.

3 Methods

3.1 High-Pressure Freezing

After preparing the high-pressure freezing machine, a specimen loading station and LN_2-filled unloading station should be set up in close proximity to the high-pressure freezer. Worms (~20–30) are loaded into a specimen carrier, lidded, and secured in a dry specimen holder. The sample in the specimen holder is inserted and frozen inside the high-pressure freezer. Frozen samples are then immediately transferred to the unloading station to be stored for FS. Once loaded into the carrier, specimens should be transferred as quickly as possible through these stations. After freezing, all tools that come into contact with the specimen carrier (i.e., forceps, cryotubes) should be precooled by submersion in LN_2 before use in order to avoid ice crystal damage. The specimen carrier and forceps should be dried with a paper towel or Kim wipe between specimen freezes.

3.1.1 Prepare High-Pressure Freezer

1. Prepare HPF machine according to the manual. In brief:
   (a) Ensure alcohol in the freezer is filled to 250 mL and the alcohol pressure gauge reads around 4 bar.
   (b) Turn on the HPF machine.
   (c) Vent the machine by running the air heater for around 1 h.
   (d) Cool the machine for 15–20 min by pressing "Start" and then "Nitrogen." When the machine is ready, the red "Nitrogen level" indicator will turn off (*see* **Note 12**).

(e) Press "Drive In" to allow the high-pressure cylinder to cycle through LN_2. This process is complete when the "Drive In" lamp turns off.

(f) Press "Auto." The oil pressure gauge should rise to ~300 bar.

2. Do 1–2 test freezes with the test specimen holder. "Pressure Maintenance" should be >0.5 s (*see* **Note 13**). The "Cooling time" should read about 6–10 ms, and the "Temperature Maintenance" indicator should read 1–4 s.

3. Assemble the unloading workstation on or near the high-pressure freezer. Place the metal working surface in a polystyrene box. Fill the box with LN_2 so the working surface is submerged about 2 cm under the LN_2 (Fig. 2) (*see* **Note 14**). Precool tweezers and the first numbered cryotubes in the LN_2-filled workstation. Arrange subsequent cryotubes in the order of the strain list so they are ready to use.

3.1.2 Loading Samples into Specimen Carrier

In this step, worms are loaded into a specimen carrier, also known as a planchette, filled with the cryoprotectant of choice. Another planchette is placed on top of the first to create a "sandwich." Once the top carrier is in place, freeze animals as quickly as possible before they become deprived of oxygen. Wear gloves and use forceps to handle all materials.

1. For ease in quick specimen loading, arrange A and B specimen carriers on separate Petri dishes lined with filter paper in the orientations shown in Fig. 4. A carriers have a 100 μm well on one side and a 200 μm well on the other side and should be arranged with the 100 μm well facing up to be loaded with worms. B carriers have a 300 μm well on one side and are flat on the other side and should be arranged with the well facing up.

2. View the selected worm plate under the microscope. Place an A planchette shallow side up on this agar plate and pipette a small drop of double deionized H_2O into the center of the well to help fill all air bubbles. Overfill the planchette with OP50, or other desired cryoprotectant, to prevent air bubbles that can allow water contamination during the freeze, but avoid any OP50 on the edges of the planchette as this will allow worms to crawl out of the well and can make it difficult to remove specimens after the freeze.

3. Transfer 20–30 worms of appropriate age into the planchette well.

4. Using forceps, place a B planchette flat side down onto the A planchette to make a sandwich. To avoid material spilling out of the carrier, allow the B planchette to slide into place.

5. Insert the sandwich into the dried specimen holder using forceps. Close the specimen holder clasp. Rotate to tighten (Fig. 1).

3.1.3 Freeze Samples

In order to work quickly and efficiently, it is useful to have one person assemble and load samples into the specimen carrier and another to freeze the samples, transfer them to cryotubes, and prepare for the next round of freezing. Before the specimen carrier is loaded, ensure the unloading workstation has enough LN_2 and forceps are precooled. Always run a test freeze or two before freezing the first sample. It is also important to keep detailed notes of your freezes because specimen carriers cannot be labeled, and it is possible that cryotube labels will become illegible after freezing in LN_2.

1. Place the specimen holder into the pressure chamber of HPF with your right hand and secure the locking pin with your left hand (Fig. 1).
2. Exhaust temperature will fluctuate from low to high. Wait for the readout to reach its lowest value and the ready light to turn green, then press JET.
3. When the pressure chamber in the HPF equilibrates to atmospheric pressure, you will feel a slight give to the lock pin. At this time, immediately, remove the locking pin with the left hand and rapidly transfer the specimen holder with right hand directly into the LN_2 of the unloading station (*see* **Note 15**).
4. To remove the specimen carrier "sandwich" from the holder, place the clasp of the holder into the groove of the working platform and rotate counterclockwise to loosen it. Raise the clasp above the groove while keeping it submerged in LN_2 and open with insulated, precooled tweezers.
5. Transfer this specimen carrier into its designated precooled cryotube filled with LN_2 for storage.
6. Dry the specimen holder using a hair dryer and paper towels.
7. Repeat this process for each strain. Typically, two samples of each strain are frozen and stored in the same cryotube.

3.1.4 Turn Off HPF

1. Follow manual instructions for shutdown. In brief:
   (a) Push "Stop."
   (b) Turn off LN_2 tank.
   (c) Turn off N_2 tank.
   (d) Open "Hydraulic valve."
   (e) Leave power on and water recirculating for 4–6 h.
   (f) Turn off the main switch.

3.2 Freeze Substitution

During freeze substitution, samples are washed in universal chambers in the AFS that allow continuous submersion in solution. Vitreous water in samples is substituted with organic solvent and fixative and embedded in resin while slowly warmed to room temperature. Described here is a protocol for morphological analysis

using TA, osmium tetroxide, and Epon resin. The protocol for immunological analysis uses UA and Lowicryl (also known as HM20) resin. Other labs use 0.1 % potassium permanganate in acetone in place of UA. Each universal chamber will require about 12 mL of solution to incubate samples, and solutions should be made fresh as needed.

3.2.1 Prepare AFS Machine

Fill the AFS machine with LN_2 and start the desired program to cool the machine to –90 °C. At this point, frozen samples are transferred to cooled universal chambers containing either TA (for the morphological protocol) or UA (for the immunocytochemical protocol) in the fume hood. Wear latex gloves at all times during FS.

1. Fill the AFS with LN_2 to 100 % capacity. Use extreme caution and do not overfill the machine.
2. Set up a program on the AFS according to the desired protocol. Follow instructions in the manual for setup (*see* **Note 16**).
3. Press START, then PAUSE the program at the first step and allow several hours for the machine to reach –90 °C.

3.2.2 Freeze Substitution and Embedding for Morphological Analysis

Protocol for morphology

Program status	Temperature	Duration	Solution
T1	–90 °C	100 h 2 h 7 h	0.1 % Tannic acid in acetone 4× Wash with acetone 2 % OsO_4 in acetone
S1	–90 °C to –20 °C in 5 °C/h increments	14 h	2 % OsO_4 in acetone
T2	–20 °C to 4 °C in 10 °C/h increments	2.5 h	2 % OsO_4 in acetone
T3	4 °C	3 h	4× Wash with acetone Add 3 h
T4	4 °C to RT	1 h	50 % Epon:acetone

1. Incubate samples in 0.1 % TA at –90 °C for 100 h.
   (a) Prepare 0.1 % tannic acid (TA) in 100 % distilled acetone. This solution should be made immediately before use. Work in a fume hood when handling TA.
   (b) Prepare universal chambers in the fume hood (Fig. 5d–f).
   - Label a flow-through ring by cutting a notch in one tube that will hold sample 1. Acetone used in FS will wash off permanent marker. Record sample positions.

- Insert a mesh-bottom vial into each arm of the ring.
- Place the ring inside a universal chamber. Each chamber can hold up to ten samples, two planchettes per mesh-bottom vial. Prepare up to three chambers for a maximum of 30 samples per FS. Leave room for at least two additional universal chambers for solution changes.

(c) Fill the unloading station with LN2 to a level half that of the universal chamber height. Avoid LN2 entering the universal chamber. This will be the workstation for FS.

(d) Using a plastic pipette, fill the assembled flow-through ring with 0.1 % TA by adding TA to the center ring so that solution distributes evenly until a little over half of each mesh-bottom vial is submerged in liquid. Remove any air bubbles as these will disrupt fixation. Use forceps to place the chamber into the workstation to freeze TA before loading the ring with samples.

(e) Transfer one sample at a time to its designated place in the flow-through ring.

- Quickly remove the first cryotube from its dewar to the workstation (see Note 17).
- Use large precooled forceps to open cryotube lids.
- Invert a single tube onto the working platform, and then move each planchette into its respective tube in the flow-through ring using fine-tipped forceps. Position samples in clockwise order relative to the notched tube, and record a diagram of sample position (*see* **Note 18**).

(f) Once all sample are placed in the flow-through ring, transfer the frozen universal chamber to the AFS. Use forceps, and only remove the universal chamber from the workstation in close proximity to the AFS, minimizing the transfer time. Once in the AFS, cover the universal chamber with an inverted plastic lid to prevent evaporation. Acetone can evaporate quickly, especially at room temperature (Fig. 5b).

(g) Check samples within an hour to ensure they remain submerged in solution at the bottom of the mesh-bottom insert vials. If samples float up in the tubes, carefully sink them using precooled fine-tipped forceps. Check the amount of LN2 in the AFS. Refill as needed, taking great care not to overfill the tank. Overfilled LN2 will seep into the chamber of the AFS and can destroy samples.

(h) Start the morphological AFS program.

(i) One hour before the first wash, fill two universal chambers with acetone and cool them in the AFS chamber to –90 °C.

Place an additional universal chamber for waste in the AFS (Fig. 5b).

2. Wash samples with acetone four times in 2 h using the following solution exchange method. This method will be used extensively throughout the remainder of these protocols.
   (a) Mark one plastic pipette for waste. Use a separate plastic pipette for washing on new solution to avoid contamination. Precool pipettes in the AFS chamber and pipet cooled acetone up and down inside the washing pipette several times to cool the entire pipette tip.
   (b) Begin a wash by removing excess fluid from the inter-spoke area of the flow-through ring with the waste pipette. Discard waste into its designated universal chamber. Then, use the waste pipette to remove solution from the center ring of the flow-through ring until samples are just covered with solution. The mesh-bottom vials will be about 1/4 full of solution. Using the wash pipette, immediately add fresh acetone outside of the ring along the perimeter of the universal chamber. Do not add fresh solution directly to samples and keep samples submerged in liquid at all times. Use the wash pipette to rotate the flow-through ring, which stirs the contents of the chamber. Repeat this process at least four times, ending with mesh-bottom vials half full of fresh acetone (Fig. 5c). This is considered one wash.
   (c) After 30 min, perform a second wash. Precool acetone for the last wash, and precool acetone to −20 °C for OsO4 solution in the next step.
   (d) After at least an hour, perform a final wash for a total of three washes in 2 h.
3. Incubate samples in 2 % OsO_4 in acetone.
   (a) Prepare OsO_4 immediately before use (*see* **Note 19**). Set up three 50 mL conical tubes: one for liquid waste, one for solid waste, and one for preparing solution. Fill the solution tube with the desired amount of acetone cooled to −20 °C (*see* **Note 20**). Clean the sealed OsO_4 ampoule with acetone and a Kim wipe. Cover the ampoule with tissue or a plastic breaker to break the ampoule and discard the top in the waste tube. Use forceps to place the ampoule in the solution tube containing cold acetone. Use a plastic pipette to transfer the acetone into the ampoule and back out into the tube until all crystals are dissolved in the tube. Pipette this solution into a universal chamber designated for OsO_4. Transfer the chamber to the AFS and allow it to reach −90 °C.
   (b) Exchange acetone surrounding the samples with 2 % OsO_4 using the solution exchange method described in **step 4**.

4. *Run AFS through program steps T1, S1, T2, and S2* to bring samples to 4 °C over 23.5 h. Check samples periodically to ensure they are submerged in solution, and maintain adequate LN_2 levels in the AFS.
5. *Wash 4× in acetone*. Wash samples in precooled acetone using the solution exchange method. Perform the second wash immediately after the first. After 30 min, wash a third time. After an hour, complete the final wash. Take precaution when handling OsO_4, and neutralize all waste products before discarding.
6. Incubate samples in 50 % Epon for 3–6 h at 4 °C.
   (a) Prepare Epon (see Note 21). Follow the directions provided by the embedding media kit.
   (b) Combine acetone and Epon as needed to make a 50 % solution in a plastic conical tube. Mix the solution by inverting.
   (c) With a plastic pipette, aliquot approximately 12 mL of 50 % Epon to a universal chamber. Cool the chamber to 4 °C in the AFS.
   (d) Exchange acetone surrounding the samples with 50 % Epon using the solution exchange method.
   (e) After 3–6 h, remove the sample-containing universal chamber(s) from the AFS to warm to room temperature in a fume hood.
7. Incubate samples in 50 % Epon for 3–4 h at room temperature.
   (a) Fill a labeled, 2 mL Eppendorf tube for each distinct sample with 50 % Epon at room temperature. Two samples of the same strain can be placed in the same tube.
   (b) After samples have reached room temperature, transfer them one at a time into their respective Eppendorf tubes. Use forceps to quickly remove a mesh-bottom insert vial from the flow-through ring and invert the samples into their designated Eppendorf tube. Repeat for each sample. Work quickly to keep samples submerged in solution at all times.
   (c) Wrap each Eppendorf tube with parafilm and rotate the samples on a shaker for 3–4 h at room temperature in a fume hood (*see* **Note 22**). Treat all waste as OsO_4 waste. Clean out AFS with acetone and turn off the machine.
8. Exchange 50 % for 90 % Epon and incubate samples for 18 h at room temperature. Use a plastic pipette with a wide tip to remove enough solution from tubes to just cover samples. Refill each tube with 100 % Epon at room temperature, which will bring the Epon concentration to roughly 90 %. Replace parafilm and rotate tubes for 18 h at room temperature (*see* **Note 23**).

9. Incubate samples in 100 % Epon for 4.5 h on a shaker. Exchange 90 % Epon for 100 % Epon as described above. Replace parafilm and rotate for 4.5 h.

3.2.3 Thin Embedding for Morphological Protocol

During thin embedding, worms are sandwiched in resin between coated slides and can later be individually cut out of the polymerized resin film and glued to a block for sectioning. Thin embedding facilitates orientation and mounting of worms on the block.

1. Prepare Teflon-coated slides (*see* **Note 24**). Lay out a glass microscope slide for each worm strain on a paper towel or other protective surface.
   (a) Spray the exposed side of the slides with Teflon spray until slides are semi-opaque.
   (b) Allow slides to dry for 5–10 min.
2. Prepare two 100 mm plastic Petri dishes for each worm strain. One dish will be a working dish to separate worms from cryoprotectant. The other dish will be for embedding and should be labeled.
3. To assemble the embedding dish, *see* Fig. 6.
   (a) Position two toothpicks parallel to each other in the bottom of the dish.
   (b) Label an uncoated glass slide according to the designated strain and position it labeled side down across the toothpicks.
   (c) Place a stack of four thin strips of Parafilm on the ends of the slide to act as spacers.
   (d) Pipet a drop of Epon into the center of the glass slide, avoiding air bubbles.
4. Pour the contents of one Eppendorf tube onto the working Petri dish.
5. Under a dissecting light microscope, use two fine needles (28G3/8) to mechanically separate worms from the cryoprotectant (*see* **Note 25**).
6. Transfer as many individual worms to the Epon drop as is feasible on the labeled embedding slide.
7. After the worms have been transferred to the slide, gently cover it with a Teflon-coated slide with the coated side facing down. Angle the Teflon-coated slide slightly offset from the bottom slide to facilitate breaking open the sandwich later.
8. Repeat this process for each strain using a new, labeled slide. Clean the needle with a paper towel before embedding the next strain to ensure strains stay separate. Use a new needle if necessary.

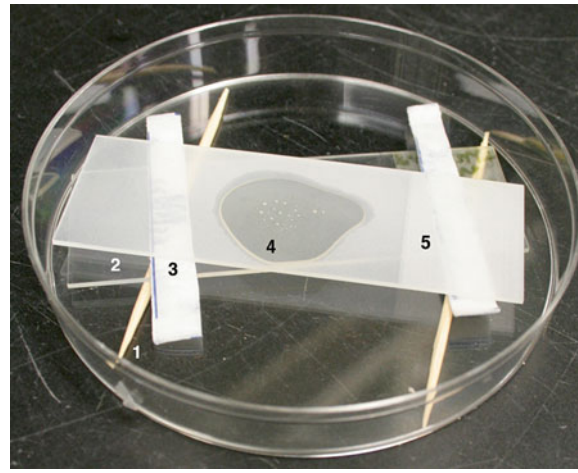

Fig. 6 Embedding dish. Assemble in the following order: (1) Two toothpicks parallel to each other. (2) Clear, labeled glass slide. Label the slide on its bottom-facing side so that Epon does not distort the label. (3) Two stacks of Parafilm strips. Use 4 layers of Parafilm strips for each stack to provide the right spacing for the Epon embedding. (4) Drop of 100 % Epon. Worms will be placed here and later cut out for mounting and sectioning. Aliquot enough Epon to embed each worm on the slide with enough space around it to cut it out of the plastic later. Too much Epon will cause the resin to drip off the edges of the slide. (5) Teflon-coated slide. This slide should be placed with the Teflon coating facing down and should be offset in its angle from the clear slide (2) to aid in breaking apart the slides after incubation

9. Follow the protocol from the embedding solution kit for incubation. Epon generally takes around 2 days to cure in a 60 °C incubator. Samples can then be removed and prepared for sectioning.

3.2.4 Freeze Substitution and Embedding for Immunological Analysis

Protocol for immunocytochemistry			
Program status	**Temperature**	**Duration**	**Solution**
T1	–90 °C	100 h	1.5 % UA in acetone
S1	–90 °C to –45 °C in 4 °C/h increments	11.15 h	1.5 % UA in acetone
T2 without UV	–45 °C	45 m 2 h 4 h 17 h 24 h	3× Wash in acetone 50 % Lowicryl/acetone 67 % Lowicryl/acetone 100 % Lowicryl 100 % Lowicryl
T2 with UV	–45 °C	48 h	Lowicryl
S3 with UV	–45° to RT in 6 °C/h increments	10–12 h	Lowicryl
T3 with UV	RT	48 h	Lowicryl

1. Incubate samples in 1.5 % UA for 104 h.
   (a) Prepare 1.5 % UA in 100 % distilled acetone immediately before use (*see* **Note 26**). Use a dark glass or foil-wrapped container as UA is light sensitive. Filter solution through a 0.22 μm filter before use.
   (b) Prepare a universal chamber to hold samples as described in **step 1** of the morphological protocol.
   (c) Fill this universal chamber with 1.5 % UA and freeze the chamber in LN_2.
   (d) Transfer samples to the flow-through ring in this chamber as described in the morphological protocol.
   (e) Transfer the universal chamber filled with UA and samples to the AFS. Cover the chamber with an inverted plastic lid. Use forceps, and only remove the universal chamber from the workstation in close proximity to the AFS, minimizing the transfer time.
   (f) Begin the immunological AFS program and run T1. Minimize light exposure to the samples by covering the viewing window of the AFS chamber. Check samples after an hour to ensure they are submerged in solution in the proper orientation and not floating up in the tubes. Check the amount of LN_2 in the AFS and fill as needed.
2. Run S1 to bring samples from –90 °C to –45 °C over 11.25 h. One hour before the next step, fill a universal chamber with acetone and cool it in the AFS chamber to –90 °C. Place a universal chamber for waste in the AFS (Fig. 5b).
3. Wash with acetone three times in 45 min at –45 °C. Use the solution exchange method. Discard all UA waste as hazardous waste.
4. Remove samples from their planchettes for embedding.
   (a) Starting with the first sample, use precooled forceps to stabilize the planchette sandwich. Using a precooled fine needle, slide one of the planchettes off of the other to expose the sample inside, also known as the galette. Dispose of the empty planchette.
   (b) With the fine needle, gently scrape around the rim of the remaining planchette to free the galette. Take care not to damage the galette.
   (c) Use the needle or a precooled plastic pipet to dislodge the galette from the planchette into the cooled acetone within the mesh-bottom insert vial. Discard the empty planchette.
   (d) Repeat for each strain, using a clean needle and forceps each time to avoid mixing strains.

5. Incubate samples in 50 % Lowicryl:acetone solution for 2 h at –45 °C. Prepare a Lowicryl stock solution according to kit instructions. Dilute the Lowicryl stock to make a 50 % solution with acetone as needed. Replace acetone in the sample-containing chamber with 50 % Lowicryl using the solution exchange method with precooled plastic pipettes (*see* **Note 27**).
6. Incubate samples in 67 % Lowicryl:acetone solution for 4 h at –45 °C. Prepare a 67 % Lowicryl:acetone solution and cool to –45 °C. Replace the 50 % for the 67 % Lowicryl:acetone solution using the solution exchange method with precooled pipettes.
7. Incubate samples in 100 % Lowicryl for 17 h at –45 °C. Cool 100 % Lowicryl stock to –45 °C. Exchange the 67 % Lowicryl:acetone solution for 100 % Lowicryl using the solution exchange method with precooled pipettes.
8. Incubate samples in 100 % Lowicryl for 24 h at –45 °C. Follow directions in the Leica manual to mount the LED UV lamp on top of the AFS chamber and connect its cable to the machine. The display screen on the machine will indicate when the UV light is successfully mounted. The UV light will be activated automatically by the AFS program in the next step.
9. Run T2 to incubate samples in 100 % Lowicryl for 48 h at –45 °C with UV light.
10. Run S3, and T3 to bring the samples to room temperature over 58 h with UV light. Lowicryl-embedded samples can now be removed and prepared for sectioning.

4 Notes

1. This protocol is written for use with the BAL-TEC HPM 010. BAL-TEC also offers a newer model, HPM100, that automatically transfers and unloads samples after freezing. For information about other machines, see [3].
2. An unloading workstation should be contained in a polystyrene box. A custom metal platform can be designed to facilitate unscrewing the specimen carrier and organizing frozen planchettes. Handheld forceps and a metal platform could be used for these purposes. The box should be filled with LN_2 and placed near or on top of the HPF machine for quick carrier transfer. Also keep an insulated pitcher of LN_2 nearby for refilling the unloading station.
3. Create holes in each tube using a heated wire or tool so tubes do not burst when cooled. Perforated cryotubes fill easily with LN_2 and remain submerged.

4. It is useful to illuminate your workspace from below the specimen in order to pick worms of the proper age and size. Once loaded in the specimen carrier, however, an overhead light source will aid in viewing the contents of the carrier to make sure worms are transferred effectively.
5. Filter paper can be coated with 1-hexadecene to facilitate handling the specimen carriers.
6. A variety of specimen carriers (also known as planchettes) may be used for different purposes. For a standard freeze, use one type A and one type B carrier (Fig. 4). To generate a more shallow well, a slot grid can be used as a spacer between the flat sides of two Type B carriers. A slot grid placed on a sapphire disc can also be used for blue light stimulation of specimens prior to fixation. See [4] for alternate arrangements and carriers.
7. 1–7 Days old OP50 *E. coli* from seeded plates is an effective cryoprotectant. Other common cryoprotectants are yeast paste, 20 % BSA in M9 medium, or alternatively pelleted *E. coli* resuspended in M9.
8. The following protocols are designed for use with the Leica EM AFS2. This equipment provides a precisely temperature controlled chamber with automatically programmed temperature changes. Alternatively, a FS apparatus can be constructed from general lab items. For details, see McDonald [4].
9. Each flow-through ring can hold 10 distinct samples, usually two planchettes of each sample per arm. It is not recommended to work with more than 30 different samples, i.e., three 10-well flow-through rings, at a time due to limited space in AFS.
10. Use the same unloading workstation used during the freeze, seen in Fig. 2. Alternatively, use a polystyrene box filled with LN_2 and working platform.
11. This protocol uses Epon and Lowicryl resins for morphological and immunocytochemical preparations, respectively. See the Electron Microscopy Services catalog for alternative embedding materials.
12. Handle LN_2 with extreme caution. Use cryoprotective gloves as well as a lab coat, mask, and footwear. Open a door or window to allow adequate ventilation. Be prepared for LN_2 to spill when filling containers.
13. If pressure is not maintained, it may be necessary to grease or change the specimen holder O-ring.
14. The LN_2 level should be maintained at a sufficient level to keep the frozen specimen submerged while the specimen holder is unscrewed and carriers are removed. However, too high of a LN_2 level will make it hard to visualize the carriers as they are removed from the holder and transferred to cryotubes.

15. Speed and consistency in this step is critical for avoiding ice crystal formation in the specimen
16. Establish a calendar according to the chosen protocol to schedule subsequent washes at convenient times. For example, if you start the morphology protocol on a Monday at 12 p.m., the next scheduled wash will occur on a Friday at 4 p.m.
17. There are various ways to store cryotubes in LN_2 before FS. It is important to transfer a frozen, LN_2-filled cryotube into the workstation as quickly as possible to maintain LN_2 temperatures. Cryocanes are useful for storing multiple tubes inside a LN_2 dewar. Remove one cryocane from the dewar and immediately submerge all attached cryotubes in LN_2. Use large forceps to liberate each numbered cryotube from the cane. Wear cryoprotective gloves.
18. Work quickly to ensure samples stay cold. Cool all forceps before use, and keep the specimen and contacting equipment submerged in LN_2 at all times.
19. Osmium tetroxide cross-links lipids and is highly toxic. Wear a lab coat with nitrile gloves tucked over the sleeves and then latex gloves over those, so that latex gloves can be replaced easily if necessary. Work under the fume hood whenever possible and wear safety goggles at all times. Use forceps and other equipment specifically designated for contact with OsO_4. Vitamin C, powdered milk, vegetable oil, or any substance rich in C = C bonds will neutralize OsO_4. These solutions will turn black and return to a normal color after OsO_4 is neutralized. All waste should be disposed of according to Material Safety Data Sheets (MSDS).
20. Depending on the number of samples and quantities of OsO_4 purchased, the amount of OsO_4 solution will vary. Always make the smallest quantity of 2 % OsO_4 solution needed. One universal chamber will require around 12 mL of this solution.
21. To minimize air bubbles that could damage the sample, make Epon about 2 h before embedding and after the last acetone wash (and degas in a vacuum chamber if available). All work with Epon should be done under a fume hood and using gloves. Solid and liquid Epon waste should be incubated at 60 °C, until Epon hardens, before disposal. Store Epon at 4 °C and aliquot as needed to make the appropriate dilutions.
22. The rotating shaker should be set to a speed that will keep the samples gently moving back and forth in the tube, but not so fast that it will create air bubbles or cause mechanical stress to samples.
23. Worms may have dislodged from the planchette and be free floating during this step. Take care not to remove worms with

the pipette, and use a new pipette for each strain to avoid mixing strains. Centrifuge tubes gently if necessary to keep worms submerged. Keep planchettes intact if possible to minimize mechanical damage to worms before embedding. If the worms have become dislodged from their planchettes, remove the empty planchette(s) with forceps to prevent mechanical damage to worms.

24. The Teflon coating will make it easier to break the sandwiched slides apart later after resin is polymerized and worms are ready to be mounted for sectioning. Alternatively, layers of Aclar film can be substituted for Teflon.
25. Take care not to damage worms during this process. Worms are fragile and should be kept intact for later sectioning. Start by scraping the middle of the planchette sample, because worms tend to stay on the sides of the planchette. Remove as much cryoprotectant as possible without damaging the worms. Osmium fixation will render the worms and cryoprotectant dark brown or black. Generally, worms that are stained the darkest will provide the best images.
26. UA is radioactive and should be handled with gloves. Dispose according to MSDS.
27. Work under a fume hood and wear gloves when handling Lowicryl. Avoid air bubbles that will reduce resin quality by degassing. Cover the lid of the AFS chamber with aluminum foil to protect samples from exposure to UV light, as Lowicryl is UV light sensitive. The Lowicryl stock should also be stored in foil. Avoid directly inhaling Lowicryl.

Acknowledgements

Protocols and expert advice have been kindly provided by Szi-chieh Yu, Elena Gracheva, Anja Habermann, Maike Kittelman, Carolin Wichmann, and Rob Weimer. Special thanks to Alex Gottschalk and Achilleas Frangakis for hosting us in their labs. Jean-Louis Bessereau provided critical feedback.

References

1. Rostaing P, Weimer RM, Jorgensen EM, Triller A, Bessereau JL (2004) Preservation of immunoreactivity and fine structure of adult *C. elegans* tissues using high-pressure freezing. J Histochem Cytochem 52:1–12. doi:10.1177/002215540405200101
2. Hall DH, Hartweig E, Nguyen KCQ (2012) Modern electron microscopy methods for *C. elegans*. Methods Cell Biol 107:93–149
3. McDonald KL, Morphew M, Verkade P, Müller-Reichert T (2007) Recent advances in high-pressure freezing: equipment- and specimen-loading methods. Methods Mol Biol 369:143–173
4. McDonald K (1999) High-pressure freezing for preservation of high resolution fine structure and antigenicity for immunolabeling. Methods Mol Biol 117:77–97

Chapter 11

Electron Tomography Methods for *C. elegans*

David H. Hall and William J. Rice

Abstract

Methods for electron tomography of the nematode *C. elegans* are explained in detail, including a brief introduction to specimen preparation, methods for image collection, and a comparison of several general methods for producing dual-axis tomograms, with or without external fiducial reference objects. New electron tomograms highlight features in software for data display, annotation, and analysis. This chapter discusses the ultrastructural analysis of cells and tissues, rather than molecular studies.

Key words Electron tomogram, High pressure freezing, Image acquisition, Image alignment, Back-projection, Denoising, Fiducial marker, Markerless alignment, Annotation

1 Introduction

Sydney Brenner chose the nematode *Caenorhabditis elegans* as a model animal for genetic studies of cell development with the idea that this small cylindrical creature had the potential for complete analysis at the EM level [1]. Brenner believed that with careful serial cross-sections, the cable-like nervous system could be fully visualized, producing a complete list of cells and cell parts that could be followed through development. The small size of *C. elegans* put a premium on the acquisition of high-quality images, since so little cell detail could be viewed by light microscopy, although GFP technology has partly solved that problem [2]. For the past 45 years, transmission electron microscopy (TEM) has often been applied to *C. elegans*, with many important results [3, 4]. Yet TEM has its limits, particularly for smaller items that are near the dimensions of a thin section. Objects such as synaptic vesicles, microtubules, or actin (5–50 nm range and below) become hidden due to overlap with other nearby objects. They become difficult to resolve separately or to quantify, and details of their local interactions are lost from view.

David Biron and Gal Haspel (eds.), *C. elegans: Methods and Applications*, Methods in Molecular Biology, vol. 1327,
DOI 10.1007/978-1-4939-2842-2_11,

Electron tomography (ET) offers an elegant solution to this quandary, with a local resolution of roughly 10 nm in any dimension when solving for structure (*see* below), and perhaps 5 nm resolution when solving for molecular details in cryo-ET where fast frozen samples are prepared without embedment or heavy staining [5]. ET was first developed several decades ago and has gradually become much more accessible as computational methods and programmable microscopes have proliferated [6, 7]. Modern electron microscopes now come equipped with a highly stable tilting stage (the goniometer) and with software that make ET image collection almost routine. The technique has benefited from modern advances in tissue preparation methods, such as high pressure freezing (HPF) and freeze substitution (FS) [8–11], which allow more accurate preservation of ultrastructure than had been originally available. Work with fast frozen animals in the absence of plastic embedment remains very difficult, but again ET can help to define the exact shapes of smaller structures, even where low contrast makes individual micrographs appear almost blank [5, 12].

TEM studies of the nematode have been impeded by the animal's thick cuticle, which slows down access to fixatives, heavy metal stains, or plastic resins [3, 4, 13, 14]. Details in these pioneering studies suffered from uneven embedment and heavy stain artifacts that made it difficult to achieve uniform results. With the advent of HPF/FS and wider access to microscopes with programmed goniometer stages, the physical barriers to ET have dropped away. As we describe in this chapter, parallel improvements in software routines required for ET image collection and image analysis have also improved dramatically. These developments set the stage for bringing more nematode-related projects into the realm of ET analysis. Below we will highlight examples where ET can contribute new understanding of *C. elegans* tissues and tissue interactions. ET is also used widely for the analysis of molecules and molecular aggregates [5, 15], but this is not the subject of this review.

ET has been used for *C. elegans* tissue studies occasionally over the past 20 years [16–18], but had not been widely adopted until recently [19–22]. Better microscope automation is a key innovation, and ET will be more widely applied in the future [23].

2 Materials

2.1 Thin Section Collection

1. Gold fiducial markers, 10 nm gold particles.
2. Pioloform for grid coating.
3. Copper slot grids.

2.2 Software Choices for Image Collection, Tomogram Creation, and Annotation

1. Leginon (Scripps Institute, CA), a common choice for microscope control during image acquisition and for tomogram production from the collected images [24].
2. Protomo (www.electrontomography.org), our preferred choice for manipulation of collected images to create tomograms without external fiducials.
3. SerialEM (http://bio3d.colorado.edu/SerialEM/), a popular choice for microscope control during image acquisition.
4. Spider (Wadsworth Center, Albany, NY), a comprehensive set of software tools, developed for automated microscope control, tomogram production, and annotation.
5. IMOD (http://bio3d.colorado.edu/imod/), a popular choice for tomogram production, annotation, and display.
6. Amira (Visage Imaging, Inc. San Diego, USA, http://www.fei.com/software/amira-3d-for-life-sciences/), a common choice for tomogram annotation and display.
7. TOM Toolbox (http://www.biochem.mpg.de/tom), a set of MATLAB extensions for tomogram production and annotation.
8. TomoJ (http://u759.curie.fr/fr/download/softwares/TomoJ), a set of ImageJ routines for tomogram production and annotation.

2.3 Useful Hardware for Tomogram Annotation

1. Data tablet/pen display (Cintiq 13HD or Cintiq 22HD, Wacom Co., Kazo, Japan).

3 Methods

3.1 Tissue Preparation

Although it is feasible to acquire ETs from animals fixed by traditional chemical immersion protocols [25], we strongly recommend the use of modern high pressure freezing (HPF) and freeze substitution (FS) protocols for achieving more "life-like" ultrastructure [7, 10, 11].

1. High Pressure Freezing: Typically, the live nematode is placed into a holding planchette in a slurry of *E. Coli* and/or 20 % BSA. The planchette is sealed and inserted into the HPF device, and live animals undergo rapid freezing under extreme pressure to become vitrified within roughly 50 μs. This is too short a time for any cells or tissues to change their shape or undergo degradation, making the technique more trustworthy than the older immersion chemistry (*see* **Note 1**). The latter involved cutting open live animals with a razor blade to allow aqueous fixative to gradually enter the cut end. The older methods required minutes to achieve a primary fixation. *See* chapter by Janet Richmond (this volume) for more details.

2. Freeze Substitution: Fast frozen worms are held at low temperature (−90 °C) while being exposed to a cold solvent containing the primary fixative(s), such as osmium in acetone. Samples are generally held at low temperature for hours or many days in a freeze substitution device, in which the frozen sample gradually melts into the fixative, so that the worm slowly becomes fixed and stained while remaining essentially frozen in place (*see* **Note 2**). The sample is then slowly warmed, rinsed in cold solvent, and sometimes restained before direct embedment into plastic resin. The animal never goes back into an aqueous phase, which precludes methods for positioning several animals in an agar block, or perhaps introducing an antibody into the sample prior to plastic embedment. *See* chapter by Janet Richmond (this volume) for more details.
3. Thin Sectioning: After the plastic-embedded worm has been cured in the oven to produce a hard plastic block, one needs to section the animal and collect the sections onto microscope grids for examination under the electron microscope. Although regular TEM is often conducted on samples cut at 50–80 nm thickness, for ET we recommend trying thicker sections, 150–250 nm each. In this manner, one can cover larger portions of the nematode anatomy within a relatively small number of serial sections. Dual-axis tomograms can be collected for the corresponding region of interest (ROI) in serial sections, then those tomograms combined to produce an ET volume covering several microns in depth. All sections might be contained on one or two Pioloform-coated slot grids (*see* **Note 3**).

   Methods for production of grids and serial sections have been described elsewhere [10, 25]. When sectioning is complete, the sections are next treated with a post-stain to increase tissue contrast. Post-stains may include uranyl acetate and/or lead citrate. Because ET uses rather thicker sections, staining times must be increased to allow better access to the deeper portions of the tissue. After post-staining, and a brief wash to remove excess stain, grids are air-dried and stored in a grid box until microscopy can begin.

   In an ideal case, the young nematode is so small that it might be possible to collect tomographic images of the whole animal without resorting to sections. One can imagine placing the fixed worm on the tip of a needle under the electron beam, and collecting images while rotating the animal/needle in rotisserie fashion to produce an electron tomogram from images taken at every few degrees of rotation, with no cone of lost information that would detract from the product. If the embedded worm were resistant to the incident electron beam and did not shrink under this treatment, a complete animal tomogram might be captured with high resolution. So far this

is only a thought experiment, but similar ETs have been possible across the thin lamellipodia of cultured amoeboid cells without sectioning [26].

4. Gold fiducial markers: External fiducial objects can be added to the sample before imaging in order to minimize drift of the ROI while calculating the tomogram. An alternative method called "markerless alignment" requires no external fiducial marks. We have had success using either method for nematode tissues.

   Small gold beads are typically used in liquid suspension. A droplet is applied on one side of the microscope grid, and then blotted to remove excess liquid and allowed to air dry. A second droplet is next added to the second side of the grid and blotted again and allowed to dry prior to microscopy. Since the gold beads now lie on the outside surface of the section, they are convenient for following the exact motions of the ROI during tilt image collection. Despite overlying the ROI itself, the very thin projection planes of the final tomogram do not allow the gold markers to become visible within the viewing area of the tissue itself. They can be added to the grid before or after post-staining the sections.

3.2 Image Collection

1. Sample Thickness, Beam Damage, and Shrinkage: Electrons interact with the specimen in two different ways. Elastic collisions of electrons with the specimen occur when the electrons are deflected without energy loss as they pass through the specimen. These electrons are appropriately focused by the lenses in the electron microscope and therefore provide high-resolution information. Since these electrons impart little energy to the specimen, they cause virtually no radiation damage. Inelastic collisions, in contrast, do transfer energy to the specimen, and therefore cause radiation damage. Worse, inelastically scattered electrons are not focused properly by the microscope (due to their energy loss), and thus contribute to noise in the image (*see* **Note 4**). Very thick specimens will appear blurry because of the dominance of inelastically scattered electrons in the image. The use of an energy filter, which removes inelastically scattered electrons, can markedly improve the images of thick sections. In practice, we have found that specimens thicker than 200–250 nm are not suitable for high-tilt tomography on a 200 kV instrument (Tecnai F20). Higher voltage (200 or 300 kV) microscopes are desirable for tomography for two reasons. First, higher voltages provide better optics and allow thicker specimens to be imaged. Second, specimen damage decreases with increasing accelerating voltage, since higher voltage lowers the cross-section for scattering. However, for the same reason, images from a higher voltage

microscope will have less contrast than those obtained from a lower voltage microscope. Remember that when tilted to 70°, a 250 nm section will have an apparent depth of almost one micron, and cannot be viewed at less than 200 kV.

2. Resolution and Electron Tomography: ET is a technique that utilizes the TEM's large depth of field to study samples from 50 to 500 nm in thickness (from whole cells to suspensions of macromolecular complexes). The resolution of the resulting tomogram will depend on the specimen preparation, microscope conditions, and image processing but is usually between 5 and 10 nm. The theoretical resolution can be calculated from the number of projections collected, and for linear tilt increments d is given by the relationship [27]:

$$d = \pi D / N$$

where d = the resolution of the reconstruction, D = diameter of the spherical object (thickness of the slab), N = number of projections recorded. (Note that these calculations are limits to maximum possible resolution, and the actual resolution of the tomogram will be lower.)

This equation is only valid if the geometrical thickness of the specimen is independent of the tilt angle and if the sample can be tilted over a full 180° angle. Neither criterion is practical for ET of thin sections, which have a slab geometry. With increasing tilt angle Θ, the specimen thickness increases with $1/(\cos(\Theta))$. Tilt angles are usually limited to −70° to +70° because of specimen holder mechanical constraints and bars from the specimen support obscuring the field of view. In practice, we usually choose a 1° or 2° increment for stained samples. We tend to use the Saxton scheme [28], by which the tilt angle increment is decreased by a factor of cos (Θ). Thus, the tilt series is sampled at finer increments as the angle increases. This reduces collection time and dataset size while minimizing effects on final resolution, and still provides an even sampling in Fourier space. For example, our typical −70° to +70° series is covered in 100 images by this scheme (2° nominal increments), versus 140 images for a standard 1° increment, a 40 % saving in collection time.

Since the collected tilt range does not cover a full 180°, there is a "missing wedge" of information when the 3D volume is calculated (Fig. 1). Data close to the electron beam normal (corresponding to the 90° tilt angle) is missing and, as a result, tomograms will have anisotropic resolution [15]. In the direction along the tilt axis (y), the resolution is limited to the nominal resolution of the microscope. In the direction perpendicular to the tilt axis (x), resolution is calculated by the equation above. In the z-direction, resolution is about half of

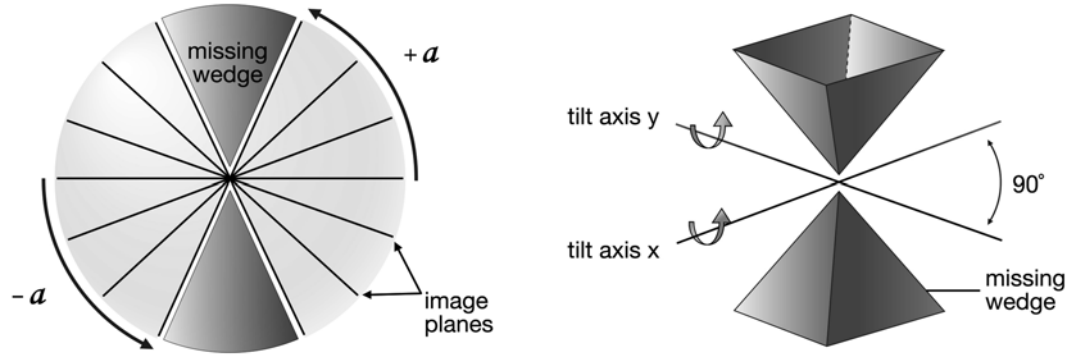

Fig. 1 Missing wedge and Fourier analysis. Images are collected at multiple tilt angles between −70° and +70° along axis *x*, then the specimen is rotated 90° to collect a second set of tilt angles along axis *y*. The dual-axis electron tomogram is calculated from the Fourier space encompassed within this included volume. The quality of the final tomogram is determined in part by minimizing the "missing wedge" of data for more extreme tilt angles. Adapted from [29]

the *x-resolution* (or $2d$ as calculated above). To reduce the effects of the missing wedge, it is common to use dual-axis tomography [30, 31], which decreases the missing wedge into a missing pyramid. This effectively increases the *z*-resolution to about 1.5 times the *x*-resolution ($1.5d$), and makes both the *x*- and *y-resolutions* the nominal resolution of the microscope. To do this, after collection of the first tilt series, the grid is rotated 90°, the ROI is refound, and a second tilt series is collected.

3. Automation of Image Acquisition: Since each tilt series covers ~70–140 images, manually collecting images at various tilt angles would be tedious, particularly since following each tilt increment, the ROI needs to be aligned and refocused. Computer control of the image acquisition process automatically corrects image shifts and focus changes during acquisition of the tilt series. These procedures also minimize the electron dose on the sample during these adjustments. A commonly used automatic focusing technique calculates image movement between two images acquired at opposite beam tilts [32]. Highly binned trial or tracking images are taken as the specimen is tilted, and these are used to keep the ROI aligned. By using the image shift coils of the microscope, alignment can be done very accurately, and more sloppy stage movements can be avoided. Tomographic data collection requires a well-aligned microscope because of all of the image shifting and beam tilting required for data collection. In addition, there are several calibrations that need to be done on the automated software being used.

   Besides automating tilt series collection, another key item is the capability to collect maps or montages. Within a "navigator" map, the ROI can be easily found and marked for automated collection. A map is essential for collecting dual-axis tilt

series. FEI provides its own software for its series of microscopes. Alternative software automation packages include Leginon (originally developed for automated single particle data acquisition) [33, 34] and SerialEM [35]. SerialEM is available for many modern microscopes and cameras, and provides a powerful interface for automated data collection. This program models the changes in image shifts and focus changes at the first few tilt angles to predict image movements for the remainder of the tilt series. By assuming that the sample follows a certain geometric rotation, the optical system characterizes the offset between the optical and mechanical axes. Thus image movement in the *x*-, *y*-, and *z*-directions due to stage tilt can be dynamically predicted with high accuracy. In our experience on three microscopes (Tecnai F20; JEOL 2100; JEOL 3200FSC), full tomogram acquisition at 2° tilt increments using the Saxton scheme can be completed in 1 h or less, which makes it possible to collect many tilt series in a given session on the microscope. This speed of acquisition becomes essential for collecting multiple tilt series across serial sections.

3.3 Image Post-processing

1. Software packages for Alignment and Reconstruction: The IMOD software suite [36] provides methods for fiducial and fiducial-free alignments and calculates reconstructions by back-projection or SIRT. It also provides means to merge tilt pairs and stack serial tomograms. It offers a complete suite for all methods and has a graphical user interface (GUI) for most techniques. The SPIDER software suite [37] also contains a set of scripts for alignment and reconstruction of tomograms. The protomo software suite [38] is mostly run through a set of command line scripts and programs, and provides means for fiducial-free alignment and reconstruction. We use a series of scripts to batch submit tomograms to a computer cluster for processing by protomo. Other software packages used for tomographic reconstructions include RAPTOR (for automated alignment of fiducials) [34], the TOM Toolbox (a Matlab extension) [39], and TomoJ (a plugin for ImageJ) [40].
2. Alignment: In most automated image acquisition systems, shifts, rotations, and magnification changes can occur during the specimen tilting process. Accurate alignment of projection images is essential for obtaining a high-quality tomographic reconstruction. For successful alignment, geometric relationships between the object of interest and the obtained projections need to be calculated. Ideally all image alignment defects should be corrected so that each image represents a projection of the same 3D object at the known projection angle. Inadequate image alignment will result in blurring or smearing of features in the reconstruction. Techniques have been developed to determine the geometric parameters for the sample throughout each projection angle or tilt increment (*see* below).

3. Fiducial marker alignment methods: The coordinates of electron dense markers such as gold particles can be helpful to align a series of tilt images [41]. Fiducial markers have the advantage of being globally consistent in alignment among the images for the full range of tilt angles. The method can also be used to correct for anisotropic and nonuniform changes occurring to the specimen during the tilt series. Markers for plastic sections should be placed above and below the sample at a concentration such that a reasonable number (~10–30) are in the field of view when imaging the ROI.
4. Fiducial-less methods: Methods have been developed for cases where markers cannot or have not been added. These generally are based on cross-correlation between successive images. The protomo software package [38] uses an iterative projection matching technique in which the full geometry of the sample in the microscope is determined (*see* **Note 5**). Besides lacking the requirement for fiducial markers, this software is scriptable since it uses only a command line interface. This makes automated simultaneous calculations of many tomograms on a computer cluster possible. The authors have found it extremely useful for *C. elegans* tilt series of serial sections (as in Figs. 2, 3, and 4).

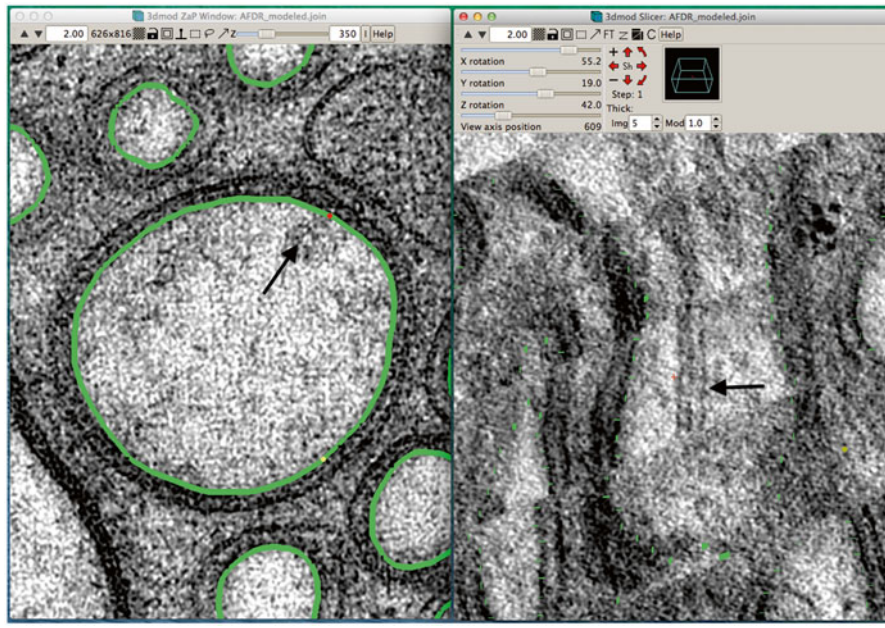

Fig. 2 IMOD window with two views for annotation. Sample working space in IMOD in which two projection planes of the same object can be seen at different angles to one another. *Left panel*. Distal dendrite of AFD is seen in "orthoslice" 350, with the main branches traced in *green. Right panel*. Same region is seen almost lengthwise, with faint *green* highlights marking outlines of cell processes. *Arrows* in each panel indicate the same object, a doublet microtubule. Tissue annotation by E. Semaya

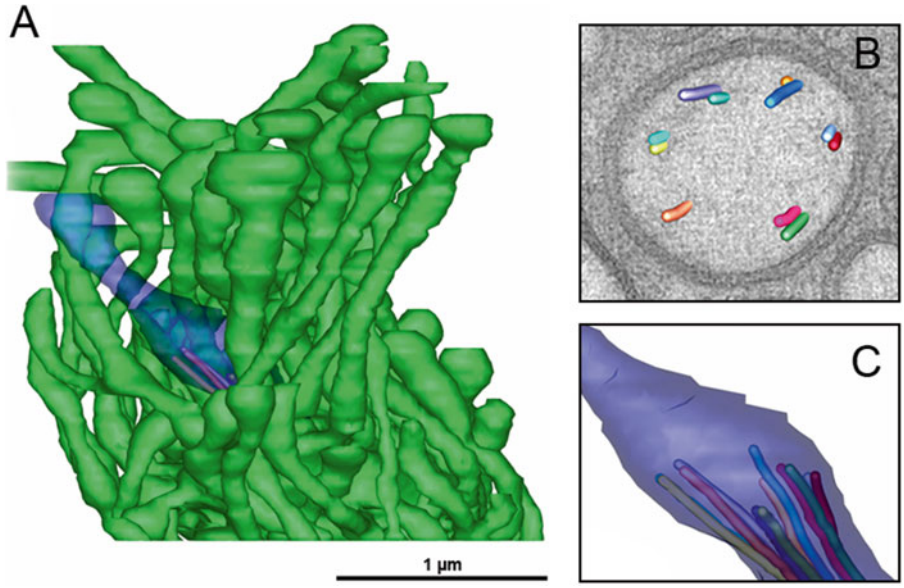

Fig. 3 3D model of AFD ending. (**a**) Complex neuron ending of the AFD neuron includes one short cilium (*purple*) and multiple microvilli (*green*) emerging from the dendrite tip. From a tomogram covering 15 serial sections. Scale bar is 1 µm. (**b**) Closer view at the base of the cilium, where microtubules are shown extruding from one slice through the tomogram. Microtubules organize as doublets here, with almost no singlet microtubules extending distally beyond the axoneme. (**c**) Individual microtubules of the cilium axoneme are modeled, showing that they all stop short and do not enter the distal tip of the cilium. Microscopy conducted by K. Nguyen and W. Liou. Tissue model created in IMOD by E. Semaya

5. 3D Reconstruction: Having collected a tilt series with predetermined tilt increments and specific angular assignments for each projection, an appropriate technique for 3D reconstruction needs to be chosen. There are three main methods used for 3D reconstruction: weighted back-projection, simultaneous iterative reconstruction technique (SIRT) [42], and algebraic reconstruction techniques (ART) [43]. The first technique is the simplest and most commonly used, and will be discussed below. The latter two techniques require knowledge of several input parameters and are computationally expensive. However, SIRT is now commonly used, since programs such as IMOD provide a GUI, and allow calculations to be performed on a GPU (graphics card) to accelerate the process.
6. Back-projection Methods: Back-projection is a simple operation to understand, as it is the inverse of the projection operation. The 2D projections are smeared out by reprojecting them along the angles at which they were collected. By summing all of these reprojections, an estimate of the original object can be formed. However, this simple summation does not reconstruct the object exactly, since low resolution terms are overweighted and high-resolution

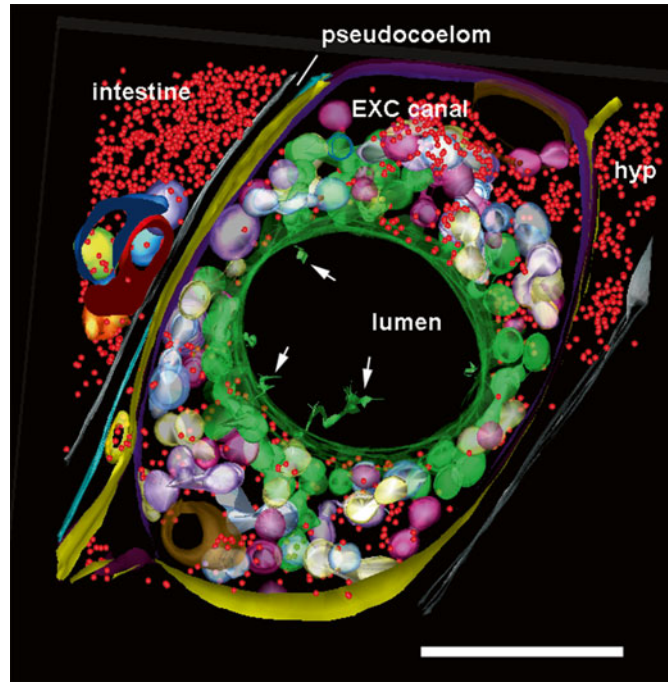

Fig. 4 Annotated adult excretory canal. The complex physical relationships between the internal organelles of the excretory canal have been modeled within three semi-thin serial sections in a dual-axis tomogram (cf. [56]). Despite the rather crowded nature of this tissue, the relationships among many smaller objects become much more visible in the tomogram compared to 50 nm thin sections, and simpler to annotate compared to a stack of serial TEM micrographs. Some features have only become apparent in the tomogram, such as the filamentous structures in the lumen (*white arrows*). Ribosomes, *red*; bead-like canaliculi, *green*, *white*, and *violet*; outer plasma membrane of canal cell, *yellow* and *purple*; plasma membrane apposed to inner lumen, *green*. Nearby tissues include the hypodermis (hyp), intestine, and an expansion of the extracellular space, the pseudocoelom. Scale bar is 1 μm. Microscopy conducted by K. Nguyen. Tissue model created in IMOD by A. Bouchelion

terms are underweighted or undersampled. Therefore, a more faithful reproduction can be obtained by weighting the summation according to $1/r^*$, where r^* is the distance from the origin in Fourier space [44]. This modified algorithm is known as weighted back-projection. All of the tomographic software suites include a weighted back-projection reconstruction as a standard technique.

7. Algebraic and Iterative Methods: The ART and SIRT methods involve back-projection, then reprojection of the newly constructed volume and comparison with the original projections. This comparison allows for corrections in the reprojection algorithm. The main difference between ART and SIRT is that ART involves successive corrections whereas SIRT calculates

simultaneous corrections of all projections. Unlike weighted back-projection, ART and SIRT are nonlinear and require estimates of several correction parameters to begin, as well as limits for number of iterations and amount of allowable corrections. ART is available in TomoJ [40]. SIRT is available in TomoJ, the TOM Toolbox [39], Spider [37], and IMOD [35].

8. Filling in the Missing Wedge: As mentioned above, after collecting one or more tilt series in the ROI, it is best to rotate the grid 90°, find the same ROI, and collect a second set of tilt series. The orthogonal data sets are then combined to reduce the missing wedge to a missing pyramid, and thus increase the signal-to-noise ratio of the final reconstruction. There are two strategies for combining the data: either all data is considered at once and combined to make a tomogram, or two separate tomograms are calculated then aligned and combined. The "all at once" method is implemented in SPIDER [31], and more recently in protomo [45], while the merging method is available in IMOD [30]. As implemented in IMOD, the merging method works with and without fiducial markers, though more manual effort is required in samples without fiducials. In both cases, after an initial alignment, the second tomogram is "warped" to match the first tomogram, and this warping takes into account any additional shrinkage which has taken place during data collection. It is not clear which method is better, as different studies have found one or the other provided better results. This is likely sample dependent, with the merging method being better for samples that have more distortions in the second tilt series [45] (*see* **Note 6**).
9. Stacking Tomograms in Three Dimensions: Quite often, one semi-thick section is not enough to cover the volume of interest, and so (dual-tilt) tomograms are collected at corresponding ROIs of serial sections. Once the tomograms are calculated and merged, they are then stacked in three dimensions to produce a larger volume. This is easily done using the IMOD suite. One selects the series of tomograms to merge, making sure that the order is correct. Subsections are chosen from the top and bottom of each set, then aligned using a GUI and automated tools. One has the option to join using only rigid body movements (rotation and translation), or magnification change and stretching can also be taken into account. A final "joined" volume contains all of the aligned tomograms. It is important to note that this volume may be very large, since each individual volume is on the order of $2000 \times 2000 \times 150$ voxels, and the final joined tomogram may be, say, ten times this size if ten volumes were merged.
10. "Large" tomograms: For even larger volumes, one may collect adjacent, overlapping ROIs and merge laterally. However, this is a somewhat difficult procedure, and it is easier to use the

TEM collection software to collect "montage" tomograms that are more than one CCD frame in width. This is possible, for example, in SerialEM. One advantage of collecting with SerialEM is that IMOD software is then capable of automatically merging the individual frames from each part into a single larger image. However, we should note that montages larger than 2×2 frames (at 2K×2K pixels per frame) would quickly run into problems due to memory considerations.

11. Denoising of tomograms: The amount of noise in the tomogram makes a simple surface view of the 3D volume nearly impossible to interpret, and also makes it difficult to identify features. Various filters can be applied to improve the signal-to-noise ratio in the ET. The simplest filter to apply is a low-pass filter, which will enhance contrast by removing high frequency information, which is likely to be noise. This could be applied with a soft cutoff at the maximum resolution determined above. While easy to perform, this sort of filter does not discriminate between signal and noise, and so real data is discarded. A better alternative is to apply a median filter, a real-space filter in which adjacent pixels are fixed to their median value. The median filter tends to enhance features, and can produce more satisfying results than the low-pass filter. It is relatively fast and can be applied consecutively, though again it does not discriminate between signal and noise.

    Advanced noise filtering methods have been developed for image post-processing which are designed to decipher the signal and separate it from the noise. These include nonlinear anisotropic diffusion (NAD) [46, 47] and a non-local means filter implemented in Amira software [48]. These filters all tend to enhance edges in the data while reducing the background noise level. This more advanced filtering requires much higher computational cost. In addition, they all have several parameters that much be specified. In general these parameters are dataset specific, and must be found by trial and error. For plastic sections, we have found that median filters are often sufficient to aid segmentation, and we go to the other filters only when needed.

3.4 Tomogram Annotation (Segmentation)

The final step in ET is interpreting the tomogram itself. If the tomogram does not consist of several repeating motifs, then one must label and identify different features in the tomogram. This annotation process is often called "segmentation" (*see* Figs. 2, 3, and 4). Resolving individual components within a tomogram is a very difficult and time-consuming process due to the low signal-to-noise ratio and the volume of data within the tomogram. In general, segmentation is done on filtered volumes, as raw tomograms are very difficult to segment. Most segmentation to date has been done manually, using software packages such as

IMOD [36] or Amira [48]. With these programs, the user goes slice-by-slice through the tomogram and manually paints the different features (*see* **Note 7**). Amira includes options such as selection by intensity and interpolation to speed up the process, and also has automated techniques for segmenting some cellular features such as microtubules. Both packages allow different orientations to be viewed (*xy*, *xz*, *yz*) and allow many objects to be created (Fig. 2). As can be imagined, annotation can be a very labor intensive process, but the final results can be striking [18–21]. The TomoJ plugin module for ImageJ is another practical choice for segmentation [40].

The generation of automated segmentation methods has been an active area of research, but in general, they have not worked as well as manual techniques. However, as computerized analysis advances, it is hoped that automated techniques will soon be more generally applicable. We use the Amira software package to produce Quicktime movies from our IMOD-based tomogram models. Amira provides much creative freedom in switching between movies of the orthoslices, and extrusion of the modeled cells and organelles. Additional examples of IMOD models and Amira-based Quicktime movies from our work on *C. elegans* can be viewed at http://www.wormatlas.org/movies.htm.

4 Notes

1. Defects are still seen within HPF-treated specimens, and some samples may need to be rejected. Poor loading can lead to freeze damage [10], pressure shocks may result in local ruptures to the eggshell or cuticle, and some animals may display a twisted pharynx just at the moment of freezing.
2. Some HPF/FS protocols are available that obviate the need for expensive high pressure freezers and freeze substitution equipment (8, 49), or that produce acceptable results in less than 1 day from freezing to final infiltration into plastic [12, 50].
3. In order for the ROI to be viewed by ET, it must lie at some distance away from the edge of the slot on the copper support grid. Otherwise as the grid is tilted, the grid itself will soon obscure the tissue lying on the support film, so that fewer tilt angles will be available.
4. Although resin-embedded and heavy metal stained biological sections are somewhat resilient to electron beam damage, they do change as they are exposed to the beam [51]. The most important and noticeable effect is specimen shrinkage, especially along the z-axis. Shrinkage occurs in two phases, fast and slow [52]. Since reconstruction algorithms assume that only the tilt angle, and not the sample itself, is changing, it is important

to minimize sample shrinkage during data collection. While it would be possible to use low-dose techniques for plastic sections, it is more common to pre-irradiate the samples before collection of tilt series data. In this way, data is collected only during the slow phase [52]. In practice, we usually set up scripts to collect images of the ROI before and after pre-irradiation. This allows us to estimate shrinkage in the $X-Y$ plane. We commonly dose to ~2000 e/A^2 before collecting tilt series. It is important to dose a significantly larger area than the ROI, since outside areas will later enter the field of view at high tilt angles and become subject to fast shrinkage. Note that a full day (or night) of EM time may be needed for the predosing step if many ROIs are to be collected.

5. We are currently using protomo software to align our tilt series. For dual tilt series, each one is processed separately. We then use custom scripts to convert the protomo output into IMOD format, and use IMOD to merge the reconstructions manually. It takes a practiced user about 30 min to merge each tilt pair. We also generally convert the final maps to "byte" format, which not only reduces the file size but also ensures that density levels of stacked tomograms are the same.
6. Calculating Tomogram Resolution. After reconstruction of a tomogram, how accurate is this model of the original structure? One criterion is the "resolution" of the tomogram: but what is meant by resolution? Resolution can be defined as the minimum distance by which two points can be separated and still identified as individual points (the point-to point resolution or Rayleigh criteria). In the case of ETs, this is not so useful, because, as discussed above, the resolution is anisotropic due to the missing wedge, or at best missing pyramid, in data collection (Fig. 1). In the case of plastic sections, the z-direction has been preshrunk by ~40 % before data collection [53]. Additional factors such as the size of the stain particles (1–3 nm) and variations in staining and preservation all add noise to the images. Finally, the thicker images collected at high tilt angles have more inelastic scattering and lower quality than un-tilted images. Therefore all projections do not contribute equally to the reconstruction. Finally, any errors in image alignment will lower the quality of the reconstruction. All of these factors cause the final resolution of the ET to be lower than any theoretical calculation based on tilt geometry. Calculation of resolution is not a trivial task, and while some methods have been proposed [54, 55], none are convenient to use or provide a simple number. In general, the resolution is best assessed by seeing the smallest features that can be reliably identified in the reconstructed volume, for example membrane bilayer structure or mitochondrial cristae.

7. A tomogram will contain information about three-dimensional structures that can be examined from any angle. The "orthoslice" is a projection image of the ET at a given depth along the z-axis, coincident with the original viewing angle of the thin sections (left panel in Fig. 2). However, by reslicing the ET at a new angle, one can bring structures into optimal view, no matter what orientation the object had in the original slices (right panel in Fig. 2). While a spherical object like a small vesicle should look rather similar from any viewing angle, a microtubule or myelin rod will be much better viewed when exactly orthogonal to its main axis or exactly lengthwise (Fig. 3). For the time being, annotation must generally be performed by hand at the computer monitor, tracing portions of the cells and organelles using a computer mouse, or using a stylus on a touchscreen or a drawing tablet, such as the Wacom Cintiq display.

Acknowledgements

We thank Ken Nguyen and Willisa Liou for help in tissue preparation and operation of the Technai20 microscope, and Ashleigh Bouchelion and Emily Semaya for annotation of the tomograms shown in Figs. 2, 3, and 4. Chris Crocker created Fig. 1. Kevin Fisher provided technical help with Amira. Access to NYSBC facilities has been supported by the Albert Einstein College of Medicine. We also thank NIH OD 010943 for support to DHH. Data collected at NYSBC was made possible by a grant from NYSTAR. The NYSBC facility was constructed with support from Research Facilities Improvement Program Grant C06 RR017528 from the NIH National Center for Research Resources.

References

1. Brenner S (1974) The genetics of *Caenorhabditis elegans*. Genetics 77:71–94
2. Chalfie M, Tu Y, Euskirchen G, Ward WW, Prasher D (1994) Green fluorescent protein as a marker for gene expression. Science 263: 802–805
3. White JG, Southgate E, Thomson JN, Brenner S (1986) The structure of the nervous system of the nematode *Caenorhabditis elegans*. Phil Trans R Soc Lond B Biol Sci 314:1–340
4. Jarrell TA, Wang Y, Bloniarz AE et al (2012) The connectome of a decision-making neural network. Science 337:437–444
5. Leis A, Rockel B, Andrees L, Baumeister W (2008) Visualizing cells at the nanoscale. Trends Biochem Sci 34:60–70
6. Frank J (2006) Electron tomography. Methods for three-dimensional visualization of structures in the cell. Springer, New York
7. Müller-Reichert T, Mancuso J, Lich B, McDonald KL (2010) Three-dimensional reconstruction methods for *Caenorhabditis elegans* ultrastructure. Methods Cell Biol 96:331–361
8. McDonald KL (1994) Electron microscopy and EM immunocytochemistry. Methods Cell Biol 44:411–444
9. McDonald KL, Webb RI (2011) Freeze substitution in 3 hours or less. J Microsc 243: 227–233
10. Hall DH, Hartwieg E, Nguyen KCQ (2012) Modern electron microscopy methods for

C. elegans. In: Rothman J, Singson A (eds) Methods Cell Biology. Academic Press, New York
11. Müller-Reichert T, Hohenberg H, O'Toole ET, McDonald KL (2003) Cryoimmobilization and three-dimensional visualization of *C. elegans* ultrastructure. J Microsc 212:71–80
12. Iancu CV et al (2006) Electron cryotomography sample preparation using the Vitrobot. Nat Prot 1:2813–2819
13. Ward S, Thomson N, White JG, Brenner S (1975) Electron microscopical reconstruction of the anterior sensory anatomy of the nematode *Caenorhabditis elegans*. J Comp Neurol 160:313–337
14. Ware RW, Clark D, Crossland K, Russell RL (1975) The nerve ring of the nematode *Caenorhabditis elegans*: sensory input and motor output. J Comp Neurol 162:71–110
15. Baumeister W, Steven AC (2000) Macromolecular electron microscopy in the era of structural genomics. Trends Biochem Sci 25: 624–631
16. O'Toole ET, McDonald KL, Mäntler J et al (2003) Morphologically distinct microtubule ends in the mitotic centrosome of *Caenorhabditis elegans*. J Cell Biol 163:451–456
17. Srayko M, O'Toole ET, Hyman AA, Müller-Reichert T (2006) Katanin disrupts the microtubule lattice and increases polymer number in *C. elegans* meiosis. Curr Biol 16:1944–1949
18. Müller-Reichert T, Mantler J, Srayko M, O'Toole E (2008) Electron microscopy of the early *Caenorhabditis elegans* embryo. J Microsc 230: 297–307
19. Stigloher C, Zhan H, Zhen M et al (2011) The presynaptic dense projection of the *Caenorhabditis elegans* cholinergic neuromuscular junction localizes synaptic vesicles at the active zone through SYD-2/liprin and UNC-10/RIM-dependent interactions. J Neurosci 31: 4388–4396
20. Topalidou I, Keller C, Kalebic N et al (2012) Both enzymatic and structural activities of the tubulin acetyltransferase MEC-17 are required for microtubule structure and organization in *C. elegans*. Current Biol 22:1057–1065
21. Doroquez DB, Berciu C, Andreson JR et al (2014) A high resolution morphological and ultrastructural map of anterior sensory cilia and glia in *Caenorhabditis elegans*. eLife 3, e01948. doi:10.7554/eLife.01948
22. Wang J, Silva M, Haas LA et al (2014) *C. elegans* ciliated sensory neurons release extracellular vesicles that function in animal communication. Curr Biol 24:519–525
23. Knott G, Genoud C (2013) Is EM dead? J Cell Sci 126:4545–4552
24. Suloway C, Pulokas J, Fellmann D et al (2005) Automated molecular microscopy: the new Leginon system. J Struct Biol 151:41–60
25. Hall DH (1995) Electron microscopy and three-dimensional image reconstruction. Methods Cell Biol 48:395–436
26. Medalia O, Weber I, Frangakis AS et al (2002) Macromolecular architecture in eukaryotic cells visualized by cryoelectron tomography. Science 298:1209–1213
27. Crowther RA, Amos LA, Finch JT et al (1970) Three dimensional reconstructions of spherical viruses by Fourier synthesis from electron micrographs. Nature 226:421–425
28. Saxton WO, Baumeister W, Hahn M (1984) Three-dimensional reconstruction of imperfect two-dimensional crystals. Ultramicroscopy 13:57–70
29. Grandfield K, Palmquist A, Engqvist H (2012) High-resolution three-dimensional probes of biomaterials and their interfaces. Phil Trans A Math Phys Eng Sci 370:1337–1351
30. Mastronarde DN (1997) Dual-axis tomography: an approach with alignment methods that preserve resolution. J Struct Biol 120: 343–352
31. Penczek P, Marko M, Buttle K, Frank J (1995) Double-tilt electron tomography. Ultramicroscopy 60:393–410
32. Koster AJ, van der Bos A, van der Mast KD (1987) An autofocus method for TEM. Ultramicroscopy 21:209–222
33. Suloway C, Shi J, Cheng A et al (2009) Fully automated, sequential tilt-series acquisition with Leginon. J Struct Biol 167:11–18
34. Amat F, Moussavi F, Comolli LR et al (2008) Markov random field based automatic image alignment for electron tomography. J Struct Biol 161:260–275
35. Mastronarde DN (2005) Automated electron microscope tomography using robust prediction of specimen movements. J Struct Biol 152:36–51
36. Kremer JR, Mastronarde DN, McIntosh JR (1996) Computer visualization of three-dimensional image data using IMOD. J Struct Biol 116:71–76
37. Frank J, Radermacher M, Penczek P et al (1996) SPIDER and WEB: processing and visualization of images in 3D electron microscopy and related fields. J Struct Biol 116: 190–199
38. Winkler H, Taylor KA (2006) Accurate marker-free alignment with simultaneous geometry determination and reconstruction of tilt series in electron tomography. Ultramicroscopy 106: 240–254
39. Nickell S, Forster F, Linaroudis A et al (2005) TOM software toolbox: acquisition and analysis

for electron tomography. J Struct Biol 149: 227–234
40. Messaoudi C, Boudier T, Sorzano COS, Marco S (2007) TomoJ: tomography software for three-dimensional reconstruction in transmission electron microscopy. BMC Bioinform 8:288–297
41. Mastronarde DN (2006) Fiducial marker and hybrid alignment methods for single- and double-axis tomography. In: Frank J (ed) Electron tomography: methods for three-dimensional visualization of structures in the cell, 2nd edn. Springer, New York, pp 163–186
42. Gilbert PFC (1972) The reconstruction of a three-dimensional structure from projections and its application to electron microscopy. II. Direct methods. Proc R Soc Lond B 182: 89–102
43. Carazo J-M, Herman GT, Sorzano COS, Marabini R (2006) Algorithms for three dimensional reconstruction from the imperfect projection data provided by electron microscopy. In: Frank J (ed) Electron tomography: methods for three-dimensional visualization of structures in the cell, 2nd edn. Springer, New York, pp 217–244
44. Radermacher M (2006) Weighted back-projection methods. In: Frank J (ed) Electron tomography: methods for three-dimensional visualization of structures in the cell, 2nd edn. Springer, New York, pp 245–274
45. Winkler H, Taylor KA (2013) Marker-free dual-axis tilt series alignment. J Struct Biol 182:117–124
46. Frangakis AS, Hegerl R (2001) Noise reduction in electron tomographic reconstructions using nonlinear anisotropic diffusion. J Struct Biol 135:239–250
47. Fernandez JJ, Li S (2003) An improved algorithm for anisotropic nonlinear diffusion for denoising cryo-tomograms. J Struct Biol 144:152–161
48. Stalling D, Westerhoff M, Hege H-C (2005) Amira: a highly interactive system for visual data analysis. In: Hansen CD, Johnson CR (eds) The Visualization Handbook. Elsevier, London, pp 749–787
49. Leunissen JL, Yi H (2009) Self-pressurized rapid freezing (SPRF): a novel cryofixation method for specimen preparation in electron microscopy. J Microsc 235:25–35
50. McDonald KL (2014) Out with the old and in with the new: rapid specimen preparation procedures for electron microscopy of sectioned biological material. Protoplasma 251:429–448
51. Egerton RF, Li P, Malac M (2004) Radiation damage in the TEM and SEM. Micron 35: 399–409
52. Luther PK, Lawrence MC, Crowther RA (1988) A method for monitoring the collapse of plastic sections as a function of electron dose. Ultramicroscopy 24:7–18
53. Lucic V, Forster F, Baumeister W (2005) Structural studies by electron tomography: from cells to molecules. Annu Rev Biochem 74:833–865
54. Cardone G, Grunewald K, Steven AC (2005) A resolution criterion for electron tomography based on cross-validation. J Struct Biol 151: 117–129
55. Unser M, Sorzano CO, Thevenaz P et al (2005) Spectral signal-to-noise ratio and resolution assessment of 3D reconstructions. J Struct Biol 149:243–255
56. Khan LA, Zhang H, Abraham N et al (2013) Intracellular lumen extension requires ERM-1-dependent apical membrane expansion and AQP-8-mediated flux. Nat Cell Biol 15:143–156

Chapter 12

Microfluidic Devices for Behavioral Analysis, Microscopy, and Neuronal Imaging in *Caenorhabditis elegans*

Ross C. Lagoy and Dirk R. Albrecht

Abstract

Microfluidic devices offer several advantages for *C. elegans* research, particularly for presenting precise physical and chemical environments, immobilizing animals during imaging, quantifying behavior, and automating screens. However, challenges to their widespread adoption in the field include increased complexity over conventional methods, operational problems (such as clogging, leaks, and bubbles), difficulty in obtaining or fabricating devices, and the need to characterize biological results obtained from new assay formats. Here we describe the preparation and operation of simple, reusable microfluidic devices for quantifying behavioral responses to chemical patterns, and single-use devices to arrange animals for time-lapse microscopy and to measure neuronal activity. We focus on details that eliminate or reduce the frustrations commonly experienced by new users of microfluidic devices.

Key words Microfluidics, *Caenorhabditis elegans*, Quantitative behavior, Locomotion, Time-lapse microscopy, Neuronal imaging, PDMS, Chemical stimulation

1 Introduction

Microfluidics refers to plumbing at a small, submillimeter scale. Microfluidic-based technologies have found numerous applications in biology over the past decade, from miniaturization of molecular biology reactions to high-throughput analysis of cellular functions. Microfluidic devices offer the advantage of increased experimental productivity by collecting more data (conditions or repeats) in less time with fewer resources and lower costs. Further, predictable fluid physics at this length scale enables dynamic and reproducible control over the fluidic environment surrounding cells or small organisms, often increasing experimental reliability.

In *C. elegans* research, microfluidic devices have been particularly useful for presenting precise physical and chemical environments, immobilizing animals during imaging, quantifying behavior, and automating phenotypic screens. A wide variety of specific *C. elegans* microfluidic devices have been surveyed in several recent reviews

David Biron and Gal Haspel (eds.), *C. elegans: Methods and Applications*, Methods in Molecular Biology, vol. 1327,
DOI 10.1007/978-1-4939-2842-2_12,

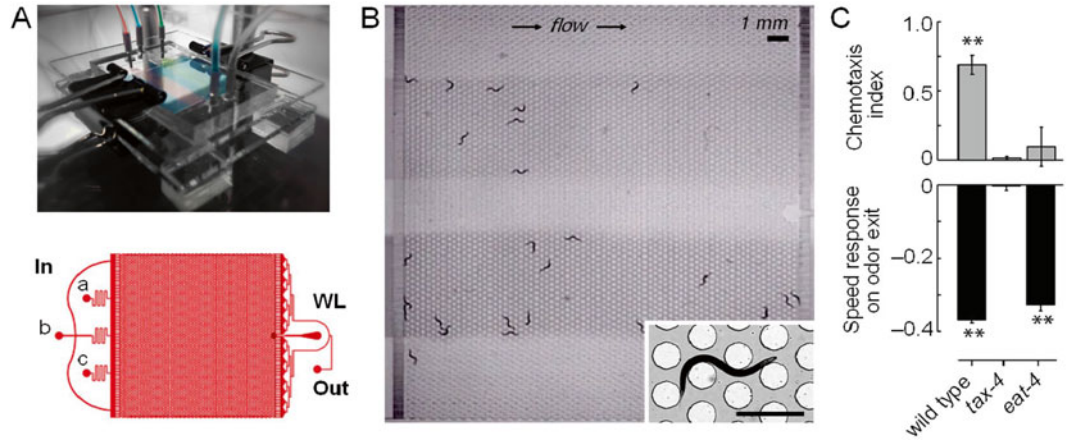

Fig. 1 Microfluidic device for quantifying behavioral responses to spatial stimulus patterns. (**a**) The device presents two stable stripes that flow from three inlet (In) ports to an outflow port (Out). Animals are loaded through a worm loading (WL) port. A completed device is shown clamped and mounted to the video capture stage (*above*). (**b**) A video frame showing 25 wild-type *C. elegans* animals responding to two horizontal stripes of the attractant isoamyl alcohol (IAA, 0.92 μM *top*, 1.84 μM *bottom*) [6]. *Inset* shows a young adult animal moving around microposts. Scale bar, 500 μm. (**c**) Quantitative behavioral data for chemotaxis index (the relative time spent inside versus outside the odor stripe, a measure of attraction to the stimulus) and for the change in speed upon exiting the odor stripe. Wild-type animals are attracted to the IAA odor and slow down upon exiting. Sensory mutant *tax-4(ks28)* shows no attraction or speed response to the odor, whereas glutamate-deficient *eat-4(ky5)* animals slow normally but do not reside in the odor due to the inability to turn appropriately [6]

[1–5]. Microfluidic devices are generally described as "easy, fast, and inexpensive," especially when fabricated from elastomeric materials such as polydimethylsiloxane (PDMS). This description is technically true, but only if the user has prior experience with microfluidic devices, already has the equipment necessary for fabrication, and uses microfluidics often enough to reduce per-device costs by purchasing raw materials in bulk.

Microfluidic designs can be as simple as a single channel with one inlet and one outlet, or as complicated as a multilayered device containing dozens of fluidic ports and integrated, computer-controlled pneumatic valves. A simple design can be operated with a syringe reservoir and thin tubing, with fluid flow driven by hydrostatic pressure. A complicated system may require precisely balanced fluid and pneumatic line pressures and computer-actuated valves or syringe pumps. Simple and elegant systems that focus on ease-of-use are preferred, not just to reduce user frustration, but to improve reliability and reproducibility of an assay.

Here we describe the preparation and operation of three simple microfluidic *C. elegans* devices that are currently in use by many research labs. The first device is a microfluidic arena for observing locomotory behavior in response to precise and stable spatial patterns of chemical stimuli, similar to a chemotaxis assay, but with greater reproducibility and data content [6] (Fig. 1). This device can be cleaned and reused dozens of times. The second and third

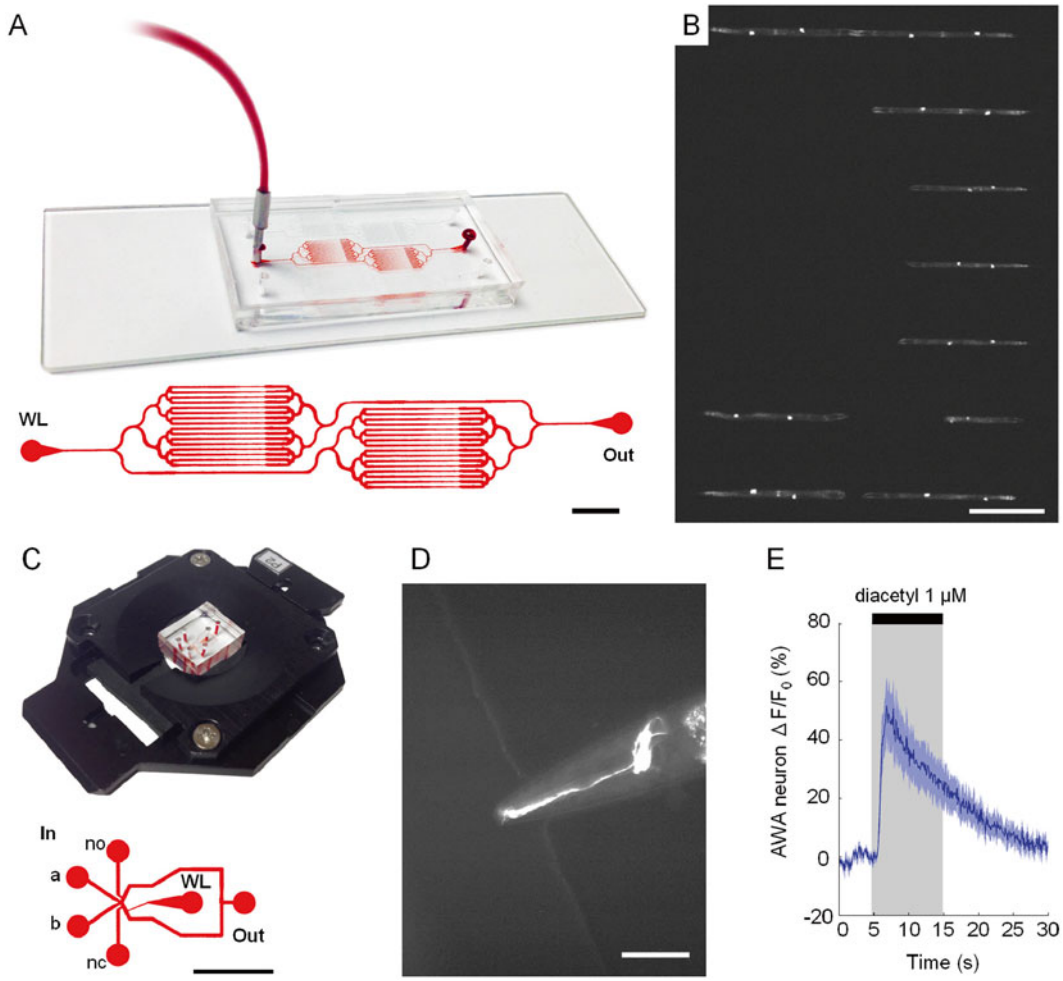

Fig. 2 Microfluidic devices for animal trapping and alignment, time-lapse microscopy, and neural imaging. (**a**) A parallel array of 32 tapering animal traps [7] is loaded via a single worm loading (WL) port. Scale bar, 2 mm. (**b**) Animals are aligned and remain in a fixed position during time-lapse imaging. Two distal tip cells are shown labeled with GFP (strain JK2868). Scale bar, 500 µm. (**c**) A neural imaging device [8] mounted in a microscope slide holder. Fluid streams from inlet (a) or (b) pass over the animal's nose depending on which control channel (no) or (nc) is open. Scale bar, 2 mm. (**d**) AWA chemosensory neurons are shown expressing the calcium sensor GCaMP2.2b (strain CX14887), Scale bar, 50 µm. (**e**) AWA neurons respond to addition of the odorant diacetyl (1 µM) with increased relative fluorescence intensity ($\Delta F/F_0$), indicating an "on" neural response [13]

devices are microfluidic worm traps for microscopy [7] and for high-resolution imaging of neural activity [8] using a fluorescent, genetically encoded calcium sensor [9] (Fig. 2). These devices are permanently bonded to a glass substrate, and most microfluidic systems are of this "single use" variety. These protocols are aimed at the user unfamiliar with microfluidic systems as well as the user who has experienced some difficulty in practice. While many details for preparing and operating microfluidic systems differ among published reports, here we highlight our preferred materials and methods and note alternatives when appropriate.

2 Materials

Microfluidic devices and accessories should be handled with gloves and pre-cleaned by washing in water, then 95 % ethanol, then water again, and dried in an air or N_2 stream (*see* **Note 1**). All solutions are prepared in sterile worm buffer at room temperature, unless noted, using aseptic technique.

2.1 Equipment

1. Vacuum desiccator.
2. Weigh balance (150 g range).
3. Magnetic stir plate.
4. Air or N_2 gun.
5. Micropipettes (10 or 20 μL, 200 μL, and 1000 μL).
6. Serological pipettes (25 mL).
7. Lab oven (65 °C) with level shelves (check with bubble level).
8. Plasma bonding system (Harrick PDC-32 or equivalent); optional, if permanently bonding the microfluidic device to a glass substrate (*see* **Note 2**).

2.2 Microfluidic Device Casting and Punching

1. Plastic or silicon master mold (*see* Subheading 3).
2. Dow Corning Sylgard 184 polydimethylsiloxane (PDMS) kit.
3. Nitrile or powder-free latex gloves (powder may inhibit PDMS curing).
4. 150 mm Petri Dish (*see* **Note 3**).
5. Large weigh boat.
6. Plastic transfer pipettes.
7. Stainless steel scalpel holder and No. 10 blade.
8. Single-edge heavy duty razor blade.
9. Scotch Magic Tape (3M cat. 810).
10. Dermal punch, 1 mm (AcuDerm P125).
11. Dark fine tip marker.
12. Self-healing cutting mat.

2.3 Microfluidic Device Accessories

1. Glass slides, 1–1.5 mm thick, cut to desired dimensions if necessary (*see* **Note 4**) using a diamond-tipped scribe. Use cover slips (#2 or #1.5 thickness) for high-resolution microscopy applications.
2. TFOCS: (Tridecafluoro-1,1,2,2-tetrahydrooctyl) trichlorosilane (Gelest SIT8174.0) for preparation of hydrophobic glass. *CAUTION: TFOCS is corrosive and toxic and must be used in a fume hood.*
3. Dremel 4000 rotary tool with workstation stand and 5/64″ diamond taper wheel point (Dremel 7134).

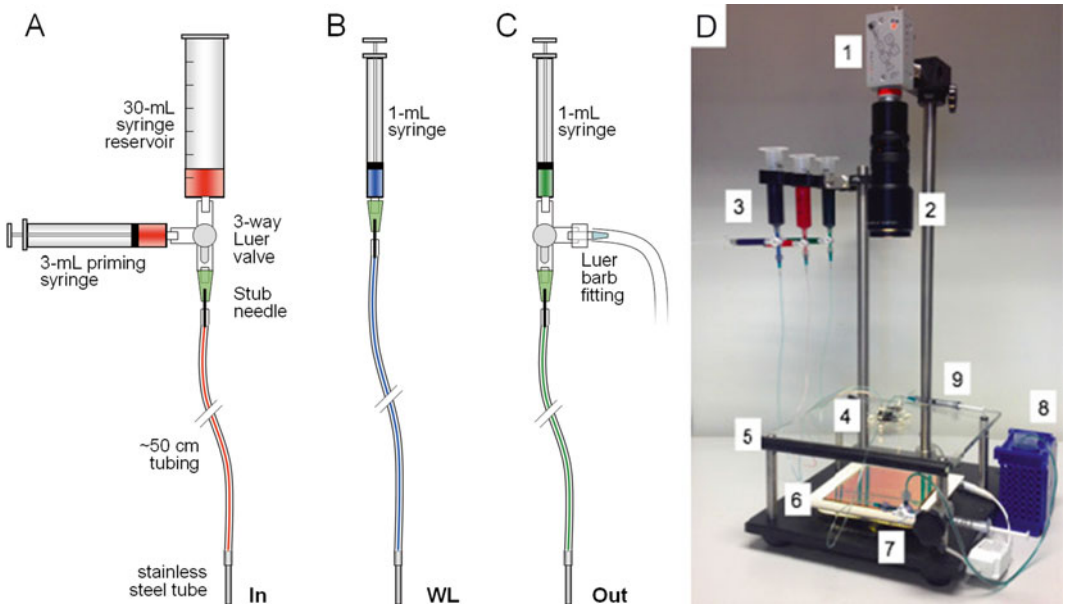

Fig. 3 Experimental setup for microfluidic flow via hydrostatic pressure. Tubing, syringes, and valves are shown for solution reservoirs (**a**), worm loading syringe (**b**), and outflow tubing (**c**). The complete video capture system (**d**) contains the (*1*) video camera, (*2*) zoom lens, (*3*) stimulus reservoirs, (*4*) microfluidic device, (*5*) glass stage, (*6*) LED backlight, (*7*) outflow syringe, (*8*) waste reservoir, and (*9*) worm loading syringe

4. Metal clamp assembly, either: (a) Small 5/16″ capacity binder clips, (b) Warner Instruments platform P-2 for small devices less than 20×20 mm^2, or (c) a custom-fabricated device holder (*see* **Note 5**).

2.4 Solutions

1. Worm buffer (*see* **Notes 6** and **7**): Dissolve 5.85 g NaCl, 1.0 g K_2HPO_4, and 6.0 g KH_2PO_4 in 1 L deionized water. Check that pH is about 6.0 and adjust if necessary. Sterilize by autoclave.
2. Dye solution (100×): 10 mg/mL xylene cyanol in worm buffer (*see* **Note 8**). Dissolve 1.0 g xylene cyanol in 100 mL worm buffer and sterilize by autoclave or syringe-tip filter.
3. Loading buffer: 5 % w/v Pluronic F127 with 0.5× dye solution. Prepare 1 mL aliquots and store at 4 °C.
4. Stimulus buffer(s): For example, a $1{:}10^7$ dilution of isoamyl alcohol (IAA, 3-methylbutanol >99.8 % purity) produces a robust attraction response (*see* **Note 9**).

2.5 Experimental Setup

1. Tubing set (five total): Insert the metal end of a blunt 23 gauge Luer stub adapter into one end of a 50 cm length of 0.020″ inner diameter (ID) Tygon tubing (*see* **Note 10**). Insert a 1/2″ (13 mm) long 19 gauge stainless steel tube (New England Small Tube NE-1027-12) about one-third of the way (4–5 mm) into the other end of the Tygon tubing as in Fig. 3a (*see* **Note 11**).

2. Solution reservoirs (three total): Connect a 30 mL syringe and 3 mL syringe to a three-way Luer stopcock valve as in Fig. 3a (*see* **Note 12**). Remove the plunger from the 30 mL syringe. Connect a tubing set (from **step 1**) to the valve.
3. Worm loading syringe: Connect a 1 mL syringe to one tubing set as in Fig. 3b.
4. Outflow tubing: Connect a 1 mL syringe, a tubing set, and a male Luer barbed fitting with ~50 cm of Tygon tubing (1/16″ ID, 1/8″ OD) as in Fig. 3c.
5. Reservoir rack and stand (Automate Scientific or Warner Instruments MSH-series).
6. Solid 1/2″ long 19 gauge stainless steel pins (New England Small Tube).
7. Video capture system as in Fig. 3d (*see* **Note 13**).

2.6 Alternative Materials

1. *Tubing*: Tygon and other lab tubing can leach chemicals such as plasticizers that elicit a weakly attractive behavioral response in *C. elegans*. We have found this effect to be negligible when testing robust stimuli or when all inlet fluids flow at an equal rate. Alternatively, high-purity Teflon PFA tubing (Upchurch IDEX, 0.020″ ID, 1/16″ OD) does not elicit any behavioral response in our experience, although it is substantially more expensive. This tubing is rigid and can be inserted directly, without a metal tube, into a larger PDMS inlet port: in Subheading 3.1, **step 10**, use a 1.5 mm dermal punch (AcuDerm P1525). This tubing also requires specific fittings (IDEX LuerTight, P-835) to connect with syringe reservoirs.
2. *Automated valves*: Automated valves are useful for precise temporal delivery of stimuli, such as a sudden application or removal of a stimulus (e.g., AutoMate Scientific). We prefer electrically actuated, computer-controlled microvalves with low swept volume and an inert wetted path.

3 Methods

This protocol assumes that the user has a microfluidic mold master (begin at Subheading 3.1) or pre-cast microfluidic devices (begin at Subheading 3.2). We recommend contacting the corresponding author of a publication presenting a microfluidic device of interest to request obtaining either a PDMS casting, a mold master, or the computer-aided design (CAD) file from which the master can be microfabricated. We encourage microfluidics-oriented labs to provide these resources openly or at modest cost where appropriate. There are a few publicly available resources for outsourcing the

microfabrication of mold masters, although they tend to have fluctuating capabilities. Commercial sources that offer prototyping services are listed at wikipedia.org/wiki/List_of_microfluidics_related_companies. Some university-based resources include the Caltech Microfluidics Foundry, the Princeton Microfluidics Laboratory, and the Stanford Microfabrication Foundry Most universities with engineering departments house a microfabrication facility, and many will either produce a mold master for nominal cost or provide training to users interested in learning fabrication methods. Finally, members of the National Nanotechnology Infrastructure Network (NNIN) offer cleanroom process capabilities. The costs of in-house production have dropped to approximately $25,000 in equipment (and also available as a kit, e.g., SoftLithoBox™ by BlackHoleLab), although substantial investment in process development is still required. Fabrication steps are relatively quick (about 2–3 h) for simple device masters and are described in detail elsewhere [10–12].

3.1 Device Fabrication: PDMS Casting from a Mold Master

1. Weigh a 10:1 (w/w) ratio of Sylgard 184 PDMS base to curing agent into a large weigh boat (*see* **Note 14**).
2. Mix PDMS base and curing agent thoroughly (*see* **Note 15**).
3. Degas the mixture in the vacuum desiccator for 30 min to 1 h to eliminate bubbles (*see* **Note 16**).
4. Clean the mold master, Fig. 4a, in an air stream if dust is visible (*see* **Note 17**).

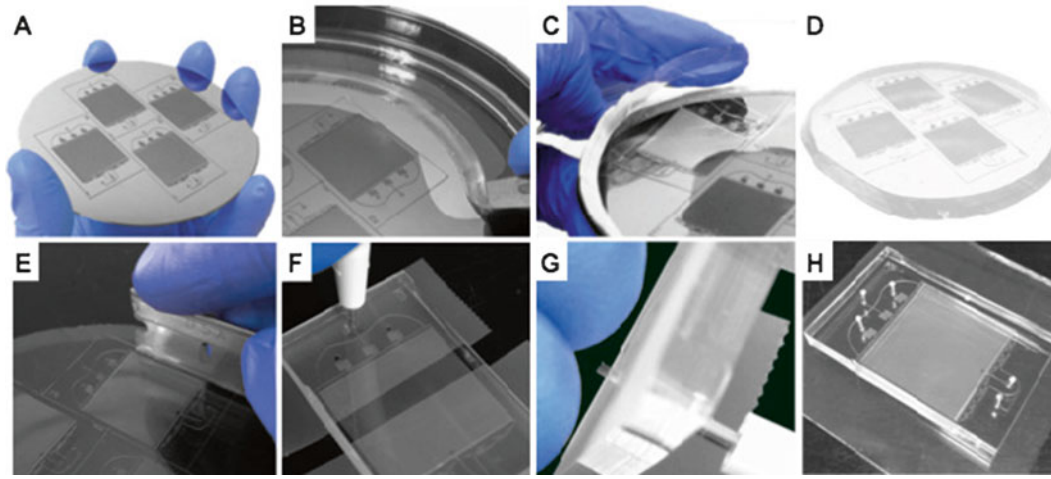

Fig. 4 Device fabrication steps. PDMS polymer is cast over a mold master such as a micropatterned silicon wafer (**a**). The cast PDMS is cut out with a scalpel (**b**), peeled from the mold master (**c** and **d**), and trimmed into individual microfluidic devices with a razor blade (**e**). Inlet and outlet ports are punched (**f**), removing excess punched material (**g**). The microfluidic device is cleaned and ready for assembly or for permanent bonding to a glass substrate (**h**)

5. Pour the PDMS mixture onto the mold master in a large (150 mm diameter) Petri dish (*see* **Note 3**), and fill to the desired device thickness, approximately 4–5 mm (*see* **Note 18**).
6. Inspect the poured PDMS and remove bubbles or dust (*see* **Note 19**).
7. Bake at 65 °C on a level shelf for between 3 h to overnight.
8. Remove the PDMS casting: Cut along the mold master perimeter with a metal-handled scalpel (*see* **Note 20**), gently peel up, and remove as in Fig. 4b–d.
9. Cut individual devices from the PDMS casting with a single-edge razor blade as in Fig. 4e (*see* **Note 21**).
10. Punch inlet and outlet holes (*see* **Note 22**) using a 1 mm diameter dermal punch as in Fig. 4f–h (*see* **Note 23**). Clean any debris remaining in the holes (*see* **Note 1**).

3.2 Device Fabrication: Glass Substrates

Microfluidic channels are formed upon sealing the PDMS casting to a flat substrate, usually a glass slide or cover slip. A reversible leak-resistant seal can be made by compressing the PDMS casting between a hydrophobic glass substrate and a second glass slide with holes drilled for tubing connections (Fig. 5a). This configuration is considered "reusable" as it can be opened after an experiment for cleaning and recovery of animals. However, it may leak under excessive fluidic pressure; thus, flow is best driven by hydrostatic pressure.

An irreversible leak-proof seal is prepared by plasma bonding a glass slide or cover slip to the PDMS casting as in Fig. 5b. Flow in bonded devices may be driven by pressurized reservoirs or syringe pumps without risk of leakage, and they are preferred for long-duration experiments and for high-resolution microscopy requiring a thin cover slip as a substrate. However, bonded devices are usually considered to be single use, as cleaning and animal recovery are difficult.

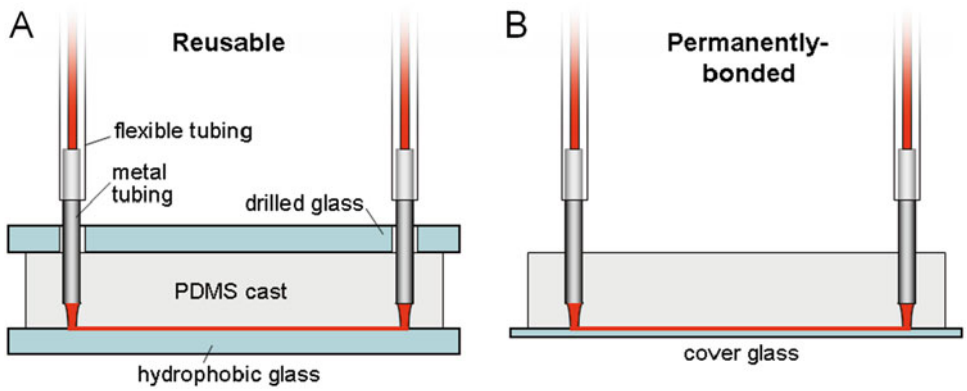

Fig. 5 Cross-sectional view of a reusable microfluidic device (**a**) and a permanently bonded microfluidic device (**b**)

3.2.1 Glass Plates for Reusable Devices

Perform these steps only for reusable, reversibly sealed microfluidic devices as in Fig. 5a, then proceed to Subheading 3.3.

1. Prepare a hydrophobic glass slide slightly larger than the PDMS device (*see* **Note 4**) by TFOCS vapor deposition (*see* **Note 24**).
2. Drill inlet holes into a second glass slide of equal dimensions: Align the PDMS device on the glass and mark hole locations (*see* **Note 25**). Drill holes under constant water lubrication (*see* **Note 26**), and clean thoroughly (*see* **Note 1**).

3.2.2 Plasma Bonding

Perform these steps only for permanently bonded microfluidic devices (Fig. 5b).

1. Seal a clean, dry, dust-free PDMS device (*see* **Note 1**) onto a $2'' \times 3''$ glass carrier slide such that the micropatterned features face up.
2. Clean the glass substrate (cover slip or slide) with ethanol while rubbing with a lint-free wipe (e.g., Kimwipe). Dry with the air/N_2 gun and remove dust with tape. Transfer to the glass carrier slide and insert into the plasma vacuum chamber (*see* **Note 2**).
3. Expose to air plasma for 60 s (*see* **Note 27**).
4. Invert the slide or cover glass onto the PDMS device (*see* **Note 28**) and briefly apply gentle pressure (*see* **Note 29**).

3.3 Device Preparation and Assembly

1. Before use, microfluidic devices should be cleaned by soaking in ethanol for several hours, rinsed with water (*see* **Note 1**), and baked for at least 1 h to evaporate residual ethanol (*see* **Note 30**).

   For permanently bonded devices, skip to step 5.
2. Seal a clean, dust-free microfluidic device against a clean, dust-free drilled top glass slide (*see* **Note 1**), aligning the drilled holes with the punched inlets. Remove any remaining dust with tape.
3. Seal a clean, dust-free hydrophobic glass slide against the micropatterned side of the device.
4. Clamp the device with binder clips as in Fig. 6 (or in a clamp apparatus, *see* **Note 5**). Holding the glass-PDMS-glass assembly

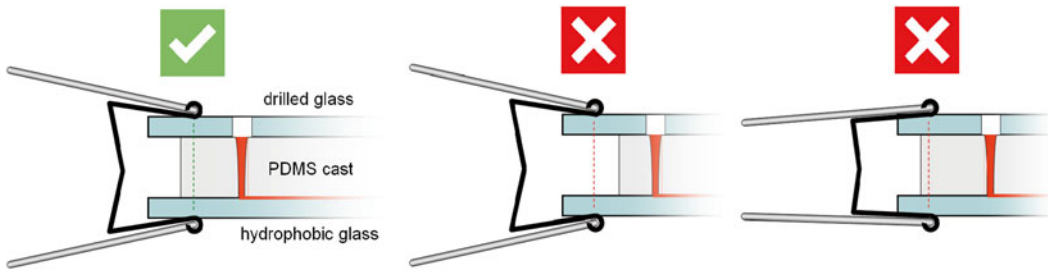

Fig. 6 Proper positioning of binder clip clamps (*left*). Avoid clamping where the glass slides are unsupported (*center*) or with a binder clip that is too small (*right*), as excess stress may crack the glass slide

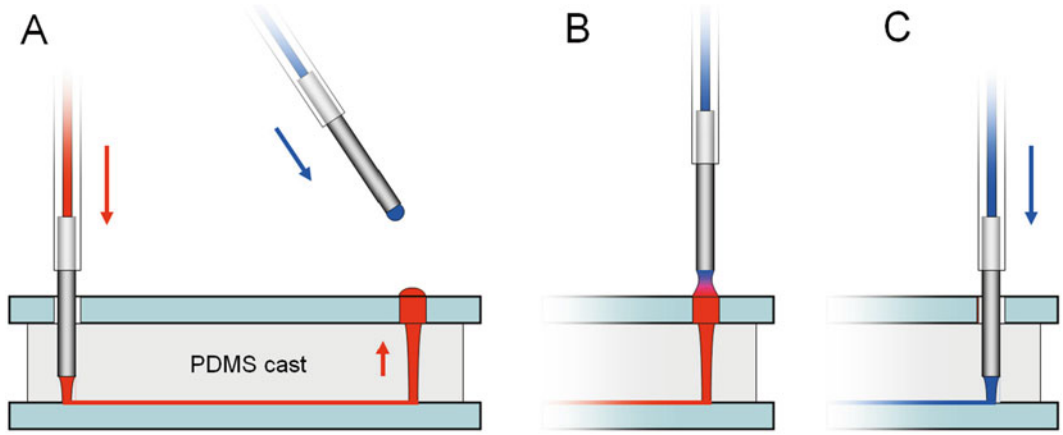

Fig. 7 Bubble-free, "drop-to-drop" insertion of tubing into a port on microfluidic device. Allow liquid to flow in the device (*red*) until a drop appears at the port, and inject liquid in the tubing to be inserted (*blue*) until a droplet hangs from the tubing pin (**a**). Bring the droplets into contact (**b**), and insert pin about 2/3 into the port (**c**)

firmly in the center, apply a binder clip to one side. Without releasing pressure, clip the opposite side (*see* **Note 31**). Test for proper compression force (*see* **Note 32**).

5. Block the worm loading port by inserting a solid blocking pin until it reaches ~2/3 (about 3 mm) through the thickness of the PDMS (*see* **Note 33**).
6. Degas the assembled microfluidic device in the vacuum desiccator for 10–30 min (*see* **Note 34**).

3.4 Device Filling

1. Prepare fluid reservoirs and tubing (as noted in Subheading 2.5). Position each reservoir on the rack and fill with stimulus or buffer solutions. Remove air bubbles (*see* **Note 35**) and fill the tubing (*see* **Note 36**).
2. Prepare outflow tubing. Fill with buffer, then draw 1 mL Loading buffer into outflow syringe.
3. Remove the device from vacuum and connect the outflow syringe to the outflow port (*see* **Note 34**).
4. Gently inject Loading buffer until it has completely filled the arena and begins to emerge as a droplet at an inlet.
5. Connect the buffer tubing to the inlet hole using a "drop-to-drop" connection as in Fig. 7 and aspirate any excess liquid (*see* **Note 37**).
6. Open the buffer valve briefly (turn to "Flow" position, Fig. 8) until another inlet hole fills, then insert the next stimulus tubing with a "drop-to-drop" connection (*see* **Note 38**). Repeat for all inlet reservoirs.

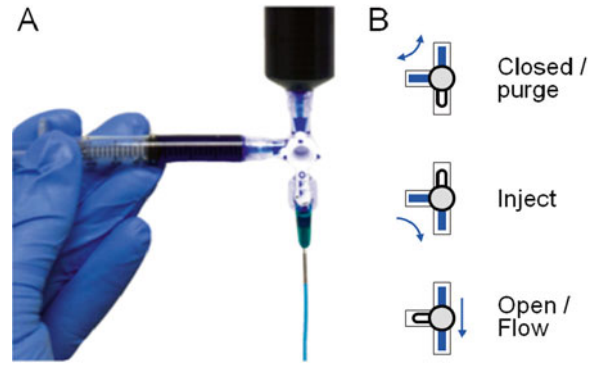

Fig. 8 (**a**) Solution reservoir filled with dye and valve in the Closed/Purge position. (**b**) Valve positions used to control fluid flow during operation of the microfluidic device. *Arrows* indicate fluid flow direction

7. Once all ports are connected with tubing (or blocked), open a buffer valve and the outflow valve to flush the arena with worm buffer and displace the Loading buffer (*see* **Note 39**).
8. Position the microfluidic device on the observation stage (*see* **Note 40**).

3.5 Worm Loading and Device Operation

1. Pick 1–50 young adult *C. elegans* (*see* **Note 41**) onto an unseeded 60 mm agar plate (*see* **Note 42**).
2. Pour ~5 mL worm buffer onto the plate.
3. Fill the 1 mL worm loading syringe with worm buffer, purge any bubbles, and draw animals into the tubing (*see* **Note 43**) using a minimal volume of buffer (*see* **Note 44**).
4. Close the outflow valve, remove the blocking pin from the worm loading port, and briefly open the buffer valve to fill it with a buffer drop. Insert the worm loading tubing with a "drop-to-drop" connection (*see* Fig. 7).
5. Open the buffer and outflow valves (Fig. 8, "Flow" position) and gently inject animals into the arena (*see* **Note 45**).
6. Once all animals have entered the arena, pinch the worm loading tubing and clamp it with a mini binder clip to prevent flow into this channel.
7. Allow animals to disperse and adapt to the micropost environment for several minutes before initiating a recording and opening the stimulus valves (*see* **Note 46**).
8. Adjust the relative heights of the stimulus reservoirs to verify the desired spatial pattern. Fluid flow rate is proportional to the height difference between fluid levels of the reservoirs and waste beaker (*see* **Note 47**). For a stripe pattern device (Fig. 1), raising a reservoir increases the width of the corresponding fluidic stripe.

9. Record animal behavior for 30–120 min (*see* **Note 48**) and analyze as desired, for example using "ArenaWormTracker" software [6].

For troubleshooting device operation, common problems and recommended solutions are listed in Subheading 5.

3.6 Device Cleanup and Storage

1. Shut off all valves (Fig. 8, "Closed" position) and remove tubing from all ports.
2. Rinse all syringe reservoirs and tubing with water and blow dry with an air or N_2 gun (*see* **Note 49**). Eject remaining liquid in worm loading tubing, rinse with water, and dry.
3. For reusable devices, open the microfluidic assembly, separate the PDMS from glass slides, and optionally recover animals to a seeded agar plate by rinsing the PDMS and glass with worm buffer.
4. Rinse the PDMS with water (*see* **Note 1**) and soak it overnight in ethanol to remove any adsorbed stimulus (*see* **Note 50**), then clean (*see* **Note 1**) and bake for at least 1 h to evaporate residual ethanol (*see* **Note 30**).
5. Devices may be stored at room temperature or in an oven at <65 °C, and reused dozens of times.

3.7 Microfluidic Devices for Microscopy and Neural Imaging

The methods described above for fabricating, cleaning, assembly, filling, loading, and operating microfluidic devices are general and can be used with most designs. Below, we describe two additional simple devices for arraying many animals in parallel for time-lapse microscopy [7] (Fig. 2a, b) and for high-resolution imaging of neural activity [8] (Fig. 2c–e).

3.7.1 Parallel Trap Array Device

This device aligns many animals within tapering channels for ease of imaging by microscopy. It is conveniently loaded through a single worm loading port and is often used for time-lapse microscopy in which individual animals can be observed over many hours.

1. Prepare the trap array device (Fig. 2a) as described in Subheadings 3.1–3.4 and fill with worm buffer from the outflow port (*see* **Note 51**).
2. Draw animals into worm loading tubing and inject them into the channels as in Subheading 3.5. Ensure the outflow valve is open during worm loading.
3. Once animal traps are filled, close the outflow valve, remove the worm loading tubing, and replace it with a buffer reservoir (*see* **Note 52**). Open the outflow valve to initiate buffer flow.
4. Monitor changes in fluorescent markers (such as position or intensity) over time (Fig. 2b).

3.7.2 Neuronal Imaging Device

Calcium imaging studies determine a neuron's response to a sudden presentation or removal of a chemical stimulus. This device traps a single animal such that its nose protrudes into a channel that is rapidly switched between two fluidic streams. Recent modifications of this design increase the number of animals and stimuli tested per experiment [13, 14] or enable neural imaging in freely moving animals to correlate neural and behavioral responses [13].

1. Prepare the imaging device (Fig. 2c) as described in Subheadings 3.1–3.3 and fill with worm buffer from the outflow port (*see* **Note 51**).
2. Prepare two stimulus reservoirs and tubing as in Subheading 3.4. Typically, one reservoir contains worm buffer (a), and the other a chemical stimulus (b).
3. Prepare a control fluid reservoir connected to the common port of a three-way actuated microvalve. Connect tubing sets to the normally open (no) and normally closed (nc) ports on the microvalve. Fill the reservoir with worm buffer (*see* **Note 53**) and prime the tubing (*see* **Notes 35** and **36**).
4. Connect all four inlet tubes to the inlet ports via drop-to-drop connections (*see* **Note 54**).
5. Inject one animal into the worm loading port. Observe the animal under the microscope, providing pressure from the worm loading syringe as necessary until it reaches the tapered clamp with its nose just protruding into the fluidic channel as in Fig. 2d.
6. Focus the objective on the neuron of interest under fluorescent excitation (*see* **Note 55**) and set up an acquisition stream (*see* **Note 56**).
7. Acquire video for 30 s to 3 min, actuating the microvalve (*see* **Note 54**) at the desired time and duration to apply a stimulus pulse, as in Fig. 2e.

4 Notes

1. All components should be stored clean, dry, and dust-free in closed containers. Rinse microfluidic devices and glass substrates first with deionized water to prevent crystallization of salts within microchannels or tubing. Flush inlet ports using squirt bottles, ensuring the fluid stream passes through each inlet. Next, clean with ethanol, wiping away any debris and smudges with gloved fingers. Finally, rinse with water and quickly blow dry with an air or N_2 gun. This step prevents evaporation which may leave a residual film that is difficult to remove, especially from microfluidic channels. Remove surface dust using tape.

2. Alternative and less expensive PDMS plasma bonding methods have been reported, although they are generally less reliable and more sensitive to exact treatment conditions. These include a handheld corona discharge wand [15] and an evacuation chamber placed in a standard microwave oven [16].
3. A disposable PDMS casting dish can be made from aluminum foil. We prefer a large 150 mm Petri dish as it has a flat and level bottom, comes with a lid, and protects the wafer from damage during handling and storage.
4. Trim glass slides as necessary to maintain about a 2–5 mm border around the PDMS microfluidic device. Use a 1.5 mm thick glass slide for devices larger than ~25 mm × 25 mm. Align a ruler along the desired cut line, firmly score once with a sharp diamond scribe, and snap the glass by applying evenly distributed pressure on each half. For best results, cut at least 12 mm away from any edge. With proper pressure, the score line should be thin and barely visible.
5. We custom machined a clamp from 1/4″ thick aluminum bar, four 1/4″-20 bolts, and four springs. Two plates each contain a central imaging window and four holes in the corners; the bottom plate holes are tapped with 1/4″-20 threads while the top holes allow free movement of the bolts. The microfluidic device is held between the top and bottom plates by the bolts that compress springs. To assemble, place and center the microfluidic assembly into the device holder, then evenly tighten the four screws in a cross-diagonal manner to prevent uneven point stresses.
6. Our preferred worm buffer is "S Basal" without cholesterol, which sustains healthy animal behavior for long durations and is easy to prepare. A common alternative is "M9 Buffer": Combine 5.0 g NaCl, 3.0 g KH_2PO_4, 6.0 g Na_2HPO_4 and 0.25 g $MgSO_4 \cdot 7H_2O$ in a beaker and add water to 1 L. Sterilize by autoclave.
7. Some chemicals may react with phosphate buffer, such as copper chloride. Choose an alternate buffered saline solution if necessary.
8. Wild-type worms may be weakly attracted to 1× xylene cyanol in the absence of other stimuli, but the dye usually does not affect behavior to a moderate stimulus. Nonetheless, it is beneficial to repeat experiments without dye to verify minimal contribution of the dye under the conditions tested.
9. Odor dilutions should be freshly prepared each day. IAA is hydrophobic, low density, and weakly soluble in aqueous buffers. Therefore, it rises to the liquid surface and adsorbs to the vial walls and to the pipette tip. We prefer the following dilution procedure: First prepare a $1{:}10^3$ dilution by adding

30 μL IAA to 30 mL worm buffer in a pre-cleaned 40 mL amber vial (ESS Vial). Pipette repeatedly to rinse the pipette tip, then quickly seal and vortex for 30 s. Transfer 3 μL diluted IAA to a second vial containing 30 mL worm buffer for a $1{:}10^7$ final dilution; if desired, include 0.5×–1× Dye solution for visualization.

10. Be careful not to gouge the inner surface of the tubing, which may result in a clog or poor seal.
11. Using gloves for improved grip, angle the metal tube into the Tygon tubing until it stretches over the metal tube. Next, push the Tygon tubing down along the metal tube while angling it back and forth. Then grip the Tygon tubing tightly at the metal tube and push firmly down on a cutting mat until it stretches about 1/3 of the way down the 1/2″ long metal tube (4–5 mm).
12. For longer duration experiments, 60 mL syringes or larger reservoirs with Luer fittings may be used.
13. Video capture can be performed with a camera attached to the trinocular port of a microscope with a transmitted light base. Alternatively, a less expensive setup can be assembled from a camera, zoom lens, and support stand, for example as described at *arenawormtracker.blogspot.com*.
14. This is a messy process: Line the work area with disposable paper, use clean gloves, and be careful to prevent spills, as it is difficult to clean off the highly viscous and oily PDMS materials. We prefer to use a large disposable weigh boat containing 100–120 g PDMS for mixing by hand, as it is easier to ensure complete mixing compared with a cup with tall sides. It is convenient to weigh the viscous base PDMS on a balance, then tare the balance and pour 1/10 (for 10:1 ratio) the weight of curing agent. Exact weights are not critical, as PDMS will cure properly with a range of base to curing agent from 5:1 to 20:1.
15. We use a transfer pipette to mix PDMS for at least 1 min, using a folding motion to combine the viscous base component with the low viscosity curing agent. Many air bubbles should be generated with proper mixing vigor. Insufficient mixing may result in partially uncured PDMS, an unusable device, and/or a messy mold master.
16. To accelerate this process, briefly vent the chamber and reapply vacuum once or twice.
17. Remove any surface smudges with an isopropanol wash, then water, then air-dry. A release agent should be applied to new, untreated mold masters. For silicon wafers, apply TFOCS as described in **Note 24**.
18. To determine the correct PDMS fill volume, first fill with water to the desired depth and note the weight of added water. After drying the mold, add the same weight of PDMS

(density 0.97 g/mL is nearly equal to water). For 4–5 mm depth, we fill 85 g PDMS in a 150 mm Petri Dish and 45 g in a 4″ diameter foil boat. To reduce bubble formation, pour quickly with the weigh boat about 1–2 cm above the mold surface while moving linearly across the mold to prevent the PDMS stream from folding upon itself and forming air bubbles.

19. Dust can be carefully removed with a transfer pipette and bubbles on the master surface can be dislodged by gently and slightly tilting the dish back and forth, allowing for viscous shear forces to release the attached bubbles. Bubbles that have risen can be removed by blowing lightly on the PDMS surface.
20. To cleanly cut out the casting, firmly grip the scalpel and insert into the PDMS at an outward angle near the edge of the mold master wafer. Then, making contact between the blade and the wafer, rotate the dish such that the blade follows the perimeter of the wafer making one continuous circumferential cut.
21. If individual devices are outlined with microchannels, it is convenient to align the single-edge razor by feeling for when it falls into the groove. Then, ensure the razor is vertical and press down firmly through to the cutting mat.
22. The punched inlet channel will taper in the direction of punching. Alignment of the inlet hole and the microfluidic features is easier when punching *from* the micropatterned side of the PDMS cast. However, we prefer punching *toward* the micropatterned side for ease of tubing insertions. Tape and mark each inlet with a fine tip marker on the micropatterned side, then insert the dermal punch from the opposite side, keeping it straight and vertical. After completely punching through the device, remove the excess PDMS from the punch before pulling it out of the device (Fig. 4g).
23. Holes punched with a damaged or dull dermal punch are prone to leakage. It is advisable to punch a test hole and observe under magnification for smooth round edges free of nicks. Use a new punch if necessary.
24. Render glass and silicon wafer surfaces hydrophobic by vapor deposition of TFOCS. Place cleaned substrates in a vacuum desiccator and add 40 μL of TFOCS to a small aluminum foil dish in the center. Treat for 1 h, then clean with isopropanol, then water, then dry in an air or N_2 stream.

    CAUTION: *TFOCS is corrosive and toxic*. Perform all steps in a fume hood.
25. Mark the drill locations on tape that is applied to the glass, to prevent the ink from washing off during drilling.
26. Hold the glass slide securely on a plastic multi-well (e.g., 96-well) plate, centering the drill hole over a well. This provides support beneath the glass during drilling. Align the bit to the

mark, apply water as lubricant and coolant, and apply gentle pressure to grind the glass at 15,000 rpm. Ensure that the bit and glass are wet at all times, or the bit will very quickly become hot and damaged. Continue grinding, releasing pressure every 3–5 s, until the hole is complete.

27. Turn on the vacuum pump and plasma power. After 10–30 s, a plasma should be visible in the vacuum chamber (purple/orange glow). Adjust the gas needle valve until the plasma appears bright red-orange due to the presence of oxygen and nitrogen gases. If no plasma is visible or it appears dim purple, pressure may be too low (open the needle valve slightly to introduce air) or too high (close the needle valve and wait for pressure to decline).
28. Plasma-activated PDMS and glass will form a covalent bond on contact, with no opportunity to reposition them. Carefully align the glass over the microchannel surface, and gently release the glass substrate upon initial contact to prevent internal stresses.
29. Gentle compression for about 10 s ensures a good bond and forces trapped air bubbles out of the device. Test for a successful bond by gently peeling up at each corner of the PDMS; the PDMS device should remain sealed against the glass substrate.
30. Ethanol causes PDMS to swell by 4 % [17]. Ensure that all ethanol is evaporated by baking at 65 °C for at least 1 h or at room temperature overnight before proceeding with assembly. Insufficient baking will result in swelling in the center of the device and a poor fluidic seal. Ethanol remaining inside PDMS can be visualized as a cloudy white haze after soaking in water or buffer; if this is observed, additional evaporation time is required.
31. Binder clips should be expanded by bending them open until a 3 mm gap remains at rest (such as by clipping a wide pen barrel and forcing the clip spine toward the barrel). Binder clips should be positioned over a supported PDMS edge without blocking the imaging area, as in Fig. 6. Avoid clamping at an unsupported region of glass or with a clamp that is too small, as stresses may cause the glass to break.
32. The binder clips should grip firmly enough to remain in place but loose enough to be easily repositioned without opening.
33. Fluid will initially flow to the port of least fluidic resistance, often the closest port. It is therefore helpful to block any open ports near the filling port to ensure rapid filling of the entire fluidic network.
34. Air bubbles that form upon initial filling of a microfluidic device are absorbed into degassed PDMS. The rate and capacity of bubble absorption increases with time under vacuum and

decreases with time outside the vacuum dessicator. Therefore, initial filling of the microchannels with liquid should occur quickly after removing the PDMS device from vacuum, ideally within a few minutes.

35. Remove bubbles from the 3 mL priming syringe by setting the valve to the "Purge" position (Fig. 8), slowly drawing liquid from the 30 mL reservoir, then quickly injecting it back. After two to three cycles, all bubbles should be purged.
36. To avoid bubbles trapped in the Luer stub, first ensure that the Luer stub and tubing are dry. Then, rotate the valve to the "Inject" position (Fig. 8) and slowly inject fluid filling the Luer fitting and tubing. If any bubbles are seen in the Luer fitting, flick the fitting while injecting to dislodge and purge them. It is important to remove these air bubbles to avoid their entry into the microfluidic channels during an experiment.
37. It is helpful to set up a vacuum line to aspirate excess liquid on the microfluidic device. Set up a vacuum trap (side-arm flask) and tubing terminated with a male Luer barb and a Luer stub needle (or a 200 μL micropipette tip, trimmed to fit).
38. It is best to flush out loading buffer from the inlet ports, as the Pluronic surfactant reduces the grip between the inlet hole and the metal tube. Flushing will reduce the chance of an inlet tube popping out during an experiment.
39. We advise testing the stimulus pattern briefly before loading animals to ensure proper device preparation and flow.
40. It is convenient to support the microfluidic device on the glass observation stage with four clean scrap PDMS pieces, each about $5 \times 10 \times 10$ mm^3. These supports seal to the stage and to the bottom of the microfluidic device assembly and hold it securely during an experiment (*see* Fig. 1a). Ensure that the scrap PDMS supports are all equal height and do not obscure the arena.
41. Wild-type animals are conveniently picked at L4 larval stage 16–24 h prior to loading as young adult animals.
42. To avoid damaging animals, it is helpful to identify the focal plane of the agar surface with a small mark or bacteria using a worm pick. It is unnecessary to wash animals before transfer to this plate, as any residual bacteria will be washed away in the microfluidic device.
43. Avoid drawing up air bubbles by keeping the metal tube submerged. Ensure that no animals enter into the syringe barrel by drawing up less volume than the tubing (~100 μL for a 50 cm length).
44. After collecting animals into the worm loading tube, deposit them slowly into a small region of the plate and draw them up

again into a minimal volume. This process speeds loading of animals into the arena. Draw up enough buffer to observe the last animal in the clear tubing, to ensure that a "drop-to-drop" contact can be made at the worm loading port without losing any animals.

45. Observe animal loading into the arena during gentle injection to ensure they are not damaged. Animals that remain stationary after fast injection may have sustained physical damage.
46. Wild-type animals move slowly for the first 10–15 min in the device. It is beneficial to flush the arena with buffer during this time to wash away any residual bacteria. Verify correct valve positions before initiating the experiment.
47. To measure total flow rate while all valves are open, briefly remove and reinsert the outflow tubing from the outflow port to introduce a small bubble. Measure the time for the bubble to move 1 cm down the outflow tubing to calculate flow rate (0.02″ ID tubing contains 2 μL/cm of length; a bubble moving 1 cm in 5 s indicates a flow rate of 2 μL/5 s or 0.4 μL/s).
48. We typically record at two frames per second at a camera resolution of about 40 pixels/mm. Adjust arena position and lens zoom such that the recorded image is level and fully contained within the video frame. Adjust illumination brightness, camera gain, and/or acquisition time such that animals have good contrast and no pixels are saturated.
49. Buffer salts that crystallize in tubing may be difficult to remove. Flush with water and air-dry by blowing with compressed air after experimentation.
50. Hydrophobic stimuli can leach into PDMS. We submerge devices in a stirred ethanol bath overnight, especially after experiments using high concentrations of hydrophobic stimuli.
51. A surfactant such as Pluronic F127 is not necessary in the Loading buffer if the microfluidic channels are narrow. However, Pluronic F127 also prevents protein and bacteria adsorption to the channel surfaces, and should be included if animals are fed bacterial food in the device.
52. Slow buffer flow helps to keep animals in the tapered clamps during time-lapse recordings. For long-term culture in traps, animals may be fed with bacteria.
53. It is useful to add a dye to the control fluid such as 1 μg/mL fluorescein to visualize and confirm proper fluid flow and operation of the valve.
54. When inlets are configured as in Fig. 2c, the animal is subjected to stimulus "a" when the valve is at rest and to stimulus "b" when the valve is energized [8].

55. Minimize photodamage and photobleaching by limiting exposure to excitation light and reducing intensity with a neutral density filter.
56. Typical GCaMP recordings are made at ten frames per second. Use a reduced region of interest (ROI) and/or image binning to reduce the acquisition file size.

5 Notes on Troubleshooting

Commonly encountered problems and recommended solutions are listed:

1. *Bubbles in a microfluidic channel or arena*. If the device was recently degassed, small bubbles will absorb into the PDMS (*see* **Note 34**). Wait 5–10 min and see whether the bubble has gotten smaller. If not, open the device, clean it, and set it up again as in Subheadings 3.3–3.4.
2. *Bubbles in inlet tubing*. Halt flow immediately by closing the outflow valve and pull out the tubing containing bubbles. Purge the bubbles by forcing them out with the syringe (valve position "Inject," Fig. 8) then reinsert using drop-to-drop contact (*see* Fig. 7).
3. *Bubbles or air in outflow tubing*. Small bubbles in the outflow tubing are ok and useful to estimate fluid flow rate (*see* **Note 47**), but large air-filled regions may slow gravity-driven flow. Be sure to fill the tubing completely to the waste beaker using the outflow syringe.
4. *Leakage at the fluorinated glass slide*. A poor channel seal may be caused by insufficient clamp pressure (*see* **Notes 31** and **32**), insufficient flatness of the PDMS device due to ethanol swelling (*see* **Note 30**), or a fabrication defect. Increase the compression force, evaporate longer in the oven, or use a new, flat device.
5. *Leakage at an inlet*. A poor seal at an inlet port may be due to insufficient tube insertion depth (ideal is ~2/3 of the port depth as in Fig. 5) or to poor punch quality. The inlet port should be punched straight with smooth walls. Damaged punches may cut a notch along the hole causing a slow fluid leak (*see* **Note 23**).
6. *Dust or particles in the microfluidic channels*. Clean devices thoroughly (*see* **Note 1**) and assemble quickly or in a clean hood. Wash inlet holes after punching. Filter solutions if necessary.
7. *Warped stimulus pattern*. Ensure no debris or bubbles disturb the flow path. If binder clips clamp too strongly and reduce channel depth at the edges, horizontal fluid stripes will bow toward the center.

8. *Fluid flow is too fast or too slow*. Adjust the height difference between reservoirs and waste beaker. For a height difference of 50 cm, flow rate in the behavioral arena is typically ~0.8 μL/s. Flow rate can be estimated as described in **Note 47**.

Acknowledgements

This work was supported by a Burroughs Wellcome Career Award at the Scientific Interface (DRA). We thank members of the authors' laboratory, L. Aurilio, K. Tran, K. Burnett, and B. Altshuler for their review and helpful comments while testing these protocols. Strains were obtained from C. Bargmann, V. Ambros, and the CGC.

References

1. San-Miguel A, Lu H (2013) Microfluidics as a tool for *C. elegans* research. WormBook, ed. The *C. elegans* Research Community. http://www.wormbook.org
2. Chronis N (2010) Worm chips: microtools for *C. elegans* biology. Lab Chip 10:432–437
3. Crane MM, Chung K, Stirman J, Lu H (2010) Microfluidics-enabled phenotyping, imaging, and screening of multicellular organisms. Lab Chip 10:1509–1517
4. Bakhtina NA, Korvink JG (2014) Microfluidic laboratories for *C. elegans* enhance fundamental studies in biology. RSC Adv 4:4691
5. Shi W, Wen H, Lin B, Qin J (2011) Microfluidic platform for the study of *Caenorhabditis elegans*. Top Curr Chem 304:323–338
6. Albrecht DR, Bargmann CI (2011) High-content behavioral analysis of *Caenorhabditis elegans* in precise spatiotemporal chemical environments. Nat Methods 8:599–605
7. Hulme SE, Shevkoplyas SS, Apfeld J et al (2007) A microfabricated array of clamps for immobilizing and imaging *C. elegans*. Lab Chip 7:1515
8. Chronis N, Zimmer M, Bargmann CI (2007) Microfluidics for *in vivo* imaging of neuronal and behavioral activity in *Caenorhabditis elegans*. Nat Methods 4:727–731
9. Tian L, Hires SA, Mao T et al (2009) Imaging neural activity in worms, flies and mice with improved GCaMP calcium indicators. Nat Methods 6:875–881
10. Qin D, Xia Y, Whitesides GM (2010) Soft lithography for micro- and nanoscale patterning. Nat Protocols 5:491–502
11. Mondal S, Ahlawat S, Koushika SP (2012) Simple microfluidic devices for *in vivo* imaging of *C. elegans*, Drosophila and zebrafish. J Vis Exp 67, e3780
12. Gilleland CL, Rohde CB, Zeng F, Yanik MF (2010) Microfluidic immobilization of physiologically active *Caenorhabditis elegans*. Nat Protoc 5:1888–1902
13. Larsch J, Ventimiglia D, Bargmann CI, Albrecht DR (2013) High-throughput imaging of neuronal activity in *Caenorhabditis elegans*. Proc Natl Acad Sci U S A 110:E4266–E4273
14. Chokshi TV, Bazopoulou D, Chronis N (2010) An automated microfluidic platform for calcium imaging of chemosensory neurons in *Caenorhabditis elegans*. Lab Chip 10: 2758–2763
15. Haubert K, Drier T, Beebe D (2006) PDMS bonding by means of a portable, low-cost corona system. Lab Chip 6:1548
16. Ginn BT, Steinbock O (2003) Polymer surface modification using microwave-oven-generated plasma. Langmuir 19:8117–8118
17. Lee JN, Park C, Whitesides GM (2003) Solvent compatibility of poly(dimethylsiloxane)-based microfluidic devices. Anal Chem 75: 6544–6554

Chapter 13

Tracking Single *C. elegans* Using a USB Microscope on a Motorized Stage

Eviatar I. Yemini and André E.X. Brown

Abstract

Locomotion and gross morphology have been important phenotypes for *C. elegans* genetics since the inception of the field and remain relevant. In parallel with developments in genome sequencing and editing, phenotyping methods have become more automated and quantitative, making it possible to detect subtle differences between mutants and wild-type animals. In this chapter, we describe how to calibrate a single-worm tracker consisting of a USB microscope mounted on a motorized stage and how to record and analyze movies of worms crawling on food. The resulting quantitative phenotypic fingerprint can sensitively identify differences between mutant and wild-type worms.

Key words Worm tracking, Automated imaging, Quantitative phenotyping, High-throughput microscopy

1 Introduction

Digital cameras are becoming smaller and cheaper, a trend that is driven in part by the mobile phone industry and that is likely to continue for some time. This trend can be exploited for worm tracking using mass-market USB microscopes as the core element of an automated motorized microscope. There are now many published worm trackers designed for a variety of applications with associated advantages and challenges. For a review of current worm trackers, *see* Husson et al. [1].

In this chapter, we will describe how to use a recently published single-worm tracker [2], including the hardware setup, basic experimental protocol, and data analysis. The main advantages of this tracking system are that it provides a high-resolution view of a single worm over time and that the subsequent analysis is automated and unbiased. Because the system is relatively inexpensive (~$4000 USD), we have been able to operate eight single-worm trackers in parallel to increase throughput.

David Biron and Gal Haspel (eds.), *C. elegans: Methods and Applications*, Methods in Molecular Biology, vol. 1327,
DOI 10.1007/978-1-4939-2842-2_13,

Automated analysis of experimental data often requires a compromise between the effort put into optimizing experimental conditions and the effort put into algorithm design: clean data can be difficult to collect but easy to analyze and vice versa. In the case of single-worm tracking, we have found that routine calibration and care during plate preparation is worth the small extra effort and makes the analysis relatively straightforward and robust. The most important factors for successful single-worm tracking are reproducible sample preparation, a thin lawn of bacterial food, and uniform lighting adjusted to give good contrast.

The expected outcome of following the method described in this chapter is a quantitative phenotype with both morphological and behavioral features that can be used to distinguish worm strains, even when the differences between them are too subtle to observe by eye.

2 Materials

The single-worm tracker used in this protocol is called Worm Tracker 2 (WT2). An assembled tracker is shown in Fig. 1. The hardware consists of a worm platform, USB microscope, motorized stage, and red-light illumination. Single worms are placed into

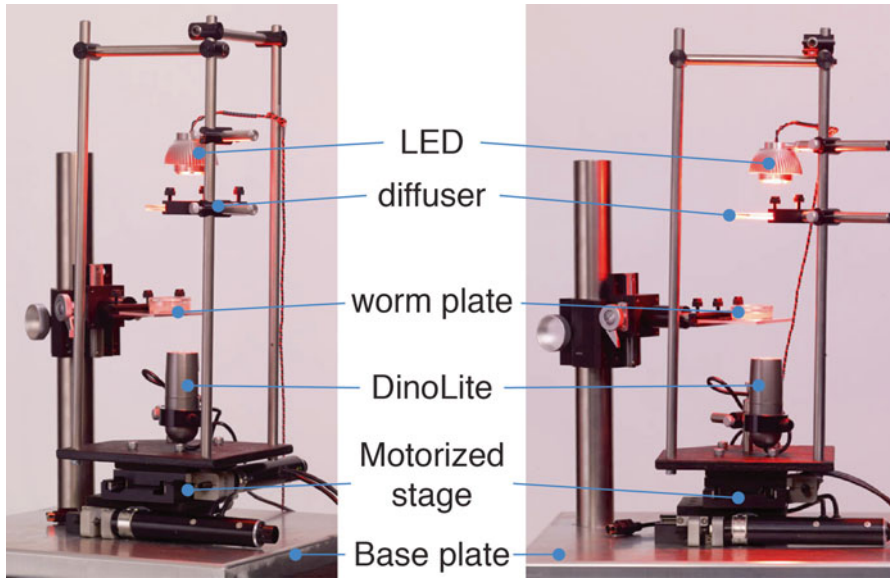

Fig. 1 WT2 tracking hardware from two angles. A worm on a plate is kept still on a platform attached to the base plate. The DinoLite USB microscope is mounted onto a motorized stage. A red LED is mounted above the plate for illumination and an opal diffuser diffuses the light from the LED to create uniform lighting within the camera's field of view. The microscope and lighting are all directly coupled to the stage and move independently of the worm on its platform, which is kept stationary with respect to the base plate

agar petri dishes. The dishes are placed on an immobile platform, shielding the worm from stage movements. The USB microscope is coupled to ~627 nm LED illumination so as to permit imaging without triggering worm avoidance behaviors (*C. elegans* sense and avoid short-wavelength light [3]). Both the camera and its illumination are mounted onto a motorized stage. A closed video loop permits the tracking software to guide the stage in pursuit of the worm while recording video of its behavior.

2.1 Worm Tracker Hardware

1. Camera: DinoLite AM413T USB microscope.
2. Motorized stage: Zaber TSB60-M translation stage plus two linear actuators (T-NA08A50 and KT-NA08A50, each with 50 mm travel, RS232 plus manual control).
3. Illumination: A red light-emitting diode (620–645 nm wavelength).
4. Optics: Fresnel lens and diffuser.
5. Computer: A computer to control the stage and camera.
6. Base and frame hardware: Mount the worm plate platform and motorized stage on a solid baseplate. Attach the microscope, LED, and diffuser on the motorized stage using standard metal posts and post holders available from multiple vendors.

2.2 Worm Tracker Software

Under the Windows operating system, the worm tracker uses the following software:

1. DinoCapture: included with the DinoLite USB microscope.
2. Java: Download version 6 or later from http://www.java.com.
3. Worm Tracker 2 and Worm Analysis Toolbox: Download the latest version from http://www.mrc-lmb.cam.ac.uk/wormtracker/.

2.3 Agar/Nematode Growth Medium Plates with Food

This subsection is adapted from WormBook.org [4].

1. Agar/Nematode Growth Medium plates: In a 2 l Erlenmeyer flask, add 3 g NaCl, 17 g agar, 2.5 g peptone, and 975 ml of distilled water. Autoclave for 50 min. Cool flask in a water bath at 55 °C for 15 min. Add 1 ml of 1 M $CaCl_2$, 1 ml of 5 mg/ml cholesterol in ethanol, 1 ml of 1 M $MgSO_4$, and 25 ml of 1 M phosphate buffer (108.3 g of KH_2PO_4, 35.6 g K_2HPO_4, made up to 1 l in distilled water). Swirl to mix. This is Nematode Growth Medium (NGM). Using sterile procedures, dispense 6 ml of NGM into 35 mm diameter petri plates using a peristaltic pump (*see* **Note 1**). Leave plates at room temperature for 2 days with the lids on to allow for detection of contaminants and to allow excess moisture to evaporate. Plates can then be stored in a sealed container at 4 °C. Note that a 4 °C plate can take ~30 min to reach 20 °C (a suitable temperature for recording worm behavior).

2. Bacterial food: Using sterile technique, streak OP50 on an LB agar plate. Pick a single colony of OP50 into 50 ml of LB in a 250 ml Erlenmeyer flask and shake overnight at 37 °C. Both streaked plates and liquid cultures should be stored at 4 °C.

3 Methods

3.1 Camera Setup

1. Run the DinoCapture software.
2. Set the camera to 640×480 resolution at 30 frames/s. Navigate to the real time image settings and set the camera to grayscale (black and white "B/W" mode). Turn off the camera's auxiliary white LEDs ("Aux LED Mode"). Save the DinoLite's configuration and quit the DinoCapture software.
3. Position the light source centered over the camera (Fig. 1).
4. Position the Fresnel lens and diffuser centered over the camera (Fig. 1).

3.2 Worm Tracker 2.0 Setup

1. Turn on the red light source and motorized stage.
2. Run the Worm Tracker 2.0 software (*see* **Note 2**).
3. On the main screen (Fig. 2c, f), set the software to record for 5 min. Make sure you are logging stage coordinates and ensure that the stage position is logged when recording video.

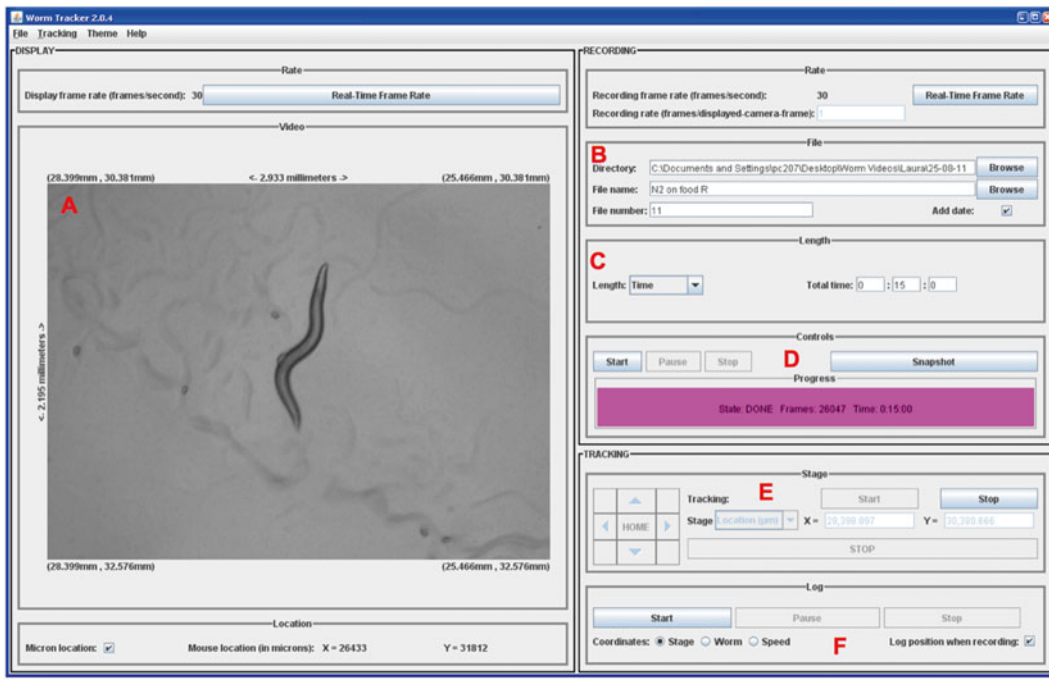

Fig. 2 WT2 main screen. (**a**) Incoming video is displayed alongside absolute coordinates and measurements. (**b**) Experiment filename information. (**c**) Recording length information. (**d**) Recording controls. (**e**) Motorized stage and tracking controls. (**f**) Stage movement logging controls

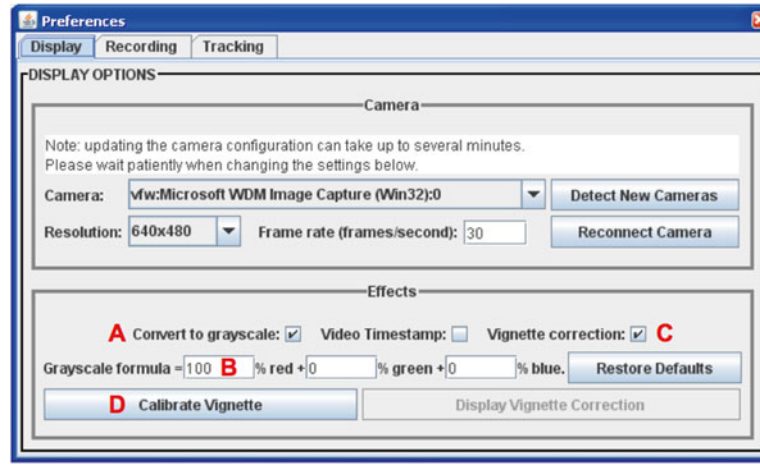

Fig. 3 WT2 display preferences. (**a**) Convert the video to grayscale. (**b**) The grayscale formula for converting the *red, green*, and *blue* channel in a color video to a single grayscale image. (**c**) Correct camera vignetting and/or dirt on the lens. (**d**) Calibrate the vignette correction using the current video image

4. Navigate to the display preferences (Fig. 3a, b). Turn on grayscale conversion and set the grayscale formula to use 100 % of the red channel and 0 % of the green and blue channels.
5. Navigate to the recording preferences (Fig. 4a). Restore the default file name date format, for example "_yyyy_MM_dd__HH_mm_ss."
6. Navigate to the tracking preferences (Fig. 5a, c–f). Set the tracking rate to 1 frame, the delay to 330 ms, and the stage type to Zaber (assuming this is the model of motorized stage you have purchased). Set the communication port correctly so that the stage responds to software commands. Set the software to move the stage using absolute coordinates. Disable the software so it does NOT check stage responses (uncheck the box). Set the software unit conversion to 20.997 steps/μm in both axes (this value is specific to the Zaber T-NA08A50; please adjust accordingly for other stage models). Set the stage speed and acceleration to the highest values that do not cause stalling or vibration; alternatively, you may try setting the speed to 6000 (Zaber uses an arbitrary unit of measurement, roughly 0.45 μm/s) and the acceleration to 100 (Zaber uses an arbitrary unit of measurement, roughly 536 $\mu m/s^2$) to test whether these values work. Set the stage's home location to its center at 25,000 μm in both axes (this value is specific to the Zaber

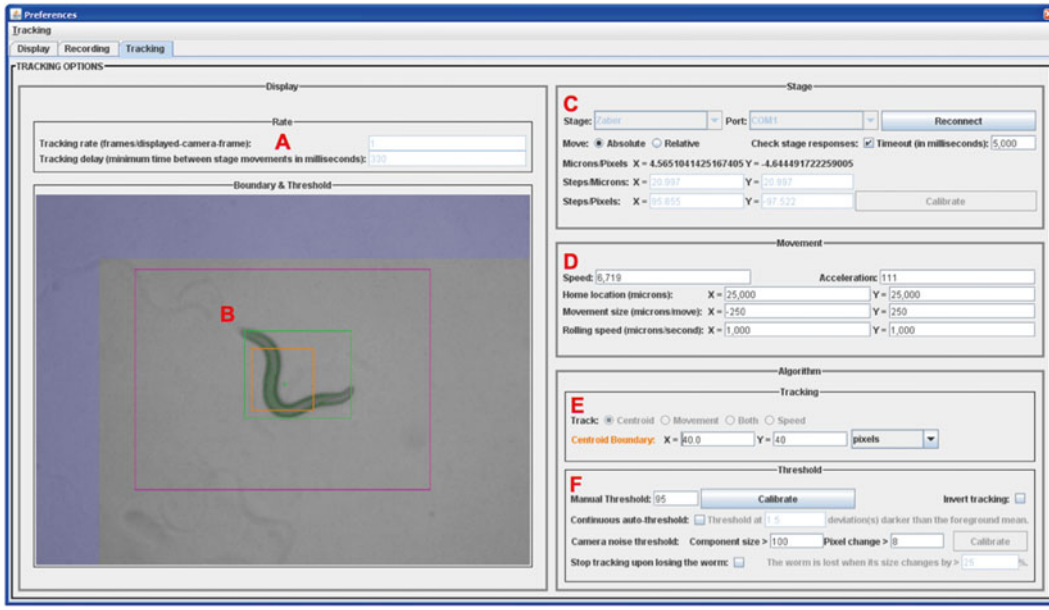

Fig. 4 WT2 tracking preferences. (**a**) The rate and delay for executing tracking stage movements. (**b**) The tracked worm, centroid, and MER (painted *green*). The centroid (painted *orange*) and movement (painted *magenta*) boundaries. Newly tracked in areas (painted *lavender*). (**c**) Motorized stage information. (**d**) Stage movement settings. (**e**) Tracking type (centroid and/or motion) information. (**f**) Tracking threshold settings

T-NA08A50; please adjust accordingly for other stage models). Set the manual stage movement size to 500 μm in both axes. Set the stage's rolling speed to 1000 μm/s in both axes. Set the software to track by centroid. Use a centroid tracking boundary of 200 μm in both axes. Set the manual threshold to 95 (unsigned 8-bit pixel intensity). Make sure the continuous auto threshold is turned off. Make sure tracking is not inverted.

7. On the main screen, save the software configuration as your default.

3.3 Camera Magnification Calibration

Ideally, the tracker should be calibrated every day before experiments are run. Alternatively, a weekly schedule of calibration can be observed with the caveat that miscalibration can lead to the loss of experimental data. Calibration should take no longer than 5–10 min.

1. Adjust the height of the Fresnel lens and opal diffuser so that the surface of the Fresnel lens is ~9 cm from the camera lens (Fig. 1).
2. Adjust the height of the light source so that the surface of the LED lens is 14 mm from the camera lens (Fig. 1).
3. Follow the worm and plate preparation procedures to prepare several *C. elegans* young adults on one tracking plate.

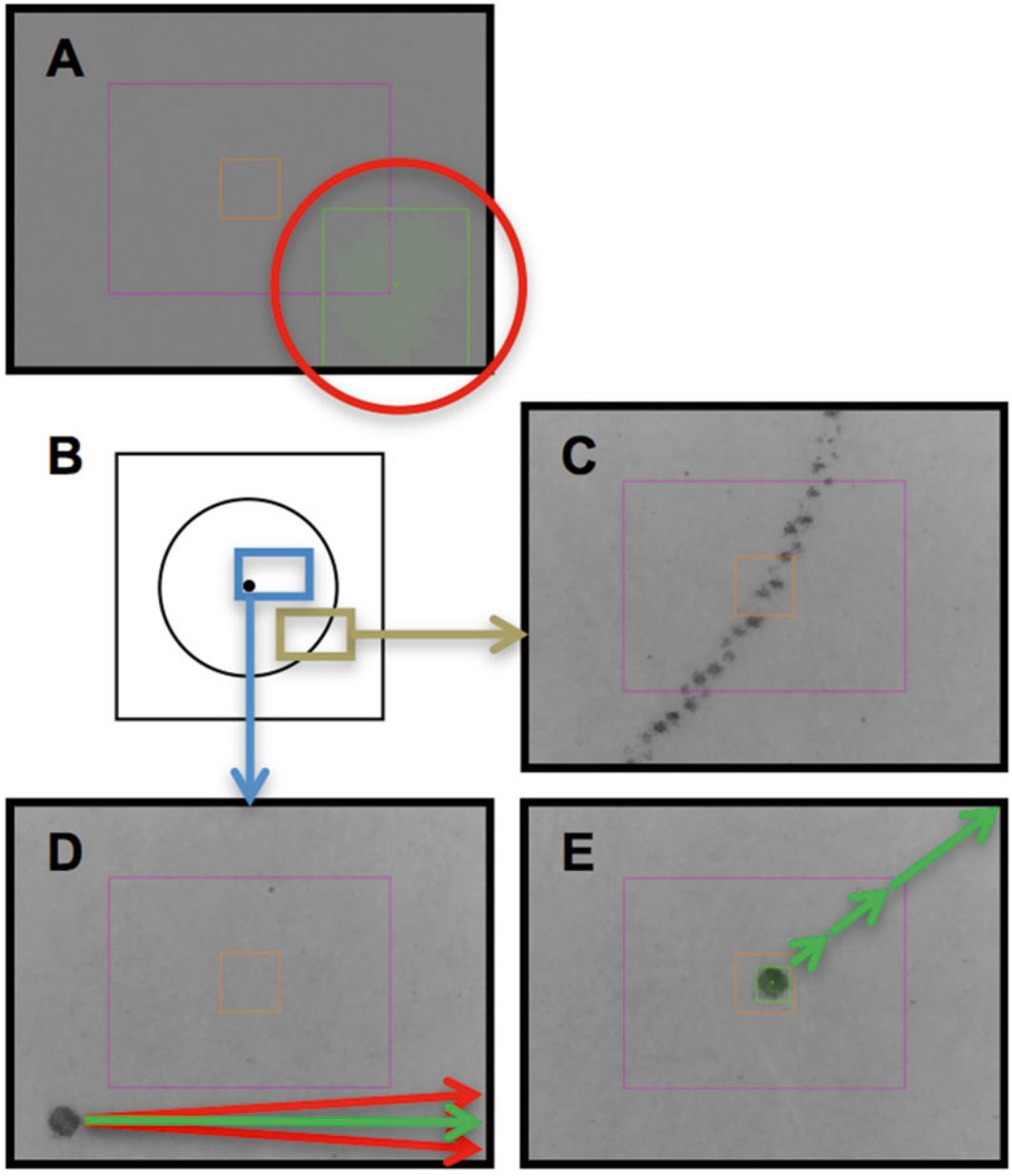

Fig. 5 WT2 calibration screenshots (on the tracking preferences screen). (**a**) The illumination, thresholded in *green*, must be centered. (**b**) WT2 comes with a PDF of squares, containing circles, which contain dots. A printout of the PDF is used for fine-scale calibration. (**c**) The circle's edge, in the printout, serves as a guide to locate the small, central dot. (**d**) The camera and stage must be aligned axially. *X*-axis stage movements must result in precise onscreen, axial dot movements (an example of axial dot movement is labeled *green*; the *red* vectors are not confined to a single axis and, therefore, indicate miscalibration). (**e**) WT2 autocalibrates the scale using the known stage step size

4. Place the plate face down such that the camera images the worm directly through a transparent lid. Filming through agar contributes to poor contrast and blurring.
5. Turn on the LED and stage.
6. Run the Worm Tracker 2.0 software.
7. Adjust the height of the platform (Fig. 1) to place the plate's agar surface in focus then navigate to locate a worm (*see* **Notes 3** and **4**).
8. Adjust the camera magnification so that the worm's length is approximately 3/4 the video image height (Fig. 2a). The actual scale of the image in microns/pixel is calibrated using the motorized stage in Subheading 3.5.
9. Focus the worm by adjusting the worm platform height (*see* **Note 5**).
10. Adjust the height of the Fresnel lens and opal diffuser to achieve good contrast (*see* **Note 6**): the worm's contour should be dark enough to be distinguished from the plate background and food lawn (especially any worm tracks). If the contrast is too light, the worm's contour will appear to be disjoint; the contour should form a continuous black line just encasing the worm. If the contrast is too dark, the worm's contour will appear to extend well beyond its body as a surrounding shadow; furthermore, tracks in the food lawn will appear as dark as the worm's contour. Contrast is dependent on larval stage and you will need to adjust the illumination should you change the life stage of recorded worms.

3.4 Camera-Illumination Calibration

1. Turn on the LED and stage.
2. Swivel the Fresnel lens and opal diffuser out of the way of the light source so that the light shines directly into the camera lens. Make sure there is nothing on the worm platform.
3. Run the Worm Tracker 2.0 software.
4. Navigate to the tracking preferences.
5. Make sure automatic thresholding is turned off. Adjust the manual threshold until the camera's vignette is painted green whereas the light source remains grayscale (Fig. 5a).
6. Center the light source in the image. The vignette should be approximately equal at all four image edges. You may need to adjust the manual threshold to see the vignette throughout this procedure. Make sure the camera lens and light source are level and parallel to each other.
7. Swivel the Fresnel lens and opal diffuser back underneath the light source. Make sure the Fresnel and opal diffuser are level and parallel to the camera lens and light source.

8. Make sure you have maintained the distances between the light source, lens, and camera.
9. Make sure the camera is not focused on anything. In the Worm Tracker 2.0 display preferences, turn on the vignette correction and calibrate the vignette.
10. Save the software configuration as your default.

3.5 Camera-Stage Calibration

1. Print the file "dots.pdf," located in your "Program Files\Worm Tracker\Documents" directory.
2. Cut out a square (Fig. 5b) from the printout.
3. Place the square face down onto an empty Petri plate. Then place this plate onto the worm platform. You can save this plate for future calibration.
4. Turn on the LED and stage.
5. Run the Worm Tracker 2.0 software.
6. On the main screen, locate and focus on an edge on the outer circle of your printout (Fig. 5c). If there is insufficient illumination, you may swivel the Fresnel lens and diffuser out of the way of the light source and/or turn on the camera's auxiliary white LEDs. Be sure to revert these changes when done.
7. Use the circle's outer edge to locate the central dot.
8. Use the software to move the dot. Twist the camera, in its holder, till the onscreen *x*- and *y*-axes match the software's manual, stage movement commands.
9. Use the software to position the dot at one of the four onscreen corners.
10. Use the software to move the dot, solely along the *x*-axis, to the opposite corner. If the dot changes its position in *y*-axis, gently twist the camera, in its holder, to precisely align the camera and stage axes. Repeat this step until the software's manual, *x*-axis, stage movement commands move the dot solely within the *x*-axis (Fig. 5d, green arrow).
11. Navigate to the tracking preferences.
12. Adjust the manual tracking threshold until the entire dot, and only the dot, is painted in green. Fine-tune the manual threshold so that the dot's centroid position, indicated as a green "+," remains as stable as possible with minimal positional jitter.
13. Use the software to position the dot in the center of the video image (Fig. 5e).
14. Press the button to calibrate the steps/pixels and wait for the calibration to complete.

15. If the difference between the steps/pixels in both axes is more than 1, repeat **steps 9**, **10**.
16. Repeat **step 14** until the steps/pixels are stable (i.e., they do not change by more than 1 from their previously calibrated values).
17. Save the software configuration as your default.
18. Navigate to the center of the motorized stages and ensure the worm platform is centered directly above the camera lens. This step ensures maximal stage coverage for the tracking plate. In other words, centering the worm platform above the camera permits the hardware to follow a worm to the edge of the plate without reaching the end of the stage's linear actuators. This can be achieved by simply navigating to the home position by pressing the "Home" button on the main screen (Fig. 2e) or using the keyboard shortcut Alt-H.

3.6 Worm Tracking Calibration

1. Follow the worm and plate preparation procedure to prepare several *C. elegans* young adults on individual low-peptone NGM plates.
2. Place a plate onto the worm platform.
3. Turn on the LED and stage.
4. Run the Worm Tracker 2.0 software.
5. Locate a worm on camera by adjusting the location of the worm plate and the height of the worm platform.
6. Focus the worm by adjusting the worm platform height.
7. Navigate to the Tracking Preferences. Adjust the manual tracking threshold until the worm, and only the worm, is painted in green (Fig. 4b). Fine-tune the threshold to paint as much of the worm as possible, without bleeding into the surrounding background of worm tracks, food, and agar.
8. You may attempt to lower the tracking delay from 330 ms to achieve faster tracking. But, when tracking, if you experience chaotic stage movements during which the stage continuously fails to re-center the worm, you will need to raise the delay value.
9. Save the software configuration as your default.

3.7 Tracking Protocol

The tracking protocol is highly dependent upon the data being analyzed. For example, while 5-min recordings may be appropriate to measure postural properties, infrequent events such as omega turns may require much longer recording to achieve sufficient sampling. It is important to achieve good image quality for the videos. Taking effort at this stage to record high quality data will ensure

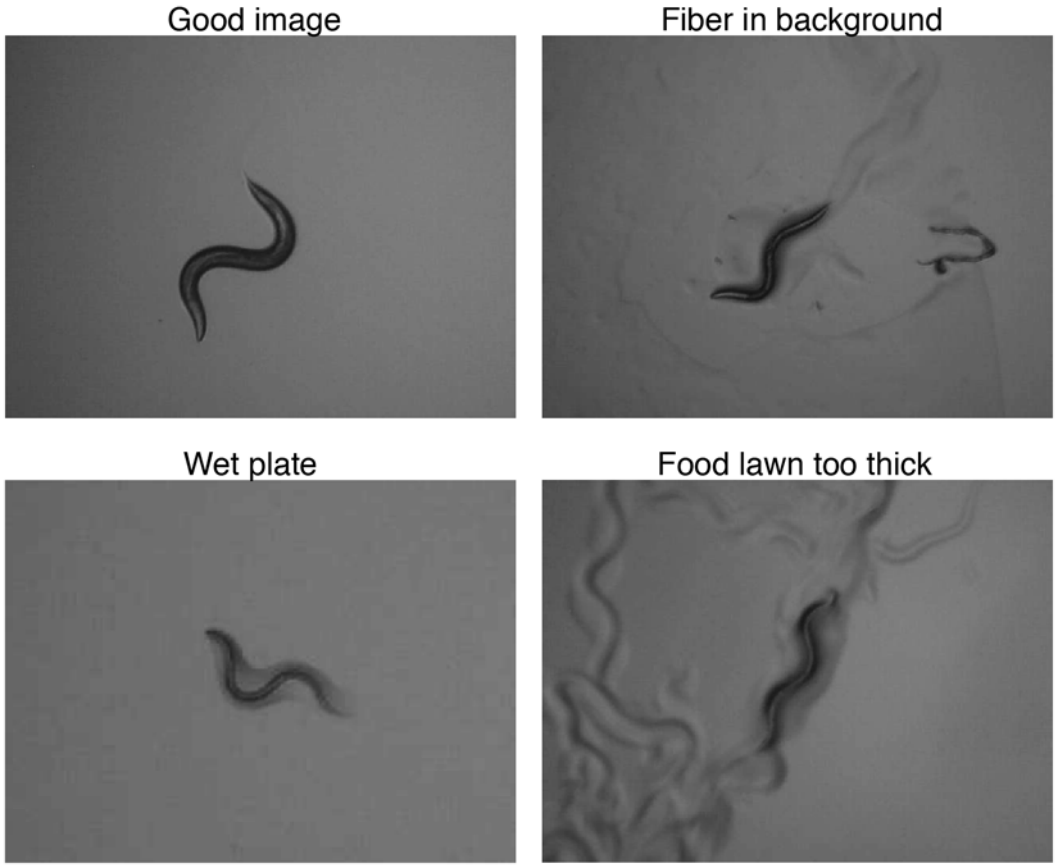

Fig. 6 Sample frames taken from a video with good contrast and magnification (*top left*) as well as videos taken from a plate with debris (*top right*), a plate that did not dry completely (*bottom left*), and a plate with a food lawn that is too thick (*bottom right*)

that the majority of videos can be analyzed and that their extracted features are accurate. *See* Fig. 6 for an example of a good image contrasted with those displaying common problems.

1. Obtain worms from the incubator. Place tracking plates and OP50 at room temperature. Discard any contaminated plates or those with imperfections such as crystals, scratches, or bubbles.
2. Resuspend the OP50 by shaking.
3. Transfer sufficient OP50 for tracking experiments to an Eppendorf. To improve imaging conditions, the OP50 can be diluted to 50 % for L4s to adults, 25 % for L2-L3s, and 10 % for L1s. Seed 20 μl onto the center of each plate. Angle the pipette when seeding plates to avoid accidentally piercing the agar. Discard any plates with imperfections in seeded bacteria.

4. Ensure that the seeded lawns on the tracking plates have dried completely, with no wet spots. At 20 °C, the OP50 lawn should take ~30 min to dry; during this time, a 4 °C plate should also reach room temperature.
5. In the worm tracking software, set the recording time.
6. Choose a tracking plate with a dry food lawn, wipe any condensation from the lid, and pick a single worm to the center of the plate taking care not to disturb the food lawn (*see* **Note 7**). Note the worm's ventral side.
7. Choose a file name and a folder to save experiments in. The following naming scheme is recommended, "<strain or worm annotation>_<room temperature>_<worm number>_<ventral side>." For example, "N2_20C_3_AC" where "AC" indicates the ventral side is anticlockwise from the worm's head.
8. Move the plate, agar/worm side down (facing the camera) onto the tracker and center it on the transparent imaging platform. If the plate is not centered, the stage may reach its travel limit during tracking and the worm could be lost.
9. Using the stage movement buttons (Fig. 2e) or their Alt-<arrow>keyboard shortcuts, find the worm.
10. Begin tracking by pressing the "Start" tracking button (*see* **Note 8**) or using the Alt-B keyboard shortcut and adjust the focus. Start recording (*see* **Note 9**).
11. When recording is finished, the recording "Progress" will change from yellow and pink to magenta. Each recording produces 4 associated files. These files share the same name, of the format "<user label>_<timestamp>." The 4 file suffixes are ".avi" (the video itself), ".log.csv" (a log of stage movements), ".info.xml" (XML formatted information regarding the experiment), and "vignette.dat" (a vignette correction for the video images). *See* **Note 10**.
12. When done tracking, the red LED illumination and motorized stage should be turned off and the camera lens covered for protection. Assuming, no more tracking will take place that day, the analysis should be run overnight for the worms tracked.

3.8 Extracting Features from Videos

1. Open Worm Analysis Toolbox.
2. Locate the "Analysis" panel and press the "Start" button.
3. Locate the "Load directory" panel and press the "Start" button.
4. Choose the directory where the worm movies are saved.
5. If you have annotated the ventral side in the filename, please check the appropriate boxes so as to inform the software.
6. Press the "Save" button to begin the analysis.

7. The analysis will run until completion and prepare feature files for each video. The feature files are stored in a "results" directory. The filename is preserved with the extension ".mat" indicating a MATLAB HDF5 formatted data file. These files can be read using an HDF5 reader without a MATLAB license. The experiment files are stored in the hidden directory ".data" (*see* **Note 11**).
8. Quit the Worm Analysis Toolbox.

3.9 Converting Features to Summary Statistics

1. Install Worm Features to Figures, available at http://csc.mrc.ac.uk/dfeatures2figures-zip/.
2. Aggregate the feature files (from the "results" directory) for your control and each comparable experiment into separate folders.
3. Label the control folder "Control-<control identifier>." The control identifier is simply a string that will be used to identify it in the output.
4. Similarly, label each experiment folder "Experiment-<experiment identifier>." The program works with 1 or more experiments. Each one is compared to the same control. For multiple experiments, statistical corrections for multiple testing extend across the entire data set.
5. Run the wormFeatures2FiguresGUI program. Please be patient, due to the MATLAB compiler runtime, the program can take a long time to start up. Note that MATLAB itself is not required to run wormFeatures2FiguresGUI.
6. Choose the directory containing the control and experiment folders by pressing the appropriately labeled button beginning with "A."
7. Convert the feature files to figures by pressing the appropriately labeled button beginning with "B."
8. Wait for the program to complete (the window will show the text "***All done!" and a message will pop up). Depending on how many files you have, this can take several hours.
9. If the program gets interrupted, relaunch to start it from where it left off.
10. The "Start/End Time for Videos (in seconds)" fields allow one to run the analysis for a subset of the recorded time.
11. The program output is stored in a "TIFs" folder, a "figures" folder, and a "statistics" folder. For an explanation of the tifs (Fig. 7), *see* [2]. The figures folder contains EPS plots with comparisons between the control and each experimental strain. In each figure, the control is darker than the experiment(s). The means are labeled as a red line. The control SEMs are the blue interval around the mean; the experiment SEMs are in pink. The standard deviations are the purple interval around the SEMs.

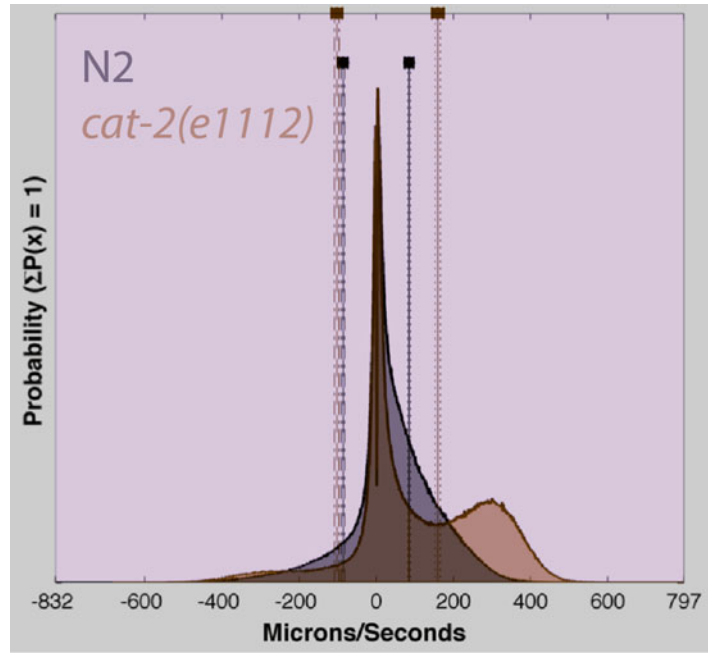

Fig. 7 Sample feature distribution produced in analysis. In this example, the mid-body speed distribution for a mutant, *cat-2(e1112)*, is compared to the laboratory reference strain N2. The *lavender* background indicates a significant difference and is used to quickly visually identify distributions of interest. The full file contains hundreds of distributions (one for each extracted feature) making this color code useful for scanning over several pages of plots

The "statistics.csv" files in the statistics folder are in comma separated value format and can be opened with many programs (e.g., Excel, Numbers, R, MATLAB). Each of the 702 features is listed in rows with a corresponding number and name. After these initial columns, the control details are listed, followed by each one of the experiments. For each of these groups, summary statistics and the results of statistical tests are included. The Shapiro-Wilk test is for normality. p-values and their q-value equivalents are shown. *See* [2] for details of the included tests and the correction for multiple comparisons (*see* **Note 12**). Additional figures and statistics files are provided within the control and experiment directories; these are described in the software's accompanying README.

4 Notes

1. Using a pump to pour a consistent volume makes focusing faster when switching plates.
2. If the camera video is not displayed the problem may lie with the DinoCapture software; in this case the software should

be reinstalled. Alternatively, if Java has been updated, locate "Program Files\Worm Tracker\Prerequisites\JMF\jmf-2_1_1e-windows-i586.exe." Run it to uninstall then reinstall the Java Media Framework (JMF).

3. If the stage does not respond to software commands, check that the stage is connected to the correct computer port and that this port is selected in the WormTracker 2.0 tracking preferences. It is also possible that the stage manual control knob is not in the neutral position. In this case, center the stage's actuator knobs in the neutral position (the LED on the knob will turn green). Then, reconnect the stage in the Worm Tracker 2.0 tracking preferences.
4. If the worm cannot be found, check that the agar surface is in focus. If there is insufficient range to focus on the surface, turning the plate over may help bring the surface within range. Alternatively, the worm may simply be too far from the camera's field of view. In this case, find a worm track on screen and use the stage to follow the track in order to locate the worm. Another option is to take the plate to a stereomicroscope, locate the worm noting its approximate location, then place the plate back onto the platform with the worm near the center of the camera to aid in locating it. If the worm has crawled off the agar to the plate edge, consider using undiluted OP50 for tracking.
5. If the image is still blurry after focusing, check that the camera lens is clean, that the platform is clean, and that there are no scratches anywhere occluding a clean focus. If necessary, clean the camera lens and platform or simply replace the platform if it is scratched. Check the lid for condensation and wipe clean when present.
6. Poor contrast can result from several problems. The food may be too thick. In that case, consider using undiluted OP50. If the DinoLite's auxiliary white LEDs are on, use the Dino Capture software to turn them off then save the configuration. The illumination may be off or too weak; make sure that it is on and being driven at its maximum power.
7. To ensure similar environmental conditions for controls and experiments, interleave strains (e.g., track one control worm, then one experimental worm, then repeat).
8. If the tracker fails to follow the worm, the tracking delay may be too long. It can be shortened in the preferences. The manual threshold may also be set incorrectly. In this case, repeat the calibration in Subheading 3.6. If the stage moves chaotically, try lengthening the tracking delay within the tracking preferences and/or recalibrating the vignette.

9. In the event that the tracker loses the worm (e.g., due to the worm reaching the edge of the plate), recording can be stopped early by pressing the "Stop" recording button. Thereafter, the associated experiment files should be discarded.
10. If recorded videos suffer dropped video frames and/or a frame rate less than 30 fps, ensure other processes are not limiting the video capture rate by quitting all applications except WT2. Additionally, ensure that the DinoLite is not using a fixed exposure. This can be checked and fixed in the DinoCapture software settings. Lastly, the grayscale conversion in WormTracker 2.0 can be processor intensive and can be disabled in display preferences.
11. Errors should be ignored until the analysis finishes. Failed videos are skipped and the analysis continues to process the next video in the queue. The most common analysis complication is the "stage_movement_detection" error. This error indicates that a problem occurred matching stage movements in video to those in the log file. Unfortunately, these videos are unsalvageable and should be replaced with more experiments. Other, less frequent errors may indicate that a critical piece of software has yet to be installed (if so, reinstall the software) or that the filenames and/or paths are too long (if so, shorten the filenames and/or the directories within which they are nested).
12. If you have an interesting, uncommon result that relates to the location of the head/tail and/or dorsal/ventral side, double-check that the head/tail and dorsal/ventral side were annotated correctly. Please check the Worm Analysis Toolbox video output. Each analyzed video should be accompanied by an annotated video with the same name and an additional suffix "_seg.avi." In these videos, the head is labeled with a green dot and the ventral side is annotated by a red dot. Please skim the video and ensure that these dots correctly label the worm. Note that if the head and tail are incorrectly labeled, the dorsal/ventral side will also end up incorrect. An easy way to determine if the head and tail are correct, as long as there are less than 25 worms, is to go to the TIF file and look at the individual path traces for the worms' "Midbody Speed." Forward movement is labeled in red and reversals are labeled in blue. Most worms rarely reverse and, when they do, the reversal is rather short. As a result, path traces should be mostly in the red tones, punctuated by a few short, blue-toned reversals. It there are significant errors, discard the offending analysis files or, retrain the head/tail classifier in the Worm Analysis Toolbox and rerun it over the videos to generate correct feature files.

Acknowledgements

This work was supported by the Medical Research Council through grant MC-A658-5TY30 to AEXB. EIY is supported by the NIH through grant T32 MH015174-37.

References

1. Husson SJ, Costa WS, Schmitt C, Gottschalk A (2012) Keeping track of worm trackers. In: The *C. elegans* Research Community (ed) WormBook. doi: 10.1895/wormbook.1.156.1, http://www.wormbook.org/
2. Yemini E, Jucikas T, Grundy LJ, Brown AEX, Schafer WR (2013) A database of Caenorhabditis elegans behavioral phenotypes. Nat Methods 10:877–879
3. Edwards SL, Charlie NK, Milfort MC, Brown BS, Gravlin CN, Knecht JE, Miller KG (2008) A novel molecular solution for ultraviolet light detection in Caenorhabditis elegans. PLoS Biol 6, e198
4. Stiernagle T (2006) Maintenance of C. elegans. In: The *C. elegans* Research Community (ed) WormBook. doi: 10.1895/wormbook.1.101.1, http://www.wormbook.org/

Chapter 14

An Imaging System for *C. elegans* Behavior

Matthew A. Churgin and Christopher Fang-Yen

Abstract

Many experiments in *C. elegans* neurobiology and development benefit from automated imaging of worm behavior. Here we describe procedures for building a flexible and inexpensive imaging system using standard optical and mechanical components.

Key words *C. elegans*, Imaging, Behavior

1 Introduction

The nematode *C. elegans* is a powerful model for investigating the neural and genetic bases of behavior, owing to its easily manipulable genome and well-mapped nervous system [1]. Much of our understanding of *C. elegans* neurobiology including synaptic function [2], sensory systems [3, 4], motor systems [5], and feeding [6] have hinged on well-designed measurements of behavior.

Many behavioral assays can be conducted by visual observation [7]. Others, such as those requiring observations over long time scales (hours to weeks), or those involving subtle details of behavior are only practical with tools for automated imaging [8].

The simplest method for digital imaging is to add a digital camera to the trinocular port on an existing stereo microscope. However, this approach may not be desirable when long-term imaging and/or simultaneous imaging on multiple setups are required. In the course of our experiments to monitor behavior during development [9] and aging [10], we have developed a table-top imaging system using commercially available cameras, optics, light sources, and mechanical components. Since the system is relatively modest in cost ($500–800 not including the computer) we have been able to construct several of these systems for various uses in our laboratory.

David Biron and Gal Haspel (eds.), *C. elegans: Methods and Applications*, Methods in Molecular Biology, vol. 1327,
DOI 10.1007/978-1-4939-2842-2_14,

2 Materials

1. Aluminum bottom plate 12″ × 12″ × ½″ (e.g., McMaster-Carr 8975K135).
2. Acrylic top plate 12″ × 12″ × ¼″ (e.g., McMaster-Carr 8505K91).
3. 1.5″ Post clamp (Thorlabs C1501), qty. 2.
4. 1.5″ Diameter stainless steel mounting post, 14″ long (Thorlabs P14).
5. 1.5″ Diameter stainless steel mounting post, 6″ long (Thorlabs P6).
6. 0.5″ diameter stainless steel post (Thorlabs TR2).
7. Post holder (Thorlabs PH2).
8. Post holder base (Thorlabs BA1 or BA2).
9. Flexible red LED strip, 4.7″ long, qty. 4 (Oznium Inc.).
10. 3–12 V power supply (e.g., Marlin P. Jones and Associates 9902PS).
11. CMOS or CCD camera (e.g., Imaging Source DMK23GP031, 2592 × 1944 pixel sensor, up to 15 images/s).
12. Power supply for camera, if needed (e.g., Imaging Source GigE23/PWR/Trig 1).
13. Data cable for camera.
14. Imaging software (e.g., Imaging Source Image Capture 2.1).
15. C-mount camera lens (e.g., Fujinon HF12.5SA-1 2/3″, 12.5 mm focal length, f/1.4).
16. C-mount extension rings (Imaging Source LAex5, LAex1).
17. Borosilicate glass sheet 8″ × 8″ × ¼″ (McMaster-Carr 8476K18).
18. Aluminum 2-hole inside corner bracket (80/20 part #4302).
19. 5-min epoxy adhesive (Devcon).
20. ¼″-20 Stainless steel cap head screws (qty 5), set screw (qty 1), and 1/4″ washer (qty 4) (e.g., Thorlabs HW-KIT1).
21. Black gaffer's tape, 1″ wide (McMaster-Carr 7612A82).
22. Binder clips (Office Depot, 5/8″ capacity).
23. Blackout fabric (Thorlabs BK5).
24. Self-adhesive bumpers (McMaster-Carr 95495K62, Polyurethane, 7/8″ Wide, 13/32″ high), qty. 4.
25. 3/16″ Hex screwdriver (e.g., Thorlabs BD-3/16).
26. *Tools required if machining top and bottom plates yourself:*
    (a) Drill press or handheld electric drill.
    (b) 1/8″ diameter drill bit.
    (c) 5/16″ diameter drill bit.

3 Methods

3.1 Designing the Imaging System

1. Decide what field of view (FOV) and resolution are needed for your experiment. The field of view FOV is related to the sensor size SS, working distance WD (distance between the lens and object being imaged), and lens focal length f by the formula $\mathrm{FOV} = \mathrm{SS} \times \mathrm{WD} / f$ (*see* **Notes 1** and **2**).

   The field of view can be adjusted by moving the camera up or down. The setup detailed in Materials will accommodate a field of view ranging from approximately 2.7 cm × 2.0 cm to 11.1 cm × 8.3 cm.
2. Select the lens. Considerations include the focal length, aperture size, and compatibility with the camera sensor size. A zoom or varifocal lens provides adjustable focal length, but may be slightly less sharp and provide slightly lower contrast than a fixed focal length lens.
3. Select the camera. Considerations include the desired pixel resolution, sensor size, and maximum frame rate. In our experience, data transfer from Gigabit Ethernet cameras is more reliable over the long term than using USB cameras.

3.2 Constructing the Mechanical Components

1. Drill 5/16″ diameter holes at the points indicated on the top (acrylic) and bottom (aluminum) plates as indicated in Fig. 1. A tolerance of ±1/8″ is acceptable. *See* **Notes 3** and **4**.
2. Wrap a 14″ × 14″ piece of blackout fabric tightly around base plate and tape to bottom of plate using gaffer's tape (Fig. 2).
3. Feel for the hole on the top of the plate previously made in the base plate. Using a razor blade, cut the blackout fabric at an approximately 1″ square around this hole and tape the fabric to the plate, leaving the hole clear (Fig. 2).

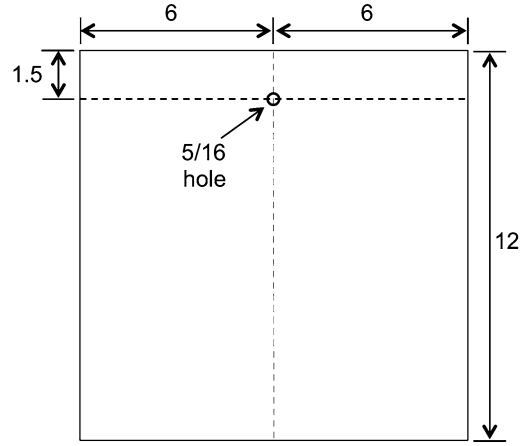

Fig. 1 Location of holes in top and bottom plates for mounting to support rod

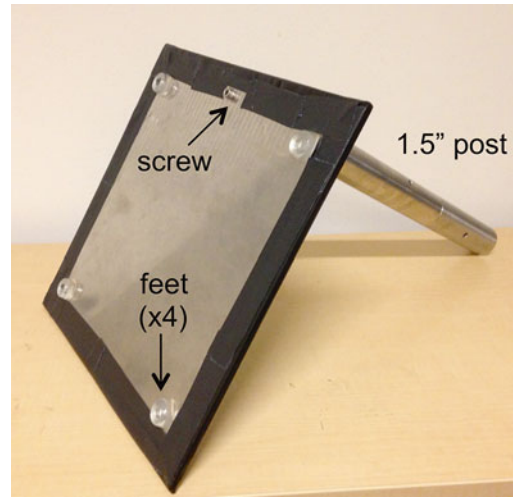

Fig. 2 Bottom view of bottom plate with blackout fabric, mounted 1.5″ diameter support rod, and feet

4. Attach 4 self-adhesive rubber feet to the bottom of the aluminum plate near the corners (Fig. 2).
5. Use a ¼″-20 hex head cap screw and 3/16″ hex screwdriver to attach the 1.5″ diameter × 14″ long stainless steel rod to the base plate (Fig. 2).
6. Using a ¼″-20 set screw, connect the two 1.5″ diameter stainless steel rods.
7. Place the first and second mounting carriers on the 1.5″ diameter rod such that the side with the tapped holes faces the front of the apparatus. To set the height, tighten the clamp using a 3/16″ hex screwdriver. When loosening either 1.5″ post carrier clamp, support the carrier with your other hand, otherwise the carrier may fall and cause damage.
8. Attach the L-bracket to the edge of the glass plate using epoxy adhesive (Fig. 3). The adhesive will harden within minutes. Allow to cure overnight for full strength.
9. Mount the glass stage onto the lower post carrier using a ¼″-20 screw with washer. Adjust so that the plate is level (Fig. 3).
10. Attach the top plate (black acrylic) to the top of the 1.5″ diameter post using a ¼″-20 screw and washer. Rotate the plate so that it is positioned directly above the base plate, then tighten the screw using the 3/16″ hex screwdriver.
11. To minimize stray light from outside the imaging system, cut a piece of blackout cloth to cover the left, right, and back sides of the imaging system, and tape to the top plate. Add another piece to cover the front of the system.

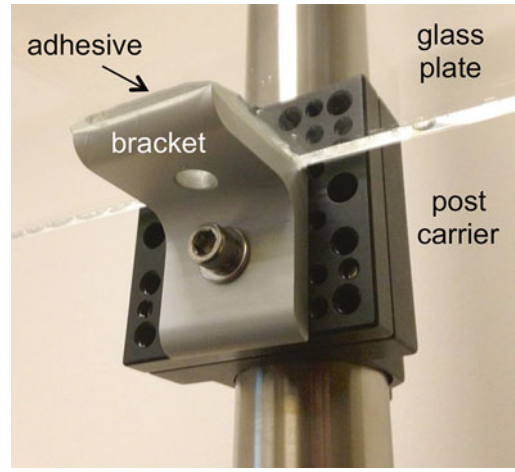

Fig. 3 View from below of post carrier mounted on 1.5″ post, 2-hole bracket, and glass platform

3.3 Assembling the Camera, Lens, and Light Source

1. Screw the lens onto the camera, separated by 5 and 1 mm extension rings. These rings allow the imaging system to focus on objects located closer than the normal minimum distance. Depending on your application, the extension distance may need to be increased or decreased. *See* **Note 5**.
2. Mount a base plate to a post holder using a 1/4″-20 socket head cap screw. Attach a 1/2″ diameter post (Thorlabs TR2) to the camera tripod mount using a 1/4″-20 set screw. Mount the post to the post holder by loosening the adjustment knob (Fig. 4).
3. Mount the camera with post and base onto the 1.5″ post carrier using at least two 1/4-20 cap screws (Fig. 4).
4. Attach the power supply and Ethernet cable to the camera. Install the camera software according to the manufacturer's directions.
5. Use a wire cutter to strip 1/2″ of the insulation off the LED wires, if needed. Connect the bare leads of the LED to the positive and negative terminals of the power supply by loosening the terminal screws, placing the bare wire behind the terminals, and retightening the terminals.
6. Place the LED strip in a ring on the base plate. Alternatively, place four shorter LED strips in a square configuration with LEDs facing inward (Fig. 5). The LEDs should be wired in parallel (each pair of leads connected to the terminals of the power supply), not in series. *See* **Notes 6** and **7**.
7. Test the LEDs by turning on the power supply. The brightness can be adjusted by varying the voltage. *See* **Note 8**.

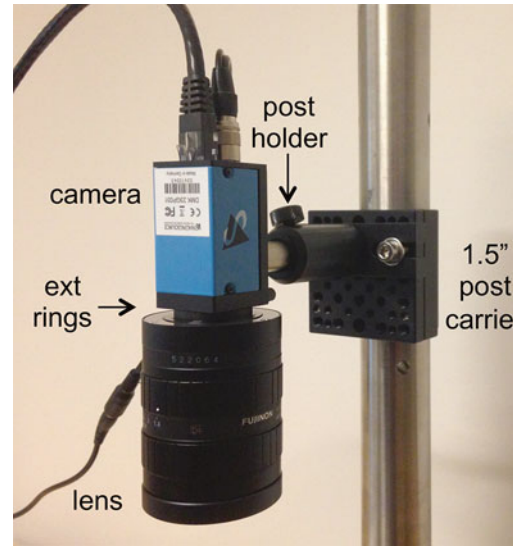

Fig. 4 Camera assembly containing camera, lens, cables, ½″ post, post holder, base, 1.5″ post carrier, and 1.5″ post

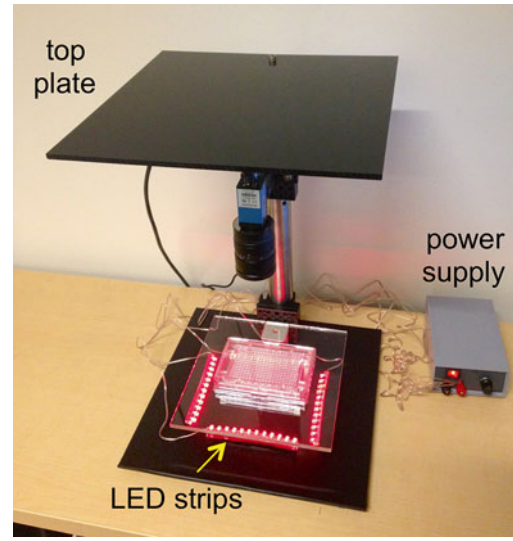

Fig. 5 Completed imaging system including LED strips, power supply, and sample to be imaged. During data acquisition, system should be completely covered by blackout curtains (not shown)

3.4 Alignment and Optimization

1. The lens has rings for adjustment of focus and aperture size. Set the lens focus near the middle of its range. Set the aperture near the middle of its range.
2. Turn on the power supply for the LEDs. Open the camera software, select the camera, and set to preview mode.

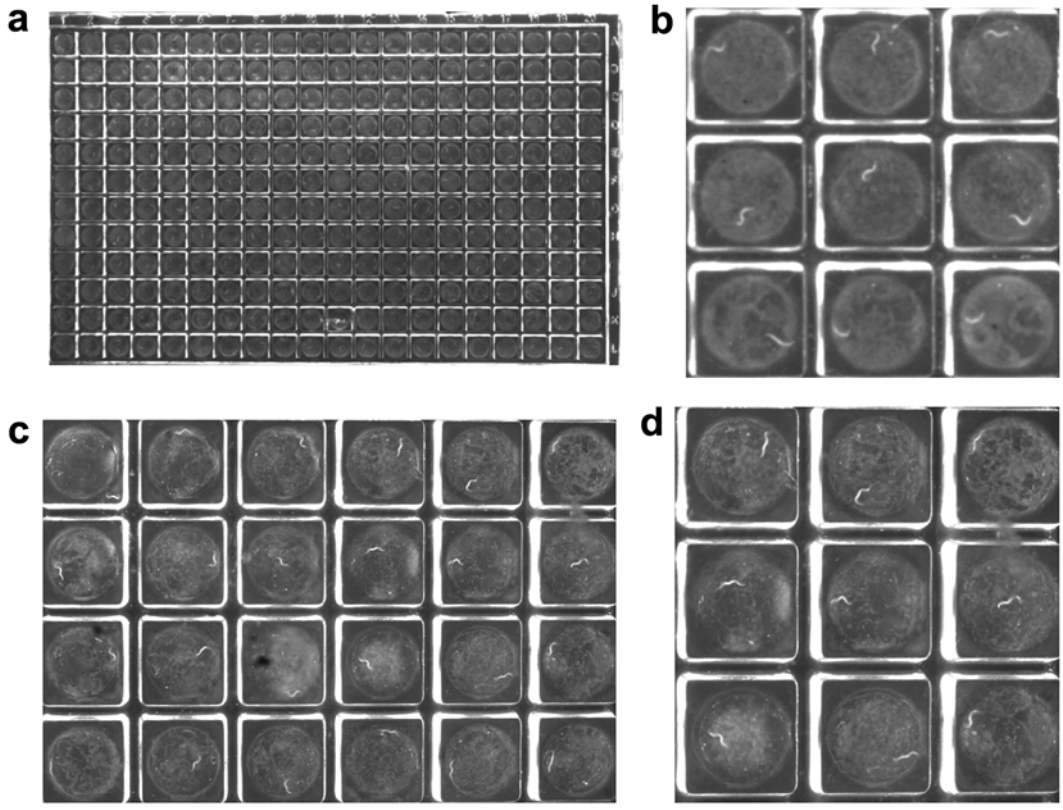

Fig. 6 (**a**) Image of a 240-well microfabricated "WorMotel" device containing one worm per well [10]. (**b**) Detail of nine wells from (**a**). (**c**) Image of 24 wells. (**d**) Detail of nine wells from (**c**). Note higher spatial resolution with smaller field of view. In all images, center-to-center spacing between wells is 4.5 mm. This imaging system also works well with glass wells [9], hanging droplets [11], and standard NGM plates

You should see an image, which may be out of focus or uniformly black or grey.

3. Place a worm plate, or any sample with height equivalent to what you will use during experiments, onto the glass stage. Adjust the height of the upper carrier to bring the object into focus (Fig. 6). Make fine adjustments using the lens focus. Familiarize yourself with the gain and exposure time settings. To minimize noise, set the gain to the minimum value and provide more light if necessary.
4. Set the lens aperture size. Opening the aperture will increase the amount of light collected and decrease the depth of field. The sharpness of the image is usually poor at the extremes of aperture (wide open or nearly closed) and best somewhere in the middle.
5. Set exposure time. Exposure should be set to collect an adequate amount of light without blurring due to movement. The optimum exposure is usually such that the brightest spots in

the important part of the image represent about 75 % of the dynamic range of the camera. If the exposure is too low, the signal-to-noise ratio will be poor. If the exposure is too high, parts of the image will be saturated (i.e., reach the maximum pixel value). The pixel values can be assayed within the IC Capture application by moving the cursor over the image.

3.5 Acquiring Image Data

1. Acquire time lapse image sequences using the in IC Capture using the Sequence Timer dialog. Save images in BMP format in a new folder devoted to the image sequence. Using JPEG format results in smaller files, but the lossy compression algorithm increases image noise.
2. To block all ambient light, close openings in the black curtains using binder clips.
3. The temperature inside the rig can be monitored by a thermometer. We use a RT100 thermistor probe and handheld meter (Omega). Note the LEDs may increase the temperature inside the rig; the voltage can be lowered to reduce LED heating. *See* **Note 9**.
4. Fogging of the plate lid can be a problem, particularly when the temperature drops. We prepare the lids with an anti-fog coating as follows: We pour a sterile-filtered solution of 20 % Tween 20 in water onto the inner surface of the lid, pour off the excess, and allow the lid to dry in a sterile hood.
5. Preparing plates in a clean hood minimizes the chances of media contamination.
6. Data can be acquired from multiple cameras using a single computer. To use multiple Gigabit Ethernet cameras, first install an Ethernet hub. Next, run a separate instance of IC Capture for each camera and configure them individually.
7. We analyze data using custom MATLAB scripts modified for each experiment. Image data acquired using this imaging system can be analyzed using worm tracking codes described elsewhere [8].

4 Notes

1. This formula is approximately valid for WD much greater than *f*.
2. The sensor size can be found in the camera specifications; the sensor of the Imaging Source DMK 23GP031 camera is 5.70 mm (H)×4.28 mm (V).
3. When working with aluminum, drilling a 1/8″ pilot hole, and use of a cutting lubricant will make machining easier. While a drill press is preferred, a hand drill can also be used. Be sure to

properly secure the workpiece during drilling and include backing material if needed to avoid damaging the surface underneath.

4. For any use of power tools, wear eye protection and consult personnel trained in their use.
5. A CS-mount camera may come supplied with one 5 mm extension ring for C-mount compatibility; an additional ring should be added.
6. For bright field imaging, a single LED source can be placed under the plate, with a diffuser made from a round piece of paper added to improve image quality.
7. The use of red LEDs reduces the behavioral effects of the illumination compared with green, blue, or white light. Infrared LEDs can also be used.
8. If you accidentally attach the LEDs in reverse, the LEDs will not light, but nothing else bad will happen.
9. In one of our setups, we placed multiple imaging rigs inside a $4' \times 4' \times 4'$ temperature-controlled chamber built using 80/20 framing and covered with black curtains. We installed a small, digital window-style air conditioner (Frigidaire Energy Star) to control the temperature inside the chamber to better than ±0.5 °C. Similarly, an electric heater with a temperature controller can be used to maintain temperature at a fixed value above the ambient.

References

1. White J, Southgate E, Thomson J, Brenner S (1986) The structure of the nervous system of the nematode Caenorhabditis elegans. Philos Trans R Soc Lond B 314:1–340. doi:10.1098/rstb.1986.0056
2. Richmond J (2005) Synaptic function. WormBook Online Rev C Elegans Biol 1–14. doi: 10.1895/wormbook.1.69.1
3. Goodman MB (2006) Mechanosensation. WormBook Online Rev C Elegans Biol 1–14. doi: 10.1895/wormbook.1.62.1
4. Bargmann CI (2006) Chemosensation in C. elegans. WormBook Online Rev C Elegans Biol 1–29. doi:10.1895/wormbook.1.123.1
5. Von Stetina SE, Treinin M, Miller DM (2006) The motor circuit. Int Rev Neurobiol 69: 125–167. doi:10.1016/S0074-7742(05)69005-8
6. Avery L, You Y-J (2012) C. elegans feeding. WormBook Online Rev C Elegans Biol 1–23. doi: 10.1895/wormbook.1.150.1
7. Hart A (2006) Behavior. WormBook. http://www.wormbook.org/chapters/www_behavior/behavior.html. Accessed 1 Aug 2012
8. Husson SJ, Costa WS, Schmitt C, Gottschalk A (2012) Keeping track of worm trackers. WormBook Online Rev C Elegans Biol 1–17. doi: 10.1895/wormbook.1.156.1
9. Yu C-CJ, Raizen DM, Fang-Yen C (2014) Multi-well imaging of development and behavior in Caenorhabditis elegans. J Neurosci Methods 223:35–39. doi:10.1016/j.jneumeth.2013.11.026
10. Churgin MA, Yu CC, Chen X, Raizen DM, Fang-Yen C (unpublished manuscript). High-throughput longitudinal monitoring of C. elegans healthspan and longevity using a multi-well device
11. Clark DA, Gabel CV, Lee TM, Samuel ADT (2007) Short-term adaptation and temporal processing in the cryophilic response of Caenorhabditis elegans. J Neurophysiol 97:1903–1910. doi:10.1152/jn.00892.2006

Chapter 15

A Method for Obtaining Large Populations of Synchronized *Caenorhabditis elegans* Dauer Larvae

Maria C. Ow and Sarah E. Hall

Abstract

The *C. elegans* dauer is an attractive model with which to investigate fundamental biological questions, such as how environmental cues are sensed and are translated into developmental decisions through a series of signaling cascades that ultimately result in a transformed animal. Here we describe a simple method of using egg white plates to obtain highly synchronized purified dauers that can be used in downstream applications requiring large quantities of dauers or postdauer animals.

Key words *Caenorhabditis elegans*, Pheromone, Stress, Dauer, Diapause, Postdauer, Egg white plate

1 Introduction

All organisms have evolved various means to survive environmental changes that may be suboptimal to their survival. The free-living soil nematode *C. elegans* shows a remarkable ability to survive harsh environments. After hatching, worms exposed to favorable conditions (plentiful food, ~20 °C temperature, and low pheromone concentrations) experience continuous development through four larval stages (L1, L2, L3, L4) before becoming reproductive adults (Fig. 1). However, when L1 larvae sense conditions that may be unsuitable to their survival (e.g., low food supply, high temperatures, or high pheromone concentrations), they make a critical developmental decision to arrest continuous development and initiate an alternative diapause stage named dauer (German for "endurance" or "permanent") (Fig. 1). Dauer can survive as non-feeding, developmentally arrested, stress resistant larvae for months. Only when conditions improve, do dauer reenter reproductive development as L4 larvae (Fig. 1) [1–4].

Although the dauer stage was previously thought of as a state of dormancy, recent work has shown that it is a highly dynamic larval stage. Notable changes in gene expression, small RNA

David Biron and Gal Haspel (eds.), *C. elegans: Methods and Applications*, Methods in Molecular Biology, vol. 1327,
DOI 10.1007/978-1-4939-2842-2_15,

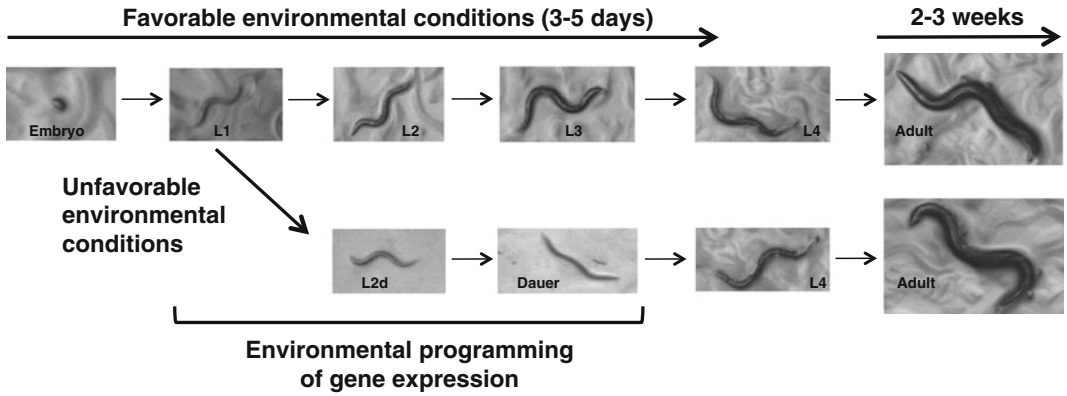

Fig. 1 Life cycle of *C. elegans*. *C. elegans* growing under non-stressful conditions undergo four larval stages before becoming reproductive adults. However, when L1 larvae sense unfavorable conditions, such as a low food supply, high temperatures, or overcrowding, they make a decision to enter an alternative non-feeding life stage, (preempted by the L2d stage) called the dauer stage where they can survive for several months. Once environmental conditions improve, dauer larvae exit the stage to become reproductive adults

populations, chromatin state, and neuronal remodeling are known to occur during dauer development [5–15]. Intriguingly, adult worms that have exited dauer (postdauers) are phenotypically and behaviorally distinct from their adult counterparts that have undergone continuous development. For instance, postdauer adults exhibit genome-wide chromatin remodeling, increased brood size, and increased mean lifespan compared to adult animals that bypassed the dauer stage [10, 14]. The mechanisms and pathways by which this physiological alteration occurs remain unknown, although chromatin remodeling and endogenous RNAi pathways have been shown to play a role [10, 14, 16–19]. Moreover, the TGF-β and insulin signal transduction pathways that mediate the entry and exit of the dauer stage are evolutionarily conserved [4], making the *C. elegans* dauer an attractive system to study the intricacies of these signaling pathways. Much of what we can learn from dauers, such as how information from the environment is sensed and transduced via sensory organs through a cascade of neuronal and signaling pathways, and how that information is translated into developmental decisions resulting in a physiologically transformed animal, constitute some of the most fundamental biological decisions of all organisms.

Often, biochemical or genomic studies necessitate large quantities of worms. Behavioral or developmental experiments also require that worms be synchronized at a particular developmental stage. Although solid media laden with thick lawns of bacterial food or large batches of liquid cultures can be used to grow large quantities of worms [20], these methods do not result in synchronized populations and may not necessarily generate large amounts of dauers. Here, we describe a detailed method of using egg white plates to

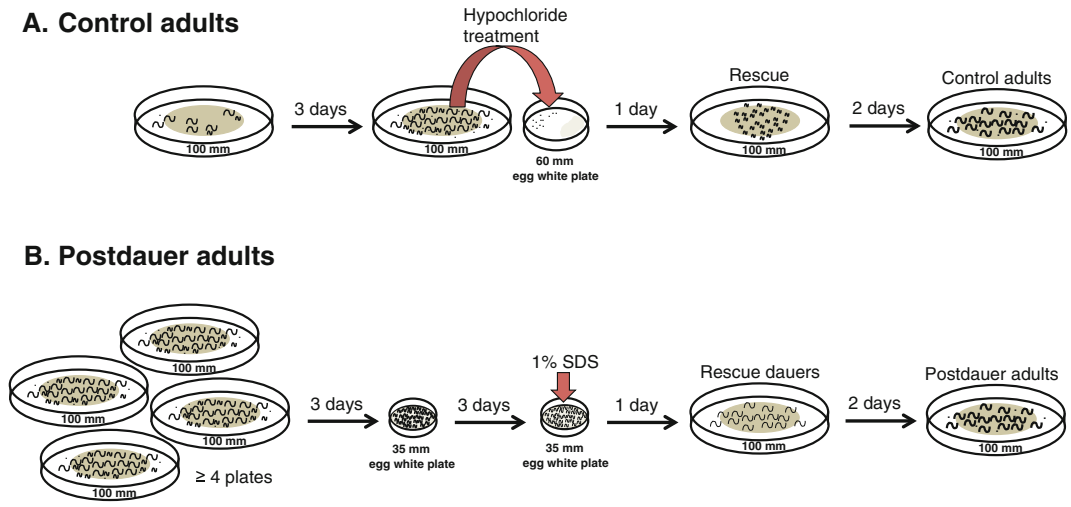

Fig. 2 Flowchart of the egg white plate method. (**a**) Control animals are obtained by adding a small drop of well-fed worms onto a seeded 100 mm NGM plate. This plate is incubated for 3 days at the desired temperature (generally 20 °C) and well-fed throughout the incubation period. After 3 days, a hypochlorite treatment is performed to isolate embryos. The embryos are transferred to a 60 mm egg white plate. The following day, a chunk of the agar with the L1 larvae is transferred to a seeded 100 mm NGM plate where they will reach the desired stage (1 day for L4 larvae and 2 days for young adults at 20 °C). (**b**) Postdauer animals are obtained by collecting densely populated worms from four 100 mm NGM plates and transferring them into a 35 mm egg white plate. The egg white plate is incubated for 3 days at the desired temperature (typically 20 °C) followed by an overnight 1 % SDS treatment. Dauers are rescued the next day by transferring them onto a seeded 100 mm NGM plate where they will exit the dauer stage and become L4 larvae or young adults (1 day or 2 days later at 20 °C, respectively)

generate large amounts of dauers by taking advantage of the high concentration of dauer-inducing pheromones secreted by the worms when overcrowded (Fig. 2) [21, 22]. The resulting dauers are highly synchronized and can be purified away from any worm or cell debris. In addition, the resulting dauers can be rescued by feeding, resulting in synchronized postdauer L4 larvae or adults. Although this method is optimized for *C. elegans*, we predict that it could be used for other nematode species that have a dauer stage.

2 Materials

The media used to maintain worms in this protocol are standard in the *C. elegans* field and have been described previously [23]. The water used to make all the solutions should be high quality water such as deionized H_2O or Milli-Q filtered water (EMD Millipore). It is important that axenic techniques be practiced when handling *C. elegans* and when preparing all the components and media described below.

2.1 Components for Nematode Growth Medium (NGM) Plates

1. 1 M $MgSO_4$: 120.4 g of $MgSO_4$ in H_2O. Bring up volume to 1 l. Sterilize by autoclaving. Store at room temperature.
2. 1 M $CaCl_2$: 147 g of $CaCl_2$ dihydrate in H_2O. Bring up volume to 1 l. Sterilize by autoclaving. Store at room temperature.
3. 5 mg/ml cholesterol: 500 mg of cholesterol (Sigma Aldrich) in 100 ml of 100 % ethanol. Do not autoclave. Store at room temperature.
4. 1 M KPO_4 buffer pH 6.0: 108.3 g KH_2PO_4 and 35.6 g K_2HPO_4 in H_2O. Bring up volume to 1 l. Sterilize by autoclaving. Store at room temperature.
5. Agar (Thermo Fisher Scientific, Waltham, MA, USA).
6. Petri dishes 35 mm, 60 mm, and 100 mm (Krackeler Scientific, Inc., Albany, NY, USA).

2.2 Components for Growth of *C. elegans* Food Source, *Escherichia coli* OP50

1. LB plates: Dissolve 10 g tryptone, 5 g yeast extract, 5 g NaCl, and 15 g agar in 950 ml H_2O. Adjust the pH to 7.0 using 1 N NaOH. Bring up volume to 1 l. Autoclave for 30 min. Allow to cool to 55 °C and pour into 100 mm petri dishes. Store any unused plates at 4 °C. Plates can be used for several months.
2. LB liquid medium: Prepare the medium as above (Subheading 2.2, **item 1**) but exclude the agar. Aliquot the medium into several bottles and autoclave for 30 min. Store at room temperature.
3. *E. coli* OP50: Can be obtained for a small fee from the *Caenorhabditis* Genetics Center (University of Minnesota, Minneapolis, MN, USA) http://www.cbs.umn.edu/research/resources/cgc.

2.3 Components for Egg White Plates

1. Egg white: A convenient source of egg white is a carton of pure egg white without any additives that can found in most grocery stores. Alternatively, chicken eggs can be used (*see* **Note 1**).
2. 1 % SDS: 10 g of sodium dodecyl sulfate (Sigma Aldrich) in 900 ml of hot water (*see* **Note 2**). Mix by stirring. Once dissolved, bring up volume to 1 l with H_2O. There is no need to autoclave the solution. Store at room temperature.

2.4 Components for Transferring Worms to Egg White Plates

1. M9 buffer: 3 g KH_2PO_4, 5 g NaCl, and 1 ml of 1 M $MgSO_4$ in H_2O. Bring up volume to 1 l. Sterilize by autoclaving. Store at room temperature.
2. 60 % sucrose: 600 g of sucrose. Bring up volume to 1 l with H_2O. Sterilize by filtration though a 0.45 μM filter. Store at room temperature. Chill on ice before use.
3. 100 mM NaCl: 5.84 g of NaCl. Bring up volume to 1 l with H_2O. Sterilize by autoclaving. Store at room temperature. Chill on ice before use.

4. Borosilicate glass $5^3/_4$ in. Pasteur pipettes (Krackeler Scientific, Inc., Albany, NY, USA).
5. Pasteur pipette rubber bulbs (Krackeler Scientific, Inc., Albany, NY, USA).
6. 15 and 50 ml conical tubes.

2.5 Components for Hypochlorite Treatment

1. 5 M KOH: Dissolve 280.6 g KOH in 1 l of water. Store at room temperature in a safety cabinet.
2. Household bleach (5 % sodium hypochlorite).
3. M9 buffer (*see* Subheading 2.4, **item 1**).
4. 15 ml conical tubes and 1.5 ml eppendorf tubes.

3 Methods

3.1 Preparation of Nematode Growth Medium (NGM) Plates

1. Dissolve 3 g NaCl, 2.5 g peptone, 17 g agar in 975 ml of H_2O. Autoclave for 30 min. Cool to 55 °C. Add 1 ml 1 M $MgSO_4$, 1 ml 1 M $CaCl_2$, 1 ml 5 mg/ml cholesterol, and 25 ml 1 M KPO_4 buffer pH 6.0. Mix by stirring.
2. Pour into 35 mm, 60 mm, or 100 mm petri dishes (*see* **Note 3**). Allow the plates to dry for 2–3 days at room temperature before using. Store unused plates at 4 °C in an airtight container to prevent them from drying. The plates can be used for several weeks.

3.2 Seeding NGM Plates

1. Grow an overnight culture from a single colony of freshly streaked *E. coli* OP50 in LB liquid medium. Using sterile technique, add 50 ml of the overnight OP50 culture to top of the 35 mm NGM plates (equilibrated to room temperature) or 1 ml of OP50 onto the 100 mm NGM plates. The 35 mm plates will serve as the base of the egg white plates while the 100 mm plates will be used to grow the worms prior to transferring them onto the egg white plates. Allow the seeded plates to dry at room temperature for 2–3 days before using.

3.3 Preparation of Egg White Mixture

1. Place a glass beaker on a hot plate. Boil 50 ml of water for every 1 egg white. Stir the mixture using a stir bar until the egg whites are fully cooked. Monitor the cooking until the egg whites start to turn slightly brown at the bottom of the beaker. Immediately remove the beaker from the hot plate to prevent the egg whites from burning.
2. Pour cooked egg mixture into a kitchen blender and puree until smooth and frothy.
3. Add a thin layer of boiled egg white mixture to the top of 35 mm NGM plates seeded with *E. coli* OP50 (Fig. 3). Add a small scoop of the egg white mixture to one side of a seeded 60 mm NGM plate (Fig. 4).

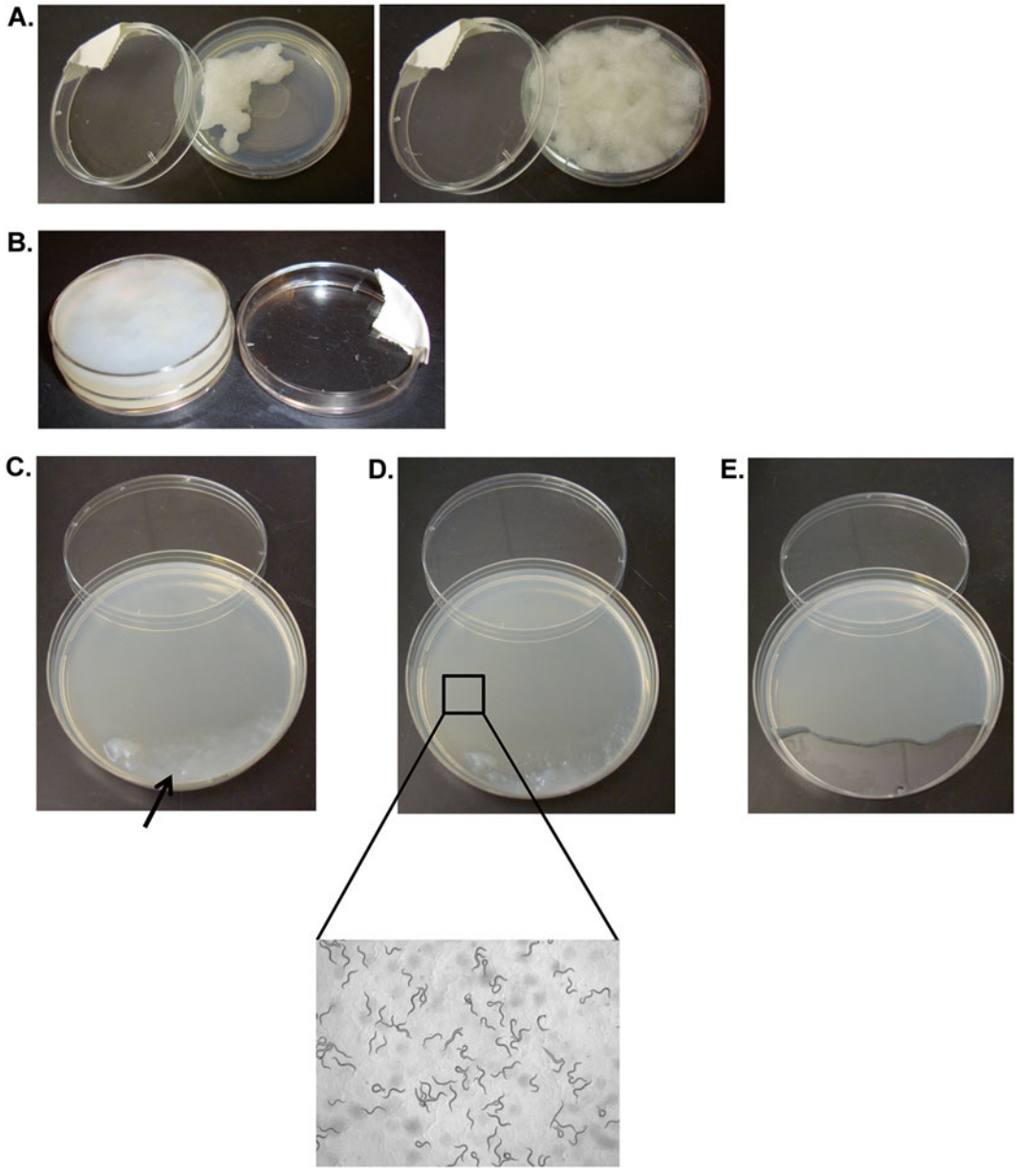

Fig. 3 35 mm egg white plate. (**a**) A 35 mm seeded NGM plate partially (*left panel*) or fully (*right panel*) filled with egg white mixture. Note the small piece of white bench tape on the petri dish cover. (**b**) A 35 mm egg white plate that was filled with 1 % SDS to select against non-dauers. (**c**) Egg white plate mixture with worms and 1 % SDS poured onto an unseeded 100 mm NGM plate (*arrow*) for dauer recovery. (**d**) Dauers (*inset*) that migrated away from the egg white mixture. (**e**) After a sufficient amount of dauers is recovered, the area with the egg white mixture is sliced and discarded

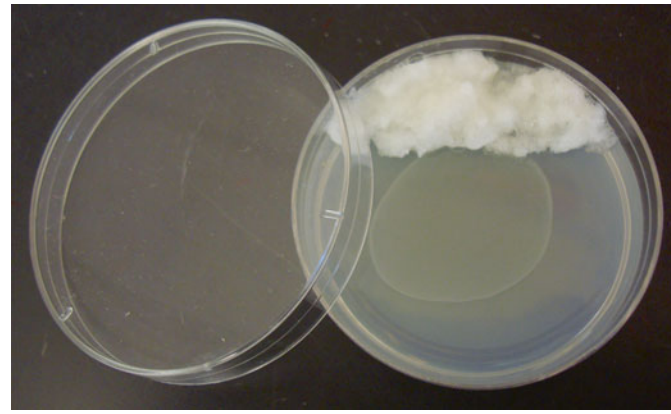

Fig. 4 60 mm egg white plate. A small amount of egg white mixture is placed on one side of a seeded 60 mm NGM plate. This plate serves to harvest control animals (Subheading 3.7)

4. Store any unused egg white mixture at 4 °C for about a month or until they appear dry. Egg white mixture can also aliquoted into 50 ml conical tubes and frozen at −20 °C indefinitely for later use (*see* **Note 4**).

3.4 Placing Worms onto Egg White Plates

1. Wash several (*see* **Note 5**) 100 mm NGM plates containing well-fed, densely populated gravid worms with M9 buffer. Collect all the worms into a 15 ml conical tube and allow the worms to settle into a pellet by gravity or by centrifugation at 845 × *g* for 30 s. Remove most of the M9 Buffer and transfer the worm pellet into an egg white plate using a Pasteur pipette. Depending on the amount of animals needed, several 35 mm egg white plates may be necessary for each strain.
2. Use a small piece of bench tape to create a gap between the petri dish lid and the base (*see* Fig. 3 and **Note 6**).
3. Incubate the egg white plate containing the worms for 60–72 h at 20 °C (or at 25 °C for worms with dauer entry difficulties).

3.5 Sucrose Wash (See Note 7)

1. After maintaining the egg white plates for 60–72 h, add 2–2.5 ml of 1 % SDS to the egg white plates. Incubate overnight at room temperature with the top lid off. Cover the plates with a darkened plastic box. This allows for the selection of non-feeding dauers from a population of worms. Incubating the plates in the dark mimics the dark conditions of a 20 °C worm incubator.
2. Next day, wash the dauers and residual egg debris from the egg plates with M9 buffer and place them into a 50 ml conical tube.

3. Prepare solutions of 100 mM NaCl and 60 % sucrose and chill to 4 °C.
4. Centrifuge the dauer and debris mixture at room temperature at 845 × *g* for 2 min.
5. Resuspend the dauer pellet in 100 mM cold NaCl. Consolidate all dauer pellets for a total volume of 22 ml of cold 100 mM NaCl. Mix well and incubate on ice for 15 min.
6. Add 22 ml of cold 60 % sucrose to the tube, mix well by inverting several times, and centrifuge for 5 min at maximum speed in a clinical centrifuge.
7. Break the narrow tip off of a glass Pasteur pipette to create a tip with a wide opening. Carefully but quickly (*see* **Note 8**) transfer the light brown layer of floating dauers into a new 50 ml conical tube containing 35 ml of cold 100 mM NaCl.
8. Pellet the dauers by spinning at 845 × *g* for 1 min in a clinical centrifuge.
9. Wash two to three times with 100 mM NaCl to remove any residual sucrose.
10. The pellet should consist of dauers free of dead worm debris.
11. For the isolation of smaller dauer populations, pour the worm-egg white-1 % SDS mixture from Subheading 3.5, **step 1** onto unseeded 100 mm NGM plates. Tilt the plate with the cover off in a sterile hood so as the dauers remain in the lowest level. Allow the dauers to crawl up from the mixture. Once a sufficient number of dauers have crawled away from the mixture, cut off the area where the mixture was poured and wash off the dauers using 1 % SDS (*see* Fig. 3 and **Note 9**).

3.6 Rescue or Recovery of Dauers

1. Following the collection of dauers described above, dauers can be allowed to recover and become postdauer L4 larvae by placing them on seeded NGM plates. Dauer larvae should exit the diapause stage and become postdauer L4 larvae after ~12 h and postdauer adults in ~48 h at 20 °C.

3.7 Preparation of Control Worms for Comparison with Postdauer Worms

This section describes the preparation of L4 larvae or adults animals that have undergone continuous development and bypassed the dauer stage. These animals are used as the control animals alongside their postdauer counterparts.

1. While placing worms onto egg white plates (Subheading 3.4), place a small drop of worms onto a seeded 100 mm plate and incubate at 60–72 h at 20 °C along with the 35 mm egg white plate (*see* **Note 10**).
2. After 60–72 h, the 100 mm plates should contain numerous gravid adults. Wash off the worms using 5–10 ml of M9 buffer in a 15 ml conical tube to perform a hypochlorite treatment (**steps 2–11**).

3. Centrifuge the tube at 845 × *g* for 30 s.
4. Remove most of the supernatant and transfer 700 ml of the M9 containing the worms into a 1.5 ml eppendorf tube.
5. Add 100 ml of household bleach (5 % sodium hypochlorite) and 200 ml of 5 M KOH. Mix the tube contents end-to-end for 2 min.
6. Centrifuge at 845 × *g* for 30 s.
7. Remove most of the supernatant and add 700 ml of M9 buffer.
8. Repeat **steps 5** and **6**. After the second hypochlorite/KOH treatment, a white pellet of embryos should be visible.
9. Remove most of supernatant and add 1 ml of M9 buffer.
10. Centrifuge at 845 × *g* for 30 s.
11. Repeat **steps 9** and **10** three more times.
12. After the final fourth wash, remove most of the supernatant and using a Pasteur pipette, transfer the embryos onto a 60 mm seed NGM plate with egg white mixture on one side of the plate (*see* Fig. 4, **Note 11**).
13. On the following day, using a sterile spatula, transfer a piece of the 60 mm plate containing the desired amount of L1 larvae onto a seeded 100 mm NGM plate.
14. These L1 larvae will be L4 larvae in ~48 h or young adults in ~72 h at 20 °C.

4 Notes

1. The shell of chicken eggs can be sterilized using a 10 % dilution of household bleach, followed by a rinse of 70 % ethanol. Care must be taken in separating the egg white from the egg yolk in a sterile manner (with the aid of an autoclaved egg separator) since any residual egg yolk in the egg white mixture can inhibit dauer entry (personal observation).
2. To prevent the inhalation of SDS, wear a dusk mask and/or use a fume hood while weighing the powder.
3. A peristaltic pump can be used to pour plates. Alternatively, the medium can be prepared and autoclaved in a 2 l polypropylene beaker with a handle and a spout (covered with aluminum foil during autoclaving) for easy dispensing into the petri dishes. Typically, 2–2.5 ml of medium per plate is sufficient (about 1/3) for the 35 mm plates and about 10 ml for the 60 mm plates. Do not pour too much medium into the 35 mm plates as space is needed for the egg white mixture and the worms. 30–35 ml can be poured into the 100 mm plates that will serve to grow worms that are to go onto the egg white plates.

4. Thaw an egg white aliquot to room temperature. Once thawed, use a sterile spatula to scoop the egg white mixture into a seeded 35 mm NGM plate. The unused portion of the egg white mixture can be stored at 4 °C.
5. Four 100 mm plates with densely populated, well-fed gravid worms are sufficient for obtaining dauers from most worm strains. This can be scaled up if using worms that are dauer entry defective. Do not allow the worms to starve on the 100 mm plates. Feed with ~1 ml of 20× OP50 if necessary. 20× OP50 is prepared by inoculating a colony of OP50 into 1 l of Super Broth (3.2 % peptone, 2 % yeast extract, 0.5 % NaCl), vigorously shaking overnight at 37 °C, collecting the OP50 by centrifugation, and washing the bacterial pellet twice with sterile water before resuspending the pellet in 50 ml of M9 buffer. Any unused concentrated OP50 can be stored at 4 °C and used for days.
6. The bench tape need not be sterilized. The gap serves to prevent an airtight closure between the lid and the base of the petri dish that can potentially suffocate the worms (Fig. 3).
7. The sucrose wash is based on ref. [24].
8. The step should be done as quickly as possible as prolonged exposure to 30 % sucrose is detrimental to dauers.
9. A secondary selection should be done if there is a mixture of non-dauers and dauers in the recovery population by incubating the worms in 1 % SDS and inverting end-to-end for 30 min at room temperature. The survival of non-dauers after an overnight 1 % SDS treatment can occur if the egg white mixture is not thoroughly blended. This can result in non-dauers finding refuge from the SDS and surviving the treatment inside the large pieces of egg white.
10. Do not allow the worms on the 100 mm plate to starve. Add 20× OP50 food if necessary (*see* **Note 5**).
11. Do not transfer too many embryos to the 60 mm egg white plate. Transferring too many embryos can result in the overcrowding (a stress-inducing condition) of L1 larvae that will be hatching. If the investigator needs a large population of control animals, the embryos can be distributed at low density to several 60 mm egg white plates.

References

1. Cassada RC, Russell RL (1975) The dauer larva, a postembryonic developmental variant of the nematode *Caenorhabditis elegans*. Dev Biol 46:326–342
2. Golden JW, Riddle DL (1984) The *Caenorhabditis elegans* dauer larva: developmental effects of pheromone, food, and temperature. Dev Biol 102:368–378

3. Riddle DL (1997) *C. elegans* II. Cold Spring Harbor Laboratory Press, Cold Spring Harbor, NY, USA, pp 739–768
4. Hu, PJ (2007) Dauer *WormBook*. In: The *C. elegans* Research Community (ed) WormBook, doi: 10.1895/wormbook.1.144.1, http://www.wormbook.org
5. Albert PS, Riddle DL (1983) Developmental alterations in sensory neuroanatomy of the *Caenorhabditis elegans* dauer larva. J Comp Neurol 219:461–481
6. Cherkasova V, Ayyadevara S, Egilmez N, Shmookler Reis R (2000) Diverse *Caenorhabditis elegans* genes that are upregulated in dauer larvae also show elevated transcript levels in long-lived, aged, or starved adults. J Mol Biol 300:433–448
7. Jones SJ, Riddle DL, Pouzyrev AT, Velculescu VE, Hillier L, Eddy SR, Stricklin SL, Baillie DL, Waterston R, Marra MA (2001) Changes in gene expression associated with developmental arrest and longevity in *Caenorhabditis elegans*. Genome Res 11:1346–1352
8. Wang J, Kim SK (2003) Global analysis of dauer gene expression in *Caenorhabditis elegans*. Development 130:1621–1634
9. Fielenbach N, Antebi AC (2008) *C. elegans* dauer formation and the molecular basis of plasticity. Genes Dev 22:2149–2165
10. Hall SE, Beverly M, Russ C, Nusbaum C, Sengupta P (2010) A cellular memory of developmental history generates phenotypic diversity in *C. elegans*. Curr Biol 20:149–155
11. Procko C, Lu Y, Shaham S (2011) Glia delimit shape changes of sensory neuron receptive endings in *C. elegans*. Development 138:1371–1381
12. Karp X, Hammell M, Ow MC, Ambros V (2011) Effect of life history on microRNA expression during *C. elegans* development. RNA 17:639–651
13. Procko C, Lu Y, Shaham S (2012) Sensory organ remodeling in *Caenorhabditis elegans* requires the zinc-finger protein ZTF-16. Genetics 190:1405–1415
14. Hall SE, Chirn GW, Lau NC, Sengupta P (2013) RNAi pathways contribute to developmental history-dependent phenotypic plasticity in *C. elegans*. RNA 19:306–319
15. Schroeder NE, Androwski RJ, Rashid A, Lee H, Lee J, Barr MM (2013) Dauer-specific dendrite arborization in *C. elegans* is regulated by KPC-1/Furin. Curr Biol 19: 1527–1535
16. Billi AC, Fischer SE, Kim JK (2014) Endogenous RNAi pathways in *C. elegans WormBook*. In: The *C. elegans* Research Community (ed) WormBook, doi: 10.1895/wormbook.1.170.1, http://www.wormbook.org
17. Wedeles CJ, Wu MZ, Claycomb JM (2013) A multitasking Argonaute: exploring the many facets of *C. elegans* CSR-1. Chromosome Res 21:573–586
18. González-Aguilera C, Palladino F, Askjaer P (2014) *C. elegans* epigenetic regulation in development and aging. Brief Funct Genomics 13:223–234
19. Guérin TM, Palladino F, Robert VJ (2014) Transgenerational functions of small RNA pathways in controlling gene expression in *C. elegans*. Epigenetics 9:37–44
20. Lewis JA, Fleming JT (1995) Basic culture methods. In: Epstein HF, Shakes DC (eds) Methods in cell biology. *Caenorhabditis elegans*: modern biological analysis of an organism. Academic Press, Inc., San Diego, pp 4–27
21. Butcher RA, Fujita M, Schroeder FC, Clardy J (2007) Small-molecule pheromones that control dauer development in *Caenorhabditis elegans*. Nat Chem Biol 3:420–422
22. Butcher RA, Ragains JR, Kim E, Clardy J (2008) A potent dauer pheromone component in *Caenorhabditis elegans* that acts synergistically with other components. Proc Natl Acad Sci U S A 105:14288–14292
23. Stiernagle T (2006) Maintenance of *C. elegans*, *WormBook*. In: The *C. elegans* Research Community (ed) WormBook, doi: 10.1895/wormbook.1.101.1, http://www.wormbook.org
24. Portman DS (2006) Profiling *C. elegans* gene expression with DNA microarrays, *WormBook*. In: The *C. elegans* Research Community (ed) WormBook, doi: 10.1895/wormbook.1.104.1, http://www.wormbook.org

Chapter 16

Sampling and Isolation of *C. elegans* from the Natural Habitat

Nausicaa Poullet and Christian Braendle

Abstract

Wild populations of the model organism *C. elegans* allow characterization of natural genetic variation underlying diverse phenotypic traits. Here we provide a simple protocol on how to sample and rapidly identify *C. elegans* wild isolates. We outline how to find suitable habitats and organic substrates, followed by describing isolation and identification of *C. elegans* live cultures based on easily recognizable morphological characteristics, molecular barcodes and/or mating tests. This protocol uses standard laboratory equipment and requires no prior knowledge of *C. elegans* biology.

Key words *Caenorhabditis elegans*, Natural genetic variation, Natural populations, Wild isolates, Natural habitat, Ecology

1 Introduction

Insights into *C. elegans* biology are almost exclusively based on the analysis of a single reference strain (N2) but recent research has started to investigate genetic and phenotypic variation among *C. elegans* wild isolates [1]. Key findings are that the reference strain N2 shows extensive laboratory adaptation [2, 3] and that *C. elegans* natural populations show overall very little genetic differentiation across the globe [4]. Nevertheless, *C. elegans* wild isolates may exhibit marked phenotypic differences, some of which have been genetically and molecularly characterized using quantitative genetic mapping approaches [1]. Such characterization of *C. elegans* natural variation generates novel insights into *C. elegans* biology and further places the wealth of mechanistic knowledge of this model organism into a much-needed ecological and evolutionary context [5].

Hundreds of *C. elegans* isolates have been collected worldwide, and the species is clearly more abundant in temperate than in tropical regions [4–8] (Fig. 1). The few *C. elegans* isolates found in the tropics occurred mostly at high altitude [8, 9] and indicate, consistent with experimental determination of thermal optima in

David Biron and Gal Haspel (eds.), *C. elegans: Methods and Applications*, Methods in Molecular Biology, vol. 1327,
DOI 10.1007/978-1-4939-2842-2_16,

Fig. 1 Geographic distribution of *C. elegans* wild isolates (adapted from refs. [4, 7, 13, 15] and C. Braendle, unpublished data). A list of available *C. elegans* wild isolates can be consulted at http://www.wormbase.org/species/c_elegans/strain#2-10-5. For information on other *Caenorhabditis* species, *see* [8] and for updates on species discovery, *see* http://evolution.wormbase.org/index.php/Main_Page

the laboratory [10], that *C. elegans* does not tolerate prolonged exposure to temperatures above 25 °C.

Current insights into the global distribution of *C. elegans* are limited due to strong sampling bias, with some regions (e.g., France) having been frequently sampled [5, 6, 11–13] whereas others (e.g., Eastern Europe) have never or only rarely been sampled. Although it is likely to colonize highly diverse habitats, *C. elegans* has primarily been isolated from anthropogenic habitats, such as gardens or agricultural lands [11–17], and only very rarely from more unperturbed sites (e.g., forests) [13], which still await in-depth sampling for *C. elegans*.

C. elegans and other *Caenorhabditis* species have been isolated from a wide variety of organic substrates, mainly decomposing vegetal matter, such as compost, fruits or plant stems [8, 18]. Despite commonly being referred to as a soil nematode, *C. elegans* has virtually never been isolated from soil samples but mostly from decaying vegetal matter on or above the soil layer. *C. elegans* has also been isolated from a range of live or dead invertebrates (e.g., beetles, isopods, millipedes, snails, and slugs) [4–6, 11, 13]. Note that in contrast to other nematode species there is no strong evidence for taxon-specific phoretic or necromenic invertebrate associations of *C. elegans* [5, 19].

In this chapter we provide a simple protocol for sampling and isolation of *C. elegans* wild isolates, chiefly aimed at researchers having minimal working knowledge using *C. elegans* as a study organism. Nevertheless, acquiring basic knowledge of *C. elegans* handling and maintenance as presented in [20] is highly recommended. Note that several alternative, yet usually more time-consuming nematode isolation protocols are available [6].

2 Materials

2.1 Collection and Storage of Substrate Samples

1. Sampling containers, e.g., resistant plastic zip-lock bags.
2. Disposable plastic gloves.

2.2 Nematode Isolation in the Laboratory

1. Dissecting stereomicroscope with transmitted light source (5–50× magnification).
2. Nematode growth medium (NGM) [20]: 1 L : 3 g NaCl, 25 g agar, 2.5 g Bacto Peptone, 975 mL H_2O. After autoclaving, add 1 mL 1 M $CaCl_2$, 1 mL 5 mg/mL cholesterol in ethanol, 1 mL 1 M $MgSO_4$, and 25 mL 1 M KPO_4. Mix well and dispense solution in Petri dishes (e.g., 90 and 55 mm diameter). (The increased agar concentration (2.5 % instead of the usual 1.7 % helps preventing burrowing of nematodes into the culture plates). Store at room temperature for 2–4 days.
3. Seed NGM plates with a central spot of *E. coli* OP50 (100–200 µL) and store at room temperature for 2–4 days. OP50 is available from the *Caenorhabditis* Genetics Center (CGC): http://www.cbs.umn.edu/research/resources/cgc.
4. Disposable plastic gloves.
5. Clean water or M9 buffer (1 L): 3 g KH_2PO_4, 6 g Na_2HPO_4, 5 g NaCl; autoclave; add 1 mL 1 M $MgSO_4$ before use [20].
6. Platinum worm pick [20].
7. Parafilm.

2.3 Morphological and Molecular Identification of C. elegans

1. Dissecting stereomicroscope with transmitted light source (50×–100× magnification).
2. Standard PCR reagents and equipment and access to sequencing service.

2.4 Genetic Identification Through Crosses with Established C. elegans Strains

1. Dissecting stereomicroscope with transmitted light source (5–50× magnification).
2. Identified *C. elegans* strain, e.g., N2 (available from the CGC: http://www.cbs.umn.edu/research/resources/cgc).
3. NGM plates (55 mm diameter) (*see* Subheading 2.2, **item 2**).

2.5 Establishment and Cryopreservation of C. elegans Wild Isolate Stocks

1. NGM plates (55 mm diameter) (*see* Subheading 2.2, **item 2**).
2. Freezing solution [20]: 300 mL: Start with 100 mL of dH_2O and add 1.76 g NaCl, 2.04 g KH_2PO_4, 1.7 mL of 1 M NaOH, 1.2 g agar, 71.6 mL glycerol. Heat to boiling until the agar is dissolved. Bring to 300 mL with dH_2O. Distribute 50 mL per 100 mL bottles; autoclave. After autoclaving or when first using, add 1.5 mL 0.1 M $MgSO_4$ and 100 µL 1 M $CaCl_2$ per 50 mL bottle [6, 20].
3. Cryovials (2 mL).
4. –80 °C freezer and liquid nitrogen storage facilities.

3 Methods

3.1 Finding Suitable Habitats and Substrate Samples

Potentially, *C. elegans* may be found in diverse, anthropogenic as well as unperturbed natural sites; however, the latter have rarely been sampled. In temperate regions of France, temporal sampling of natural populations uncovered *C. elegans* from September to November, but rarely during the summer months [13]. Such population fluctuations further depend on the specific habitat and substrate sampled, given that certain habitats, e.g., composts heaps in gardens [12], may represent more stable habitats than others, such as, seasonally occurring fruits. As a general rule, hot, dry or very cold habitats are very unlikely to yield *C. elegans* although individuals in the dauer stage may be uncovered at low densities.

Substrates potentially containing *C. elegans* encompass any organic sample that contains or contained microbial organisms serving as possible *C. elegans* food source, including fruits, plant stems and leaves, compost, animal carcasses, animal feces. Fruits in advanced stages of decomposition on the ground represent ideal target samples due to their high microbial content and likely also because they attract diverse invertebrates that might carry *Caenorhabditis* nematodes [5]. Direct sampling of such invertebrate carriers (arthropods, including insects, isopods as well as mollusks, such as snails or slugs) has yielded *C. elegans* and other *Caenorhabditis* species [5, 6, 12]. Sampling success is highest for rotting fruit/plant material that is not dry and not directly exposed to sun light.

3.2 Collection and Storage of Substrate Samples

1. Using disposable plastic gloves, collect samples from suitable habitat (*see* above) and place into container, ideally transparent plastic zip-lock bags for plant substrates (for invertebrates, use hard plastic containers, e.g., Falcon tubes). Leave ample air in the bag and add some paper towel if the sample is very liquid, to avoid fermentation.
2. Note date of collection, locality (e.g., GPS coordinates), habitat, and substrate type (e.g., take photographs).

3. Store samples in the dark, and keep at temperatures of 15–25 °C (above 25 °C may lead to sterility in *C. elegans*). Before processing in the laboratory, substrate samples may be stored for several weeks in plastic bags but samples should be regularly aerated. For high success in nematode recovery, analyze substrates within 1 week after sampling.

3.3 Nematode Isolation in the Laboratory

1. Place substrate samples on large (e.g., 100 mm diameter) NGM plates seeded with a spot of *E. coli* OP50 in the center of the plate. Tear up or cut large samples into smaller pieces and place them around the *E. coli* spot (sacrifice live invertebrates). Add 1–3 mL of clean water or M9 buffer onto the substrate. Avoid damaging the agar plates as this will facilitate burrowing of nematodes into the culture plates, making subsequent visual observation difficult. Cover the plate with lid. Samples, such as rotting fruit, usually contain diverse invertebrates (e.g., mites, insect larvae, flies): to avoid their spread and cross-contamination among plates, wrap plates with Parafilm. Keep samples at 15–20 °C.
2. Bactivorous nematodes, such as *C. elegans*, will crawl onto the *E. coli* lawn and can be easily observed using a standard dissecting stereomicroscope equipped with a transmitted light source. Nematodes may colonize the *E. coli* lawn within minutes to hours after placing the sample on the culture plate, but for samples with low densities (or individual dauer individuals) it may take several days to detect the nematodes. Keep sampling plates for 5–7 days and, after nematode isolation, autoclave before disposal.
3. Check for the presence of nematodes on the plate using a dissecting scope. Diverse bacteria and fungi stemming from the sample will also grow on the NGM plate, making observation difficult over time (*see* **Note 1**). If this is the case, cut out a piece of agar containing nematodes and transfer to a new plate to facilitate visual observation.
4. Pick individual nematodes to fresh NGM plates (55 mm diameter) using a platinum worm pick and amplify population (*see* **Note 2**).

3.4 Morphological and Molecular Identification of C. elegans

The following protocol for rapid and easy identification of *C. elegans* uses minimal morphological knowledge of *C. elegans* allowing an efficient initial elimination of nematodes that do not represent members of the genus *Caenorhabditis*. In a second step, only nematodes with a hermaphroditic mode of reproduction are selected. After these two initial steps of selection, analysis using species-specific DNA sequence-tag is performed to distinguish between different hermaphroditic *Caenorhabditis* species [8], which are morphologically very similar. Currently, only three androdioecious

(hermaphrodite-male) *Caenorhabditis* species have been described: *C. elegans*, *C. briggsae*, and *C. tropicalis* (*C.* sp. 11); all other species (>23) show a gonochoristic (female-male) mode of reproduction [8, 21]. For a detailed overview of *Caenorhabditis* identification methods, *see* [6].

1. Diverse nematode taxa may be uncovered in substrate samples, but a given sample often contains only one or two different nematode species. To check whether picked nematodes may represent *C. elegans*, use the following two criteria:
   (a) The pharyngeal head region contains two distinct bulbs: the middle and the basal pharyngeal bulbs, the latter bulb exhibits a grinder (Fig. 2). This morphology is typical for all *Caenorhabditis* species [6] and can be examined using a dissecting scope at 50× or higher magnification (or using light microscopy).
   (b) Test whether reproduction occurs through self-fertilizing hermaphrodites: isolate juvenile stages onto individual NGM plates and determine whether fertile progeny is produced after a 2–5 days of growth at 20°. (For isolation of gonochoristic *Caenorhabditis* species, *see* **Note 3**).

   Note that several additional simple morphological criteria (e.g., long and pointy tail, central vulva, oval embryos) are characteristic for *Caenorhabditis* and may also be used for identification [6]; for detailed morphological characterization of *Caenorhabditis* species, *see* [8, 22, 23].

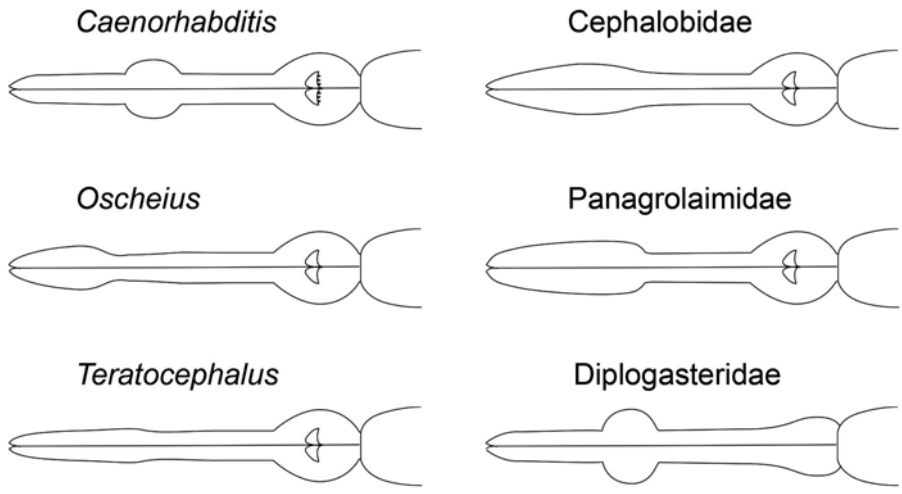

Fig. 2 Morphological characteristics of the *C. elegans* pharynx compared to a selection of other nematode taxa (adapted from [6, 24]). The presence of two circular pharyngeal bulbs is a distinctive feature of *Caenorhabditis* species and can be observed using a dissecting stereomicroscope at >50× magnification and good illumination. Commonly found in the same habitat/substrate are nematodes of the genus *Oscheius*, which superficially show an overall morphology and size similar to *C. elegans*, yet present a clearly different pharyngeal structure

2. Molecular identification of *C. elegans*: Kiontke et al. [8] have established a *Caenorhabditis* species barcoding method using sequencing of the ITS2 (Internally Transcribed Spacer) region, localized between the 5.8S and 28S rDNA genes. To amplify the region of approximately 2 kb, use the following primers:

   5.8S-1: 5′-CTGCGTTACTTACCACGAATTGCARAC.

   and

   KK28S-4:5′-GCGGTATTTGCTACTACCAYYAMGATCTGC.

   Sequence the amplified fragment with the sequencing primer KK-28S-22 (5′-CACTTTCAAGCAACCCGAC) [8].

   Use NCBI Blast to check for species identity of sequence. *Caenorhabditis* ITS2 sequences are highly species-specific and isolates of a given species differ by a maximum of two nucleotide polymorphisms [8].

3.5 Genetic Identification Through Crosses with Established C. elegans Strains

In combination with ITS2 sequence analysis (Subheading 3.4), or as an alternative, presumptive *C. elegans* species identity of a new isolate can be verified through crosses with known *C. elegans* strains, e.g., the reference strain, N2 (available from the CGC). Place three to four L4 hermaphrodites of the new isolate together with five to ten males of the identified *C. elegans* strains, and vice versa. The presence of a high proportion of males (>30 %) in the F1 progeny indicate successful crossing, thus confirming *C. elegans* species identity.

(Note that *C. elegans* does not produce any cross progeny with any other known *Caenorhabditis* species.)

3.6 Establishment and Cryopreservation of C. elegans Wild Isolate Stocks

1. Strain establishment: derive any new *C. elegans* isolate (i.e., strain) from an isolated single L4 stage hermaphrodite and amplify resulting populations over 4–5 generations, so that isolates can be considered nearly isogenic [6]. Unless individuals are isolated within hours after sampling, it is advisable to derive only a single isolate from a given sampling bag/unit. Given that *C. elegans* proliferates very rapidly, also within the sample after collection, this procedure limits strain establishment of isolates with identical genotypes. Each new *C. elegans* isolate should have a unique name, ideally following *C. elegans* strain naming procedures, i.e., Lab name abbreviation followed by number ID [20].
2. Cryopreservation: All *Caenorhabditis* species can be cryopreserved [6] using standard *C. elegans* protocols, and stored at −80 °C and liquid nitrogen [20]. For a given isolate to be frozen, grow 5–10 NGM plates (55 mm diameter) until starvation when cultures contain a maximum of freshly starved L1 animals. Collect individuals from plates using M9 buffer and place solution into sterile test tube (e.g., 15 mL Falcon tube) and place on ice for 15 min. Centrifuge tube and keep 3 mL of solution containing worms, then add an equal volume

of Freezing Solution to tube and mix well. Aliquot mixture to three cryovials, labeled with strain name. Place cryovials in a small Styrofoam box with slots for holding microtubes (to ensure slow freezing of the worms) and place box in a −80 °C freezer overnight. Transfer tubes to stock collections at −80 °C or liquid nitrogen.

3. Database entry: Add strain information of newly discovered *C. elegans* wild isolates to Wormbase using the following form: http://tazendra.caltech.edu/~azurebrd/cgi-bin/forms/wild_isolate.cgi.

4 Notes

1. To limit fungal contaminations on NGM plates, add 0.01 % thimerosal to water or M9 solution used to moisten the substrate samples.
2. Substrates may harbor diverse microbes that are pathogenic to *C. elegans* [5]. *C. elegans* and other nematode species therefore may show pathologies preventing development or growth, and may also complicate morphological analysis. Moreover, many bacterial contaminants generate thick films on NGM plates rendering observations difficult. To generate clean plates and *C. elegans* cultures, use NaOH–sodium hypochlorite mixture to decontaminate [20].
3. To isolate gonochoristic *Caenorhabditis* species, place either a single mated female (often visible by the presence of a mating plug) or a female plus male to a fresh plate. For detailed isolation methods of gonochoristic *Caenorhabditis* species, *see* [6].

Acknowledgments

This protocol makes use of diverse contributions from the worm community and is primarily based on *Caenorhabditis* isolation methods established by Antoine Barrière and Marie-Anne Félix. Our research is financed by the Centre National de la Recherche Scientifique, France.

References

1. Gaertner BE, Phillips PC (2010) as a platform for molecular quantitative genetics and the systems biology of natural variation. Genet Res (Camb) 92:331–348
2. Andersen EC, Bloom JS, Gerke JP et al (2014) A variant in the neuropeptide receptor npr-1 is a major determinant of *Caenorhabditis elegans* growth and physiology. PLoS Genet 10, e1004156

3. McGrath PT, Xu Y, Ailion M et al (2011) Parallel evolution of domesticated Caenorhabditis species targets pheromone receptor genes. Nature 477:321–325
4. Andersen EC, Gerke JP, Shapiro JA et al (2012) Chromosome-scale selective sweeps shape *Caenorhabditis elegans* genomic diversity. Nat Genet 44:285–290
5. Félix M-A, Braendle C (2010) The natural history of *Caenorhabditis elegans*. Curr Biol 20:R965–R969
6. Barrière A, Félix M-A (2014) Isolation of C. elegans and related nematodes. In: The C. elegans Research Community (ed) Wormbook. http://dx.doi.org/10.1895/wormbook.1.115.2
7. Gimond C, Jovelin R, Han S et al (2013) Outbreeding depression with low genetic variation in selfing Caenorhabditis nematodes. Evolution 67:3087–3101
8. Kiontke K, Félix M-A, Ailion M et al (2011) A phylogeny and molecular barcodes for *Caenorhabditis*, with numerous new species from rotting fruits. BMC Evol Biol 11:339
9. Dolgin ES, Felix MA, Cutter AD (2008) Hakuna Nematoda: genetic and phenotypic diversity in African isolates of *Caenorhabditis elegans* and *C. briggsae*. Heredity 100: 304–315
10. Anderson JL, Albergotti L, Ellebracht B et al (2011) Does thermoregulatory behavior maximize reproductive fitness of natural isolates of *Caenorhabditis elegans*? BMC Evol Biol 11:157
11. Barrière A, Félix M-A (2005) High local genetic diversity and low outcrossing rate in *Caenorhabditis elegans* natural populations. Curr Biol 15:1176–1184
12. Barrière A, Félix M-A (2007) Temporal dynamics and linkage disequilibrium in natural *C. elegans* populations. Genetics 176: 999–1011
13. Felix MA, Duveau F (2012) Population dynamics and habitat sharing of natural populations of Caenorhabditis elegans and C. briggsae. BMC Biol 10:59
14. Haber M, Schüngel M, Putz A et al (2005) Evolutionary history of *Caenorhabditis elegans* inferred from microsatellites: evidence for spatial and temporal genetic differentiation and the occurrence of outbreeding. Mol Biol Evol 22:160–173
15. Petersen C, Dirksen P, Prahl S et al (2014) The prevalence of *Caenorhabditis elegans* across 1.5 years in selected North German locations: the importance of substrate type, abiotic parameters, and *Caenorhabditis* competitors. BMC Ecol 14:4
16. Sivasundar A, Hey J (2005) Sampling from natural populations with RNAI reveals high outcrossing and population structure in *Caenorhabditis elegans*. Curr Biol 15: 1598–1602
17. Caswell-Chen EP, Chen J, Lewis EE et al (2005) Revising the standard wisdom of *C. elegans* natural history: ecology of longevity. Sci Aging Knowl Environ 40:pe30
18. Felix MA, Jovelin R, Ferrari C et al (2013) Species richness, distribution and genetic diversity of *Caenorhabditis* nematodes in a remote tropical rainforest. BMC Evol Biol 13:10
19. Kiontke K, Sudhaus W (2006) Ecology of Caenorhabditis species. The C. elegans Research Community (ed) Wormbook. http://dx.doi.org/10.1895/wormbook.1.37.1
20. Stiernagle T (2006) Maintenance of C. elegans. The C. elegans Research Community (ed) Wormbook. http://dx.doi.org/10.1895/wormbook.1.101.1
21. Felix MA, Braendle C, Cutter AD (2014) A streamlined system for species diagnosis in *Caenorhabditis* (Nematoda: Rhabditidae) with name designations for 15 distinct biological species. PLoS One 9, e94723
22. Sudhaus W, Fitch D (2001) Comparative studies on the phylogeny and systematics of the Rhabditidae (Nematoda). J Nematol 33:1–69
23. Sudhaus W, Kiontke K (1996) Phylogeny of Rhabditis subgenus *Caenorhabditis* (Rhabditidae Nematoda). J Zoo Syst Evol Res 34:217–233
24. Chiang JT, Steciuk M, Shtonda B et al (2006) Evolution of pharyngeal behaviors and neuronal functions in free-living soil nematodes. J Exp Biol 209:1859–1873

Chapter 17

A Primer on Prototyping

Dylan Lynch and David Biron

Abstract

Standard mechanical components, such as adapters or mounts, are ubiquitous in research laboratories, *C. elegans* labs included. Recently, in-house prototyping and fabricating both standard and custom mechanical parts has become simple and cost effective. Here we describe the basic steps, equipment, and considerations required for rapid prototyping of a handful of simple yet useful designs. These examples were chosen for their simplicity, as well as for demonstrating specific practicalities. They are thus appropriate as training exercises.

Key words Prototyping, Fabrication, Laser cutting, 3D printing

1 Introduction

1.1 In-House Prototyping

Mechanical components of instrumentation are not the first thing that springs to mind when thinking of a *C. elegans* lab, but they are abundant and often essential. These may include holders for pipettes, tubes, or other common items, or custom designed and fabricated parts such as adapters, mounts, or frames required for a specific experimental setup. New technologies for rapid prototyping have lowered the cost of design and production such that the cost of prototyping equipment can be offset by average usage. When multiple iterations of design and trials are required, in house prototyping equipment can speed up research and become highly cost effective. Moreover, such equipment can be seamlessly and effectively shared between several labs with similar prototyping needs, a department, a center, or an institute.

Two primary technologies, laser cutting and 3D printing, are particularly interesting due to their abilities to create complex objects from a wide variety of materials with minimal user experience and training. Laser cutters are able to quickly cut a wide variety of materials, many of them inexpensive and biocompatible. A typical instrument would achieve a tolerance of 0.01″. Importantly, translating an idea to a physical prototype merely

David Biron and Gal Haspel (eds.), *C. elegans: Methods and Applications*, Methods in Molecular Biology, vol. 1327,
DOI 10.1007/978-1-4939-2842-2_17,

requires an electronically drawn design using widely available software. Alternatively, 3D printers can quickly fabricate complex 3D shapes, and achieve tolerances of 0.001″. Designing 3D objects on a Computer Aided Design (CAD) program can become involved, as compared to 2D illustrations. However, a great number of useful designs are simple and require only a minimal level of training and skills. Thus, a novice user can learn to effectively use a laser cutter in several hours and a 3D printer in several days. In contrast, standard machine shop techniques typically require significant training and practice, while purchasing mechanical parts may be expensive, time consuming, or both.

1.2 Laser Cutting

Laser cutting enables in house rapid prototyping of custom objects that may require several design iterations. Complex prototypes can be quickly cut from a large variety of materials, including plastics, woods, rubbers, foams, papers, cloth or thin leather, and thin metals. Importantly, materials intended for cutting should not contain chloride or emit other poisonous fumes, e.g., PVC, Acrylonitrile butadiene styrene (ABS), chlorine-containing rubbers, or fiberglass. Tables detailing materials recommended and not recommended for cutting are readily available online. Acrylic is a particularly attractive material for laser cutting: it offers durability and strength, it is inexpensive, and it can be chemically welded to allow for layered 3D constructions. Delrin (POM) can also be used when higher rigidity and solvent resistance is required with the tradeoff that the resulting objects are more difficult to bond. We have found that laser-cut parts are sufficiently strong for a large number of applications in the lab and can often successfully replace machined metal. Moreover, complex shapes can be very difficult to machine. Thus the benefits of cutting often outweigh the loss in strength and precision as compared to machined metal.

While the model and power of individual laser cutters will dictate some specific details, the basic design rules apply broadly. The laser allows for vector cutting, vector engraving, and raster engraving. The vector modes follow paths drawn in a vector-editing program while the raster mode can use grayscale bitmaps to engrave images. The software provided with the instrument automatically translates the vector drawing to the commands required to physically move the laser "knife" in a path that will result in performing the required work. Commonly, laser cutters operate using colored hairline vectors and therefore any program capable of generating such files will be sufficient. A few commonly available options are listed in Subheading 2.

When drawing paths, care must be taken to maintain proper connectivity of points. Otherwise, the laser cutter may make cuts in an undefined order, which can lead to unexpected results. For instance, internal holes should be physically cut prior to the outline of the part that contains them. Cutting the outline first may result in

the part shifting inside the instrument and, as a result, holes being cut at an offset with respect to their intended positions. A proper vector drawing would translate to a proper path of physical cutting.

We present examples of laser cut prototypes below, chosen for their simplicity and wide applicability. These or similar examples can be used to train a user in laser cutting. The first example is a pipette holder assembled from four individually cut parts. The second is a microfluidic junction that provides an example of a layered construction. This junction uses a single cut of the laser to make channels. The width and shape of the channel can be altered in a fraction of the time and cost it would take using common lithography methods for microfluidics. However, the minimum feature size of 0.01″ is large as compared to the one attainable by lithography. The third example demonstrates the ease of fabricating custom mounts for microscope slides. The turnaround time from design to prototype can be as short as 1 h—significantly shorter than machining using traditional methods.

1.3 Three-Dimensional Printing

There are several types of 3D printers and this technology is still rapidly evolving. Currently, the most common types used for scientific research are fused deposition modeling (FDM), stereolithography (SLA), and fused powder printing. Between these technologies, a myriad of materials can be printed. Examples include Acrylonitrile butadiene styrene (ABS), polylactic acid (PLA), photopolymer resins such as methylacrylate acid ester, water-soluble plastics such as polyvinyl alcohol (PVA) for support structures, and even metals such as titanium. Shapes can be printed that would be impossible to fabricate using traditional machining methods. The finer points of 3D printing could fill a book [1]. Here we will briefly describe the basic process and the major benefits and drawbacks of each of the three common technologies.

While some commercial printers use proprietary communication protocols, the basic steps of prototyping are the same for every type of printer. At the core, 3D printing is based on standard Computer Numerical Control (CNC) machining technology: a process that uses a computer to control machine tools such as lathes, mills, or grinders in 3D space. After an initial CAD design is created, it requires translation to specialized CNC machining language. This language is specifically designed for programming the exact positioning, velocity, and coordination of the tool. Thus, control software is required to serve as an interface between the user-made CAD design and the CNC machine.

After modeling an object using a CAD program (*see* Subheading 2), the file is exported to a slicing application. This application allows the user to orient the model in the machine's build volume, automatically adds support structures, and computationally slices the model into horizontal planes. Finally, the slicing program generates the tool path instructions for the printer

head, i.e., the physical path in real space that the printer head will follow in order to fabricate the desired 3D shape. This file is then sent to the aforementioned control software that translates it to appropriate commands for the machine. These separate tasks can be combined within one program or done separately.

FDM printers are the least expensive machines on the market. They are often small and can easily fit on a desktop. An FDM printer functions by heating a thermoplastic filament and depositing the material in a vectored manner. Acrylonitrile butadiene styrene (ABS) and polylactic acid (PLA) are the two workhorse materials. However other materials can be printed including nylon and Delrin (POM). FDM printers can print multiple materials in one print, which can be used to print water-soluble temporary support structures. The cost of these machines currently ranges from $200 to 20,000. Many open-source do-it-yourself designs of FDM printers exist, as well as a variety of commercial printers. The inexpensive (sub $2000) printers offer professional level printing but suffer from poor reliability and require significant maintenance and technical skills in order to keep them functional. More highly priced production printers are capable of running with little intervention beyond basic upkeep.

Stereolithography instruments are typically slightly more expensive ($1000+). An SLA printer uses a UV laser to cure a liquid resin. Instead of drawing layers in a vectored format, SLA printers expose entire layers to the curing laser in a single pass. As a result, their print time is much quicker than that of FDM printers and only depends on the height of the target object. An important limitation of this technology is that the materials printed are required to be photopolymer resins. As a result, material costs are higher as compared to FDM printing and biocompatibility, if required, should be verified in advance. A major advantage of SLA technology is that it is capable of easily producing very thin layers. Consequently, extremely fine structures can be printed quickly. While the majority of SLA printers are commercial grade machines, some open-source designs do exist. However, considerable technical expertise would be required for safely operating an open-source stereolithography instrument.

Finally, fused powder machines use chemical binders or heat to fuse granular material together one layer at a time. As the part is printed, single layers of powder are sequentially added to its top-side and the particles are bonded according to the target design. A major advantage of this technology is that it can make use of a wide range of materials. Some fused powder printers can even print in full color. Materials ranging from powdered sugar to powdered titanium can be printed with resolutions that depend on the binder and the size of the original particles. The high cost associated with this technology is a major drawback—an affordable model can cost several tens of thousands of dollars. Therefore, this technology is more common in industrial production environments. Still, for some

research applications, the ability to work with exotic materials and achieve high precision and complexity can be crucial.

We present two examples of 3D printed objects that can be useful in a *C. elegans* lab environment. The first is a camera mount that would be considerably more difficult to construct in a standard machine shop. The design securely couples a small scientific camera to a customized microscope body. The second application is a 3D model of the *C. elegans* nematode that can be used for instruction and demonstration. The CAD files for the model nematode are available from the Virtual Worm Project [2].

2 Materials

2.1 Laser Cutting of Acrylic Sheets

1. A cast acrylic sheet.
2. Acrylic welding solution: 10:1 dichloromethane to glacial acetic acid.
3. Gap-filling acrylic glue: add 5.0 g acrylic scrap to 50 ml acrylic welding solution and allow to dissolve.
4. Illustration software, e.g., Inkscape, Corel Draw, Illustrator.

2.2 Three-Dimensional Printing with an FDM Printer

1. A thermoplastic filament, e.g., ABS or PLA.
2. CAD program, e.g., Sketchup, Blender3D, Autodesk 123D.
3. Slicer/Control Program, e.g., Cura, Pronterface, Slic3r, Simplify3D.

3 Methods

3.1 A Laser-Cut Microfluidic Junction

1. Refer to the documentation for your specific laser cutter for safety information and operating instructions.
2. Draw the object as a vector file—an example design is depicted in Fig. 1. Pieces can be nested to save material. For precise fitting, account for the kerf of the laser (the width of the laser cut is typically ~0.01″).
3. Use single lines to cut channels with a minimum channel width of the laser kerf.

Fig. 1 A Y-Junction for microfluidics made of 1/32″ clear cast acrylic. (**a**) The design of the six layers of the part. (**b**) An image of the part

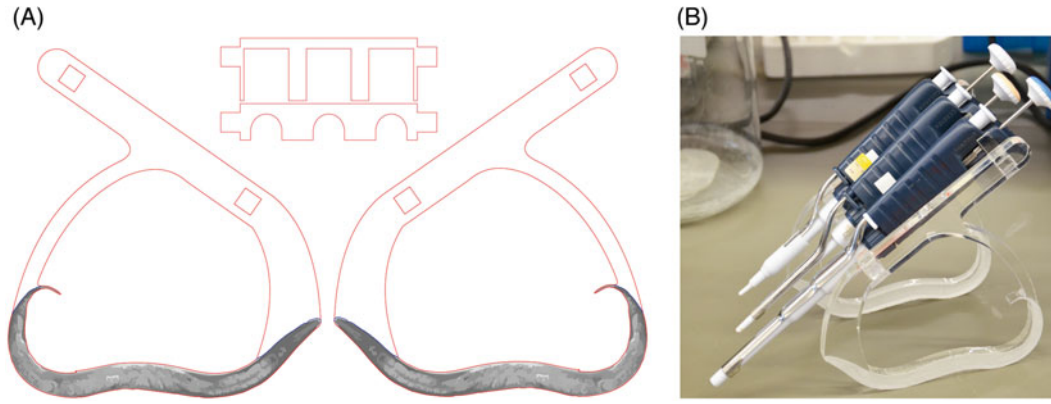

Fig. 2 A micropipette rack with an engraved *C. elegans* design made of 3/8″ clear cast acrylic. (**a**) The design of the four components of the part. (**b**) An image of the part

4. Separate the parts and remove any backing paper from the acrylic. Use tape to clean any ash from the parts.
5. Lay all of the parts together on a paper towel stacked in their final configuration.
6. Using a micropipette, weld the parts by bringing a drop of welding solution near the space between parts. Capillary action will draw the solvent between the parts. Run along all spaces until the capillary forces no longer visibly wick the solvent.
7. Leave the acrylic undisturbed for 30–60 s, at which point the joint will be set permanently. The bond will strengthen over the first 24 h.

3.2 A Laser Cut Pipette Holder

1. *See* **steps 1** and **2** above. An example design is depicted in Fig. 2.
2. Incorporate in the design a system of tabs and slots to hold the parts together. Butt joints are often weak due to small irregularities in the laser cut edge.
3. The engraved graphics are provided for the purpose of illustration. In this example, they were designed as greyscale bitmaps for raster engraving augmented with vector engraving lines to accent different parts of the drawing.
4. Separate the parts and remove any backing paper from the acrylic. Use tape to clean any ash from the parts.
5. Assemble the parts on a paper towel in their final configuration.
6. Use a similar approach to **step 6** above to weld spaces with tight clearance. For larger gaps, apply space-filling glue to fill the gap. Multiple applications of gap filling glue may be necessary to fill larger spaces.
7. Allow 2 h for the glue to set and 24 h to fully cure.

3.3 A Laser Cut Microscope Mount

1. *See* **steps 1** and **2** above. An example design is depicted in Fig. 3.
2. Since properly centering the parts is important in this design, use vector engraved lines to aid alignment when welding.
3. The laser generates some amount of ash and dust that needs to be cleaned in a sink before welding the parts in order to prevent debris from reaching optical components.
4. The black acrylic helps to prevent glare and reflections that could occur with clear acrylic.
5. Note that this design used $5 of materials and 15 min to design and cut.

3.4 An FDM Printed Camera Mount

1. Design the file in your CAD program of choice. The example design depicted in Fig. 4 was created with Blender3D (*see* Subheading 2).
2. This design uses a circular barrel to fit into the microscope mount and a square receptacle for the camera. This is an example of a shape that would be significantly more difficult to machine using traditional subtractive methods.

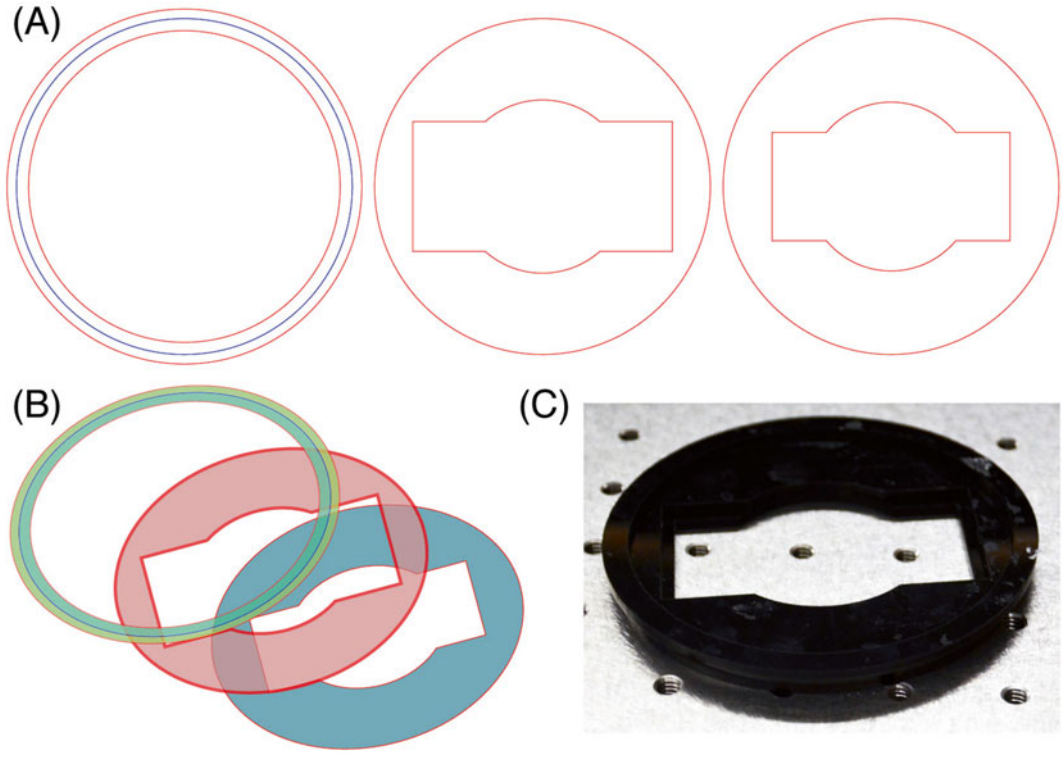

Fig. 3 A laser-cut microscope mount for glass slides made of 1/8″ black cast acrylic. (**a**) The design of the three layers of the part. (**b**) A sketch of the assembly of the three concentric layers. The bottom layer supports the slide, the middle layer positions the slide, and the top layer fits into a standard round microscope stage port. (**c**) An image of the part

3. The design was printed in at 0.2 mm layer height in PLA. The cost of the material was under 10 cents and the print took 10 min.
4. If the sizing needs adjustment, changes can be made and a new part can be quickly printed. The object depicted in Fig. 4 was correctly sized after three iterations. In this simple design, the aluminum thread of the microscope body threads the soft plastic.

3.5 An FDM Printed Three-Dimensional Model of C. elegans

1. Download the files from the OpenWorm project [2]. The freely available files can be edited using Blender3D.
2. We selected the cuticle model and hid other features—*see* Fig. 5. However, OpenWorm models are organized according to anatomical systems such that particular aspects of the anatomy can be individually printed. For instance, using water-soluble supports would enable printing the complex nervous system.
3. In order to prepare the model for printing it must be a closed mesh. Use Blender3D to close the holes in the model for the mouth, secretory pore, and vulva. Delete the inner geometry

Fig. 4 A custom microscope mount for a scientific camera printed in white PLA. (**a**) An image of the 3D computer-aided design of the part. (**b**) An image of the printed part with and without a scientific camera. The barrel was designed to fit a non-standard microscope thread

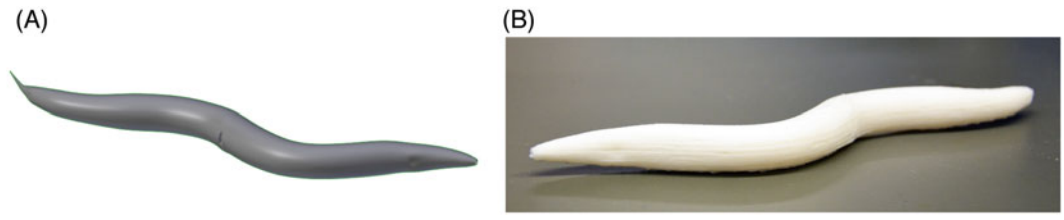

Fig. 5 A *C. elegans* adult hermaphrodite printed in white PLA. (**a**) An image of the 3D computer aided design of the part. (**b**) An image of the printed part

of the model to leave only the geometry of the outer shell. Prior to printing, it is recommended to use a tool for automatically identifying unprintable features (available in Blender3D).

4. The design was printed in at 0.2 mm layer height in PLA with support structures and inner fill. The cost of plastic was under $1 USD and the print took about 40 min.
5. The printed object can show fine details and structures and can be useful for demonstration of worm anatomy.

4 Notes

1. During production, acrylic sheets are either *cast* or *extruded*. Mixing liquid ingredients in molds, resulting in a homogeneous material, produces cast acrylic. In contrast, continuously extruding acrylic through a form results in varying mechanical properties, depending on the direction (relative to the extrusion direction). Cast acrylic is more convenient for laser cutting because extruded acrylic stores stresses from the extrusion process and can thus bend or break more easily.
2. As either form of acrylic is, in principle, suitable for laser cutting, additional considerations may apply. Extruded acrylic has a lower melting point and results in fire-polished glassy edges when cut; however, engraving performance is poor. Cast acrylic has slightly hazy edges when cut but turns frosted when engraved, resulting in improved visibility. Most importantly cast sheets have a very high tolerance (~15 %) and designs should account for the measured, rather than specified, thickness of the sheet.
3. The consistency of acrylic glue should be similar to two-part epoxy. The solution can be stored in an airtight container for long periods of time.
4. A pinned tenon joint can help align the layers in a repeatable way.
5. Using force to hold the joints together will cause crazing in the acrylic when it is bonded. Any tape will trap solvent and mar the surface of the acrylic.
6. Clear acrylic is easy to work with since the glue is visible. To get optically clear joints flood the joint and leave undisturbed.
7. In our experience, the welded joint is often stronger than the acrylic and the part will mechanically fail before the joint does.
8. The vaporizing acrylic leaves a slightly beveled edge that is not suitable for butt joints.
9. FDM printers often produce holes approximately 2 % smaller than designed. If so, account for this tolerance in the design file.

Acknowledgements

This work was supported by the NSF IOS grant no. 1256989. We thank E. Efrati for useful discussions.

References

1. Lipson H, Kurman M (2013) Fabricated: the new world of 3D printing. Wiley, Indianapolis, IN
2. Palyanov A, Khayrulin S, Larson SD, Dibert A (2012) Towards a virtual *C. elegans*: a framework for simulation and visualization of the neuromuscular system in a 3D physical environment. In Silico Biol 11(3-4):137–147

Chapter 18

A Primer on Quantitative Modeling

Iulia Neagu and Erel Levine

Abstract

Caenorhabditis elegans is particularly suitable for obtaining quantitative data about behavior, neuronal activity, gene expression, ecological interactions, quantitative traits, and much more. To exploit the full potential of these data one seeks to interpret them within quantitative models. Using two examples from the *C. elegans* literature we briefly explore several types of modeling approaches relevant to worm biology, and show how they might be used to interpret data, formulate testable hypotheses, and suggest new experiments. We emphasize that the choice of modeling approach is strongly dependent on the questions of interest and the type of available knowledge.

Key words Mathematical modeling, Developmental patterning, Computational neuroscience, Behavior

1 Introduction

Many of the characteristics that make *C. elegans* an ideal model organism for studying wide range of biological phenomena also make it particularly suitable for acquisition of quantitative data. These properties include the transparency of the worm, which allows quantitative measurements of gene expression, neural activity and molecular dynamics in vivo, its small size, which allows tracking of individual and group behavior, and its short generation time and lifespan, which permits quantitative characterization of aging and evolutionary dynamics. In order to fully take advantage of these quantitative measurements, quantitative modeling is required. A model, formulated and analyzed in mathematical terms, can be used to mine the data, formulate hypotheses, and suggest new experiments.

The problem of formulating a quantitative model of a real biological scenario may often seem ill posed, since it is frequently the case that many of the biological details, such as kinetic rates or complete descriptions of underlying mechanisms, are not available. Yet, provided that the levels of details assumed by the model correctly represent the scale of available data, and that the

David Biron and Gal Haspel (eds.), *C. elegans: Methods and Applications*, Methods in Molecular Biology, vol. 1327,
DOI 10.1007/978-1-4939-2842-2_18,

assumptions made in designing the model are explicit and well defined, much progress can be made by crafting a model tuned to address a well-defined question. A successful model will combine the available data and the researcher's intuition, and will have the power to make testable predictions.

Fruitful quantitative modeling of biological systems requires knowledge and insight in both a quantitative discipline (e.g., applied math, physics, or computer science) and in the relevant branch of biology. Not surprisingly, many successful examples are the product of interdisciplinary collaborations, yet construction of simple models is within reach of any scientist.

The aim of this chapter is to introduce some of the ideas, opportunities, and considerations of modeling complex biological systems. Through several examples from the recent *C. elegans* literature we present a few modeling approaches that handle partial knowledge at different levels of abstraction. We describe these approaches in broad strokes and put emphasize on their distinctive advantages, while suppressing technical details. These can be found in the primary literature or in textbooks on mathematical and systems biology.

2 Modeling with Partial Information: The Case of Vulva Development

2.1 Background

The development of the worm vulva is a much-studied example for pattern formation and cell differentiation. The simple geometry of the vulva and the small number of well-specified cell types make it an attractive model for quantitative modeling. In wild-type worms a line of 6 vulval precursor cells (VPCs) adopt an invariant pattern of cell fates (denoted 1°, 2°, and 3°) in a robust pattern (3°3°2°1°2°3°). This pattern is specified by two signaling pathways, EGF signaling emanating from the anchor cell proximal to the 1° VPC, and lateral Notch signaling between neighboring VPCs. Over the years an array of mutants that show perturbed patterns has been characterized. Interestingly, many mutant lines show variable phenotype between different (but genetically identical) worms.

Despite the apparent simplicity of this system and the substantial progress made in elucidating molecular mechanisms that drive its developmental patterning, it is still true that little is known about the quantitative properties of this system such as kinetic rates, the profile of the (presumed) EGF gradient, the biochemical properties of the mutual inhibition between EGF and Notch, and more. Nevertheless, much progress has been made in applying multiple modeling methodologies to this system, thus making it a convenient context for exploring possible approaches of general applicability.

2.2 Formal Models

Every researcher who studies a natural system has some working model that summarizes his or her assumptions about how that system works. New data is interpreted within this model and is used to update it. The model in turn guides the formulation of new

hypotheses and the design of new experiments. Quite often the current version of the model is depicted with blocks and arrows on the whiteboard in the researcher's office: parts of the diagram may have been drawn years ago and are no longer dry-erasable, while others have been added more recently based on the latest results from the lab. Often the most updated version of this model appears in figures accompanying the discussion sections of published papers.

Formal models are a computational approach that aims to turn these pictorial models into executable computer programs. These models define modules of the system (such as cells or pathways) as semi-independent entities that evolve among a finite set of states according to some predefined rules, which may depend on the state of other modules. The main advantage of these approaches is that they require very little quantitative input; their main drawback is their limited capacity for quantitative predictions. Still, formal models are excellent for systematically challenging the working model, for identifying potential inconsistencies, and for formulating new hypotheses.

For example, a formal model for vulval patterning has been developed by Fisher and coworkers [1–3] based on a working model proposed by Sternberg and Horvitz [4]. Execution of the model revealed that it could account for all known phenotypes only if one prohibits simultaneous commitment of cells to their final fate, and explained the unstable phenotype associated with a particular mutant as a consequence of the loss of the sequential signaling. The model thus resulted in a testable hypothesis that had been later verified experimentally. A systematic analysis of the model, using a methodology known as *model checking*, exposed discrepancies between model predictions and known phenotypes, and led the authors to conjecture a previously unknown negative feedback loop.

Formal models and model checking are popular tools used in hardware and software development. Tools that implement them—including Petri-nets, interacting state machines, hybrid automata, and more—are available online, and examples for their adaptation for analyzing complex biological phenomena can be found in the literature.

2.3 Kinetic Models and Phase Space Analysis

While formal models offer a high level abstraction of the underlying logic of a system, kinetic models may be more appropriate for addressing questions about the roles and relative importance of molecular mechanisms, the sensitivity of the systems to particular parameters, and the kinetic response to quantitative perturbation.

Kinetic models are cast in the form of coupled differential equations. Each equation described the way the time evolution of a component (e.g., the spatial profile of a signaling molecule, the concentration of an mRNA, or a protein species in each cell) depends on the concentrations of other molecules in the system. Of major concern is the fact that these equations are specified in terms of many kinetic and biochemical parameters that are not

known but are absolutely required for simulating the model. Still, a correct formulation of the model can yield significant insight and offers possible answers to well-formulated questions.

For example, a kinetic model of vulval development has been developed by Giurumescu and coworkers [5, 6]. Rather than attempting to model all known components of the system, the authors focused on two key signals in each cell, the MAP kinase and the Notch signal. Analyzing such models starts by identifying ways to combine parameters, such that the model behavior does not depend on each parameter separately but on the way parameters are related with each other. This step can already reveal constraints on the design of the system: It allowed Giurumescu et al. to ask how lateral coupling among VPCs enhances the response of the system to the extracellular EGF gradient while keeping the system robust.

Combining microscopic parameters into effective ones reduces the dimensionality of the *phase space* of the model. Each point in phase space corresponds to a particular assignment of values to the different effective parameters. The reduction in dimensionality allows effective scanning of the phase space and predicting—within the model—how different phenotypes arise from different combinations of parameters. Characterization of the phase space of the proposed kinetic model for vulval patterning showed that significant regions of this space yield phenotypes observed in *C. elegans*, while other regions correspond to phenotypes observed in other species of the *Caenorhabditis* genus. It also uncovered the fact that other choices of parameters may lead to many phenotypes that are not observed experimentally, presumably due to the fact that none of these phenotypes occupied a significant area in phase space.

Thus, analysis of the phase space of a kinetic model can lead to insights about the plasticity and evolvability of the network, even in the absence of detailed knowledge of the underlying parameters. Kinetic modeling allows exploring wide range of possible parameter values, unlike overexpression experiments and genetic knockouts, which explore the extreme ends of this range.

2.4 Phenomenological Models

The fates of cells were famously described by Waddington in terms of valleys in an epigenetic landscape [7]. Within the theory of dynamical systems, cell fates correspond to alternative fixed points and the valleys correspond to their basins of attraction.

Detailed kinetic models like the one discussed above can be analyzed within the framework of dynamical systems to classify potential fixed points and the "decision points" between them, and to investigate their stability and parameter dependence. However, this route assumes that a correct detailed model is available. An alternative option is to step back from the molecular scale and describe the dynamics in terms of a flow in a phase space that

harbors the expected fixed points. Knowledge of the signals that drive the system and the outcomes of genetic perturbations dictate the modeled geometry of this phase space, which in turn allows formulation of new hypotheses. Ultimately, translating these predictions to experimental design requires detailed familiarity with underlying molecular mechanisms, but does not depend on its details and is not sensitive to its parameterization.

This approach is beautifully demonstrated in a model of vulval development by Corson and Siggia [8]. The developmental dynamics of each cell is described in terms of a flow in a phase space that carries three fixed points (corresponding to fates 1°, 2°, and 3°) starting from an initial point (that is identical for all cells). Phase space is assumed to be effectively two dimensional (corresponding loosely to the two signaling pathways that govern the dynamics). Signals received by each cell shift the boundaries between the different basins of attractions, thus placing different cells in the basin of attraction of different fixed points. The equations that govern the dynamics in this phase space are not meant to describe any molecular mechanism: rather, they are constructed as the minimal model that captures the current understanding of how the signaling network functions and recovers known experimental results. Genetic and ablation perturbations are then described in terms of the structure of these boundaries, and epistatic interactions are understood as the cumulative effect mutations have on their geometry. In this model, for example, epistasis between Notch and EGF signaling is captured by the fact that to cross a boundary line between two fates that is not parallel to either axis requires either a large step in one direction (corresponding to induction of one of the signals) or the combination of two smaller step in both directions (corresponding to weaker simultaneous induction of both signals).

The mapping between the fate of a cell and the basin of attraction in which it resides can also be used to understand partial penetrance and sensitivity to noise. For example, a mutation that places a transition line close to the developmental trajectory of a cell would make this cell more sensitive to noise, as small fluctuations may send this cell across the transition line and towards a different cell fate.

Phenomenological models are a powerful tool because they are minimally parameterized, and their qualitative features are used to determine the flow topology. This allows making direct testable predictions that challenge the fundamental understanding of the functionality of the system, without being obscured by arbitrary choices of parameters. The success of such a model, however, strongly depends on the ability to clearly define the questions that it aims to address, making sure that some presumed answers to these questions are not already present in the very definition of the model.

3 Models of Neural Control of Behavior

3.1 Background

C. elegans are a neuroscientist's playground. The nervous system of an adult hermaphrodite is comprised of a mere 302 neurons, eight orders of magnitude smaller than that of a human. Nonetheless, such a simple system is capable of complex behaviors, such as sexual behavior, foraging for food, learning and memory, stimuli response and locomotion. As opposed to the crippling computational complexity faced when attempting to theoretically and computationally model many neural circuits, the small size of this system provides many opportunities for modeling.

Like any system in biology, the nervous system can be studied at different scales. As we exemplify next, different mathematical modeling approaches can be used to address questions at different scales, or can be used to bridge between them.

3.2 Modeling a Single Neuron: Linear–Nonlinear Models

A robust method for generating phenomenological models of neuronal responses to current inputs is the linear–nonlinear (LN) cascade. The approach is particularly useful when one is looking for a qualitative understanding of the overall temporal dynamics of a network, without necessarily being interested in its biophysical details. This method estimates the output of a neuron by successively applying a linear temporal filter and a static nonlinear transformation to the sensory signal [9]. The linear filter accounts for how the neuron integrates the stimulus over time; its output is a linear function of the input. The nonlinearity is equivalent to the neuron's input–output function.

The literature provides several options for choosing the linear filter, and the final choice is likely to depend on personal preference and the nature of the analyzed data [10, 11]. One of the easier options is to define the filter as the sum of orthonormal basis functions of increasing frequency $F_{\mathrm{NL}}(t) = \sum_j a_j \sin 2\pi jt/\tau$ for $t \le \tau$. The nonlinearity can be a power law function fitted to the measured output response [11].

The LN model is therefore a powerful tool, since its properties can be directly associated with different behaviors and mechanisms. Once the model has been obtained from input–output measurements, it can be used to predict response and characterize its accuracy for other types of stimuli. In the study of *C. elegans*, as well as for other organisms, this method is useful in the study of neurons that produce responses that vary over time. For example, chemosensory neurons in *C. elegans* respond precisely to stimulus perturbations; the LN model was used to understand how sensory signal transduction mutations disrupt the response and how the neuron dynamics affect sensory-driven behaviors [11].

3.3 Modeling a Neural Circuit

Neural circuits can be modeled, in analogy with electric circuits, as a wiring of resistors and capacitors. From a modeling perspective, one of the advantages of *C. elegans* neurons is that they are assumed to be isopotential and do not generate sodium-based action potentials, such that a neuron's membrane potential V_i can be used to describe its state. Each neuron is modeled as a capacitor with capacitance C_i that receives input from three different sources: the postsynaptic activity of a different neuron, leakage current due to its input resistance R_i, and perhaps also neurons or cues external to the circuit [12]. A network of interacting neurons can be described by a set of coupled nonlinear differential equations:

$$Ci\frac{dV_i}{dt} = -\frac{1}{R_i}V_i + \sum_j g_{ij}I_j + I_i^{\text{ext}}.$$

The matrix g in this equation accounts for the active connections between neurons. The last ingredient of a concrete model is a mapping between the activity of neurons and the behavior in question.

Such models allow understanding how different classes of neurons interact to produce robust responses to external stimuli, and can elucidate how behavior results from network topology. Several simple yet powerful circuits in *C. elegans* have been successfully modeled using this method. For example, the motor circuit for forward movement is made up of eight classes of motoneurons, whose connectivity motif is consistent along the animal's length. A simulation of this circuit was able to reproduce the oscillatory behavior associated with crawling [13]; a similar model yielded a connection between the frequency of the oscillations and muscle gap-junction coupling [14].

3.4 The Connectome

A focus of current neuroscientific research is connectomics, the effort to produce exhaustive maps of the synaptic connections within the nervous system. For many organisms, however, the overall system is too complex to be thoroughly mapped, and thus it is difficult to infer function from the network connectivity. On the other hand, the wiring diagram of the *C. elegans* neural system has already been mapped for more than 25 years, and is being actively investigated [15, 16]. Advances in electron microscopy will make the acquisition of such extensive data easier and cheaper, and techniques from graph theory will become more and more essential in extracting relevant information.

A graph is a collection of nodes (also called vertices) and edges, specified by an adjacency weight matrix A such that the element A_{ij} accounts for the presence (and sometimes weight) of a connection between node i and node j. Mathematical software packages such as Matlab provide straightforward resources for obtaining relevant

properties from the adjacency matrix. For example, properties of individual nodes (such as the number of nodes it is connected to or the number of shortest paths in the graph that go through it) can indicate the centrality of its role in the functionality of the network, and global properties of the network (such as its diameter or modularity) provide information about its organization. In addition, many clustering algorithms that aim to identify modules in the networks are widely available and used in systems biology and systems neuroscience.

Using techniques from graph theory one can sort through the extensive data that is already associated with the *C. elegans* connectome, and identify areas of interest where further research can be focused. For example, analyses of network properties have helped identify groups of highly connected interneurons of the locomotor circuits; these neurons might be responsible for the nematode's coordinated movement [17]. Centrality analysis of the pharyngeal connectome was used to understand how neuronal rewiring is responsible for the differences in feeding behavior between of *C. elegans* and the predatory nematode *Pristionchus pacificus* [18].

3.5 Compressed Representation of Behavior

Dimensional reduction is a popular concept in data science, where a large number of correlated observations are represented by a smaller set of uncorrelated features. A popular method of dimensional reduction is principal component analysis (PCA) that is of abundant use in genomics and systems biology.

C. elegans produce reproducible, repetitive, stereotypical shapes. A snapshot of a worm posture can be represented by a set of coordinates along its midline, but these coordinates are highly correlated. To reduce dimensionality of the data, one can alternatively represent each worm posture as a superposition (that is, a linear combination or a weighted sum) of a small set of stereotypical shapes, popularly called "eigenworms" [19]. A particular shape is then specified in terms of the weight (or "amplitude") of each eigenworm in the sum, and the motion of the worm is captured by the temporal changes in these weights.

Behavioral data in the form of trajectories of individual worms can be captured at large scale and high precision, and dimensional reduction of these data is required to facilitate its analysis. Indeed, representation of these data in terms of eigenworms enabled to detect subtle differences in movement strategy among dopamine receptor mutants [20], to cluster genetic perturbations based on their impact on locomotion [21], and to study the response of worms to stimuli [22].

4 Notes

1. Mathematical modeling is an efficient way to summarize knowledge, formulate the current view of a system's mechanisms and functionality, test the implications of these views

and formulate new hypotheses and testable predictions. When formulated correctly, mathematical modeling is useful even if the knowledge of underlying details is limited. We emphasize the importance of matching the modeling approach to the questions of interest and to the available data.

2. The models discussed above focus on signaling and information flow, and do not account for the physical aspects of the systems in question. Physical properties of cells, organisms and their environment (such the mechanics of membranes, the hydrodynamic interactions among vesicles and cellular organelles, or the viscosity of the surrounding liquid) play important role in development, signaling and behavior. Physical models of soft materials have been extremely valuable, for example, in understanding the specification of zygotic cell polarity [23–25] or the action of the pharyngeal pump [26].
3. This chapter provides examples for alternative modeling approaches at different scales, with emphasis on examples from the *C. elegans* literature. This list is in no way comprehensive, and many other valuable examples can be found in the primary literature.

Acknowledgements

This work was supported by the NSF grants MCB-1413134 and PHY-1205494.

References

1. Fisher J, Piterman N, Hubbard EJA, Stern MJ, Harel D (2005) Computational insights into Caenorhabditis elegans vulval development. Proc Natl Acad Sci U S A 102:1951–1956
2. Fisher J, Piterman N, Hajnal A, Henzinger TA (2007) Predictive modeling of signaling crosstalk during C. elegans vulval development. PLoS Comput Biol 3, e92
3. Nusser-Stein S, Beyer A, Rimann I, Adamczyk M, Piterman N, Hajnal A, Fisher J (2012) Cell-cycle regulation of NOTCH signaling during C. elegans vulval development. Mol Syst Biol 8:618
4. Sternberg PW, Horvitz HR (1989) The combined action of two intercellular signaling pathways specifies three cell fates during vulval induction in C. elegans. Cell 58:679–693
5. Giurumescu CA, Sternberg PW, Asthagiri AR (2006) Intercellular coupling amplifies fate segregation during Caenorhabditis elegans vulval development. Proc Natl Acad Sci 103:1331–1336
6. Giurumescu CA, Sternberg PW, Asthagiri AR (2009) Predicting phenotypic diversity and the underlying quantitative molecular transitions. PLoS Comput Biol 5, e1000354
7. Waddington CH (1957) The strategy of the genes; a discussion of some aspects of theoretical biology. Allen & Unwin, London
8. Corson F, Siggia ED (2012) Geometry, epistasis, and developmental patterning. Proc Natl Acad Sci U S A 109:5568–5575
9. Ostojic S, Brunel N (2011) From spiking neuron models to linear-nonlinear models. PLoS Comput Biol 7, e1001056
10. Ozuysal Y, Baccus SA (2012) Linking the computational structure of variance adaptation to biophysical mechanisms. Neuron 73:1002–1015
11. Kato S, Xu Y, Cho CE, Abbott LF, Bargmann CI (2014) Temporal responses of C. elegans chemosensory neurons are preserved in behavioral dynamics. Neuron 81:616–628

12. Hopfield JJ, Tank DW (1986) Computing with neural circuits: a model. Science 233:625–633
13. Kunert J, Shlizerman E, Kutz JN (2014) Low-dimensional functionality of complex network dynamics: Neurosensory integration in the Caenorhabditis connectome. Phys Rev E Stat Nonlin Soft Matter Phys 89(5):052805
14. Karbowski J, Schindelman G, Cronin CJ, Seah A, Sternberg PW (2007) Systems level circuit model of C. elegans undulatory locomotion: mathematical modeling and molecular genetics. J Comput Neurosci 24:253–276
15. White JG, Southgate E, Thomson JN, Brenner S (1986) The structure of the nervous system of the nematode Caenorhabditis elegans. Philos Trans R Soc Lond B Biol Sci 314:1–340
16. Jarrell TA, Wang Y, Bloniarz AE, Brittin CA, Xu M, Thomson JN, Albertson DG, Hall DH, Emmons SW (2012) The connectome of a decision-making neural network. Science 337: 437–444
17. Towlson EK, Vértes PE, Ahnert SE, Schafer WR, Bullmore ET (2013) The rich club of the C. elegans neuronal connectome. J Neurosci 33:6380–6387
18. Bumbarger DJ, Riebesell M, Rödelsperger C, Sommer RJ (2013) System-wide rewiring underlies behavioral differences in predatory and bacterial-feeding nematodes. Cell 152: 109–119
19. Stephens GJ, Johnson-Kerner B, Bialek W, Ryu WS (2008) Dimensionality and dynamics in the behavior of C. elegans. PLoS Comput Biol 4, e1000028
20. Stephens GJ, Johnson-Kerner B, Bialek W, Ryu WS (2010) From modes to movement in the behavior of Caenorhabditis elegans. PLoS One 5, e13914
21. Brown AEX, Yemini EI, Grundy LJ, Jucikas T, Schafer WR (2013) A dictionary of behavioral motifs reveals clusters of genes affecting Caenorhabditis elegans locomotion. Proc Natl Acad Sci 110:791–796
22. Neagu I, Nagy S, Levine E, Biron D. Fluctuations and response during C. elegans sleep-like behavior. Unpublished
23. Mayer M, Depken M, Bois JS, Jülicher F, Grill SW (2010) Anisotropies in cortical tension reveal the physical basis of polarizing cortical flows. Nature 467:617–621
24. Brangwynne CP, Eckmann CR, Courson DS, Rybarska A, Hoege C, Gharakhani J, Jülicher F, Hyman AA (2009) Germline P granules are liquid droplets that localize by controlled dissolution/condensation. Science 324: 1729–1732
25. Zwicker D, Decker M, Jaensch S, Hyman AA, Jülicher F (2014) Centrosomes are autocatalytic droplets of pericentriolar material organized by centrioles. Proc Natl Acad Sci U S A 111:E2636–E2645
26. Avery L, Shtonda BB (2003) Food transport in the C. elegans pharynx. J Exp Biol 206: 2441–2457

INDEX

David Biron and Gal Haspel (eds.), *C. elegans: Methods and Applications*, Methods in Molecular Biology, vol. 1327,
DOI 10.1007/978-1-4939-2842-2, © Springer Science+Business Media New York 2015

L

M

N

O

P

R

S

T

V

W